NASA TECHNICAL NOTE

NASA TN D-7817

NASA TN D-7817

EFFECTS OF NOZZLE INTERFAIRING MODIFICATIONS ON LONGITUDINAL AERODYNAMIC CHARACTERISTICS OF A TWIN-JET, VARIABLE-WING-SWEEP FIGHTER MODEL

David E. Reubush and Charles E. Mercer

Langley Research Center
Hampton, Va. 23665

NATIONAL AERONAUTICS AND SPACE ADMINISTRATION • WASHINGTON, D. C. • FEBRUARY 1975

1. Report No.	2. Government Accession No.	3. Recipient's Catalog No.
NASA TN D-7817		

4. Title and Subtitle	5. Report Date
EFFECTS OF NOZZLE INTERFAIRING MODIFICATIONS ON LONGITUDINAL AERODYNAMIC CHARACTERISTICS OF A TWIN-JET, VARIABLE-WING-SWEEP FIGHTER MODEL	February 1975
	6. Performing Organization Code

7. Author(s)	8. Performing Organization Report No.
David E. Reubush and Charles E. Mercer	L-9802
	10. Work Unit No.
	760-17-01-11

9. Performing Organization Name and Address	11. Contract or Grant No.
NASA Langley Research Center Hampton, Va. 23665	
	13. Type of Report and Period Covered
	Technical Note

12. Sponsoring Agency Name and Address	14. Sponsoring Agency Code
National Aeronautics and Space Administration Washington, D.C. 20546	

15. Supplementary Notes

16. Abstract

A wind-tunnel investigation has been made to determine the effects of nozzle interfairing modifications on the longitudinal aerodynamic characteristics of a twin-jet, variable-wing-sweep fighter model. The model was tested in the Langley 16-foot transonic tunnel at Mach numbers of 0.6 to 1.3 and angles of attack from about -2° to 6° and in the Langley 4-foot supersonic pressure tunnel at a Mach number of 2.2 and an angle of attack of 0°. Compressed air was used to simulate nozzle exhaust flow at jet total-pressure ratios from 1 (jet off) to about 21. The results of this investigation show that the aircraft drag can be significantly reduced by replacing the basic interfairing with a modified interfairing.

17. Key Words (Suggested by Author(s))	18. Distribution Statement
Afterbody drag Boattail drag Interfairing modifications Fighter model	Unclassified – Unlimited STAR Category 02

19. Security Classif. (of this report)	20. Security Classif. (of this page)	21. No. of Pages	22. Price*
Unclassified	Unclassified	126	$5.75

*For sale by the National Technical Information Service, Springfield, Virginia 22151

EFFECTS OF NOZZLE INTERFAIRING MODIFICATIONS ON LONGITUDINAL AERODYNAMIC CHARACTERISTICS OF A TWIN-JET, VARIABLE-WING-SWEEP FIGHTER MODEL

By David E. Reubush and Charles E. Mercer
Langley Research Center

SUMMARY

A wind-tunnel investigation has been made to determine the effects of nozzle interfairing modifications on the longitudinal aerodynamic characteristics of a twin-jet, variable-wing-sweep fighter model. The model was tested in the Langley 16-foot transonic tunnel at Mach numbers of 0.6 to 1.3 and angles of attack from about -2° to 6° and in the Langley 4-foot supersonic pressure tunnel at a Mach number of 2.2 and an angle of attack of 0°. Compressed air was used to simulate nozzle exhaust flow at jet total-pressure ratios from 1 (jet off) to about 21.

The results of this investigation show that the aircraft drag can be significantly reduced at both subsonic and transonic speeds by modifications to the basic interfairing (termination of interfairing upstream of the cruise nozzle exit plane and addition of a contoured body to the center) without significantly affecting airplane lift or pitching moment. The addition of vortex generators mounted on the engine nacelles upstream of the nozzles reduced nozzle drag but resulted in an overall increase in drag.

INTRODUCTION

Military fighter aircraft are often configured to have twin engines within their fuselages with the exhaust nozzle exits located at the rear of the fuselage. In contrast to the podded engine arrangement, this type of engine-fuselage arrangement offers compactness and a reduction of the one-engine-out stability problem, although it generally presents other problems, such as difficulty in integrating the airframe and the nozzles. The flow over the aft portion of a typical fighter configuration is complex and includes disturbances from such sources as horizontal and vertical tails, ventral fins, and for carrier-based airplanes, the tail hook which interacts with the expansion and succeeding recompression on the nozzle boattails. With such a complex flow field, often a relatively minor change in some aircraft component can have a major effect on the aircraft drag.

One aircraft component which can be relatively easily changed and offers promise of a large payoff in drag reduction is the interfairing between the nozzles. The purpose of this investigation was to determine the effects on airplane aerodynamic characteristics (drag, lift, and pitching moment) which result from modifications to the interfairings between the nozzles of a variable-wing-sweep fighter airplane configuration. Also, the addition of vortex generators on the engine nacelles just upstream of the nozzles was investigated for possible drag reduction.

The model used in this investigation had two fixed wing-sweep positions: 22° for subsonic speeds and 68° for supersonic speeds. Exhaust nozzles representative of power settings for cruise, partial afterburning, and maximum afterburning for two different engine packages were utilized. Nozzle exhaust flow was simulated by use of high-pressure air at about room temperature. In addition to the basic interfairing, six alternate interfairings were investigated. Data for the model with the various nozzles and basic interfairing have been previously reported in reference 1, and data obtained through the use of an aerodynamic model of this configuration with some of these alternate interfairings and others have been reported in reference 2.

This investigation was conducted in the Langley 16-foot transonic tunnel at Mach numbers from 0.6 to 1.3 and in the Langley 4-foot supersonic pressure tunnel at a Mach number of 2.2. Angle of attack was varied from -2° to 6° in the Langley 16-foot tunnel and was held constant at 0° in the Langley 4-foot tunnel. The jet total-pressure ratio was varied from 1 (jet off) to about 21, depending on Mach number.

SYMBOLS

All force and moment coefficients are referenced to the stability-axis system and are based on the geometry of the model having a wing leading-edge sweep of 20°. The origin of this axis system is at fuselage station 0.9127 m and water line 0.3175 m. All reference dimensions are given in meters; model dimensions are shown in centimeters.

A_e nozzle exit area, m^2

A_t nozzle throat area, m^2

b wing span, 1.6289 m

C_D afterbody-nozzle drag coefficient, $\dfrac{\text{Aft-end drag + nozzle drag}}{q_\infty S}$

$C_{D,n}$ nozzle drag coefficient obtained from integration of nozzle pressures, $\frac{\text{Drag of two nozzles}}{q_\infty S}$

C_L afterbody-nozzle lift coefficient, $\frac{\text{Aft-end lift + nozzle lift}}{q_\infty S}$

C_m afterbody-nozzle pitching-moment coefficient, $\frac{\text{Aft-end pitching moment + nozzle pitching moment}}{q_\infty S\bar{c}}$

ΔC_x incremental coefficient due to a change in model configuration from a baseline to a modified configuration (x is a dummy variable)

$\bar{c}$ mean aerodynamic chord of wing, 0.2490 m

l reference length from airplane nose to tip of tail, 1.5685 m

M free-stream Mach number

$p_{t,j}$ jet total pressure, N/m^2

p_∞ free-stream static pressure, N/m^2

q_∞ free-stream dynamic pressure, N/m^2

S wing reference area, 0.3645 m^2

x longitudinal distance from model nose (station 0), positive rearward, m

α angle of attack, deg (see fig. 2(b))

θ angle of radius from nozzle center line to nozzle surface pressure orifice (clockwise positive for left nozzle, counterclockwise positive for right nozzle; facing upstream, 0^o is at top of nacelle), deg

Λ wing sweep angle, deg

Abbreviations:

A/B afterburning

BL buttock line

FS fuselage station

max maximum

S. L. sea level

WL water line

APPARATUS AND PROCEDURE

Wind Tunnels

This investigation was conducted in the Langley 16-foot transonic tunnel and in the Langley 4-foot supersonic pressure tunnel. The Langley 16-foot transonic tunnel is a single-return, continuous, atmospheric wind tunnel with a slotted octagonal test section. The tunnel speed is continuously variable between Mach numbers of 0.2 and 1.3. The Langley 4-foot supersonic pressure tunnel is a single-return, continuous wind tunnel with a stagnation pressure range of 27.58 kN/m^2 to 206.84 kN/m^2 and a stagnation temperature range of 309 K to 322 K. By use of interchangeable nozzle blocks, the Mach number can be varied from 1.25 to 2.2.

Model

Photographs of the model mounted in the Langley 16-foot transonic tunnel and in the Langley 4-foot supersonic pressure tunnel are shown in figure 1. A sketch showing the principal dimensions of the model is shown in figure 2(a). The model was supported in the Langley 16-foot tunnel by a thin sweptback strut attached to the bottom of the fuselage just aft of the nose, as shown in figure 2(b). The strut blended into a sting which had a constant cross section beginning at the intersection with the strut trailing edge and extending downstream to a station well aft of the model. Model details and dimensions are presented in figure 3.

The model was tested with two wing-sweep positions: 22° for subsonic speeds ($M < 1.0$) with extendible glove vanes retracted and horizontal tails normally set at 0°, and 68° for transonic and supersonic speeds ($M \geq 1.0$) with glove vanes extended and horizontal tails set at -2°. (Tails were set at -2° at transonic and supersonic speeds to insure that the balance did not foul out.) The inlets, located on each side of the fuselage, maintained true geometric lines but were closed to flow passage a short distance inside the inlet lip. The model consisted of three parts: the forebody and wings, the aft fuse-

lage and empennage (hereafter referred to as the afterbody), and the engine exhaust nozzles. The forebody and wings were rigidly attached to the support system and were not metric. The afterbody was the metric portion of the model and started at the model metric break (station 1.1261 m); it included the horizontal and vertical tails, ventral fins, tail hook and fairing, aft fuselage, and interfairing between the engines. The metric break is indicated in the sketches of figure 2 and can be seen in the photographs shown in figure 1. A flexible teflon strip inserted into slots machined into the metric and nonmetric portions of the model was used as a seal at the metric-break station to prevent flow through the gap between the afterbody and the forebody.

Two different sets of exhaust nozzles representing various power settings of two different nozzle types were tested. One set represented various power settings of a convergent-divergent iris type of nozzle (type A) and the second set, various power settings of a convergent-divergent balance-beam type of nozzle (type B). Photographs and geometric details of these nozzles are shown in figures 1 and 4, respectively. The nozzle exhaust flow was simulated by use of a high-pressure compressed air system similar to that described in reference 3. The nozzles have been given configuration numbers, which conform to the configuration numbers used in references 1 and 4 and are as follows:

Configuration number	Nozzle type	Power setting	A_e/A_t
03	A	Cruise	1.05
07	A	Maximum afterburning	1.21
09	B	Cruise	1.02
10	B	Sea-level maximum afterburning	1.19
11	B	Transonic maximum afterburning	1.37
18	B	Supersonic maximum afterburning	1.41

For this investigation, the model was supplied with seven interchangeable interfairings: the basic one and six alternates. (Note that the interfairing is defined as that part of the fuselage afterbody located between the engine nacelles and nozzles.) Details of the interfairings are presented in figure 3 and photographs of the various interfairings installed on the model are shown in figure 1. Interfairings 1, 2, 4, and 5 were of similar design, an uncambered wedge with varying droop angles (inclination of upper and lower surfaces to the horizontal). Interfairing 1 was of the same length as the basic interfairing, whereas the trailing edge of interfairings 2, 4, and 5 terminated slightly upstream of the nozzle exit plane (type A cruise). Interfairing 3 was a truncated basic interfairing but was not as short as interfairing 2. Interfairing 6 was interfairing 4 with the addition of a contoured centerbody extending aft of the wedge trailing edge.

In addition to the various interfairings, the model was supplied with vortex generators which could be mounted on the engine nacelles just upstream of the nozzles. The vortex generator blades were 0.762 cm long, 0.635 cm high, and 0.038 cm thick. They were arranged in opposing pairs with each blade inclined 15° to the free stream and their midpoints separated by 0.826 cm. The rings supporting the vortex generators could be installed above the interfairing and horizontal tail (fig. 1(s)) or below, or both sets could be installed at the same time.

Instrumentation

External static-pressure orifices were located on the exhaust nozzles as indicated in table I. In addition, internal static-pressure orifices were located in the afterbody cavity and at the seal station in the gap between the forebody and afterbody. The total pressures and temperatures of the jet simulation air were measured in each tail pipe by use of a total-pressure probe and a thermocouple. Forces and moments on the metric portion (afterbody) of the model were obtained by use of a six-component strain-gage balance. An electronic flowmeter was used to measure the air mass flow rate to the nozzles.

Tests

Data were obtained for Mach numbers from 0.6 to 1.3 at angles of attack from -2° to 6° and for a Mach number of 2.2 at 0°. The average Reynolds number per meter varied from 1.00×10^7 at $M = 0.6$ to 1.41×10^7 at $M = 1.3$ in the 16-foot tunnel and was about 1.19×10^7 at $M = 2.2$ in the 4-foot tunnel. The jet total-pressure ratio was varied from 1 (jet off) to about 21, depending on Mach number.

Transition was fixed on the model by means of 3.2-mm-wide strips of No. 120 carborundum grains. The transition strips were located on the ventral fins and on the horizontal- and vertical-tail surfaces at a distance of 5.08 mm measured normal to the leading edge. The transition strips on the wing were located as shown in figure 5. A 3.2-mm-wide ring of transition grit was also located 13.5 mm aft of the nose of the fuselage.

Tests were conducted with the model equipped with the basic interfairing and six alternate interfairings and with the various nozzles listed previously. In addition to the tests with the various interfairings, other variables were investigated at subsonic speeds. One nozzle-interfairing combination was tested with horizontal-tail settings of $+2^{\circ}$ and -2°. Another nozzle-interfairing combination was tested with two arrangements of vortex generators mounted on the engine nacelles just upstream of the nozzles (fig. 1(s)).

Data Reduction

Model data recorded on magnetic tape were used to compute standard force and pressure coefficients. All force and moment data in this paper are referenced to the stability axes through the airplane center of gravity. Model angle of attack was corrected for support deflection due to loads and for tunnel upflow. The angle of attack was corrected by calibrating the support system for deflection due to loads and by using the lift curves from reference 5 to calculate the loads on the entire configuration for the various conditions. No correction was made for strut interference since data from references 6 and 7 indicate that the effect is small for a similar type of support system.

The afterbody axial force was obtained from the reading for balance axial force corrected for pressure-area terms which consisted of internal-cavity and seal-cavity forces. The axial force on the exhaust nozzles was obtained from pressure measurements by assigning an incremental projected area to each nozzle pressure orifice (locations shown in table I) and summing the incremental forces.

The afterbody force and moment increments and the drag increment of the nozzle boattail due to interfairing variation were obtained by subtracting the force or moment coefficient value obtained with a particular nozzle configuration and the basic interfairing from the value obtained with the same nozzle configuration and one of the alternate interfairings. The increments due to the other test variables were obtained by subtracting the force and moment coefficients obtained with a given nozzle-interfairing combination without the variation (for example, no vortex generators) from those obtained with the same nozzle-interfairing combination with the variation (for example, with vortex generators).

RESULTS AND DISCUSSION

Basic Force and Moment Data

Basic afterbody-nozzle force and moment coefficient data for the various configurations investigated are presented in figures 6 to 28. Afterbody-nozzle force and moment data for the configurations with the basic interfairing have been previously reported in reference 1 and therefore are not presented here. These figures present the afterbody-nozzle force and moment data as a function of the jet total-pressure ratio for the various Mach numbers and angles of attack. It should be noted that these aerodynamic forces and moments represent only those measured on the aft portion of the model (afterbody-nozzle combination, approximately one-third of the model length) and do not include forces and moments on the wings or forward portion of the fuselage. Since the purpose of this report is to investigate the effect of changing from the basic interfairing to the alternates, these basic data will not be discussed and only the incremental data will be discussed.

Incremental Force and Moment Data

Figure 29 presents typical engine operating pressure-ratio schedules with Mach number for the two nozzle types used in this investigation. Data have been cross-plotted at these jet total-pressure ratios, and from these cross plots, incremental data have been obtained and are presented in figures 30 to 39.

Effects of interfairing modifications.- The primary purpose of this investigation was to determine the effects of modifications of the interfairing between the nozzles on aircraft drag. The incremental changes in aerodynamic characteristics from those of the basic configuration are shown in figures 30 to 35 for all configurations tested.

The subsonic drag increments $\left(\Delta C_D\right)$ in figure 30 for the truncated basic interfairing (interfairing 3) show that this relatively minor change in the interfairing was not successful since it generally resulted in increased drag for both the type A and type B cruise nozzles. Conclusions derived from examination of just the drag increment for the other interfairings (which all result in reduced drag for both nozzle types) could be erroneous because changes in aircraft lift and pitching moment could result in a trim drag penalty. Therefore, to obtain a valid answer as to which interfairing gives the best performance, both lift (fig. 31) and pitching-moment (fig. 32) increments must be examined in conjunction with the drag increments.

Interfairings 1, 2, and 5 do not give the best performance since they exhibit relatively large changes in the afterbody-nozzle lift and pitching moment at all subsonic speeds for nozzle type B and these changes would result in a trim drag penalty. Interfairing 4, a symmetrical uncambered wedge ending slightly upstream of the type A cruise nozzle exit, reduced the drag coefficient of the airplane aft end by about 0.0020 (with type B cruise nozzles installed) at subsonic speeds without significantly affecting the lift and pitching moment. However, interfairing 4 may not be a practical configuration because of the necessity of shielding the tail hook for carrier-based aircraft and of the requirement for additional volume to house the chaff and flare dispensers and the fuel dump.

Interfairing 6 (interfairing 4 with the addition of a contoured body at the center to provide a more gradual change in airplane area distribution in the vicinity of the nozzle exits, protection for the tail hook, and additional required volume) has a very slight drag advantage compared with interfairing 4 at subsonic speeds, whereas the lift and pitching-moment characteristics are about the same. At transonic speeds ($M = 1.2$, fig. 34), interfairing 4 produces a less beneficial drag increment for both type A and type B nozzles than interfairing 6. At supersonic speeds ($M = 2.2$, fig. 35), interfairing 2, which was the only interfairing modification tested at those speeds, shows little effect of interfairing geometry on any of the aircraft characteristics and this small effect is probably typical of any of the short wedge interfairings. Therefore, it must be concluded that interfairing 6

is the best of the interfairings investigated and does provide significant performance advantages at both subsonic and transonic speeds.

By comparing the nozzle drag increments ($\Delta C_{D,n}$, fig. 33) with the total drag increments (ΔC_D, fig. 30) it can be seen that the largest percentage of drag improvement due to the interfairing modifications is obtained on the nozzles. This is probably due to the fact that at subsonic speeds with the short interfairings, the recompression which occurs at the end of the interfairings can feed over to help pressurize the nozzle boattail, whereas with the long basic interfairing, the recompression occurs downstream of the nozzles. At transonic speeds, the addition of the contoured body (designed with help of a wave-drag program) which extends downstream of the trailing edge of interfairing 6 helps to smooth out the area distribution without moving the recompression rearward. Therefore, interfairing 6 is successful in reducing drag at both subsonic and transonic speeds. This result agrees with that found in reference 2.

For configurations with relatively wide-spaced nozzles, these results show that for the best performance at subsonic speeds, the nozzle interfairing should end upstream of the nozzle exits. For the best performance at transonic speeds, the interfairing for subsonic speeds may be modified by the addition of a body at the center to allow for a smooth area distribution without adversely affecting the subsonic performance.

Effects of the addition of vortex generators.- Because of the flow separation on the cruise nozzles, an attempt was made to improve aircraft drag without modifying the basic interfairing by testing the model with two vortex generator configurations mounted on the engine nacelles just upstream of the beginning of the nozzle boattail. One configuration had vortex generators completely encircling the nacelles and the other only had them on the top half of the nacelles between the interfairing and the horizontal tails. The results of this investigation are shown in figures 36 and 37. Neither of these two vortex generator configurations reduced aircraft drag; however, both configurations reduced nozzle drag, as was expected. The full set of vortex generators was generally slightly more than twice as effective as the half set. However, the overall drag increased because the drag on the vortex generators was generally about twice the value of the reduction in nozzle drag. (See figs. 36 and 37.) The full set of vortex generators was generally slightly more than twice as bad as the half set.

Effects of horizontal-tail incidence.- In an effort to evaluate the possible drag penalties associated with retrimming the aircraft at subsonic speeds to allow the use of interfairing 2, for example, the model was tested at $M = 0.7$ and 0.8 with the horizontal tails set at $\pm 2^\circ$ as well as at the normal 0°. The results (figs. 38 and 39) show that a tail deflection of 2° or less is sufficient to retrim the aircraft for any of the interfairings investigated. However, this change in tail angle can have significant effects on aircraft drag, depending on aircraft angle of attack and tail setting. These results tend to support

the effectiveness of interfairing 6, which changed aircraft lift and pitching moment very little, as the best type to improve airplane range capability.

CONCLUSIONS

An investigation of the effects of interfairing modifications and of other minor configuration modifications on the longitudinal aerodynamic characteristics of a twin-jet, variable-wing-sweep fighter model has indicated the following conclusions:

1. The replacement of the basic interfairing with a shortened symmetric uncambered wedge with a contoured body at the center resulted in significant drag reductions at both subsonic and transonic speeds without significantly affecting the aircraft lift or pitching-moment characteristics.

2. For the best performance at subsonic speeds of a similar configuration with relatively wide-spaced nozzles, the nozzle interfairing should end upstream of the nozzle exits. For the best performance at transonic speeds, the interfairing for subsonic speeds may be modified by the addition of a body at the center to allow for a smooth area distribution without adversely affecting the subsonic performance.

3. The addition of vortex generators on the engine nacelles upstream of the nozzles reduced nozzle drag but resulted in an overall drag increase.

Langley Research Center,
National Aeronautics and Space Administration,
Hampton, Va., December 11, 1974.

REFERENCES

1. Mercer, Charles E.; and Reubush, David E.: Sting and Jet Interference Effects on Longitudinal Aerodynamic Characteristics of a Twin-Jet, Variable-Wing-Sweep Fighter Model at Mach Numbers to 2.2. NASA TM X-2825, 1973.

2. Putnam, Lawrence E.: Effect of Nozzle Interfairings on Aerodynamic Characteristics of a Twin-Engine Variable-Sweep-Wing Fighter Airplane at Mach 0.60 to 2.01. NASA TM X-2769, 1973.

3. Mercer, Charles E.; and Berrier, Bobby L.: Effect of Afterbody Shape, Nozzle Type, and Engine Lateral Spacing on the Installed Performance of a Twin-Jet Afterbody Model. NASA TM X-1855, 1969.

4. Reubush, David E.; and Mercer, Charles E.: Exhaust-Nozzle Characteristics for a Twin-Jet, Variable-Wing-Sweep Fighter Airplane Model at Mach Numbers to 2.2. NASA TM X-2947, 1974.

5. Putnam, Lawrence E.: Effects of Modifications and External Stores on Aerodynamic Characteristics of a Fighter Airplane With Variable-Sweep Wing and Twin Vertical Tails at Mach 0.65 to 2.01. NASA TM X-2366, 1974.

6. Re, Richard J.; Wilmoth, Richard G.; and Runckel, Jack F.: Investigation of Effects of Afterbody Closure and Jet Interference on the Drag of a Twin-Engine Tactical Fighter. NASA TM X-1382, 1967.

7. Runckel, Jack F.; Lee, Edwin E.; and Simonson, Albert J.: Sting and Jet Interference Effects on the Afterbody Drag of a Twin-Engine Variable-Sweep Fighter Model at Transonic Speeds. NASA TM X-755, 1963.

TABLE I.- EXTERNAL NOZZLE ORIFICE LOCATIONS

[Configuration number in parentheses]

θ, deg	x/l (03)	x/l (07)	θ, deg	x/l (09)	θ, deg	x/l (10)	x/l (11)	x/l (18)
Engine type A nozzles			Engine type B nozzles					
Left nozzle								
0	0.935	0.932	12	0.909	12	0.919	0.919	0.919
20	.905	.909	12	.936	12	.937	.937	.937
35	.935	.932	12	.970	12	.955	.957	.959
35	.949	.940	54	.909	54	.919	.919	.919
35	.963	.947	71	.936	71	.937	.937	.937
50	.905	.909	60	.948	60	.943	.943	.943
75	.949	.940	60	.957	60	.955	.957	.959
75	.963	.947	60	.970	60	.974	.973	.974
95	.935	.932	108	.909	108	.919	.919	.919
135	.905	.909	108	.948	108	.937	.937	.937
135	.935	.932	108	.957	108	.943	.943	.943
135	.949	.940	108	.970	108	.974	.973	.974
180	.905	.909	180	.909	180	.919	.919	.919
180	.963	.947	180	.936	180	.937	.937	.937
225	.905	.909	180	.948	180	.943	.943	.943
225	.935	.932	180	.957	180	.955	.957	.959
225	.949	.940	180	.970	180	.974	.973	.974
264	.905	.909	228	.909	228	.919	.919	.919
264	.921	.921	228	.948	228	.937	.937	.937
264	.945	.937	228	.970	228	.955	.957	.959
275	.963	.947	276	.957	276	.955	.957	.959
287	.905	.909	290	.927	290	.926	.929	.929
287	.921	.921	324	.909	324	.919	.919	.919
287	.945	.937	324	.936	324	.937	.937	.937
315	.935	.932	324	.948	324	.943	.943	.943
315	.949	.940	324	.957	324	.955	.957	.959
315	.963	.947	324	.970	324	.974	.973	.974
350	.905	.909	348	.919	348	.919	.919	.919
Right nozzle								
0	0.949	0.940	36	0.936	84	0.926	0.929	0.919
0	.963	.947	36	.948	84	.943	.943	.943
35	.905	.909	36	.957	88	.974	.973	.974
75	.935	.932	228	.936	252	.943	.943	.943
135	.963	.947	264	.927	252	.974	.973	.974
180	.921	.921	264	.943	264	.909	.909	.909
180	.935	.932	264	.957	264	.926	.929	.929
180	.949	.940	276	.970	290	.909	.909	.909
225	.963	.947	290	.943	300	.943	.943	.943
315	.905	.909	290	.957	300	.974	.973	.974

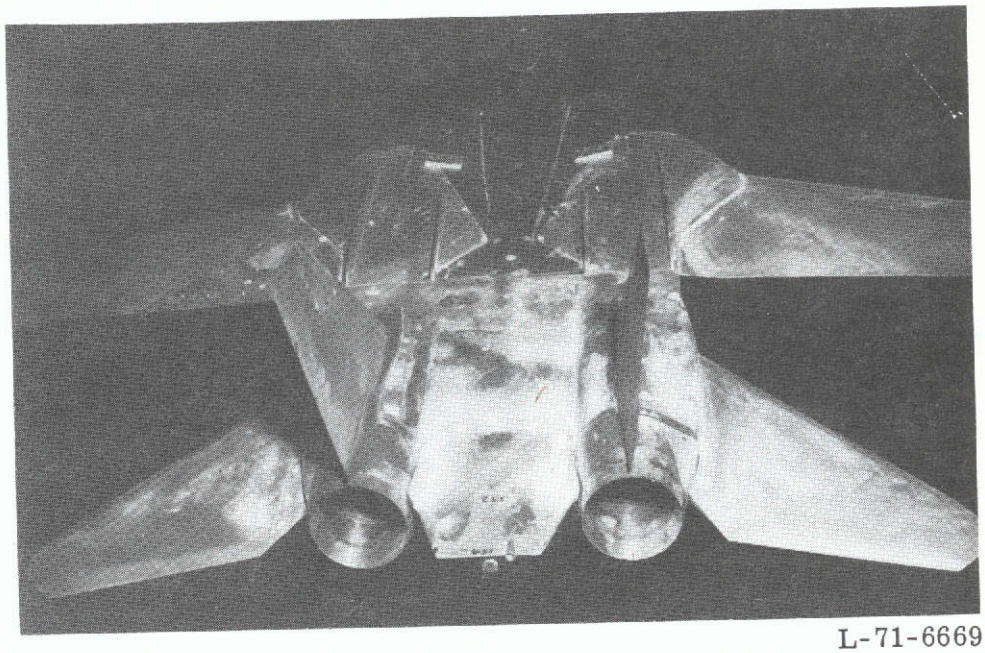

L-71-6669

(a) Top rear view of nozzle type A, maximum afterburning power setting, with basic interfairing.

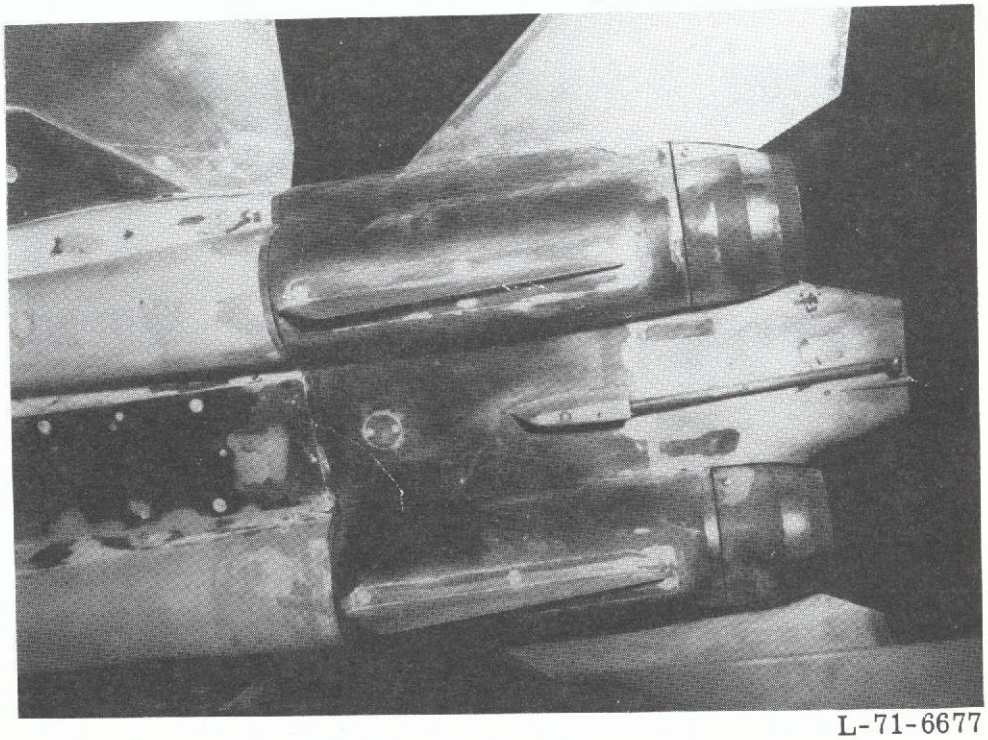

L-71-6677

(b) Bottom rear view of nozzle type A, maximum afterburning power setting, with basic interfairing.

Figure 1.- Photographs of model installed in Langley 16-foot transonic tunnel and 4-foot supersonic pressure tunnel.

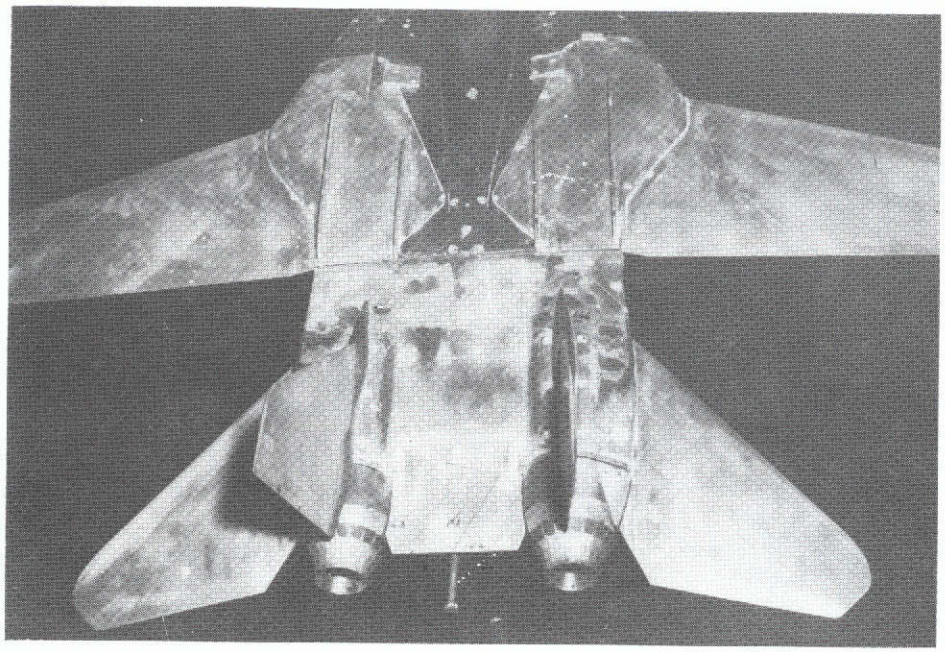

L-74-3939

(c) Top rear view of nozzle type A, cruise power setting, with typical short wedge interfairing.

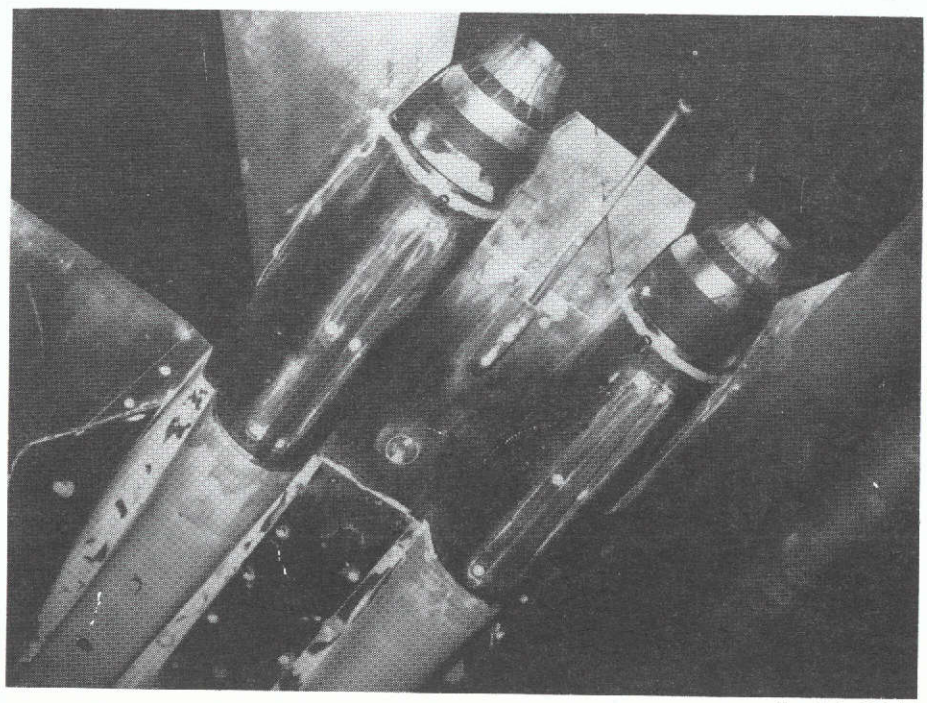

L-74-3941

(d) Bottom rear view of nozzle type A, cruise power setting, with typical short wedge interfairing.

Figure 1.- Continued.

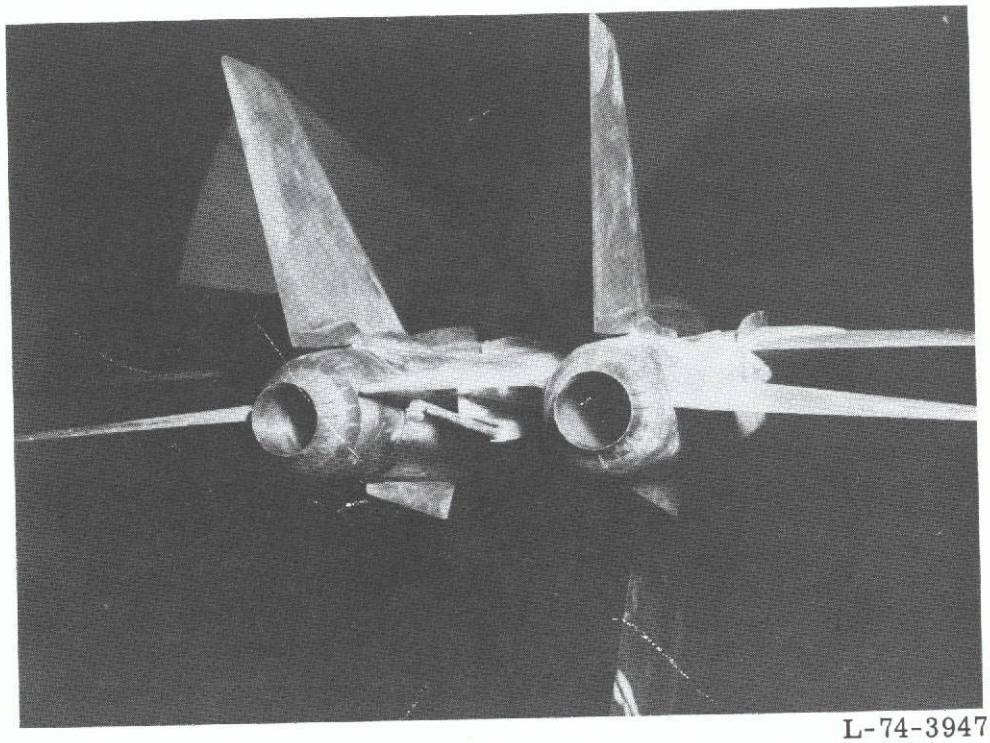

L-74-3947

(e) Rear view of nozzle type A, cruise power setting, with interfairing 2.

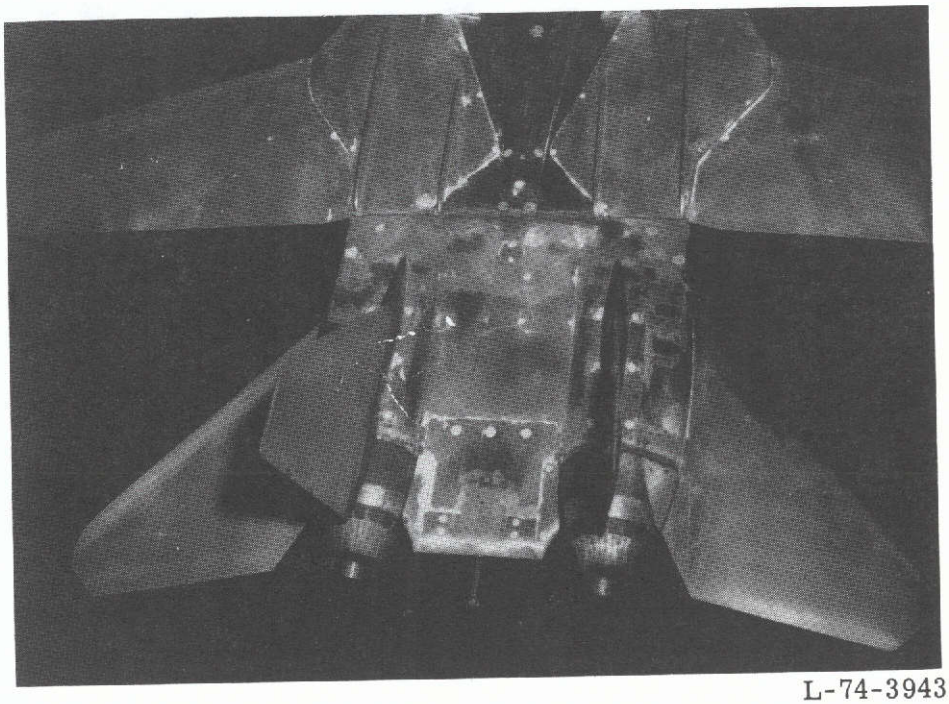

L-74-3943

(f) Top rear view of nozzle type A, cruise power setting, with interfairing 3.

Figure 1.- Continued.

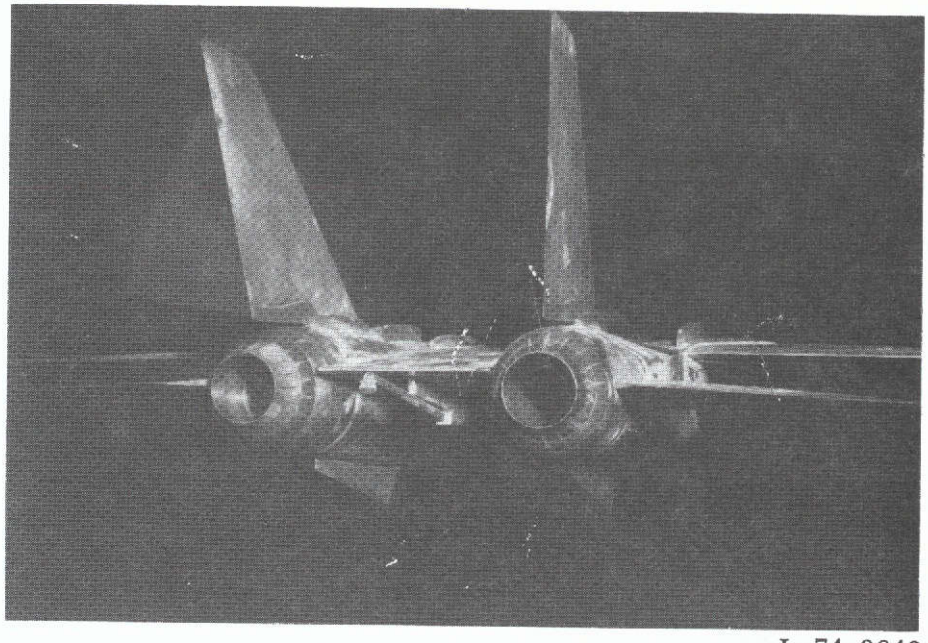

L-74-3940

(g) Rear view of nozzle type A, cruise power setting, with interfairing 4.

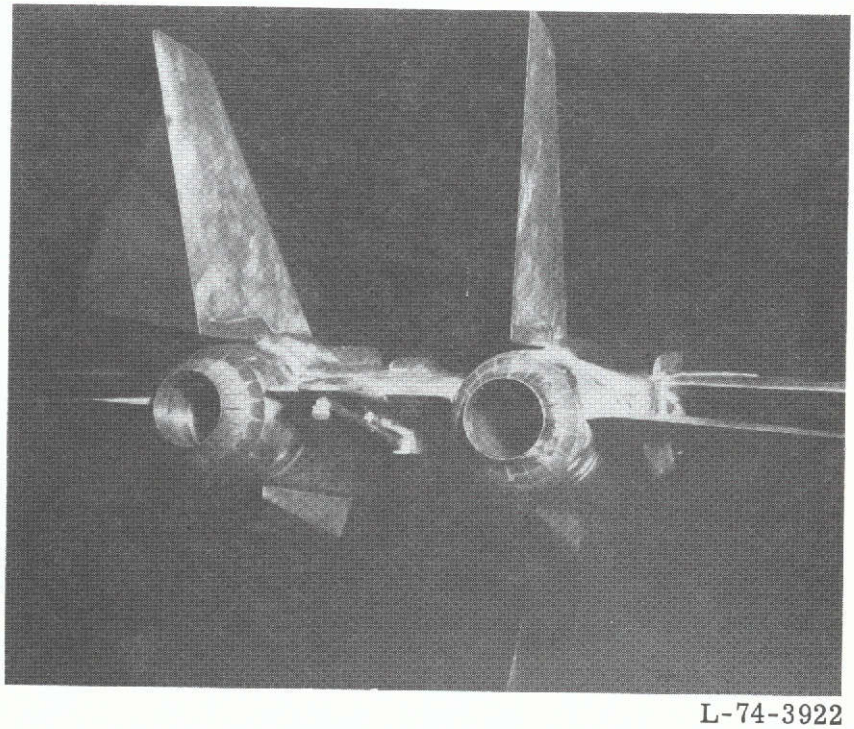

L-74-3922

(h) Rear view of nozzle type A, cruise power setting, with interfairing 6.

Figure 1.- Continued.

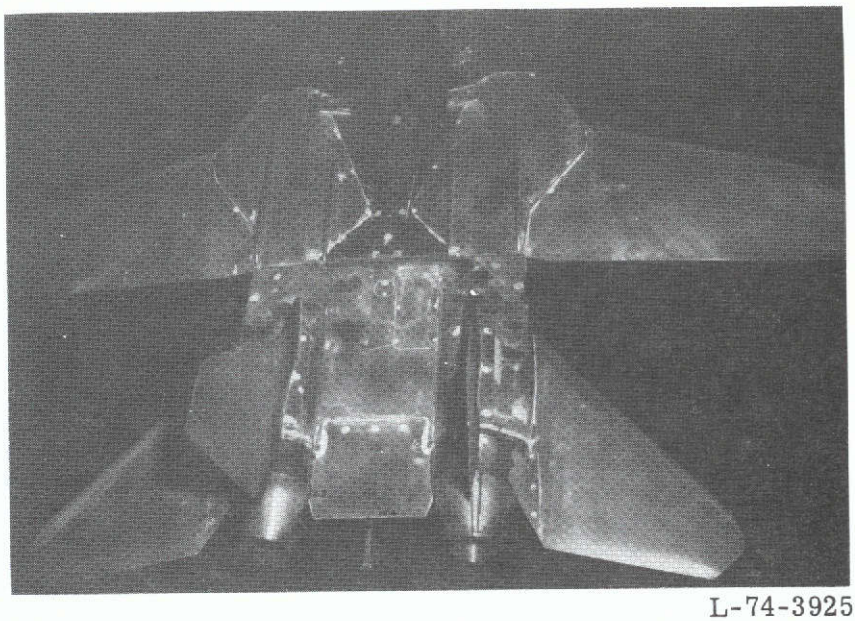

L-74-3925

(i) Top rear view of nozzle type B, cruise power setting, with typical short wedge interfairing.

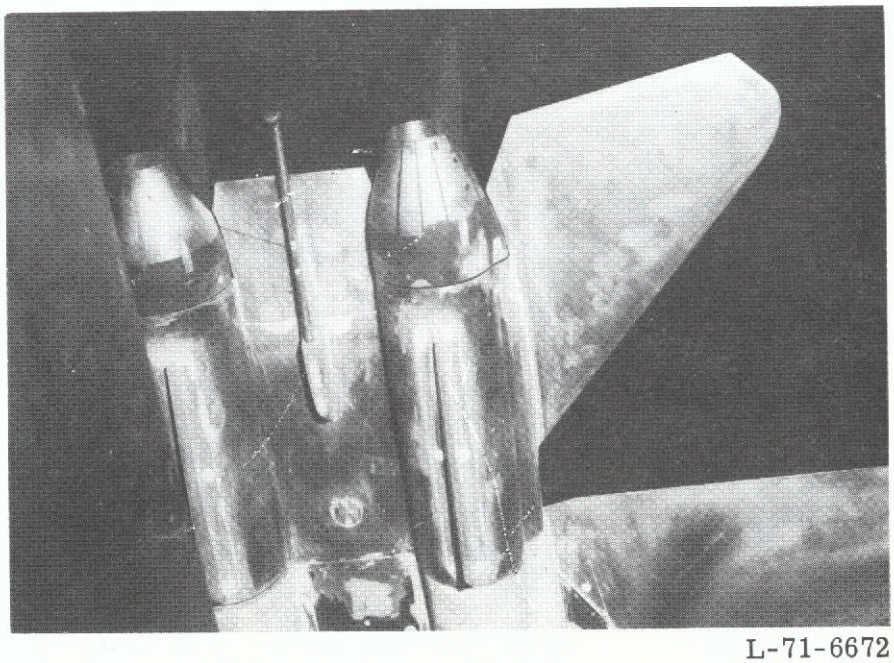

L-71-6672

(j) Bottom rear view of nozzle type B, cruise power setting, with typical short wedge interfairing.

Figure 1.- Continued.

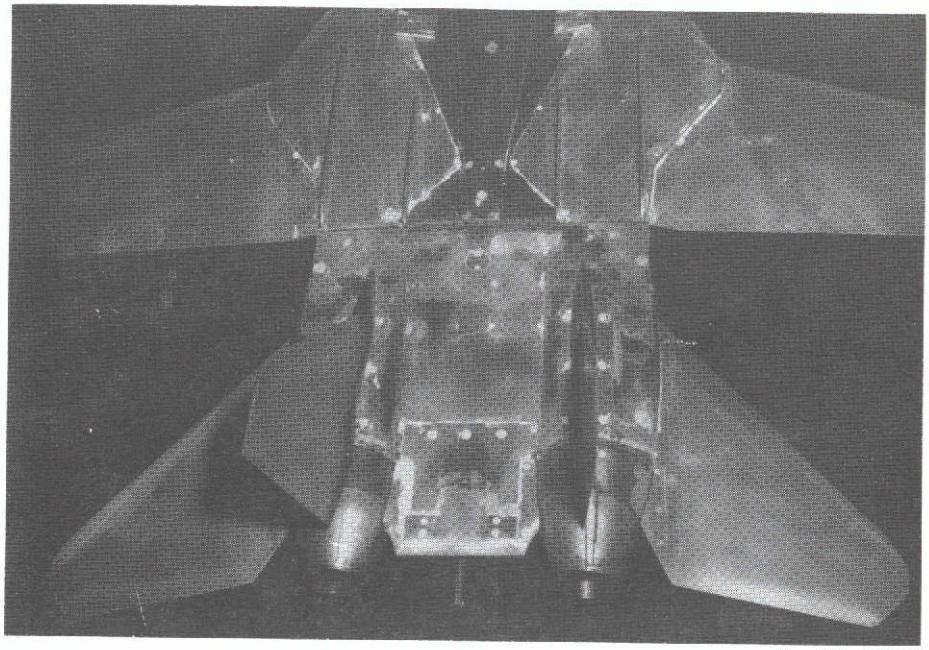

L-74-3920

(k) Top rear view of nozzle type B, cruise power setting, with interfairing 3.

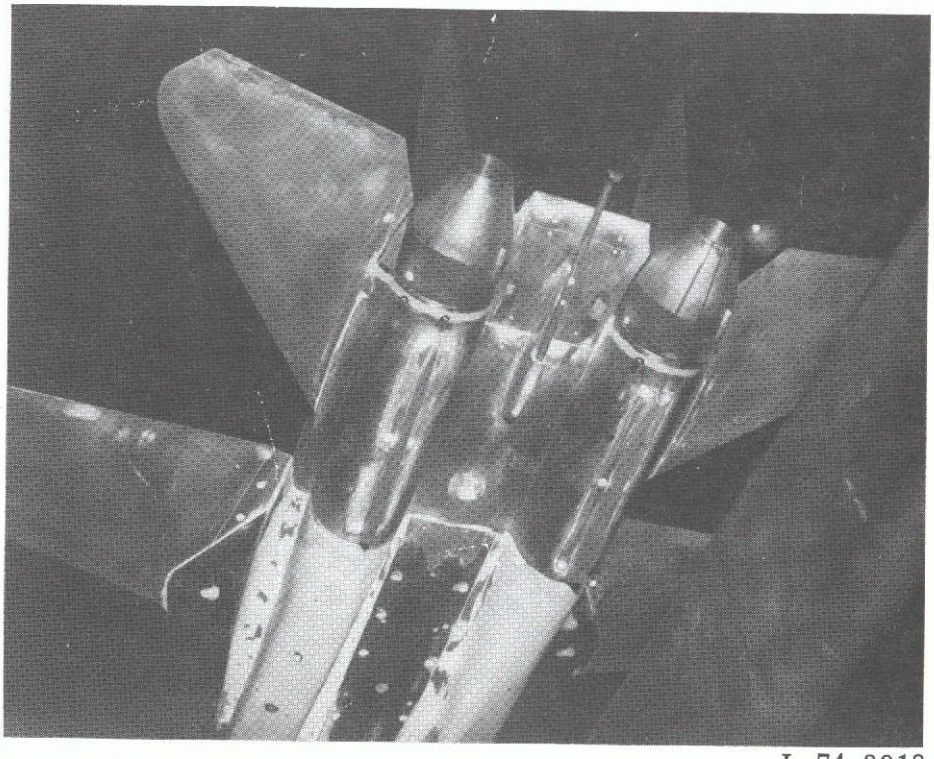

L-74-3918

(l) Bottom rear view of nozzle type B, cruise power setting, with interfairing 3.

Figure 1.- Continued.

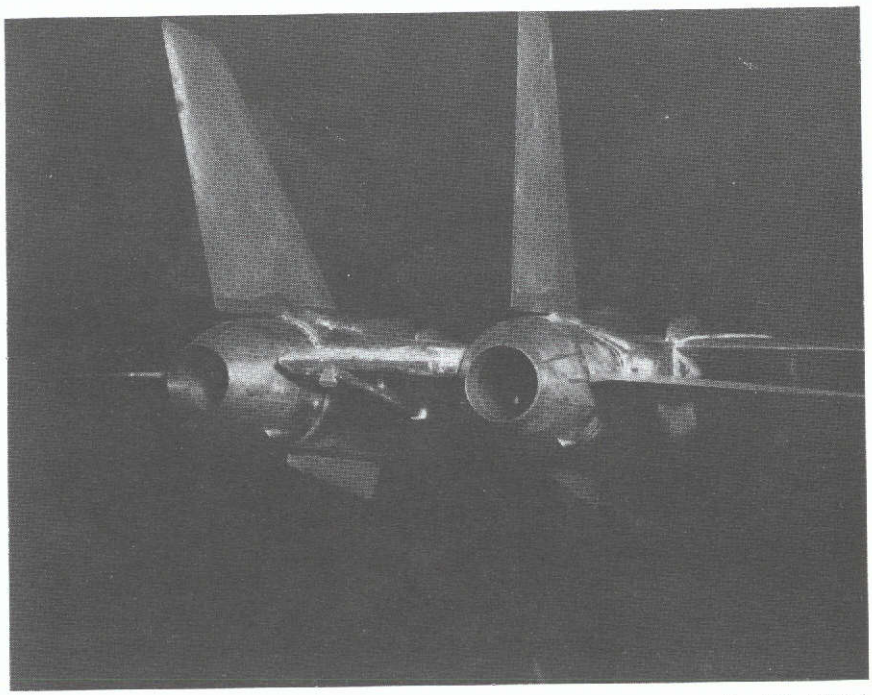

L-74-3921

(m) Rear view of nozzle type B, cruise power setting, with interfairing 3.

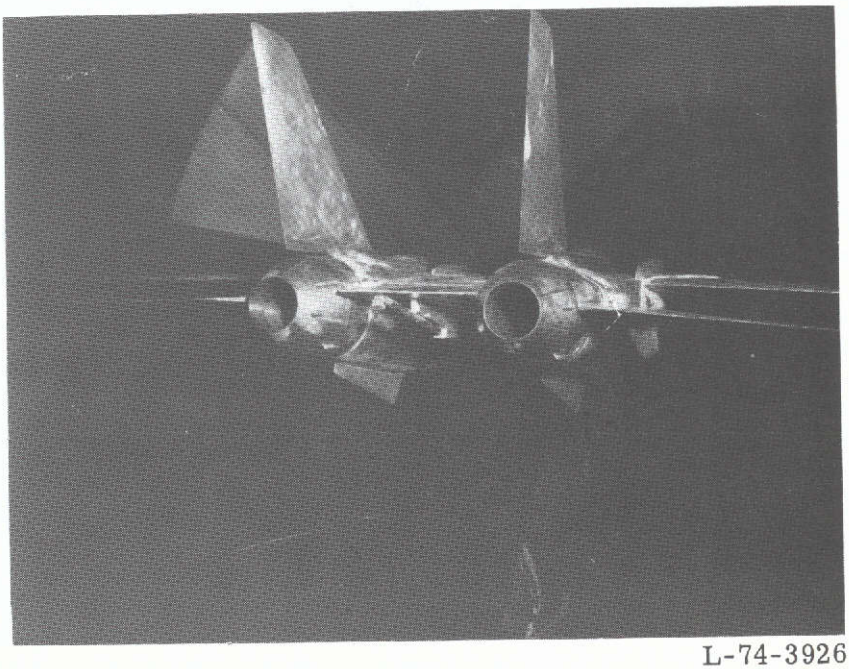

L-74-3926

(n) Rear view of nozzle type B, cruise power setting, with interfairing 4.

Figure 1.- Continued.

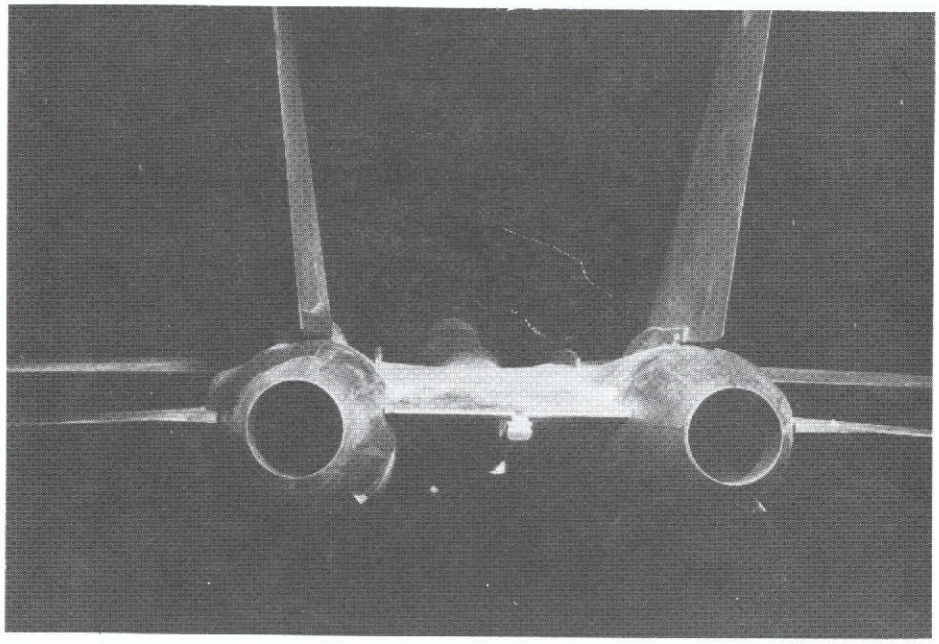

L-74-3928

(o) Rear view of nozzle type B, cruise power setting, with interfairing 5.

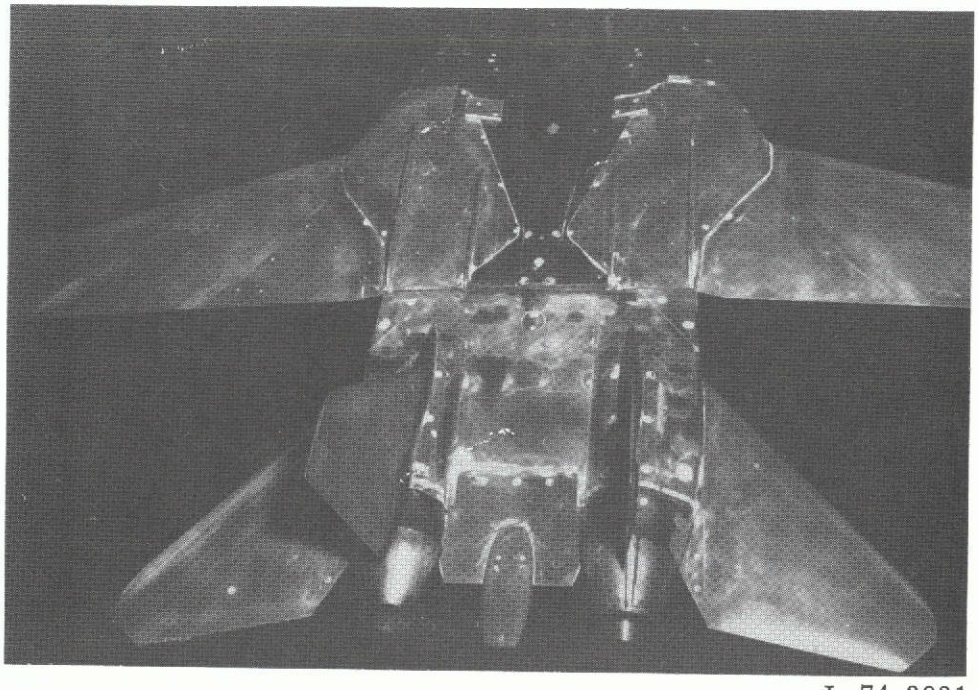

L-74-3931

(p) Top rear view of nozzle type B, cruise power setting, with interfairing 6.

Figure 1.- Continued.

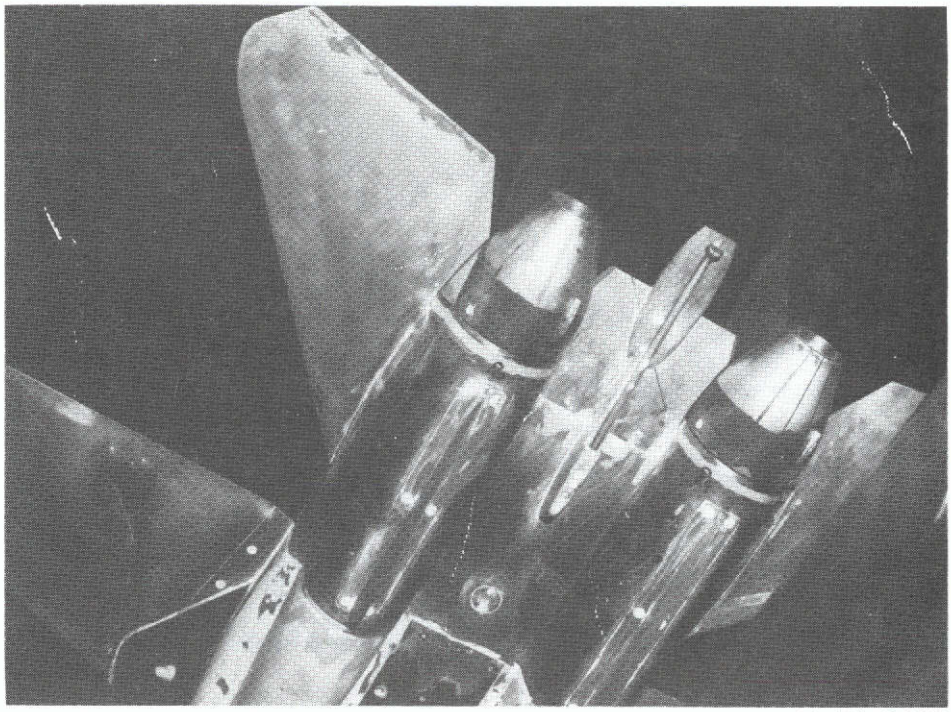

L-74-3932

(q) Bottom rear view of nozzle type B, cruise power setting, with interfairing 6.

L-74-3933

(r) Rear view of nozzle type B, cruise power setting, with interfairing 6.

Figure 1.- Continued.

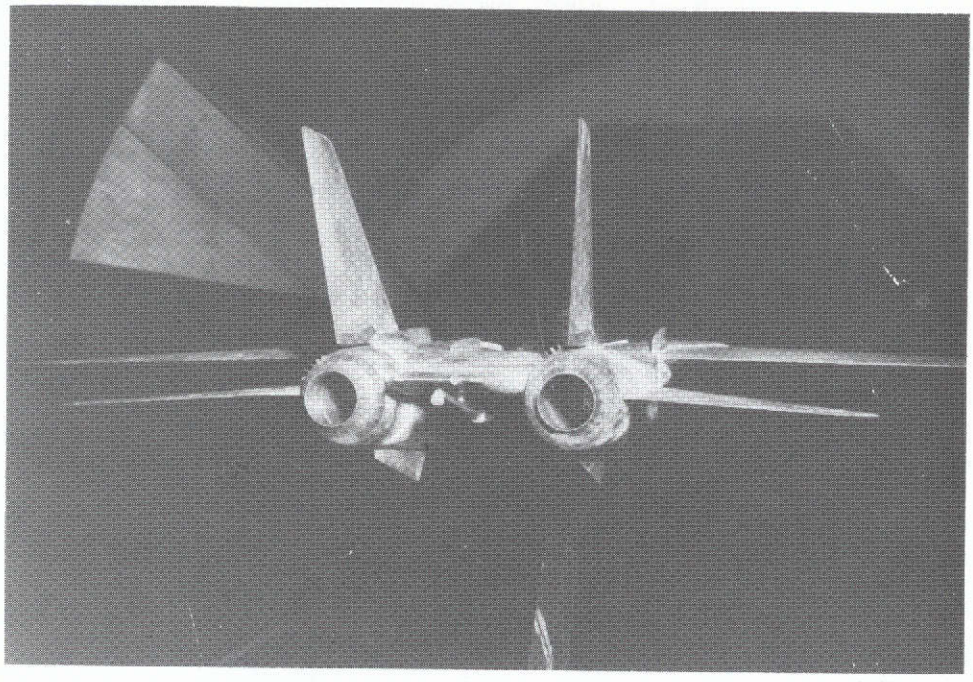

L-74-3944

(s) Rear view of nozzle type A, cruise power setting, with basic interfairing and vortex generators on top of nacelles.

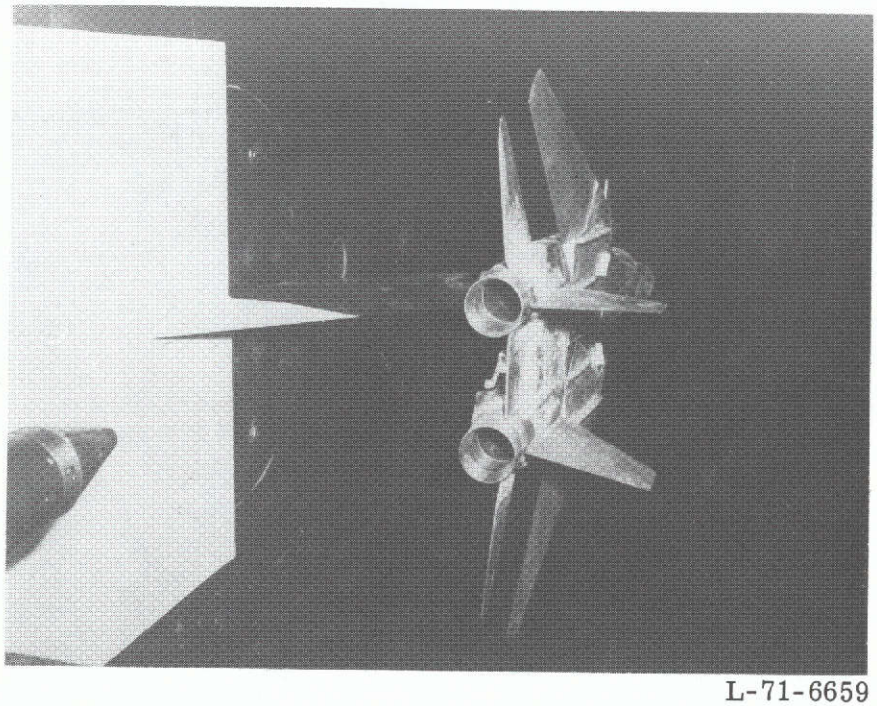

L-71-6659

(t) Rear view of nozzle type B, supersonic maximum afterburning power setting, with interfairing 2 in 4-foot tunnel; model mounted on side wall.

Figure 1.- Concluded.

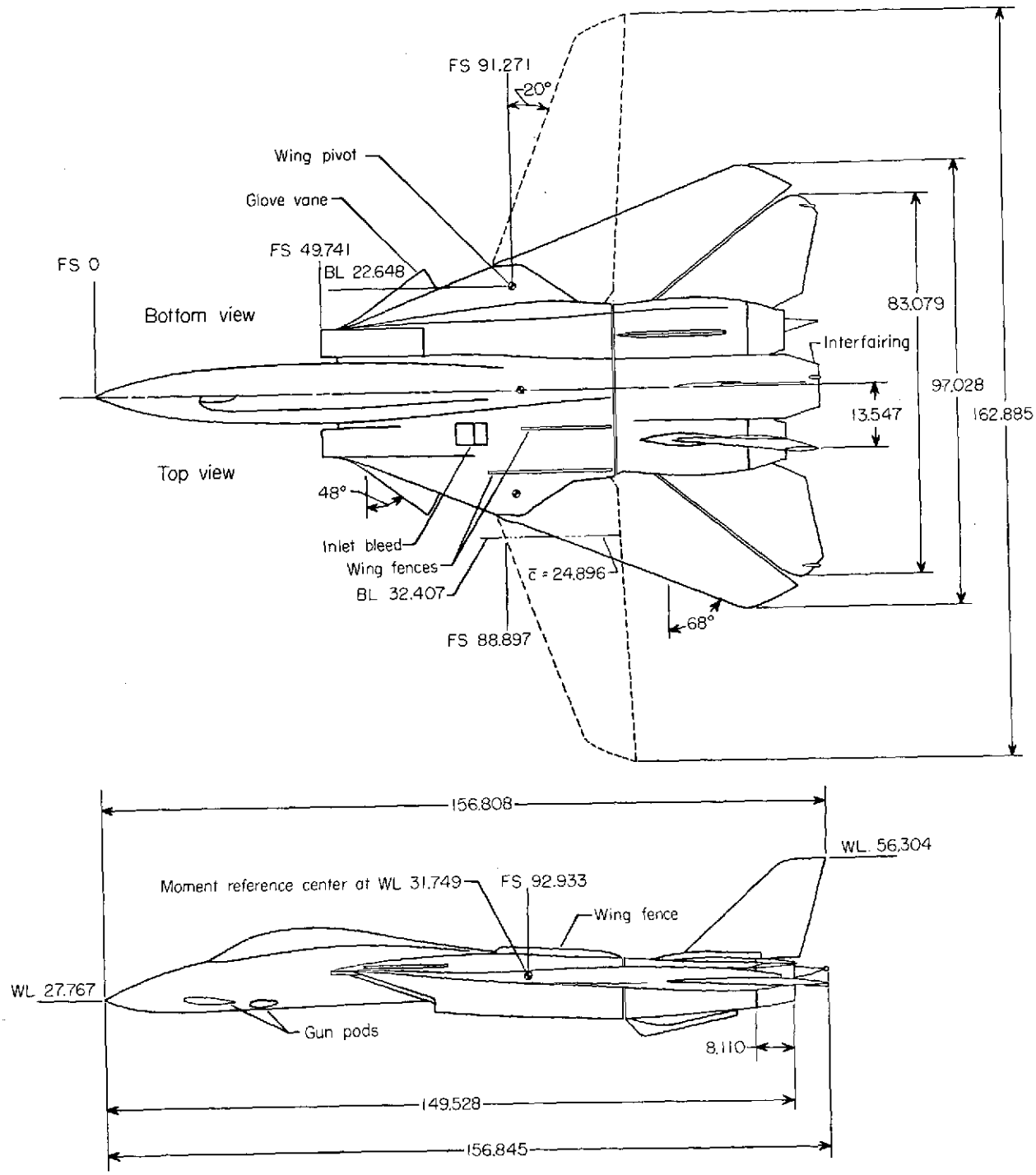

(a) Model with nozzle type A and maximum afterburning power setting nozzles installed.

Figure 2.- Sketch of model and geometric details of model support.
All dimensions are in centimeters unless otherwise specified.

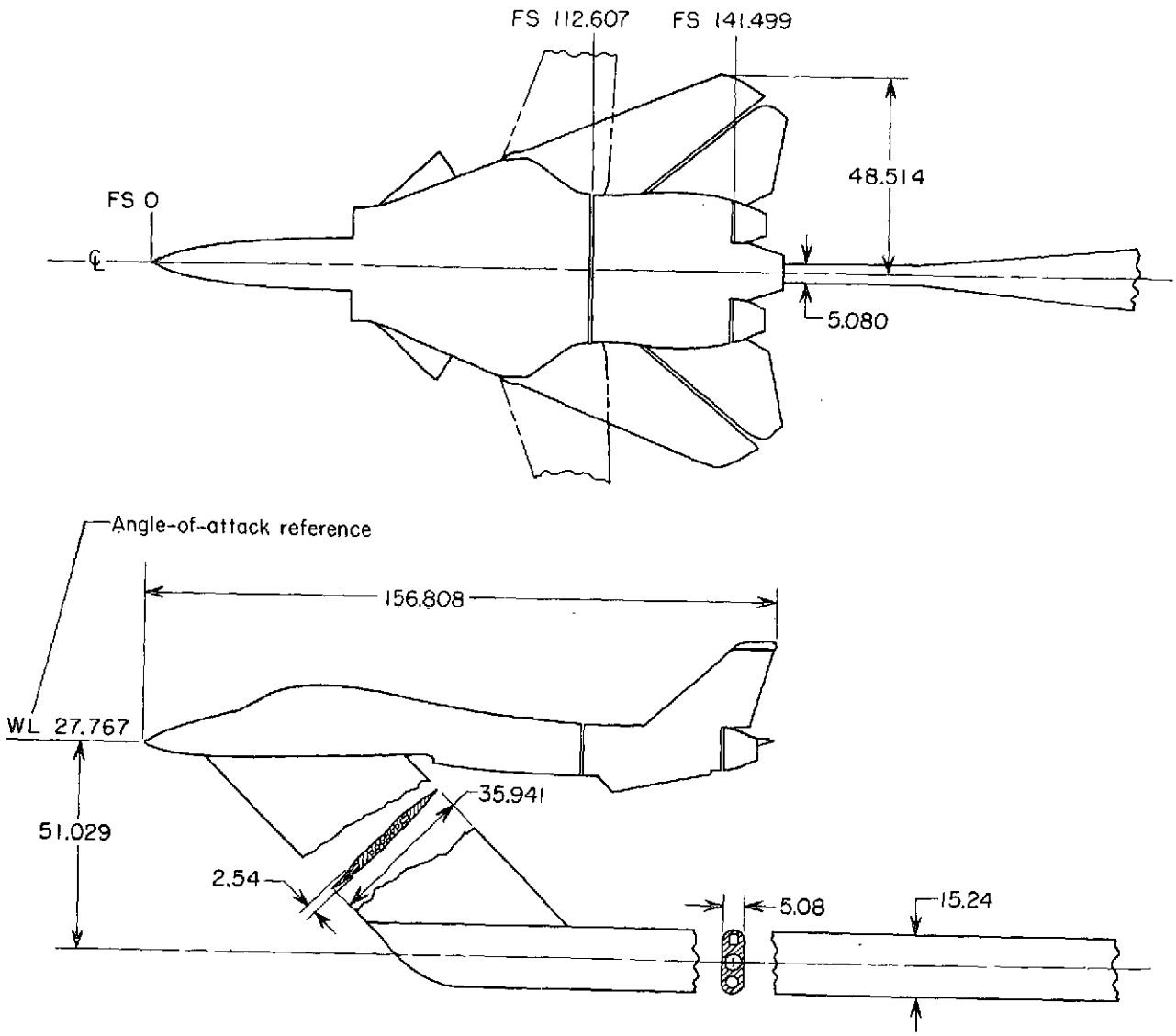

(b) Geometric details of model support.

Figure 2.- Concluded.

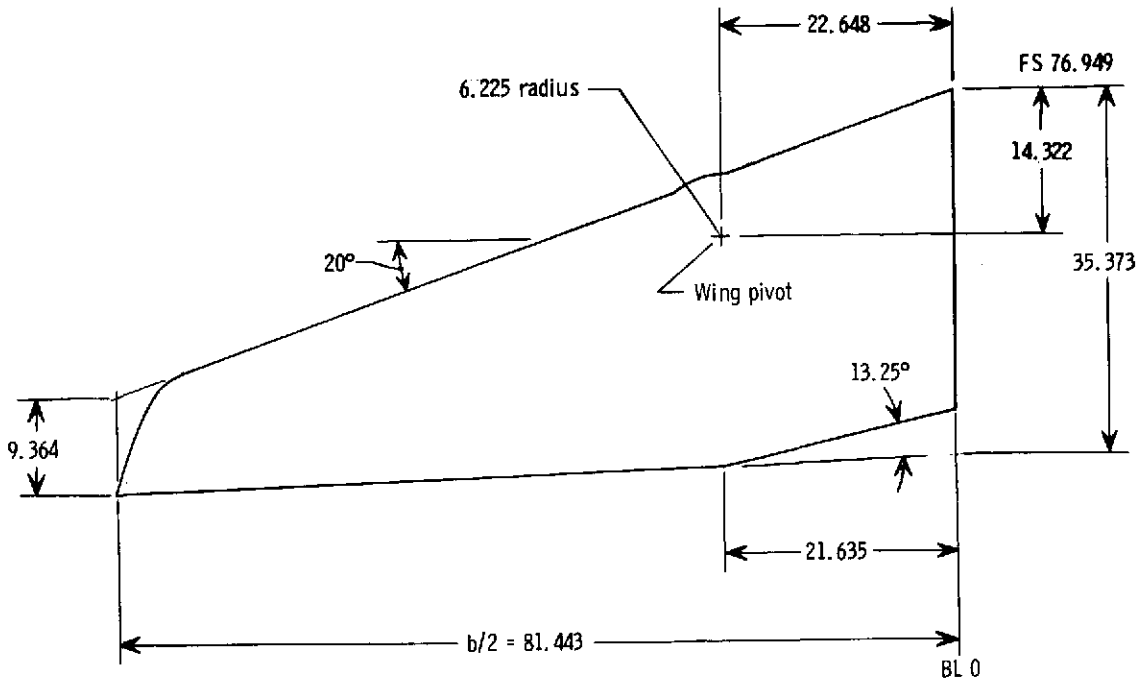

(a) Wing.

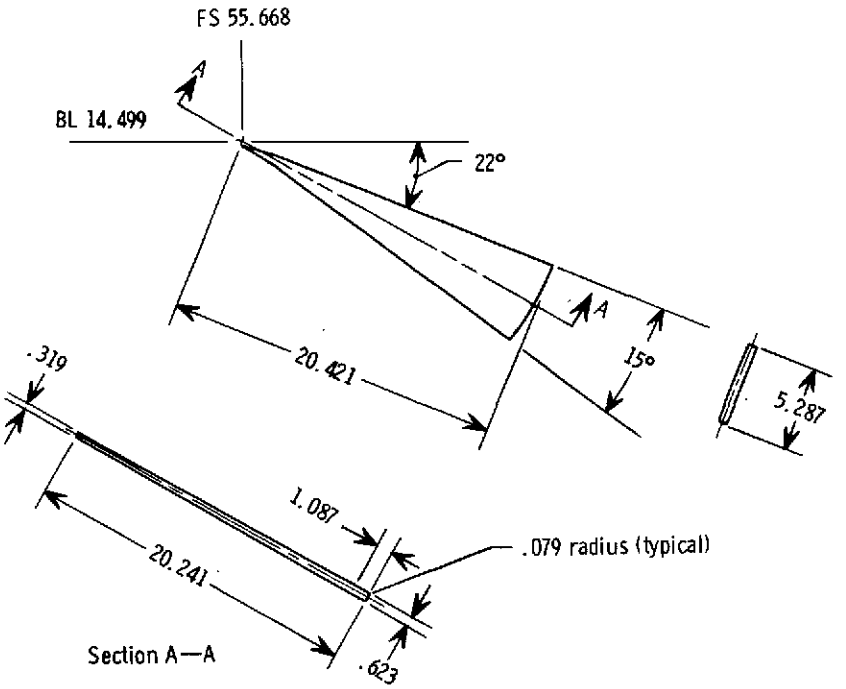

(b) Glove vane.

Figure 3.- Details of model. All dimensions are in centimeters unless otherwise specified.

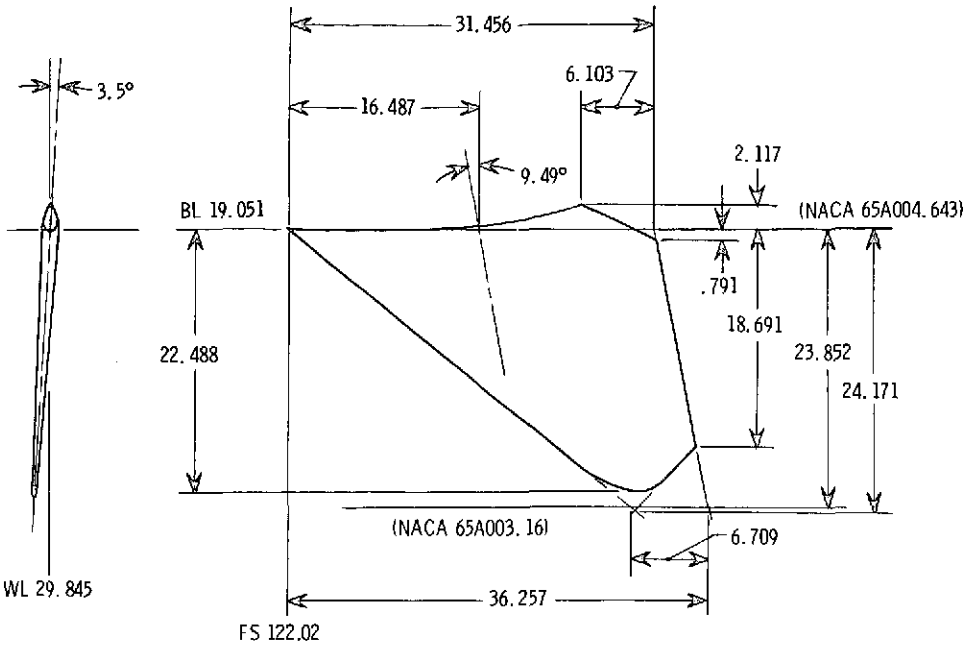

(c) Horizontal tail.

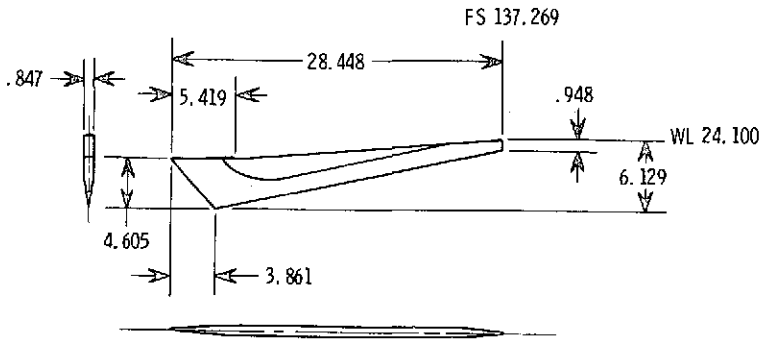

(d) Ventral fin.

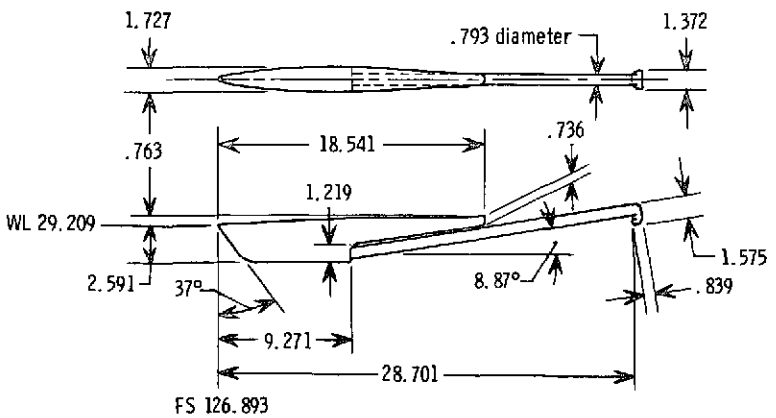

(e) Tail hook and fairing.

Figure 3.- Continued.

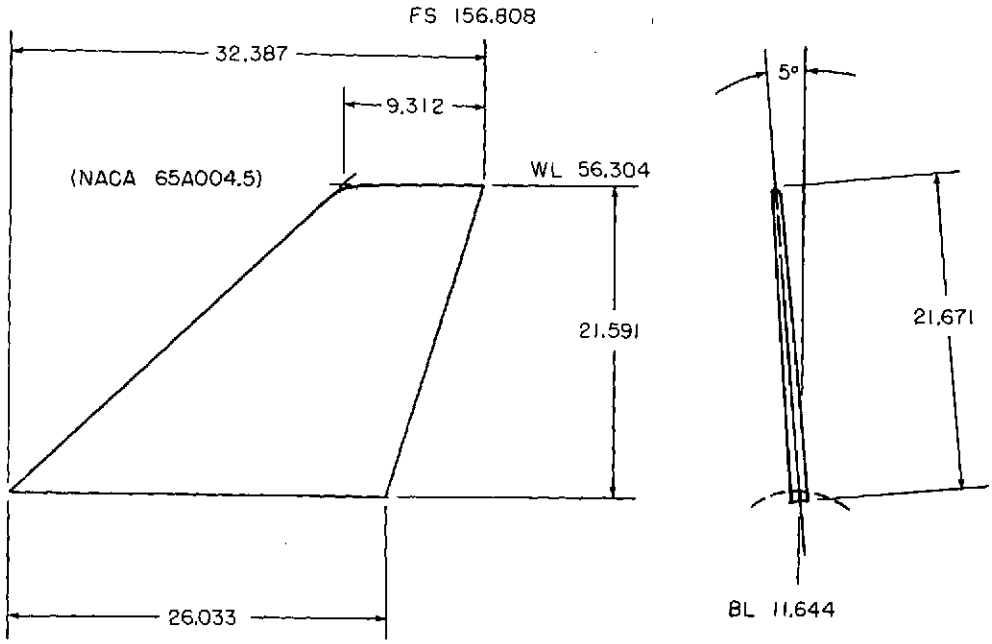

(f) Vertical tails (left shown). Vertical tails are toed in 1°.

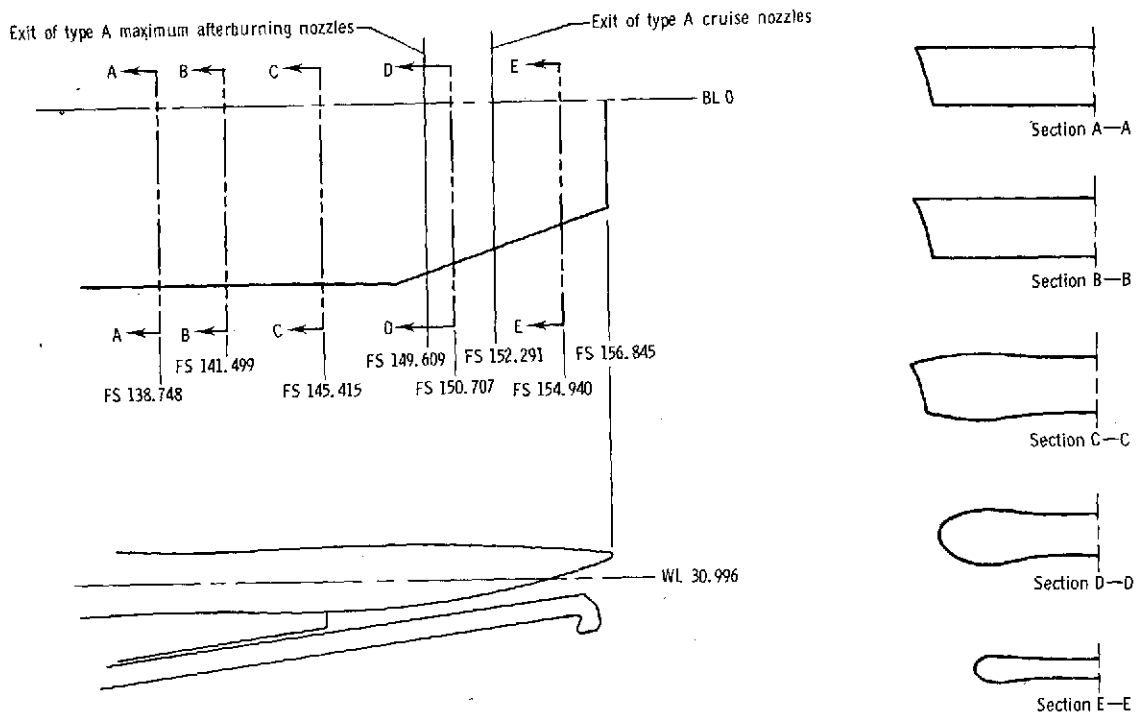

(g) Basic interfairing.

Figure 3.- Continued.

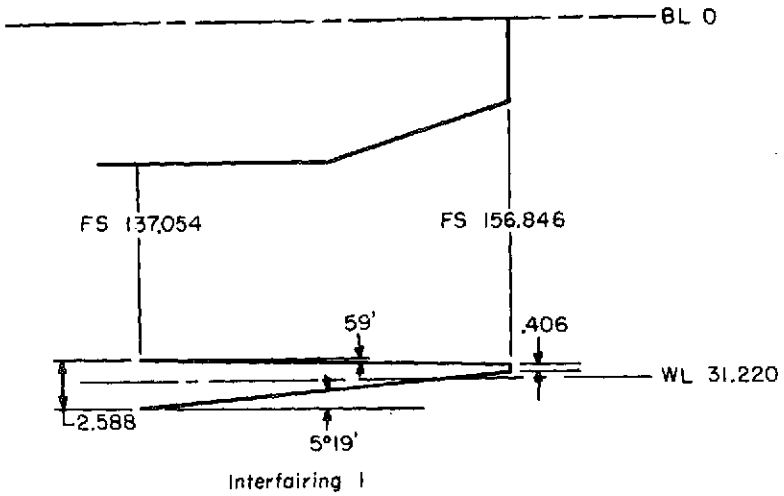

(h) Interfairing 1.

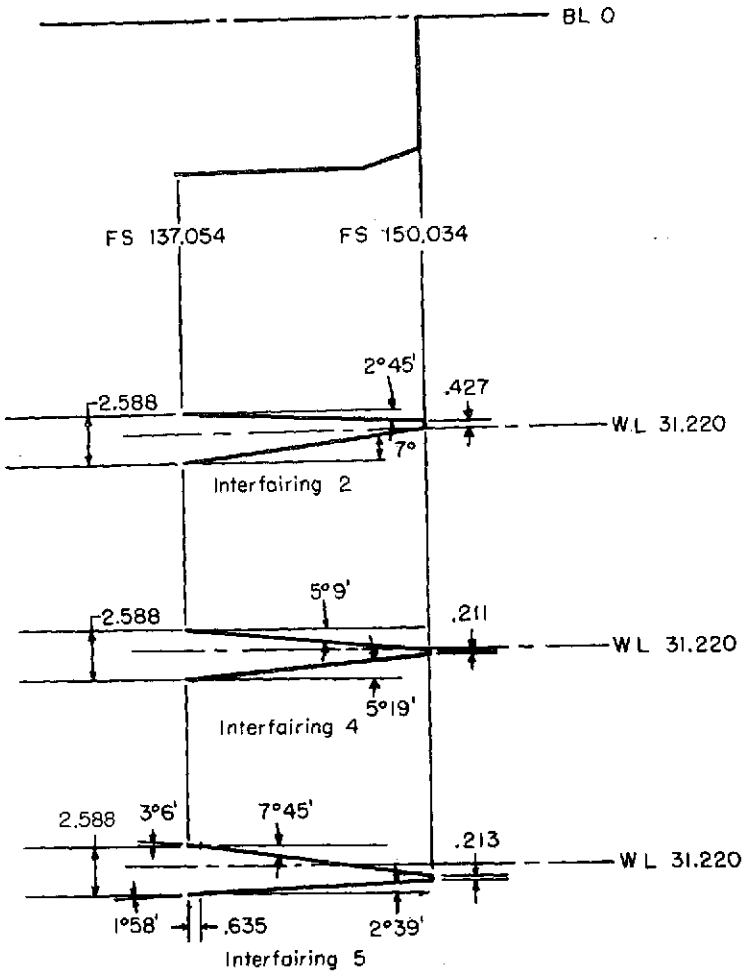

(i) Interfairings 2, 4, and 5.

Figure 3.- Continued.

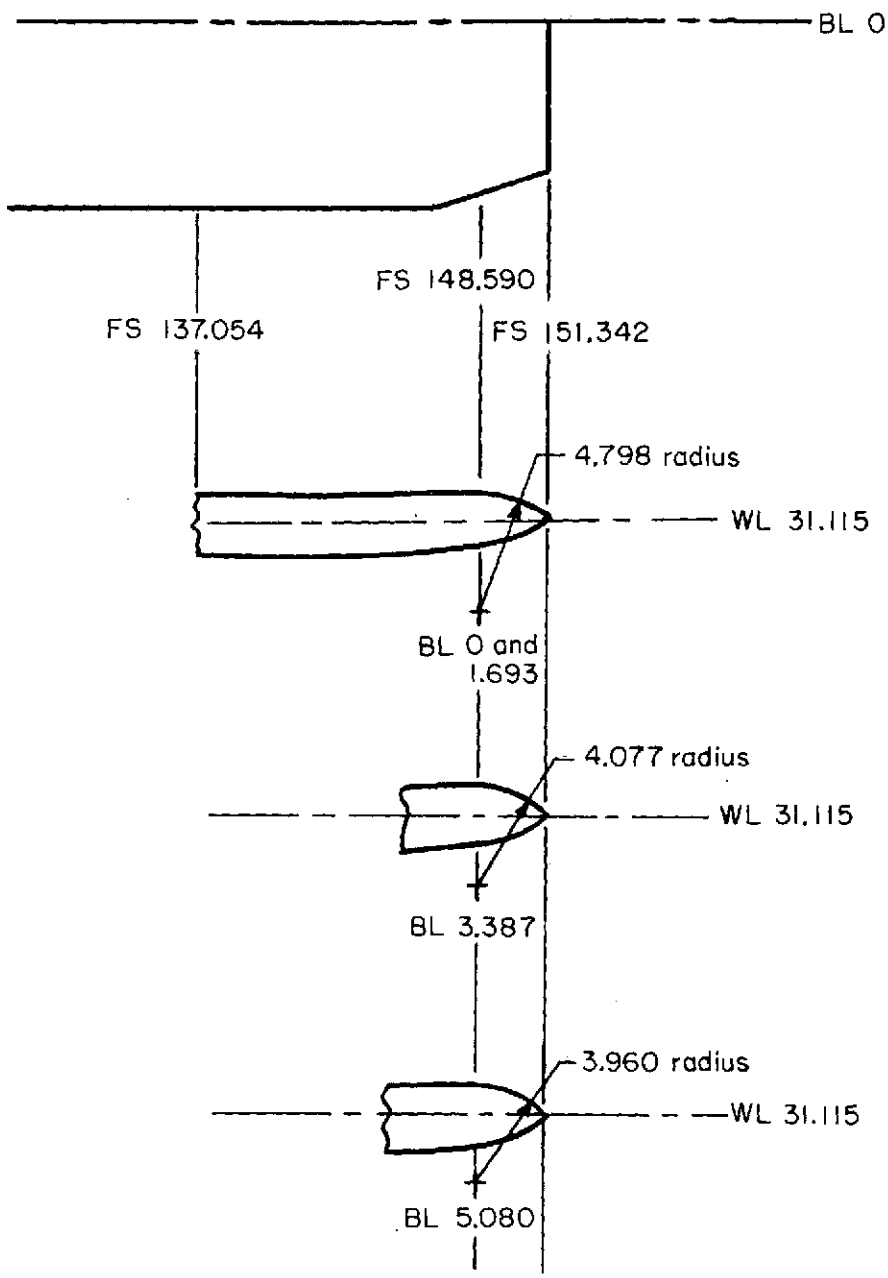

(j) Interfairing 3.

Figure 3.- Continued.

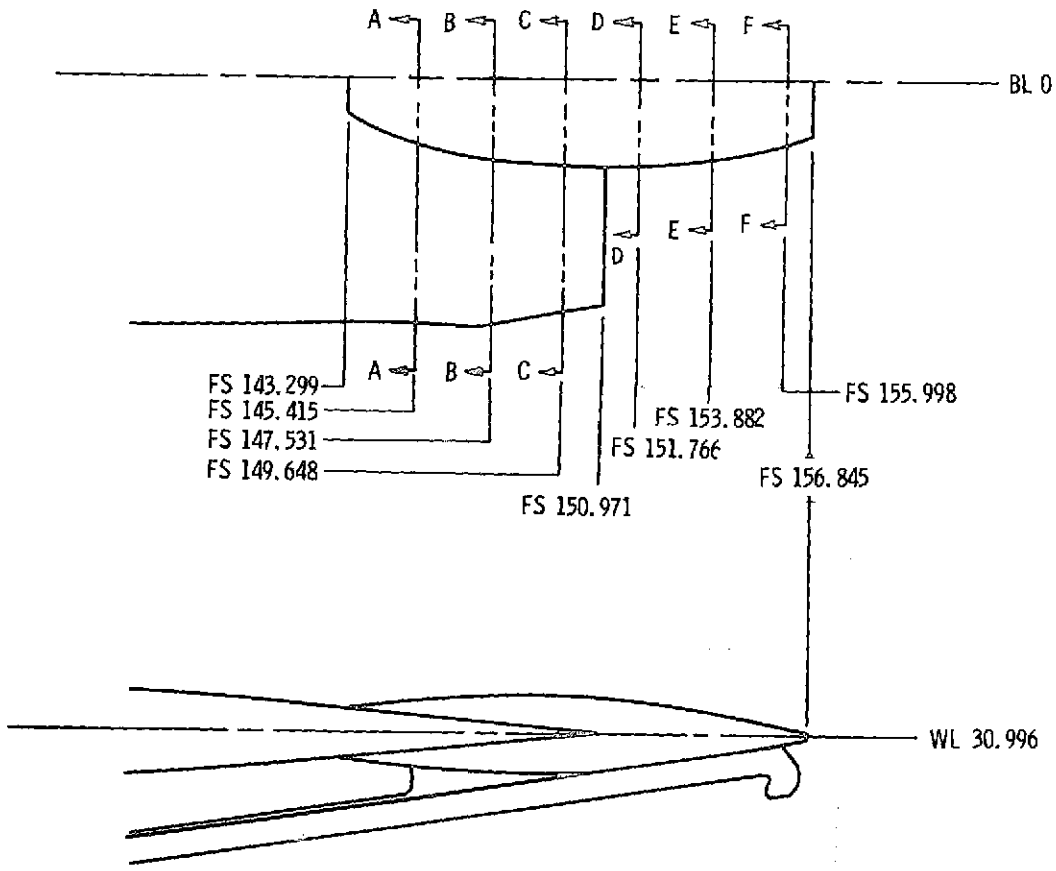

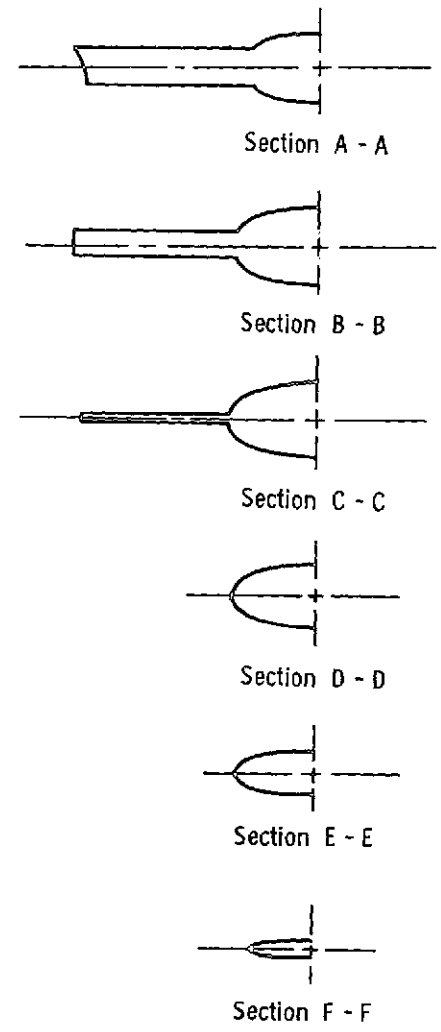

(k) Interfairing 6.

Figure 3.- Concluded.

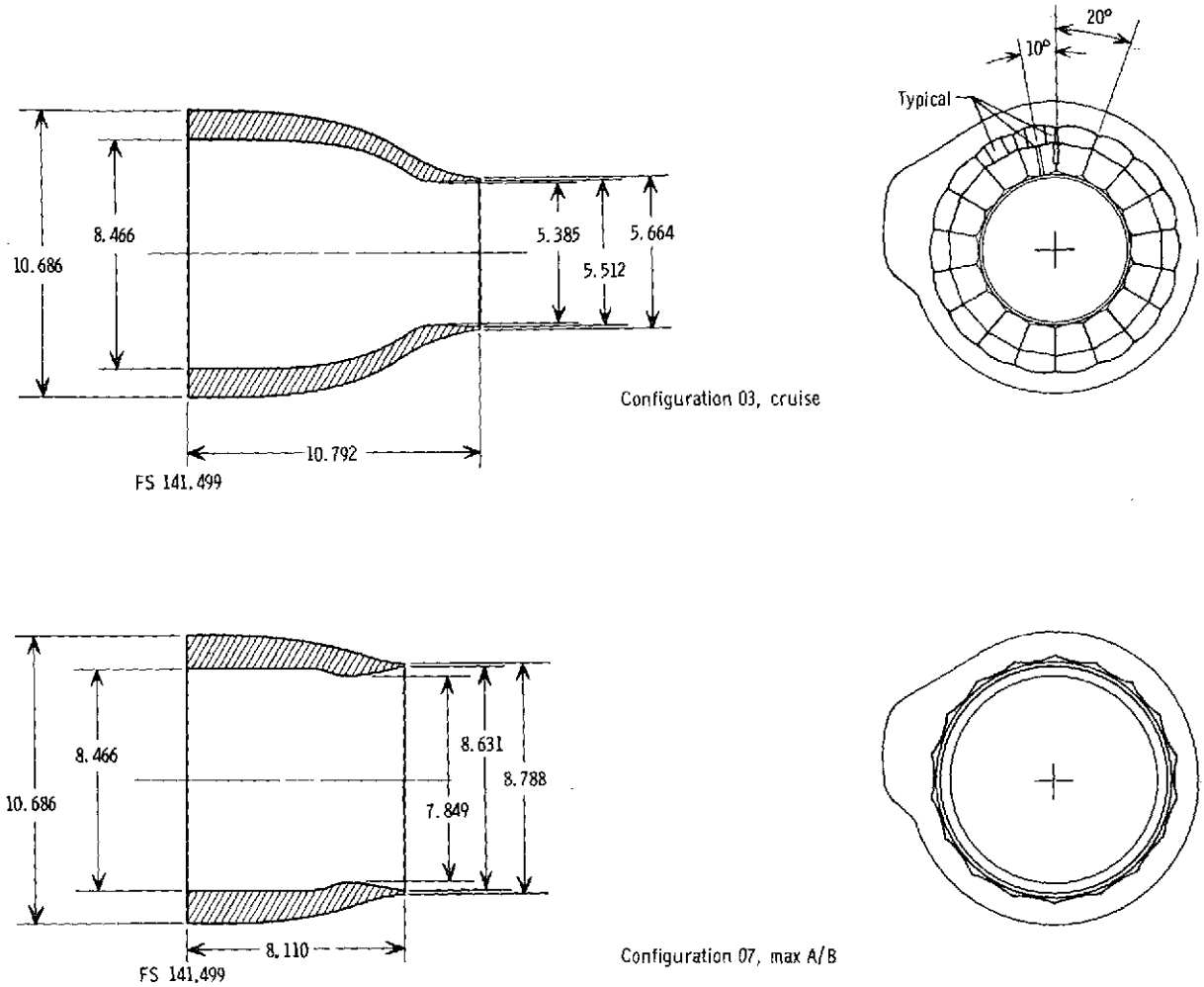

(a) Nozzle type A, cruise and maximum afterburning nozzles.

Figure 4.- Sketches of nozzle configurations. All dimensions are in centimeters.

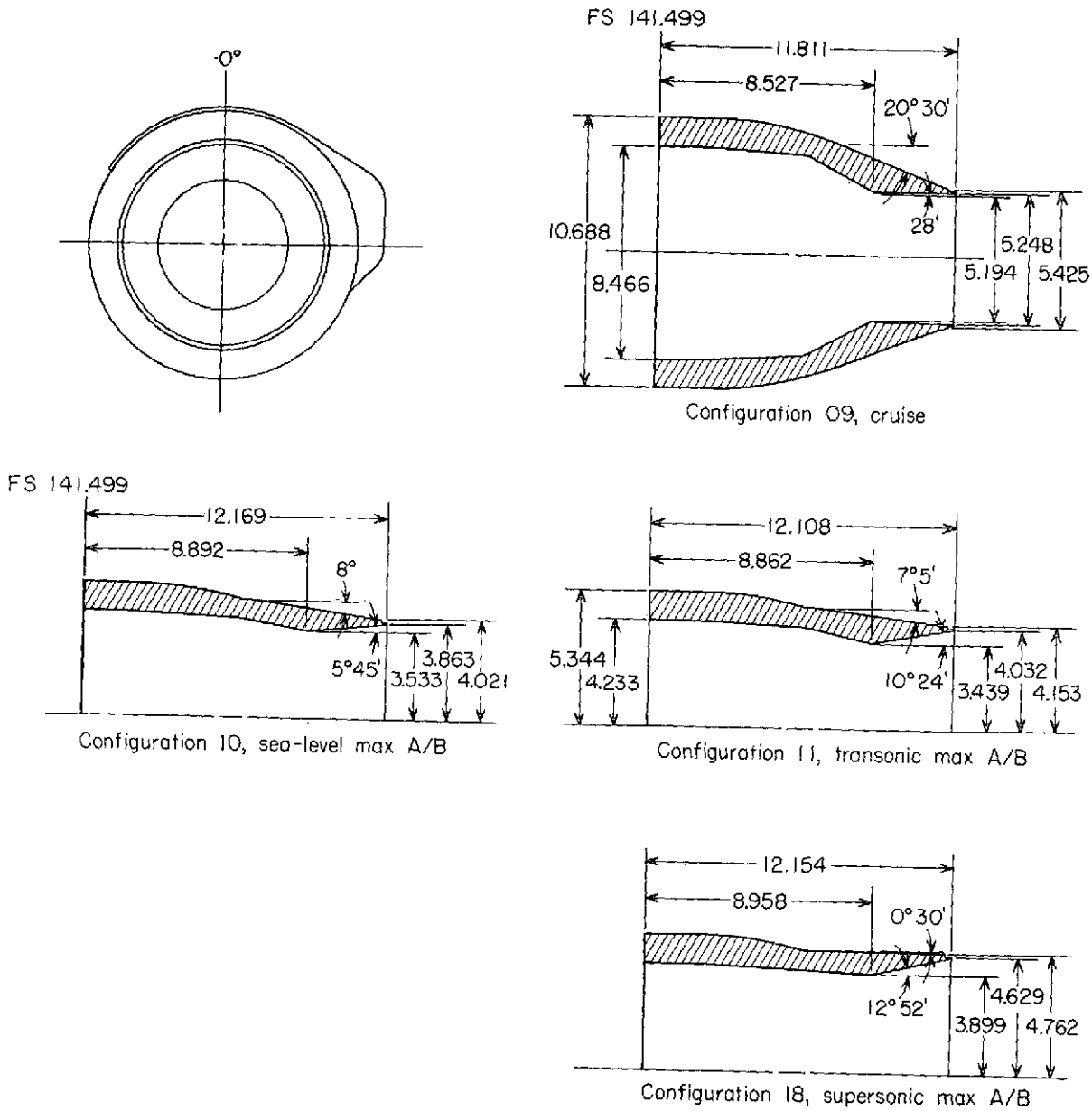

(b) Nozzle type B.

Figure 4.- Concluded.

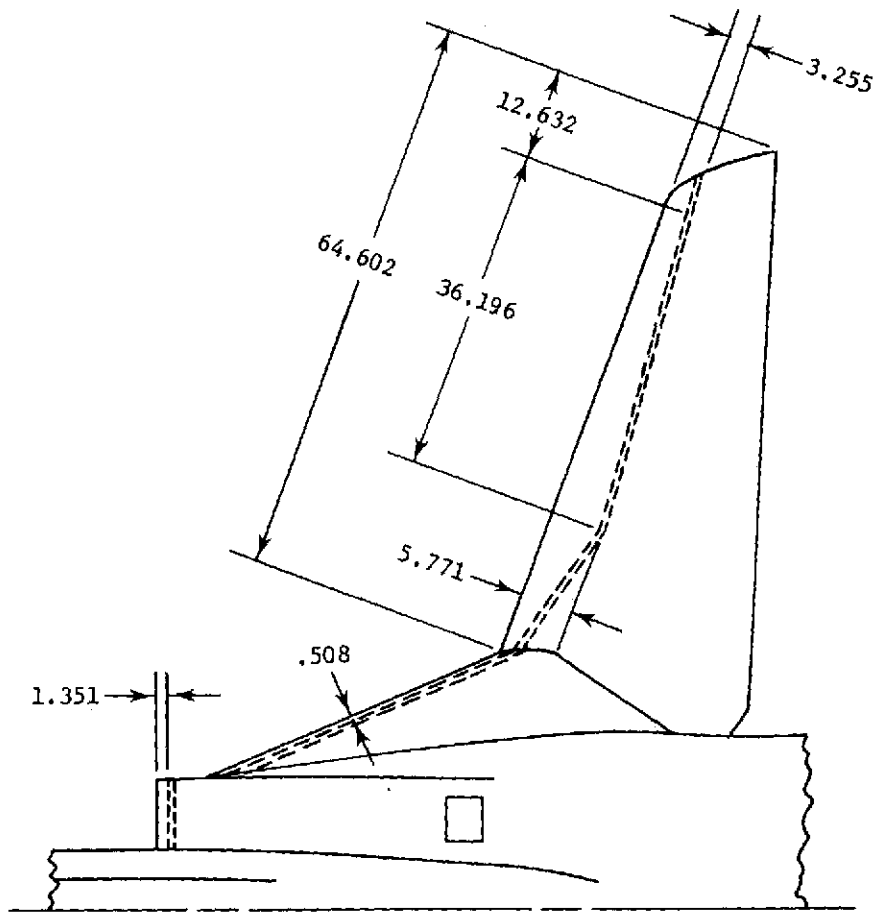

Figure 5.- Sketch showing transition location on upper wing surface for configurations with $\Lambda = 22^{o}$. All dimensions are in centimeters.

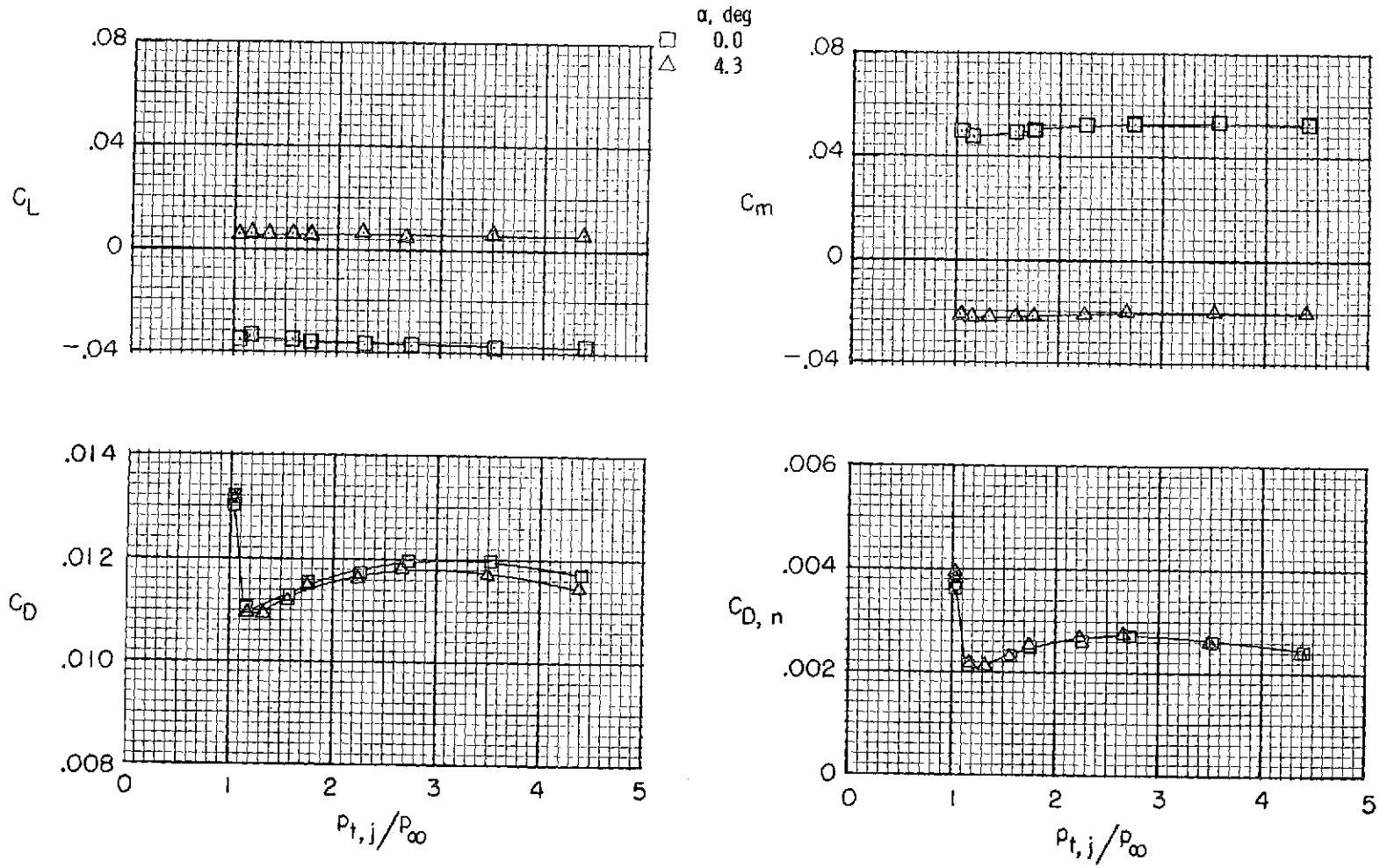

(a) M = 0.60.

Figure 6.- Effect of jet total-pressure ratio on afterbody-nozzle aerodynamic forces and moments for type A cruise nozzles and interfairing 1.

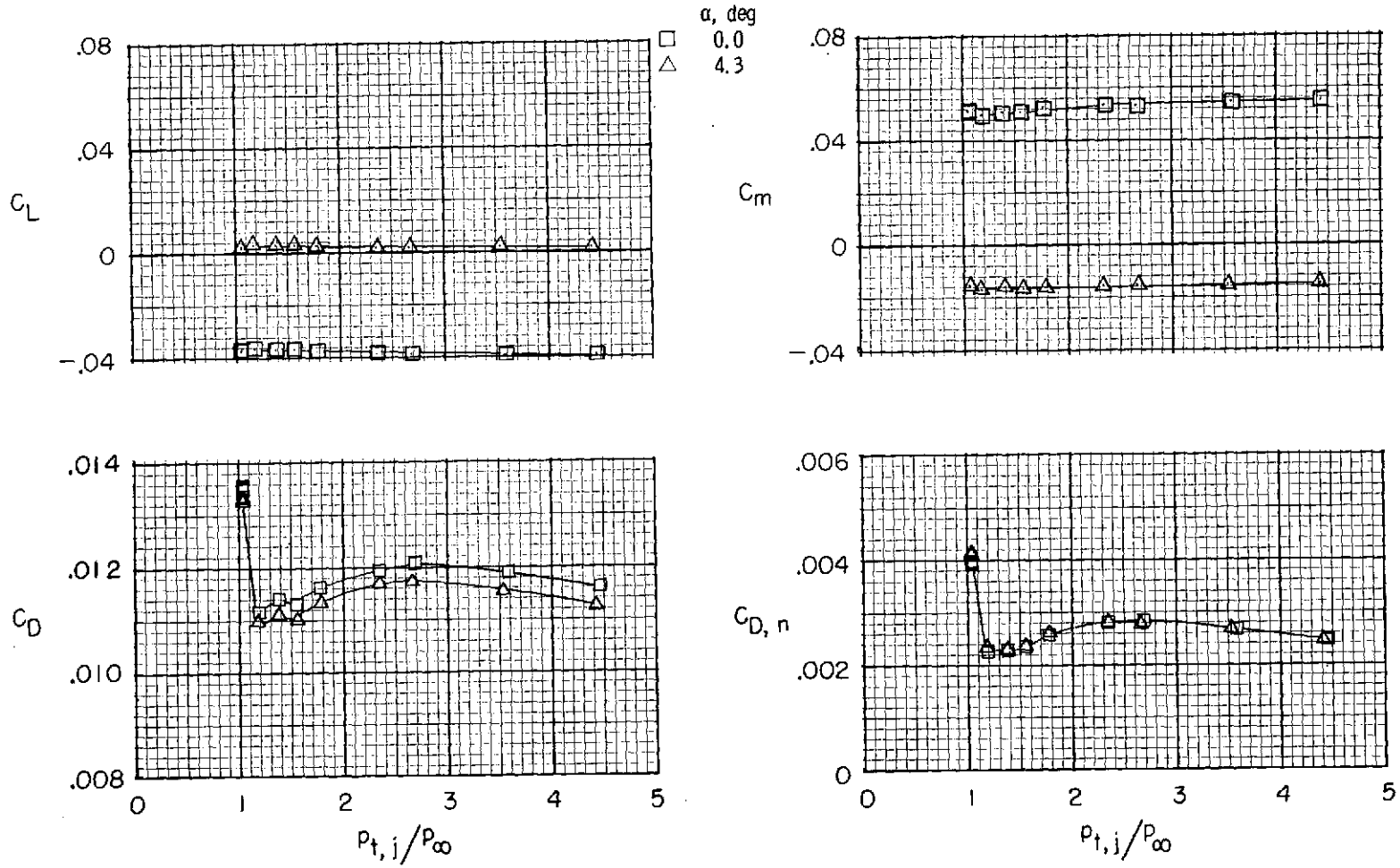

(b) M = 0.70.

Figure 6.- Continued.

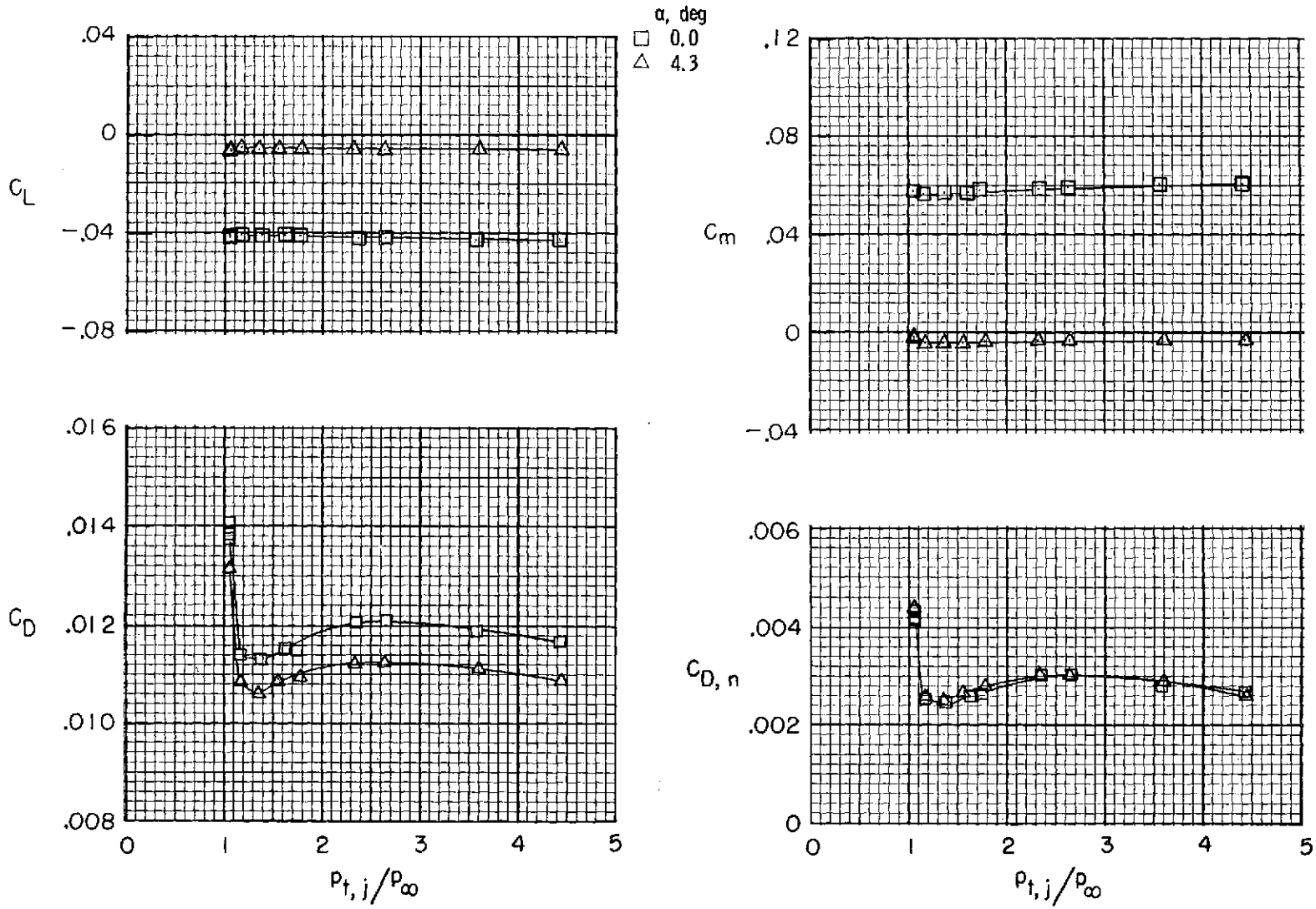

(c) M = 0.80.

Figure 6.- Continued.

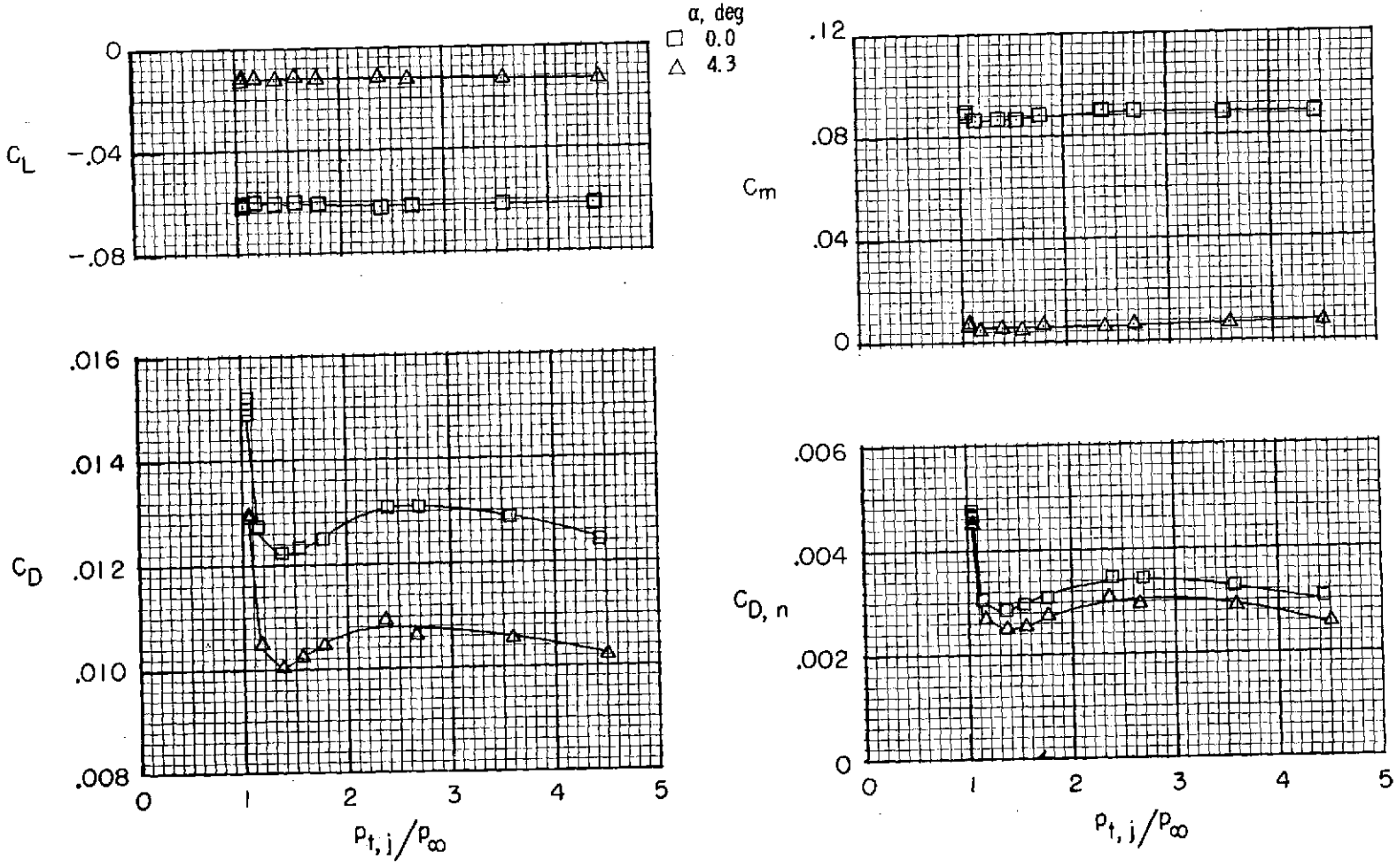

(d) M = 0.90.

Figure 6.- Concluded.

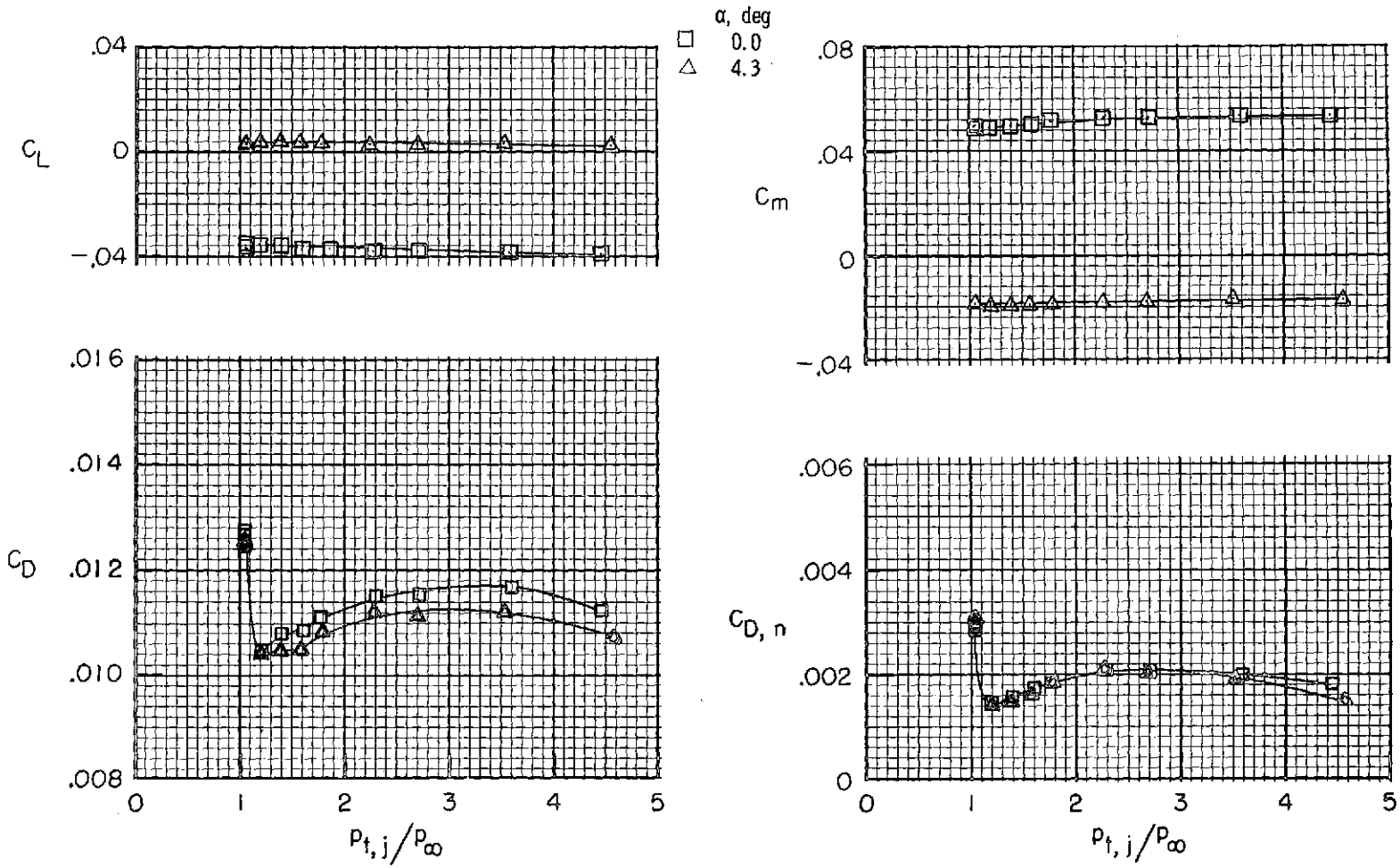

(a) M = 0.60.

Figure 7.- Effect of jet total-pressure ratio on afterbody-nozzle aerodynamic forces and moments for type A cruise nozzles and interfairing 2.

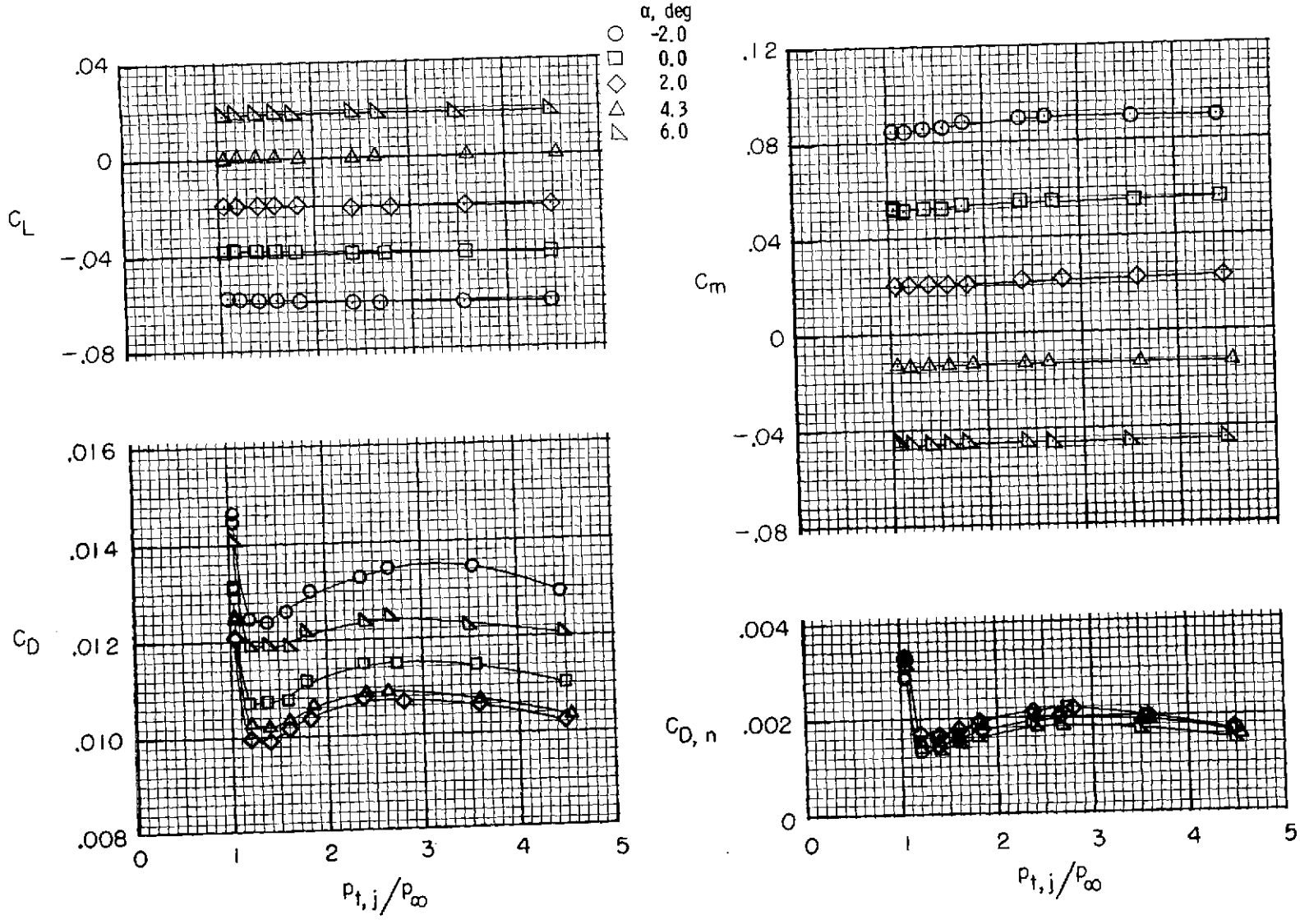

(b) M = 0.70.

Figure 7.- Continued.

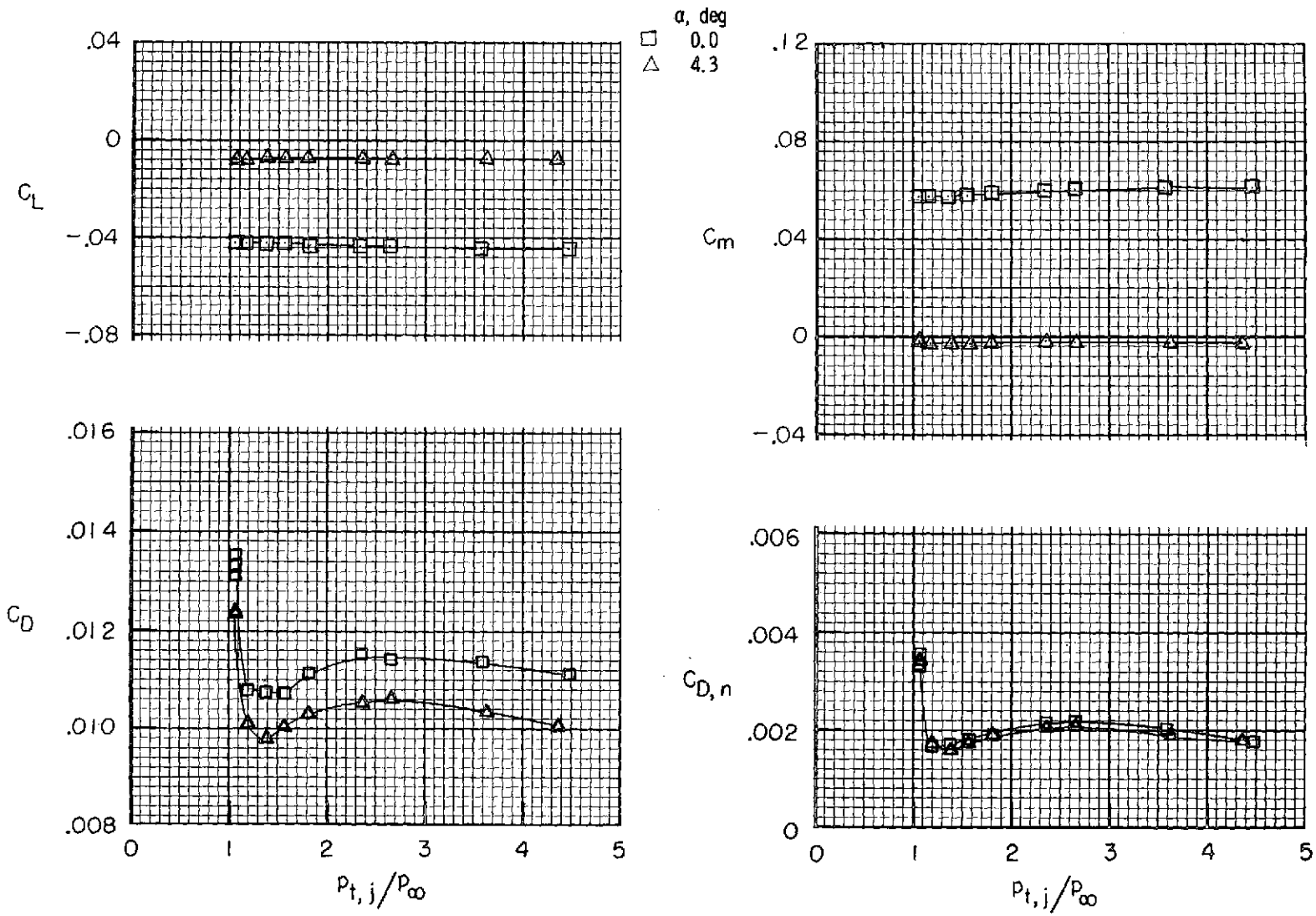

(c) M = 0.80.

Figure 7.- Continued.

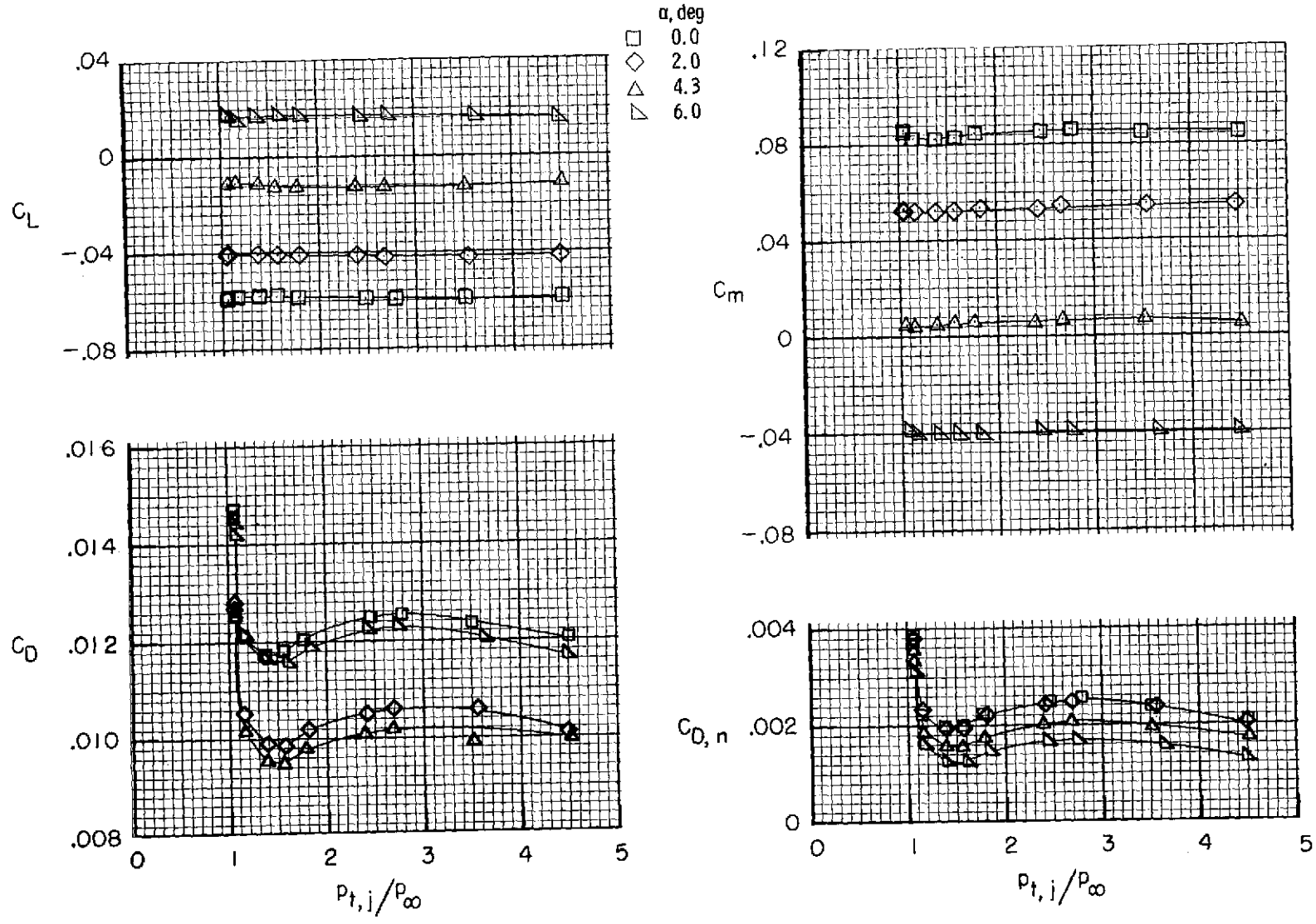

(d) M = 0.90.

Figure 7.- Concluded.

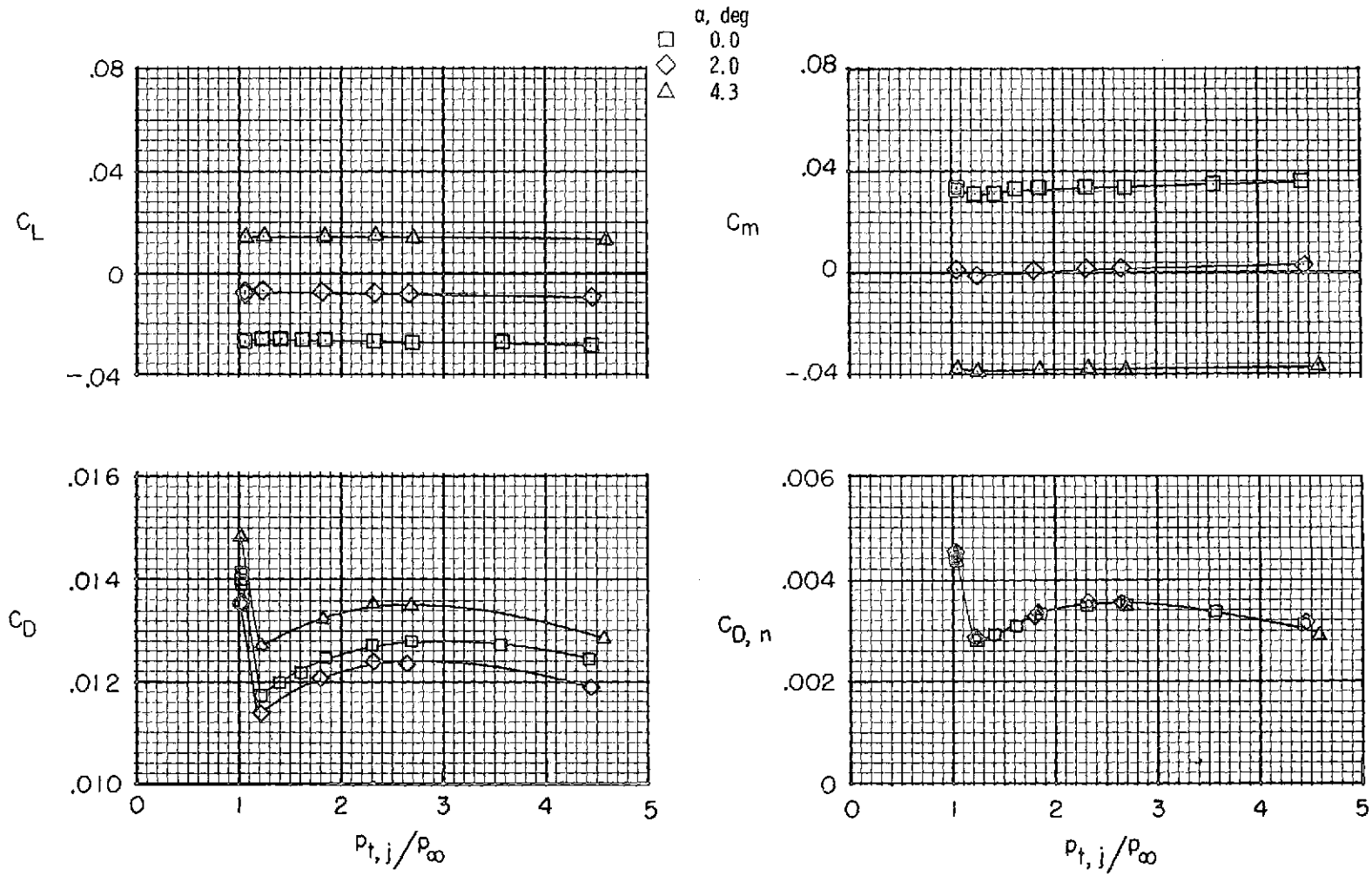

(a) M = 0.60.

Figure 8.- Effect of jet total-pressure ratio on afterbody-nozzle aerodynamic forces and moment for type A cruise nozzles and interfairing 3.

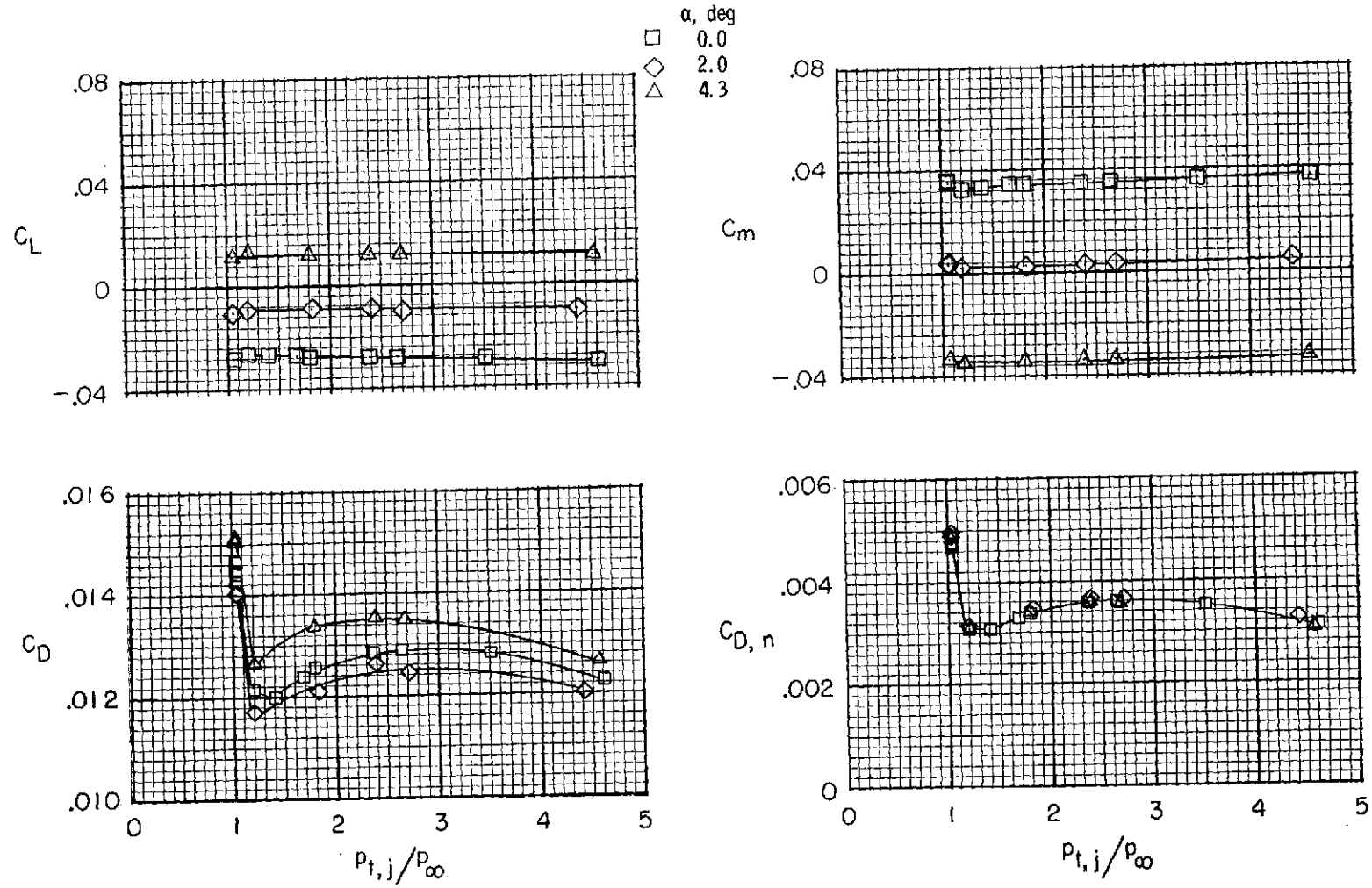

(b) M = 0.70.

Figure 8.- Continued.

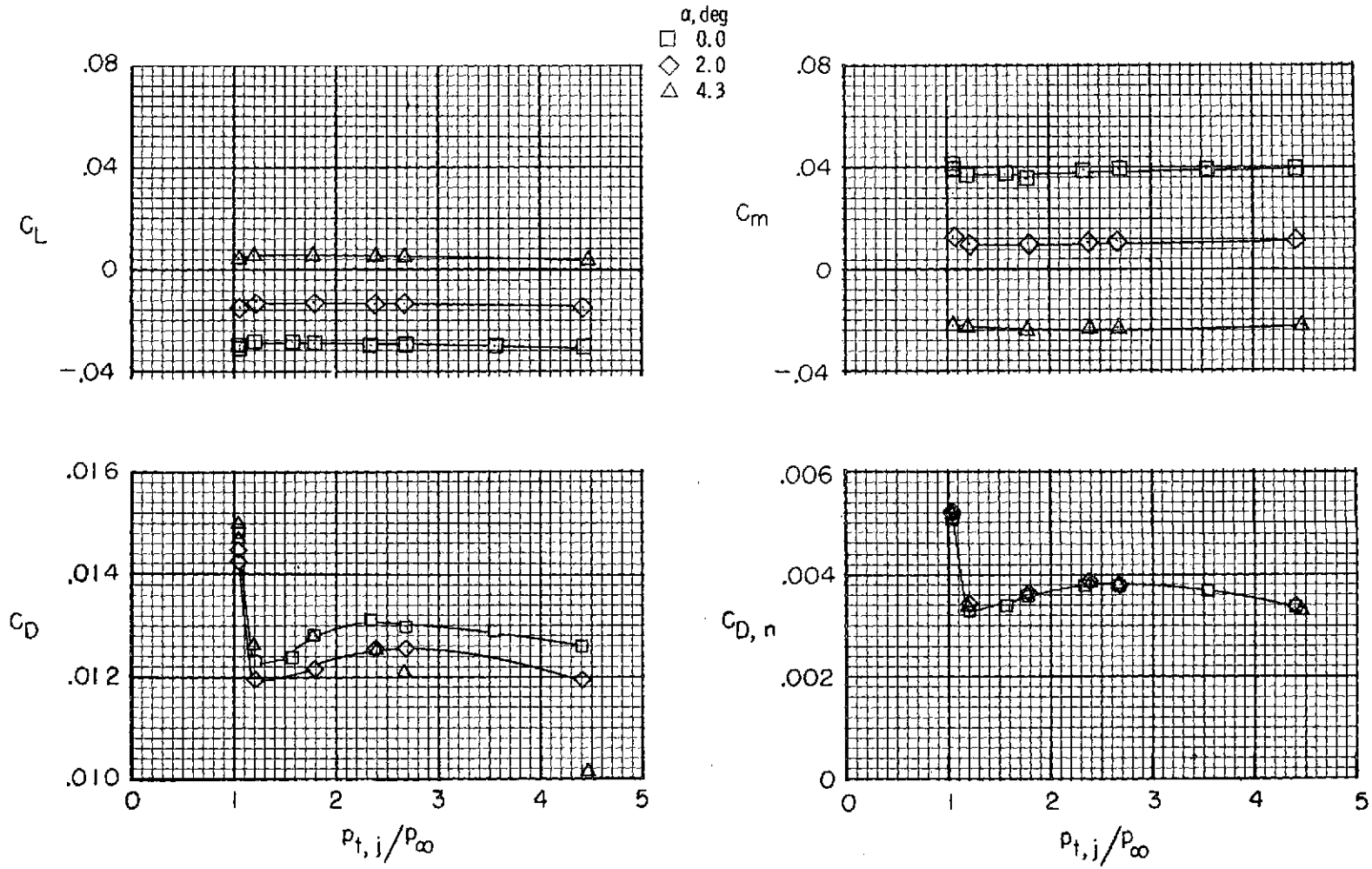

(c) M = 0.80.

Figure 8.- Continued.

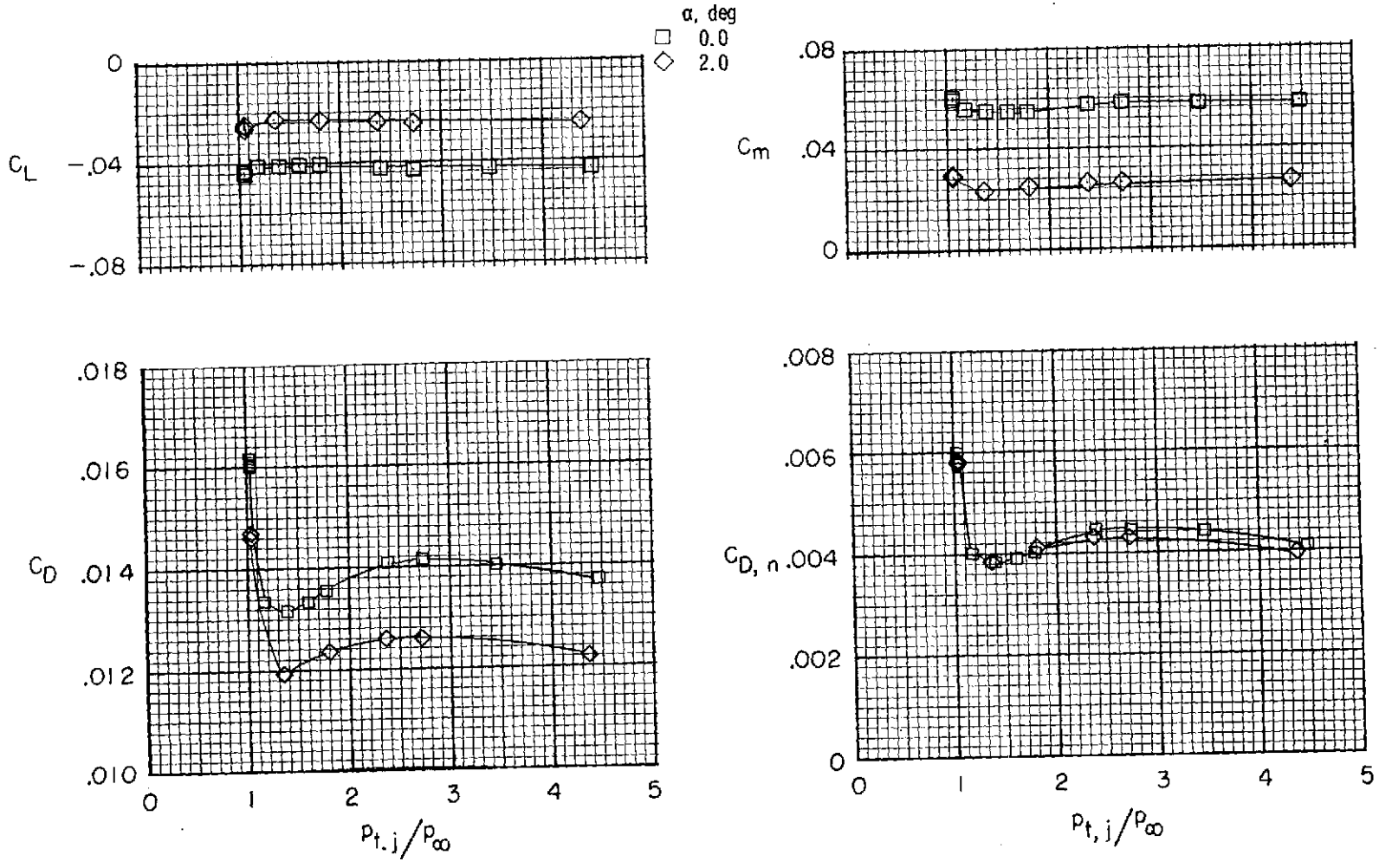

(d) M = 0.90.

Figure 8.- Concluded.

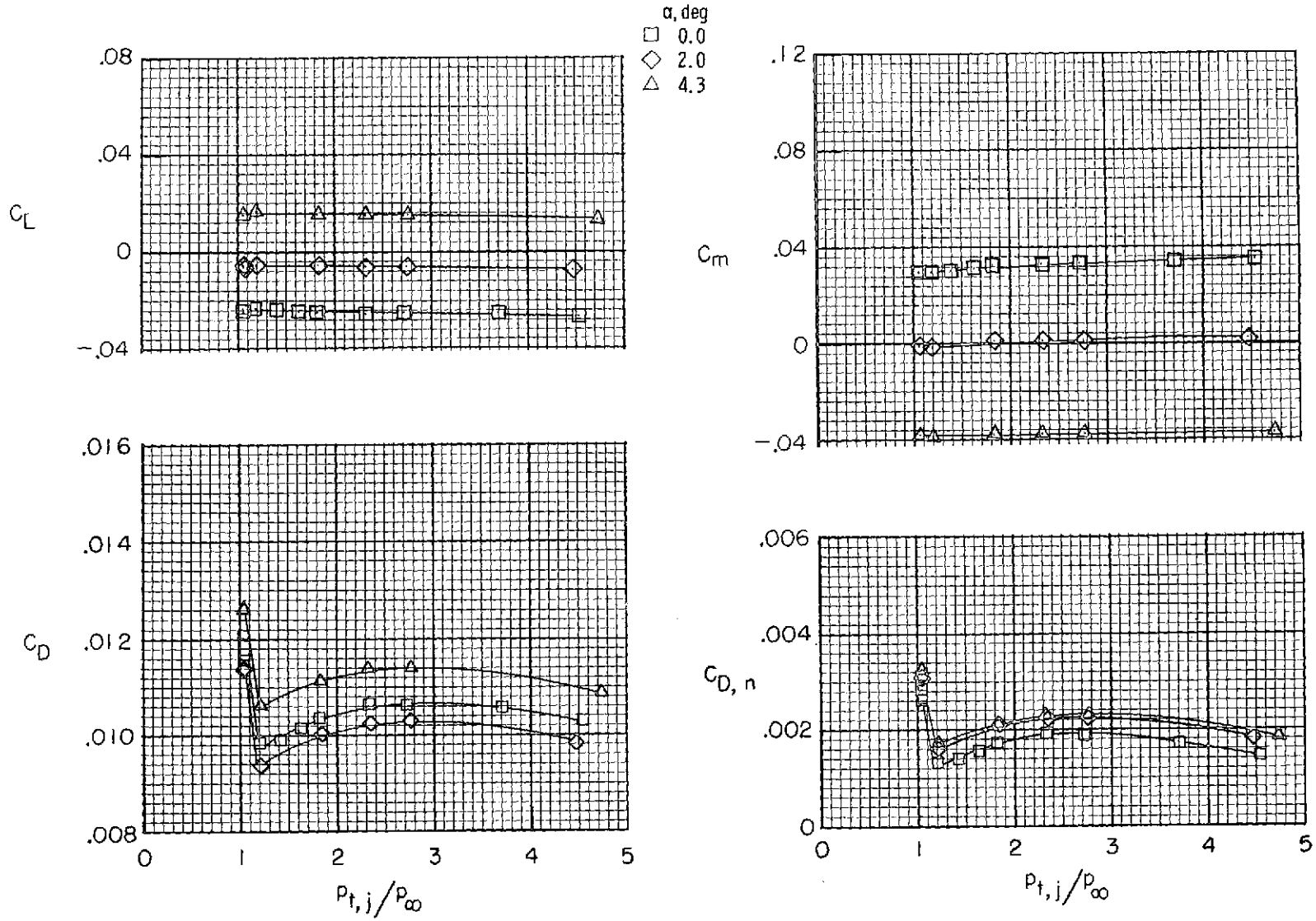

(a) M = 0.60.

Figure 9.- Effect of jet total-pressure ratio on afterbody-nozzle aerodynamic forces and moments for type A cruise nozzles and interfairing 6. Dashed line indicates possible fouling.

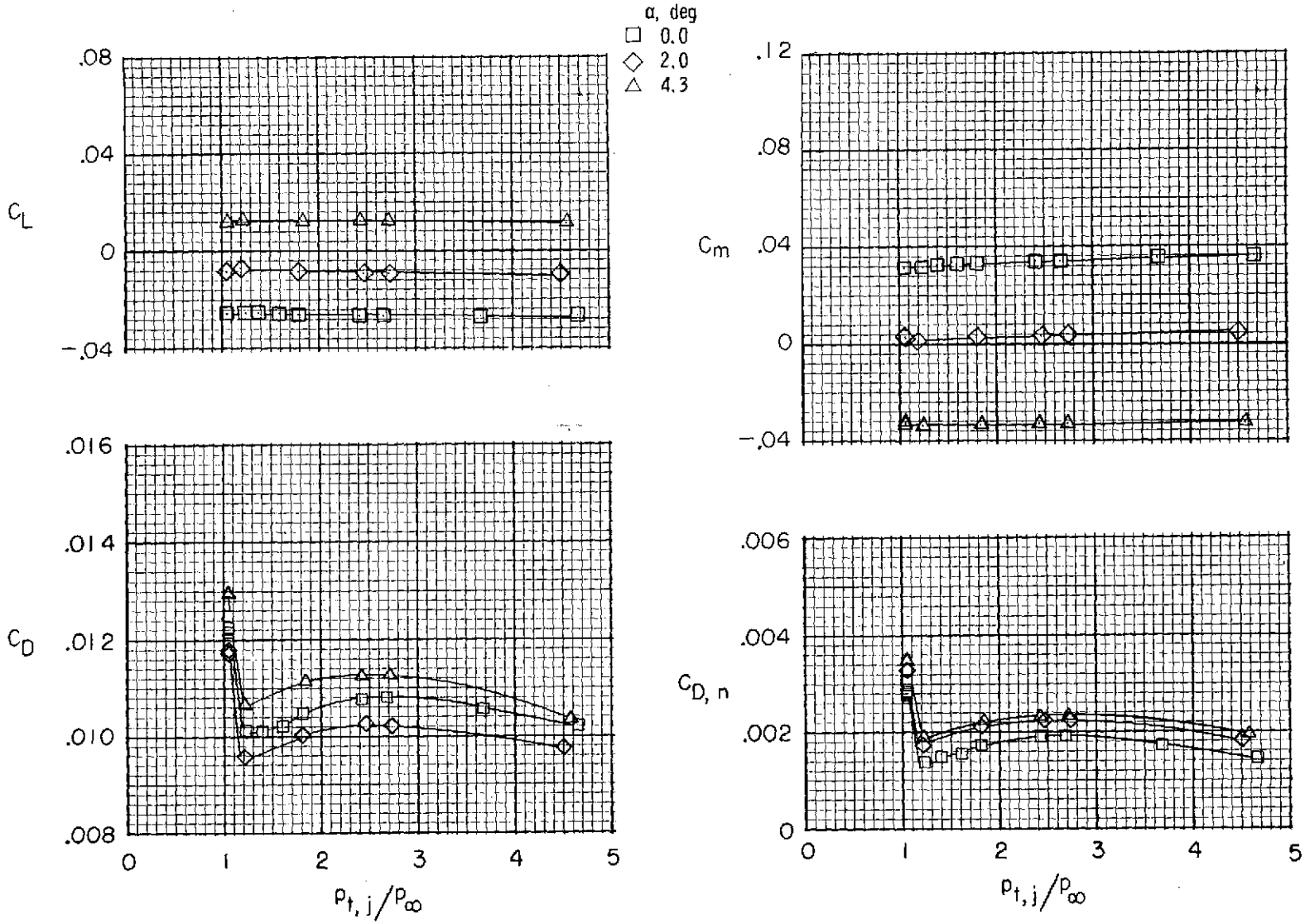

(b) M = 0.70.

Figure 9.- Continued.

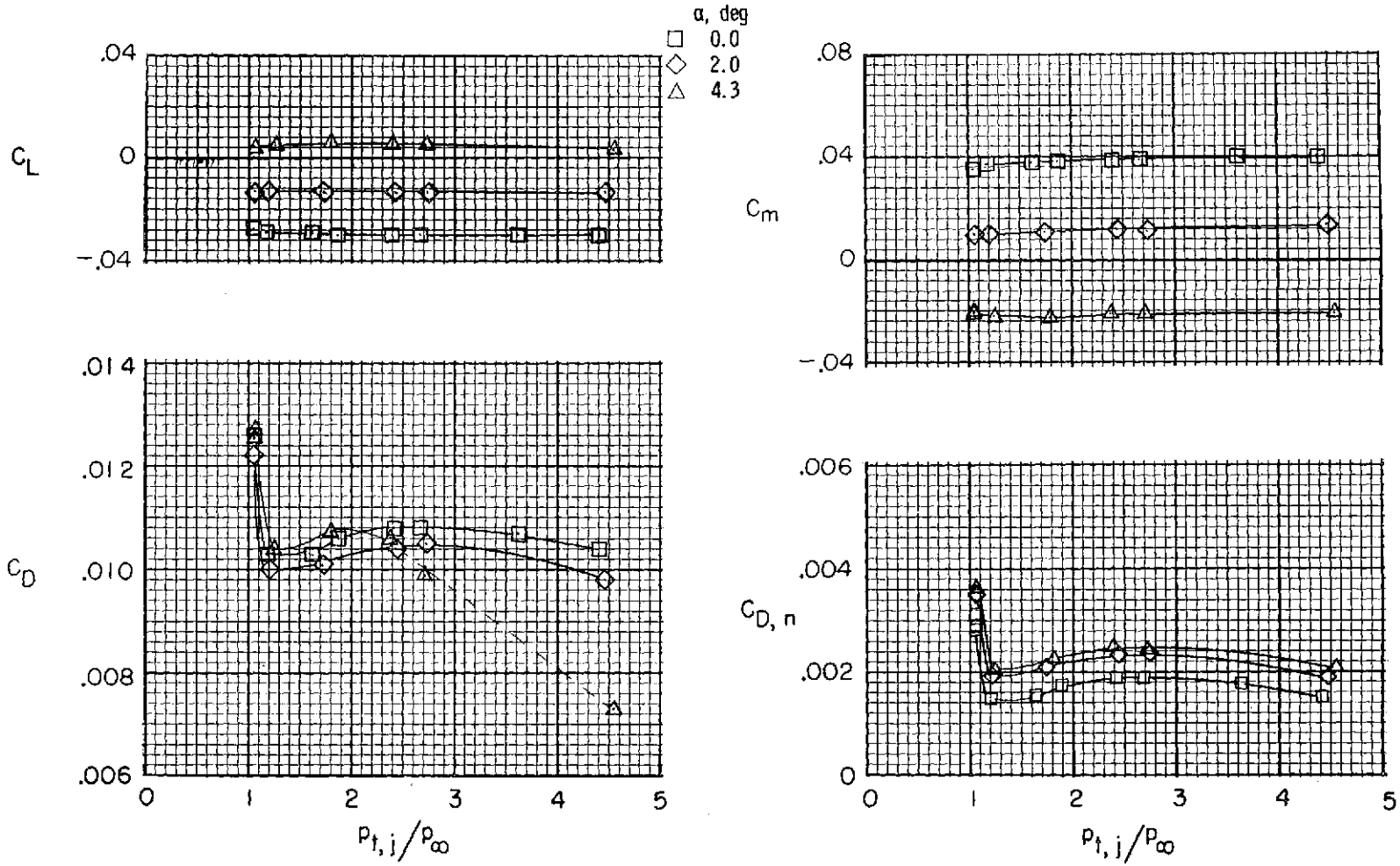

(c) M = 0.80.

Figure 9.- Continued.

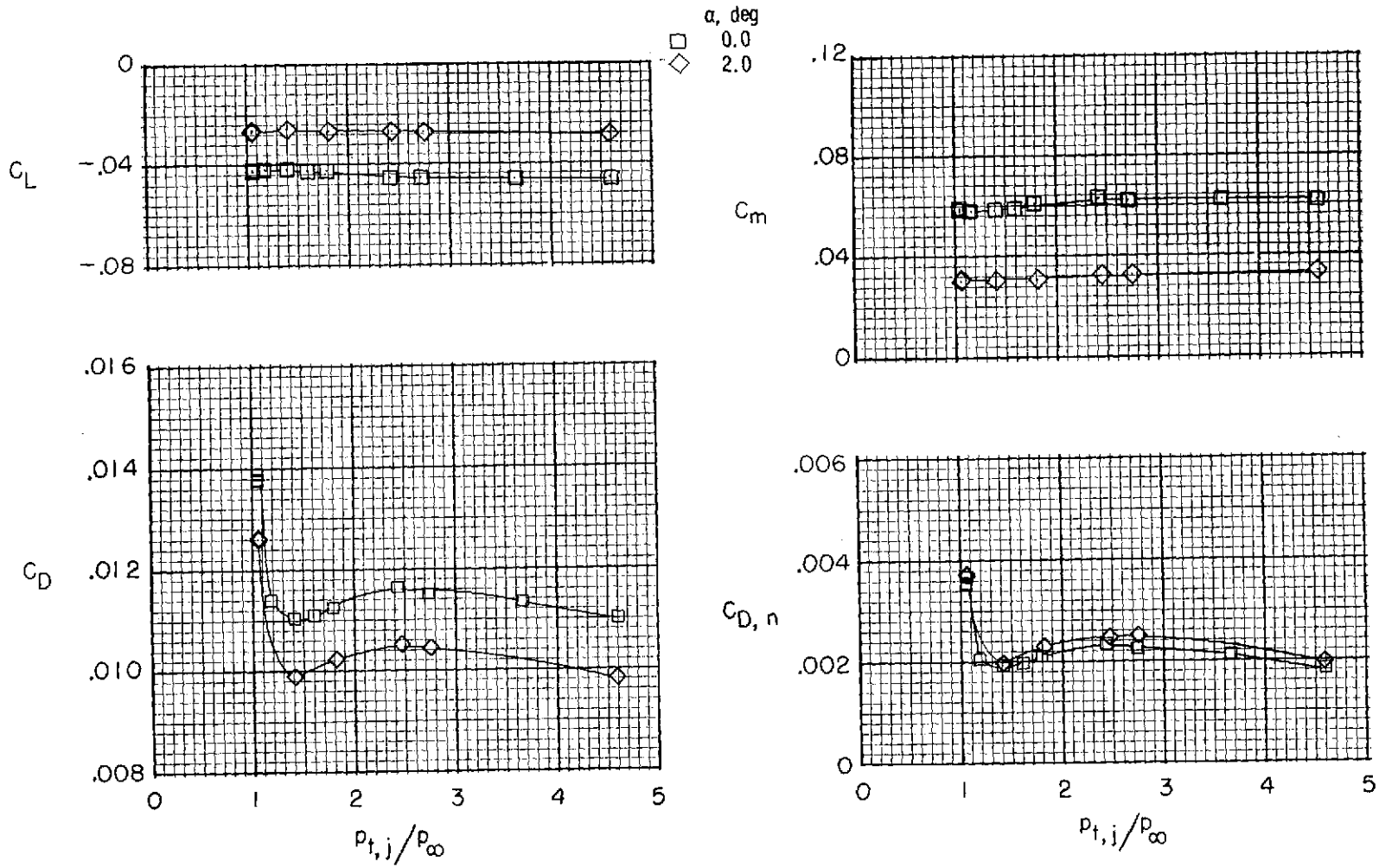

(d) M = 0.90.

Figure 9.- Concluded.

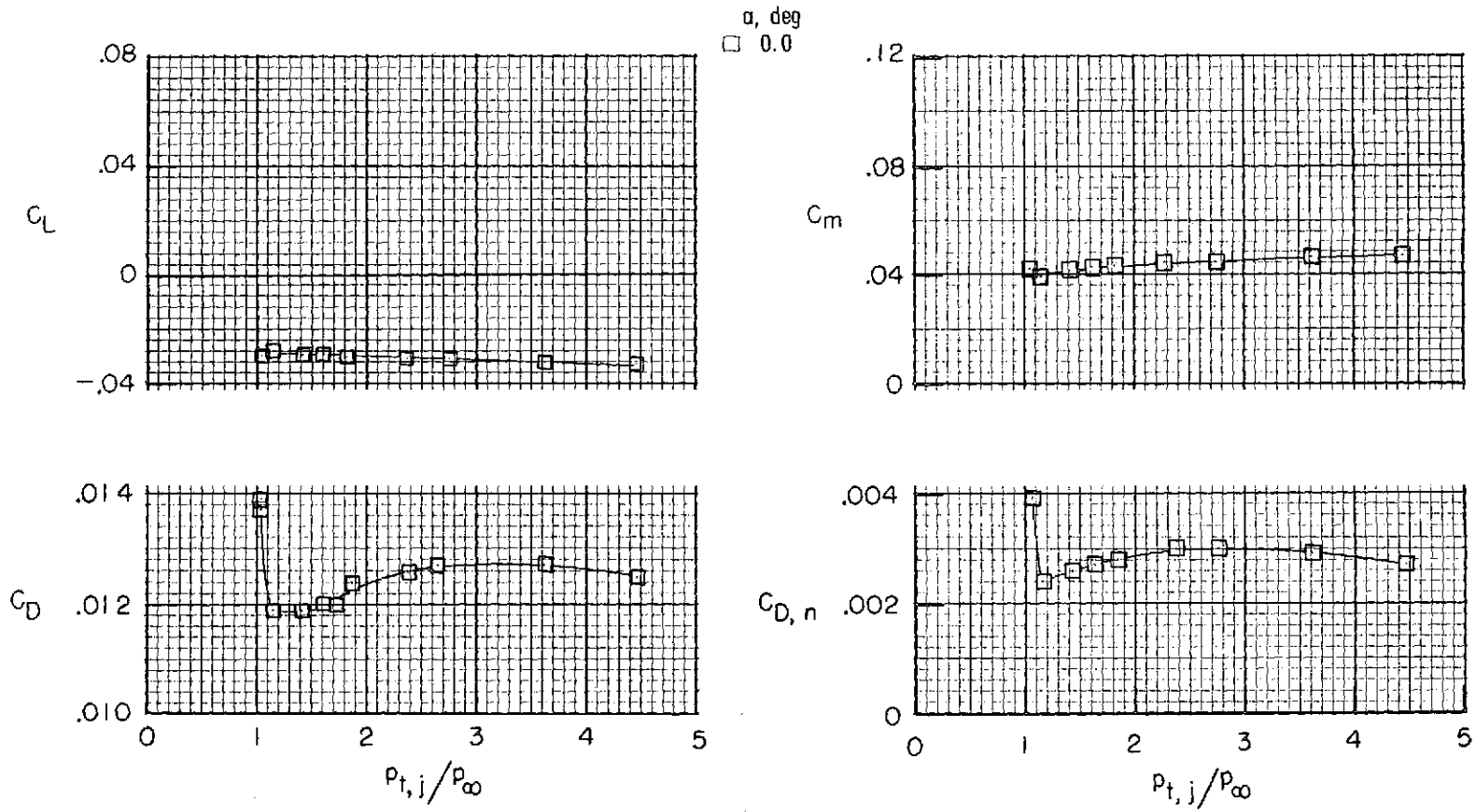

(a) M = 0.60.

Figure 10.- Effect of jet total-pressure ratio on afterbody-nozzle aerodynamic forces and moments for type A cruise nozzles, basic interfairing, and vortex generators on top of nacelles.

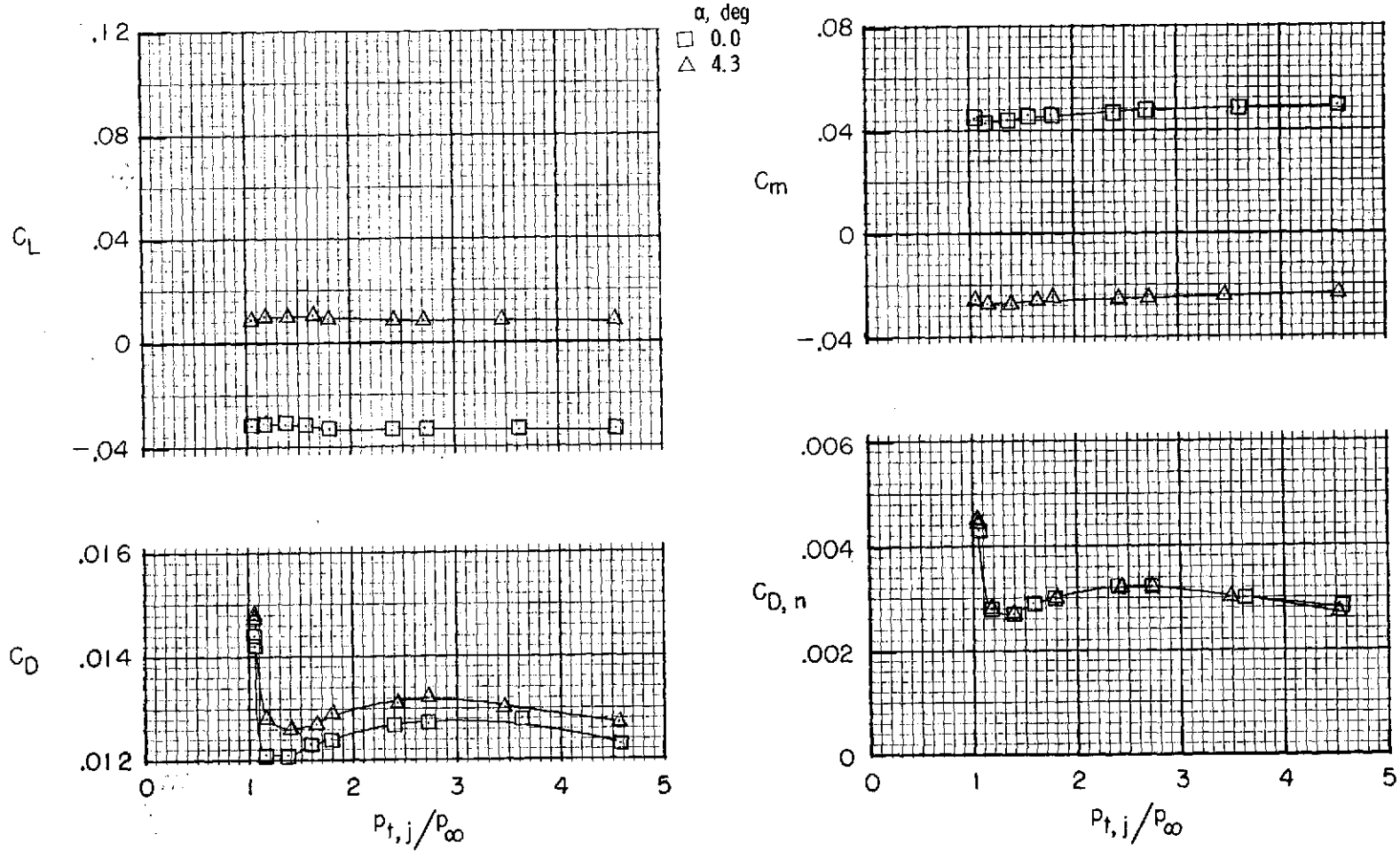

(b) M = 0.70.

Figure 10.- Continued.

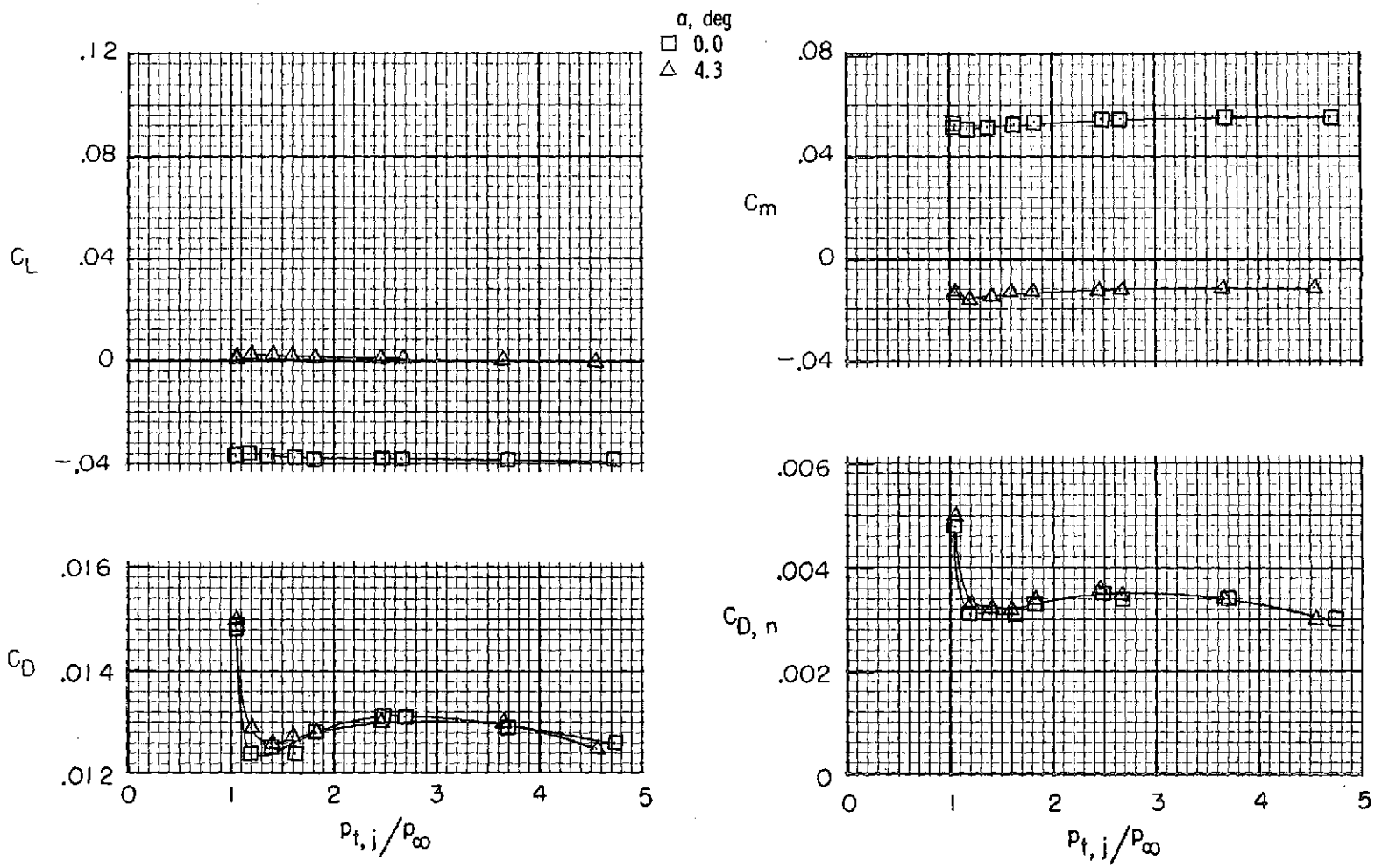

(c) M = 0.80.

Figure 10.- Concluded.

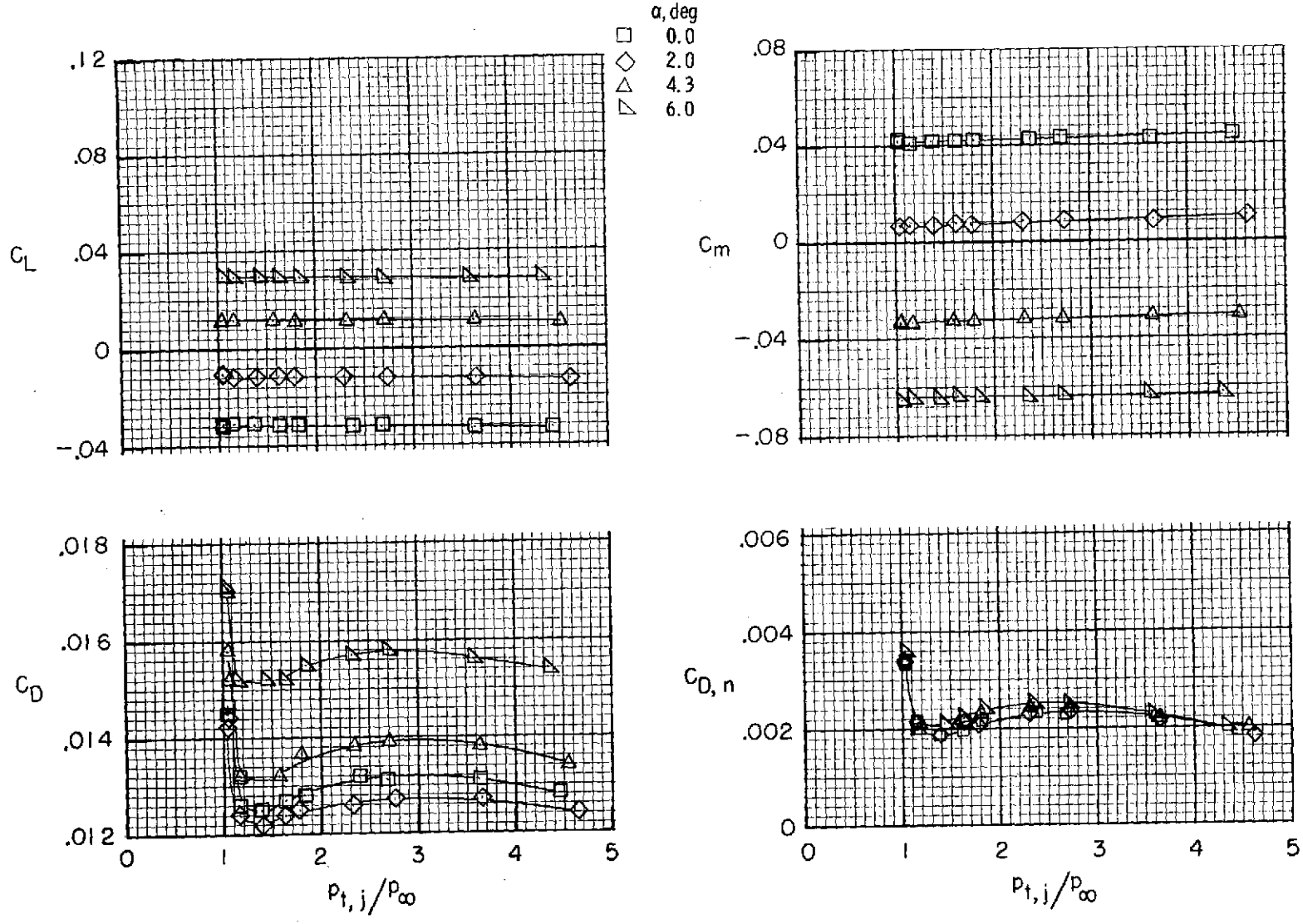

(a) M = 0.60.

Figure 11.- Effect of jet total-pressure ratio on afterbody-nozzle aerodynamic forces and moments for type A cruise nozzles, basic interfairing, and vortex generators encircling nacelles.

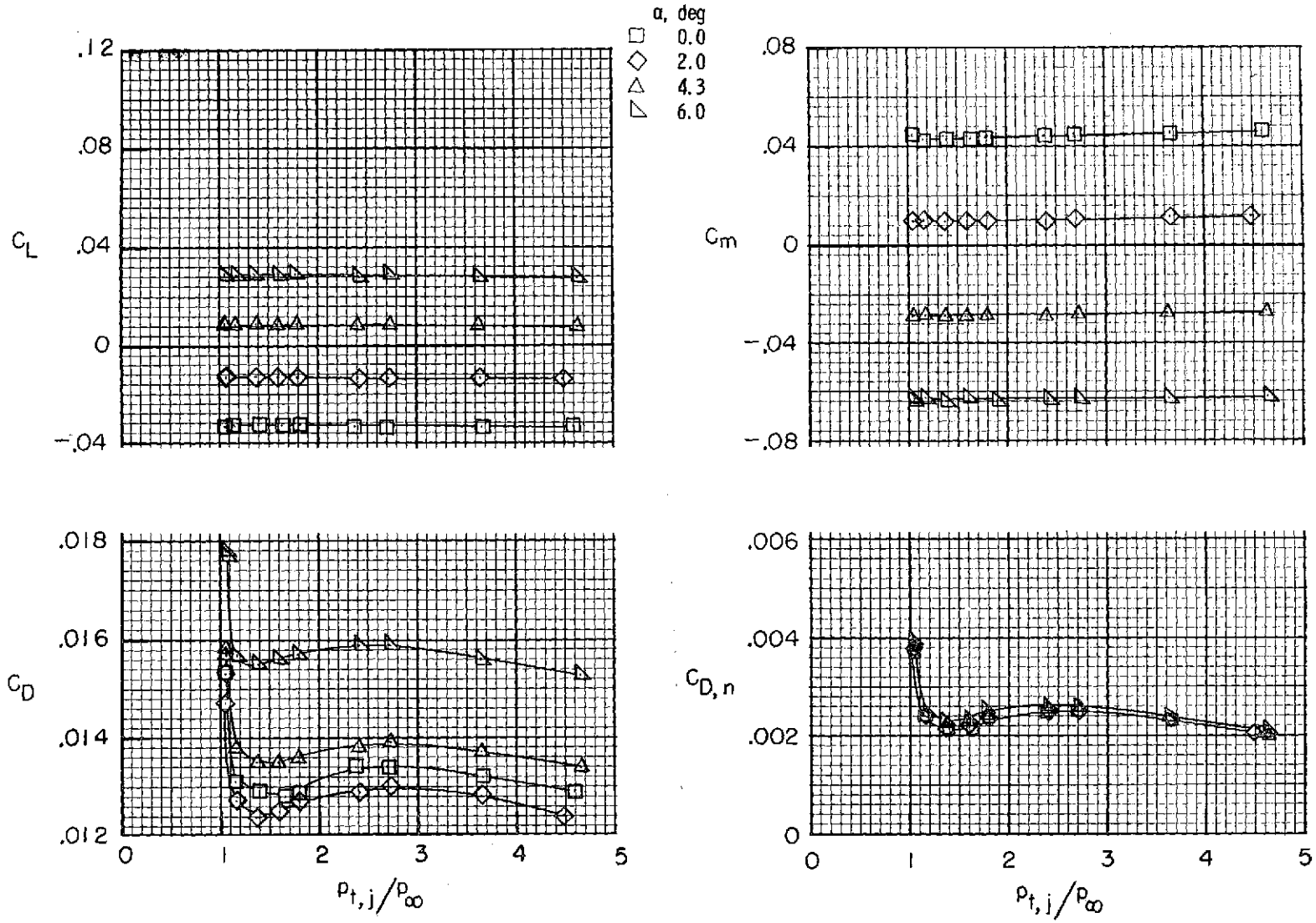

(b) M = 0.70.

Figure 11.- Continued.

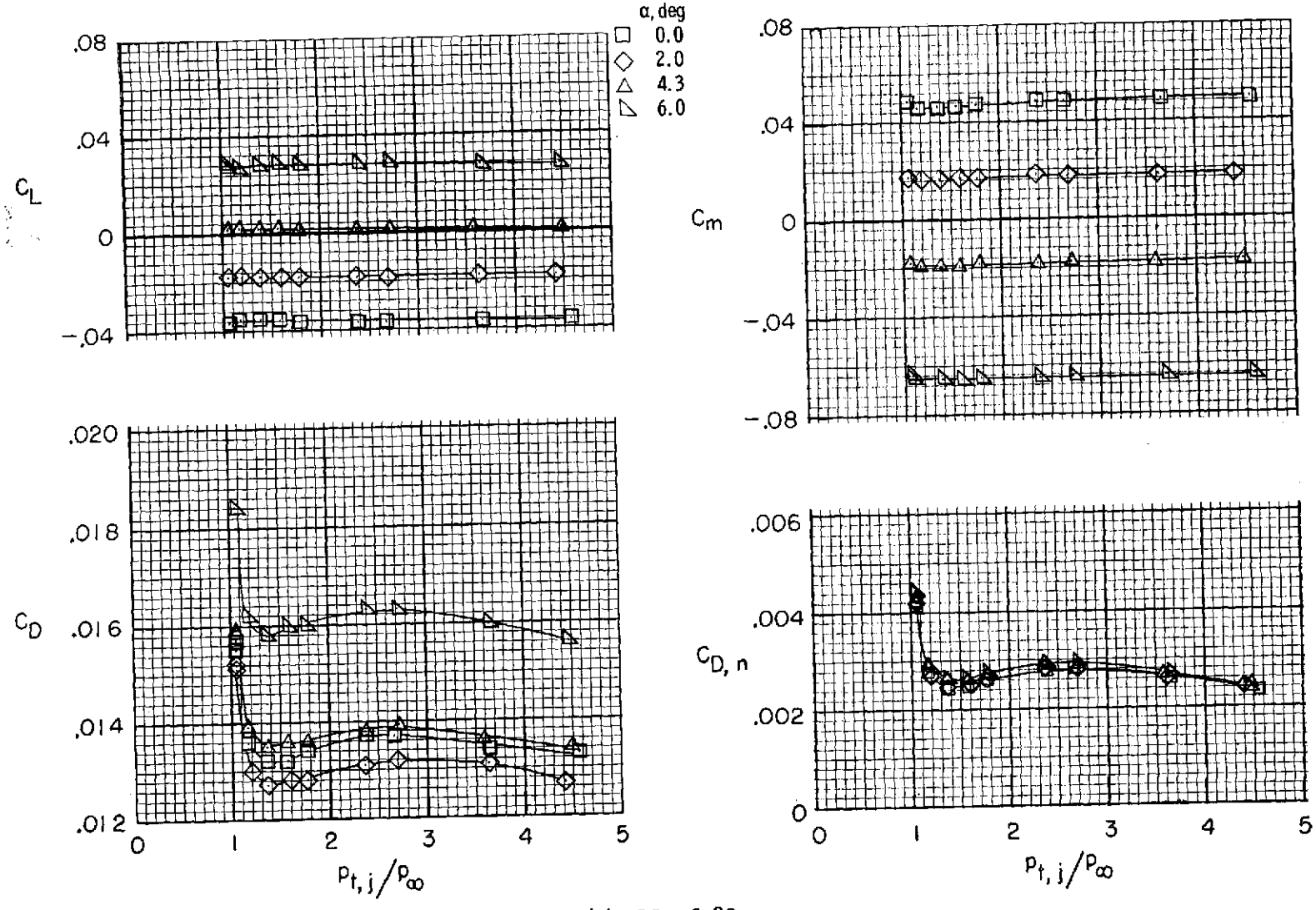

(c) M = 0.80.

Figure 11.- Continued.

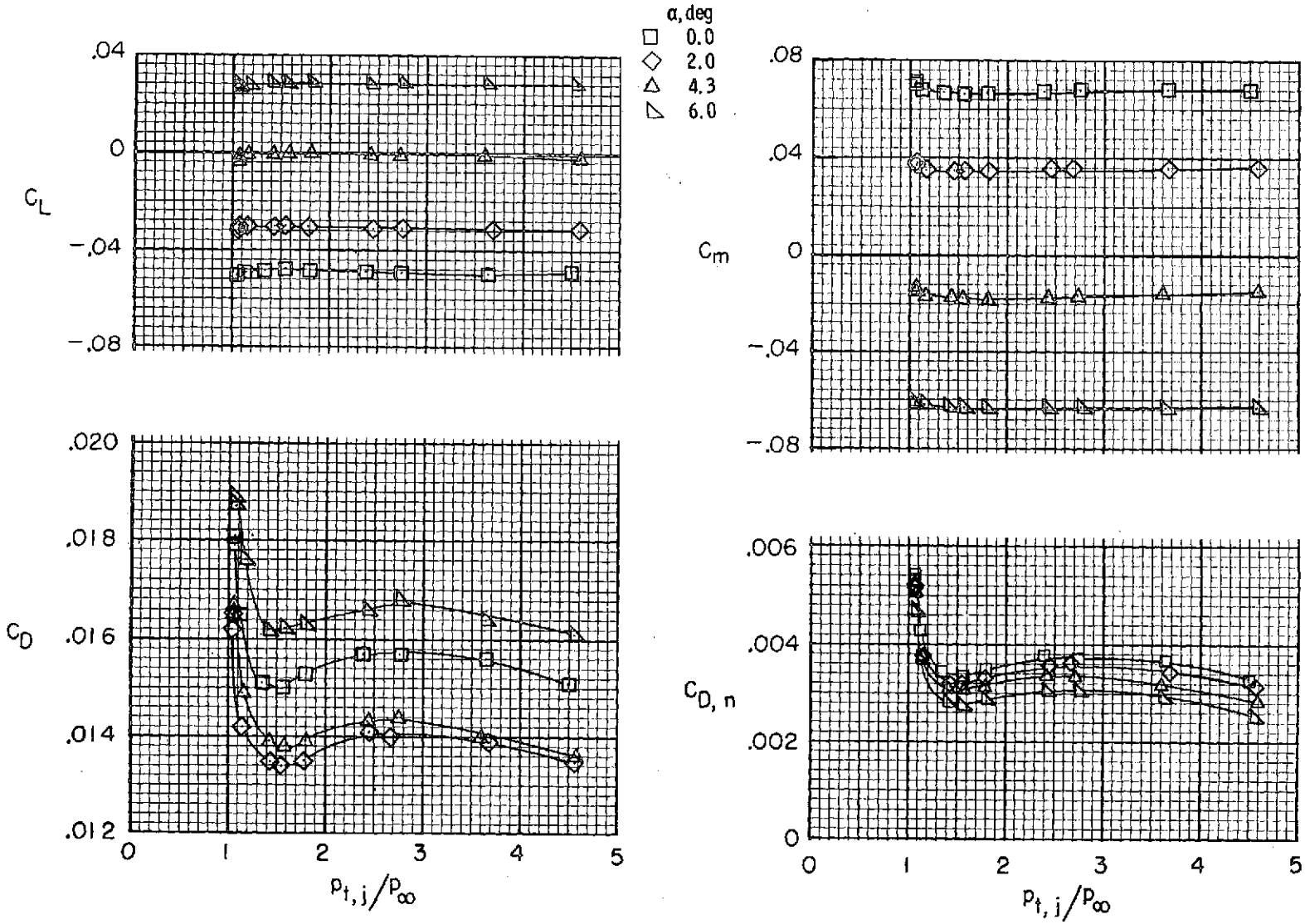

(d) M = 0.90.

Figure 11.- Concluded.

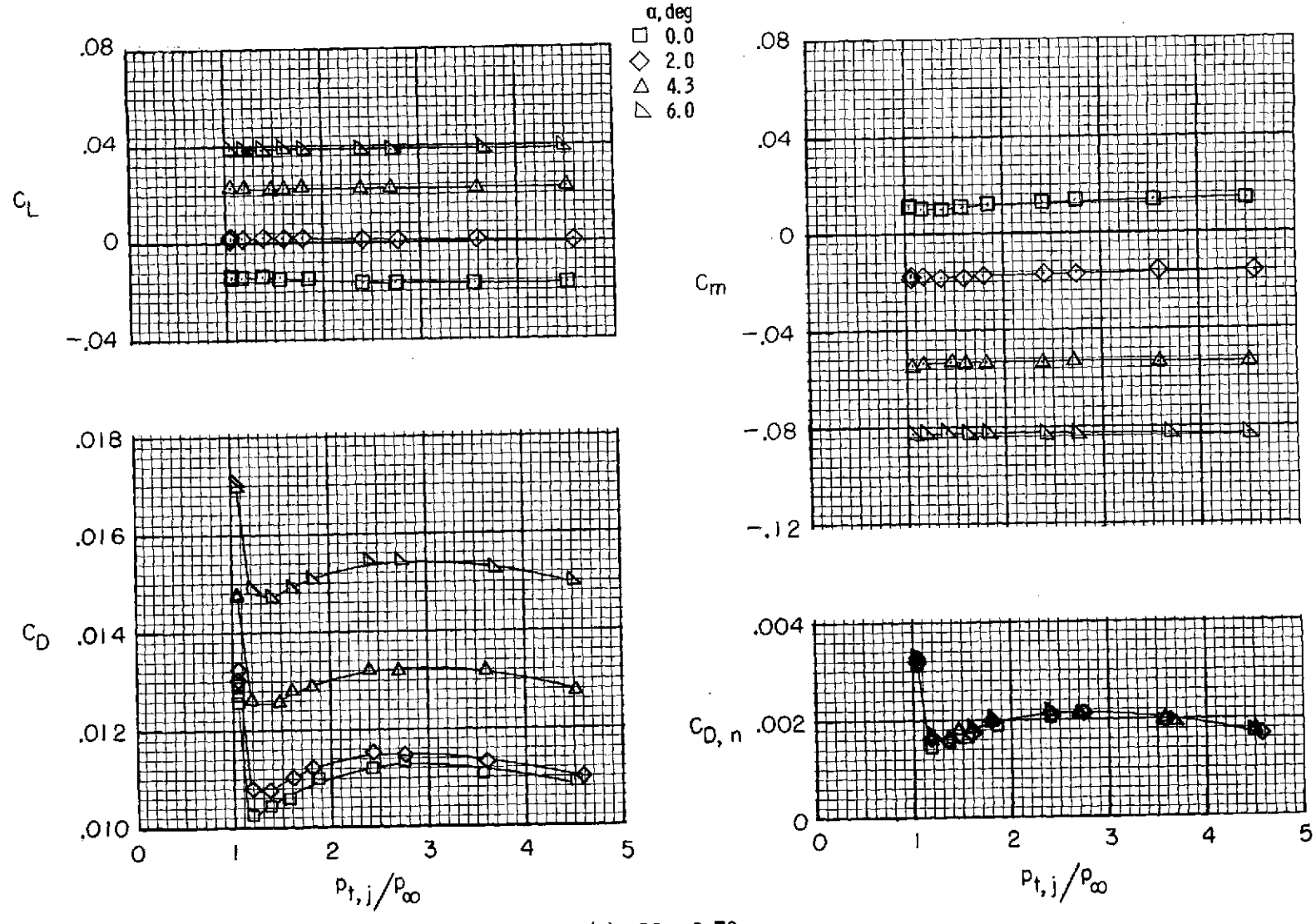

(a) M = 0.70.

Figure 12.- Effect of jet total-pressure ratio on afterbody-nozzle aerodynamic forces and moments for type A cruise nozzles, interfairing 2, and horizontal tails set at +2°.

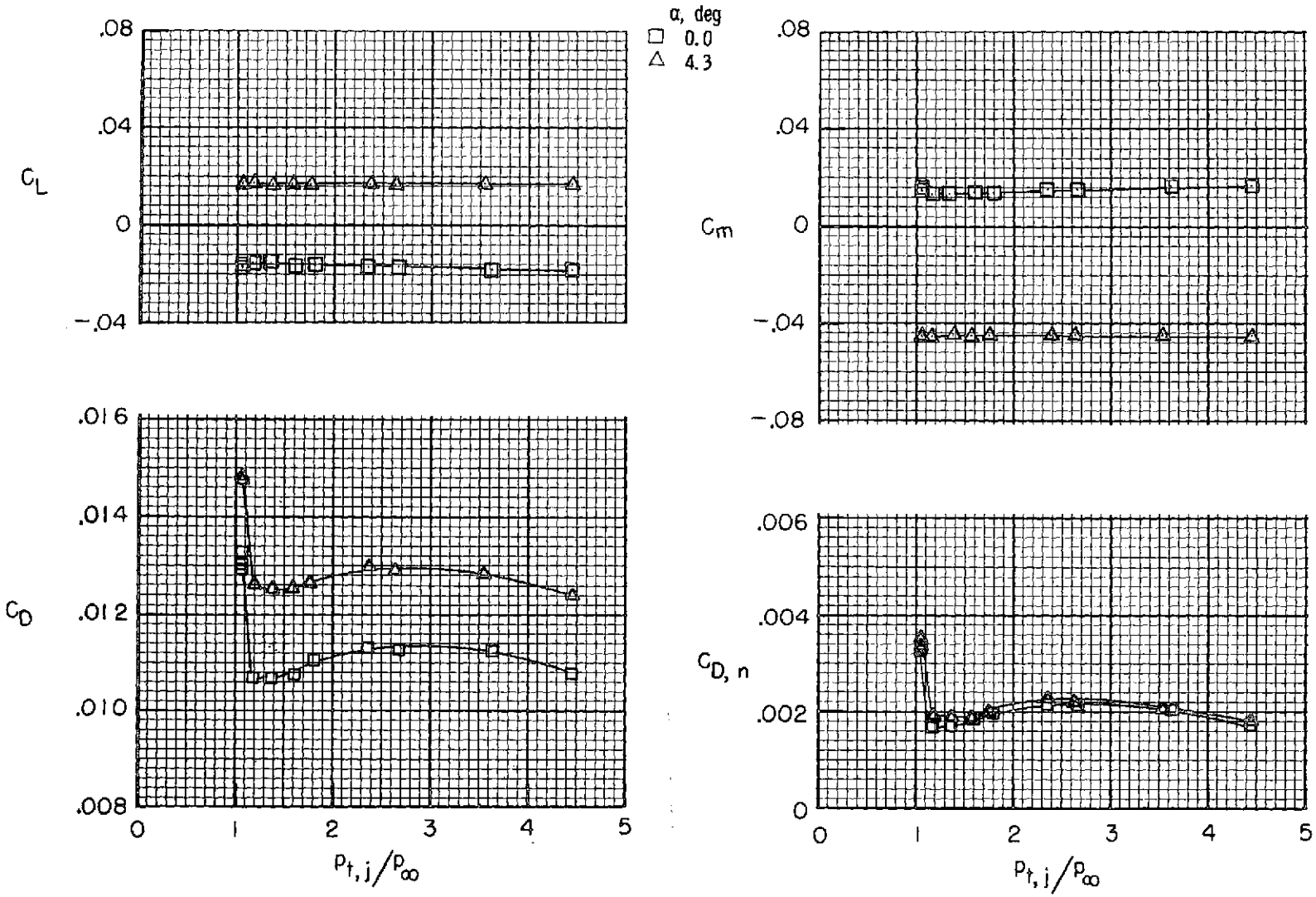

(b) M = 0.80.

Figure 12.- Concluded.

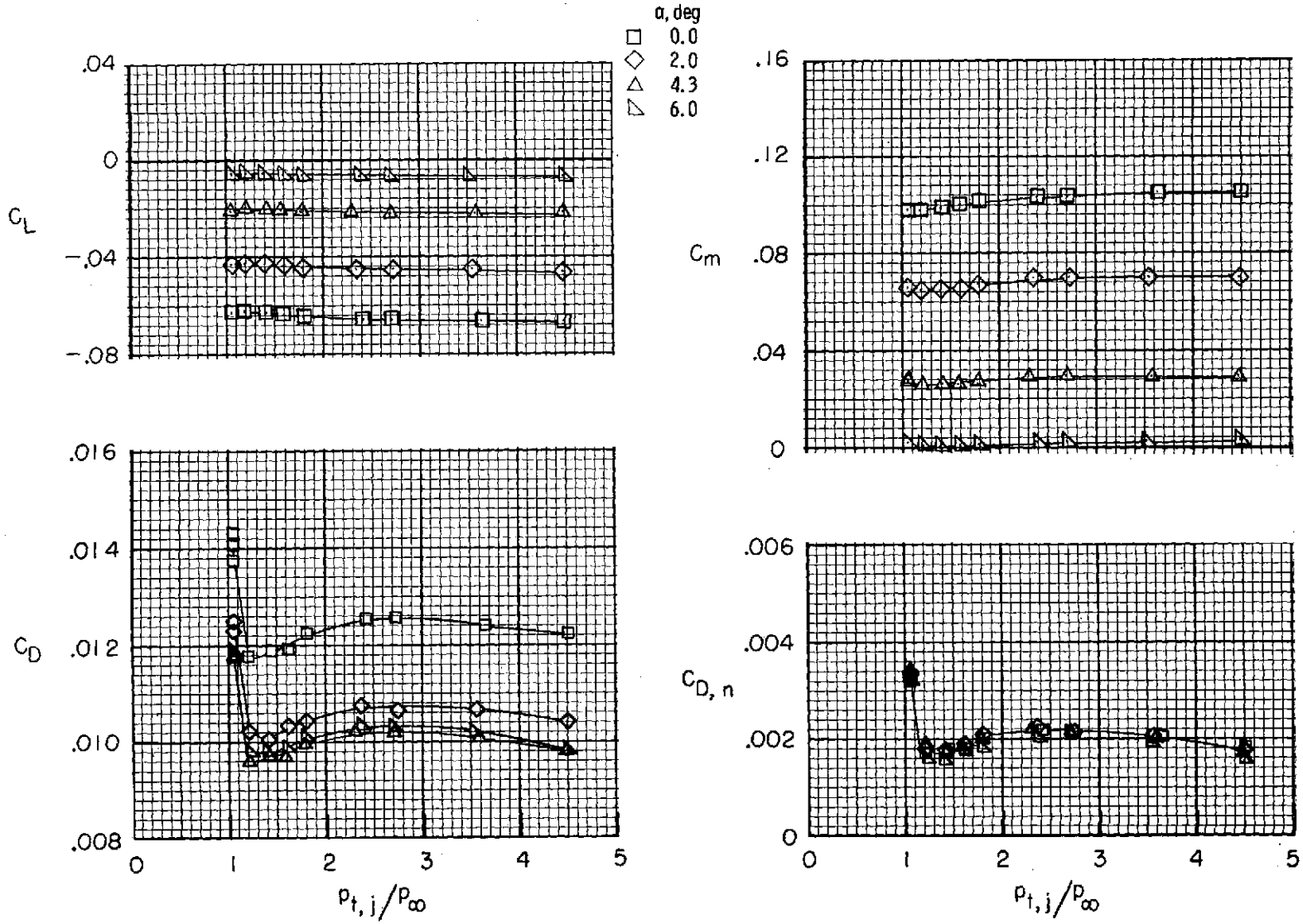

(a) M = 0.70.

Figure 13.- Effect of jet total-pressure ratio on afterbody-nozzle aerodynamic forces and moments for type A cruise nozzles, interfairing 2, and horizontal tails set at -2°.

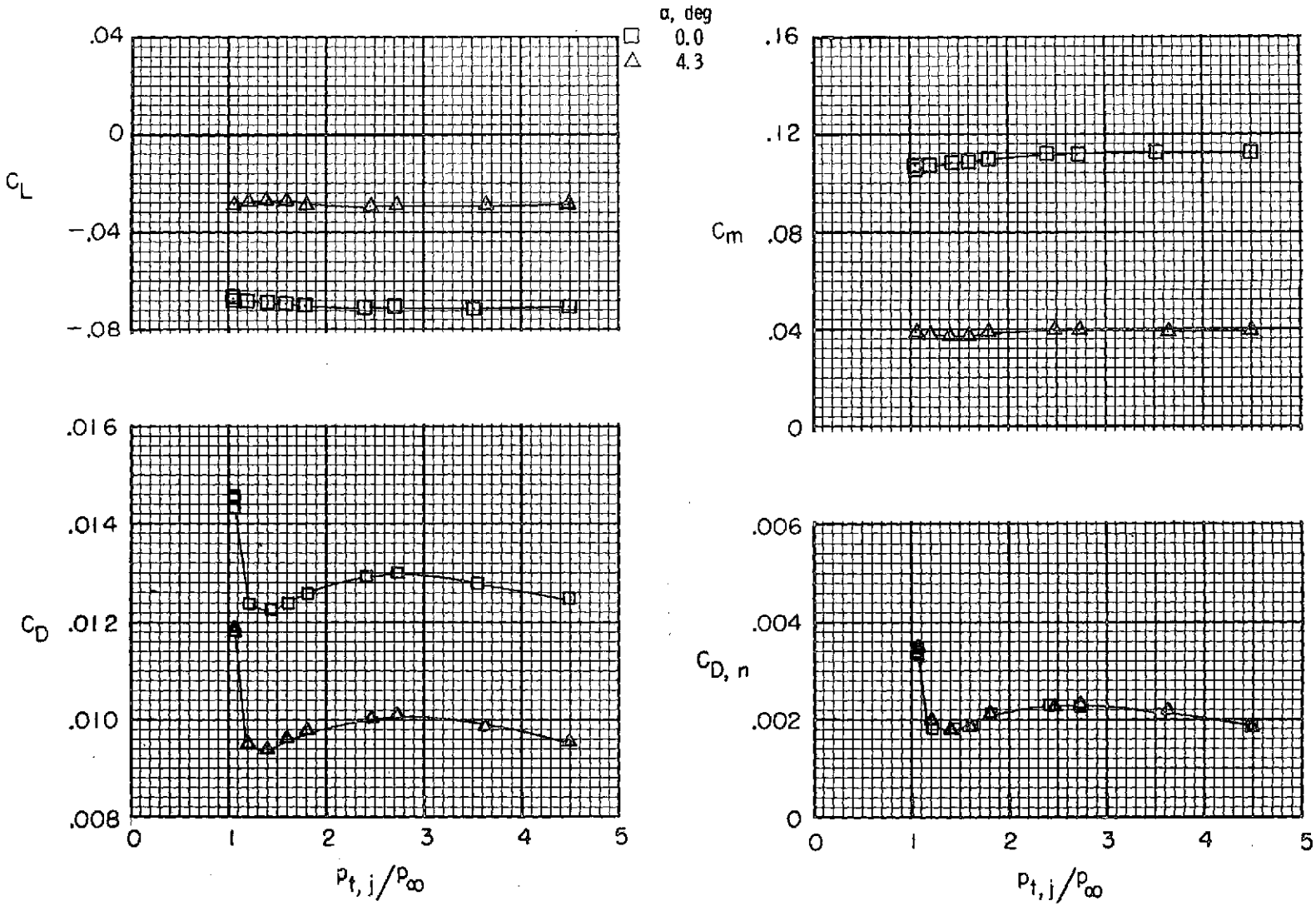

(b) M 0.80.

Figure 13.- Concluded.

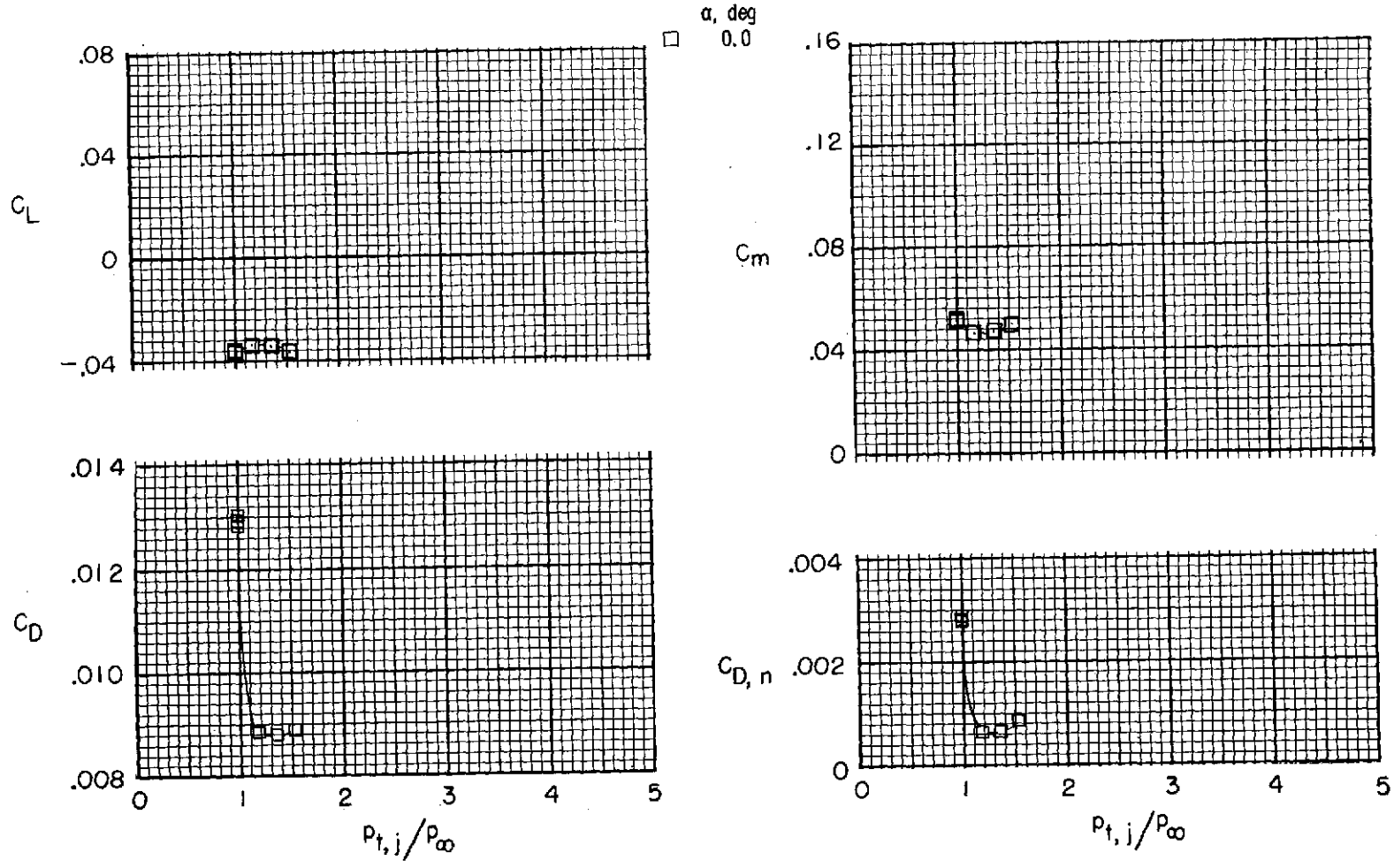

(a) M = 0.80.

Figure 14.- Effect of jet total-pressure ratio on afterbody-nozzle aerodynamic forces and moments for type A maximum afterburning nozzles and interfairing 2.

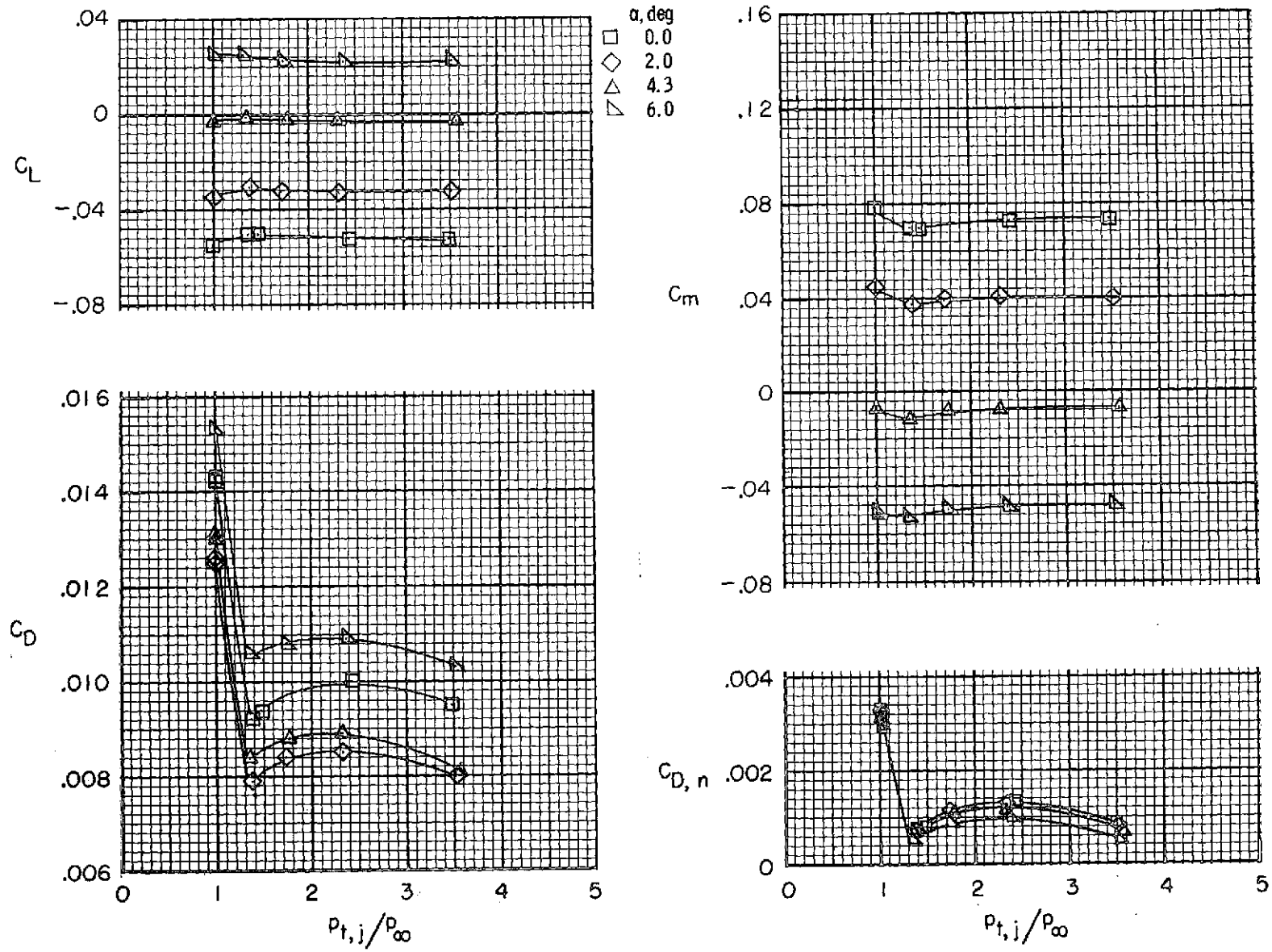

(b) M = 0.90.

Figure 14.- Continued.

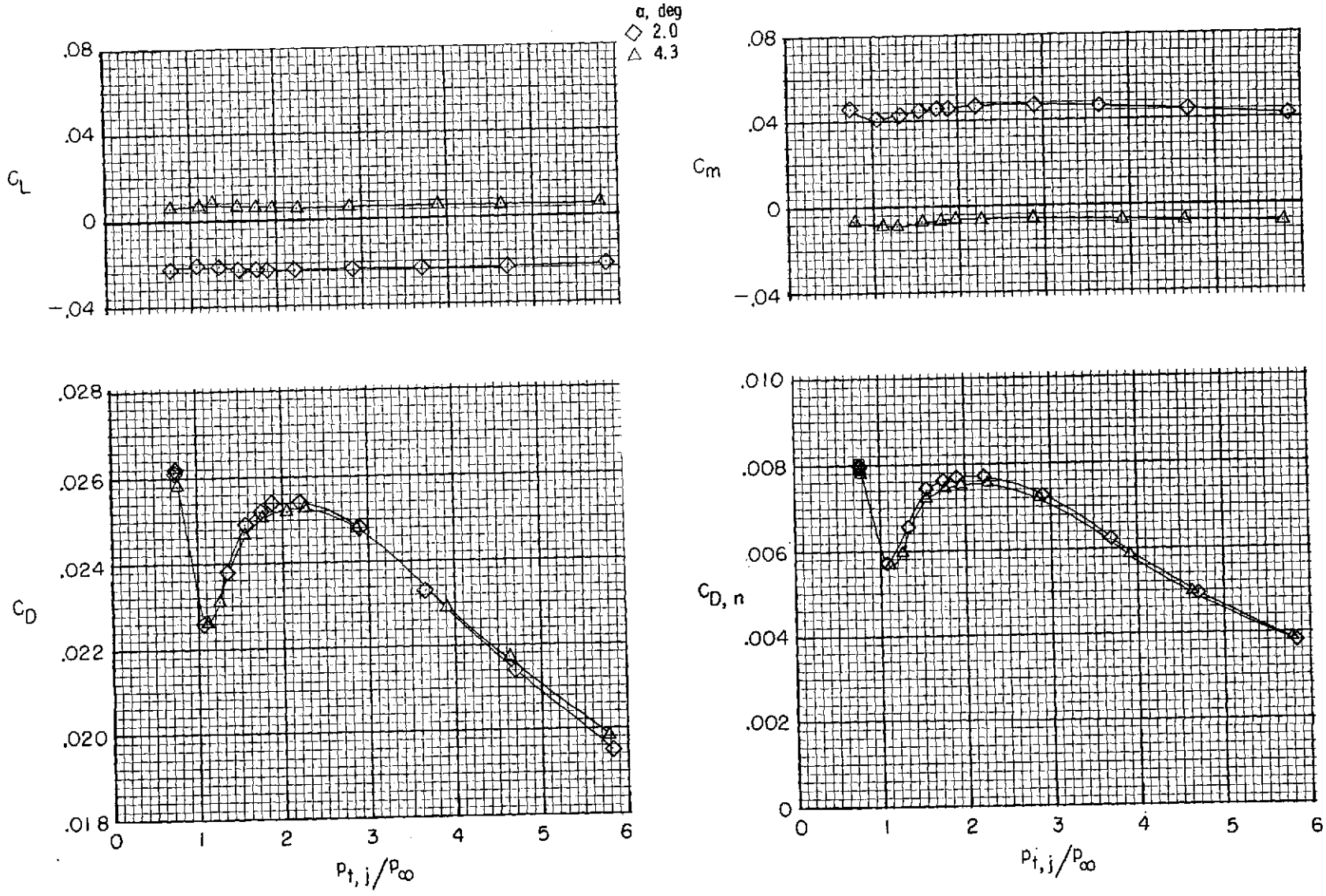

(c) M = 1.20.

Figure 14.- Continued.

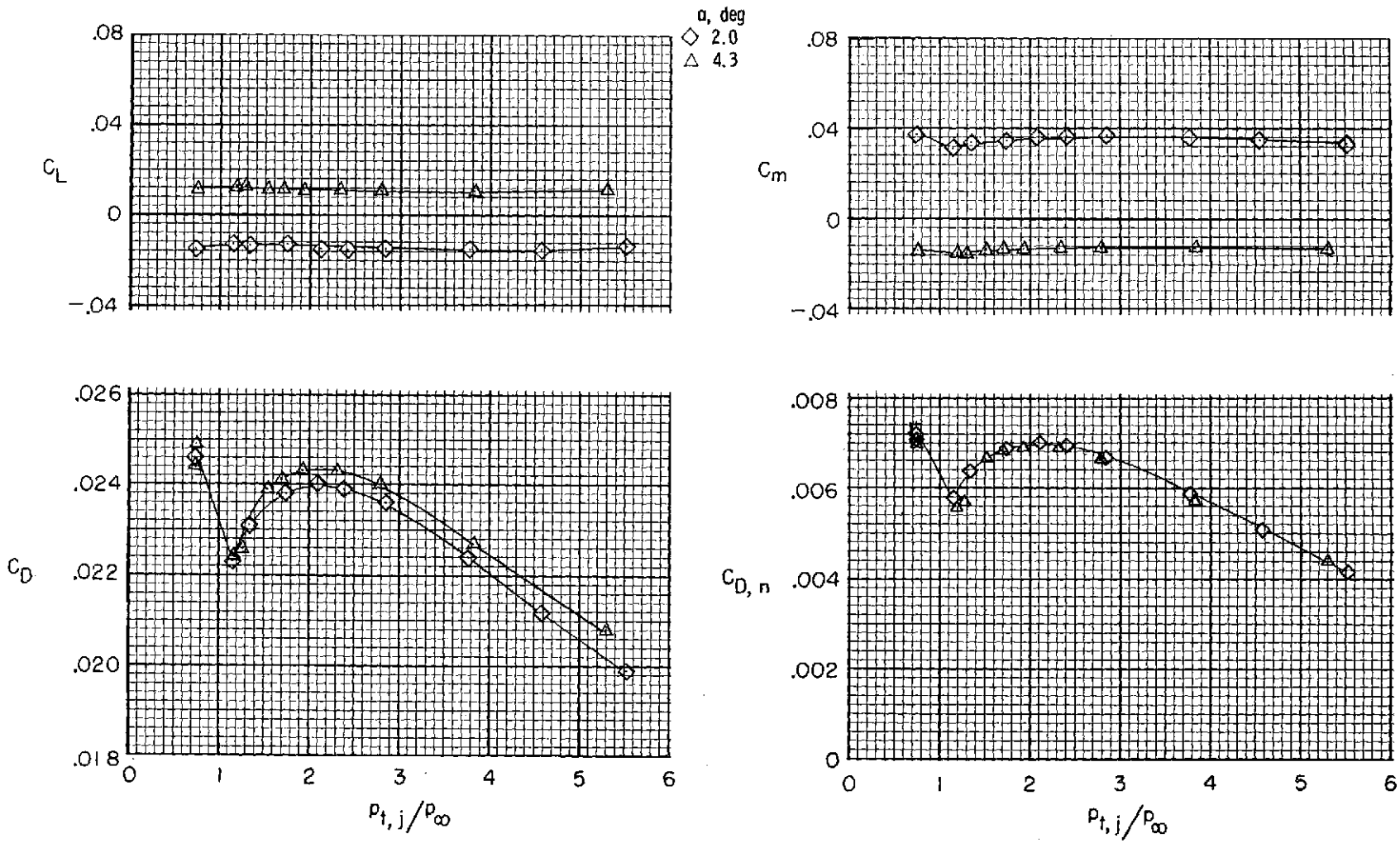

(d) M = 1.30.

Figure 14.- Continued.

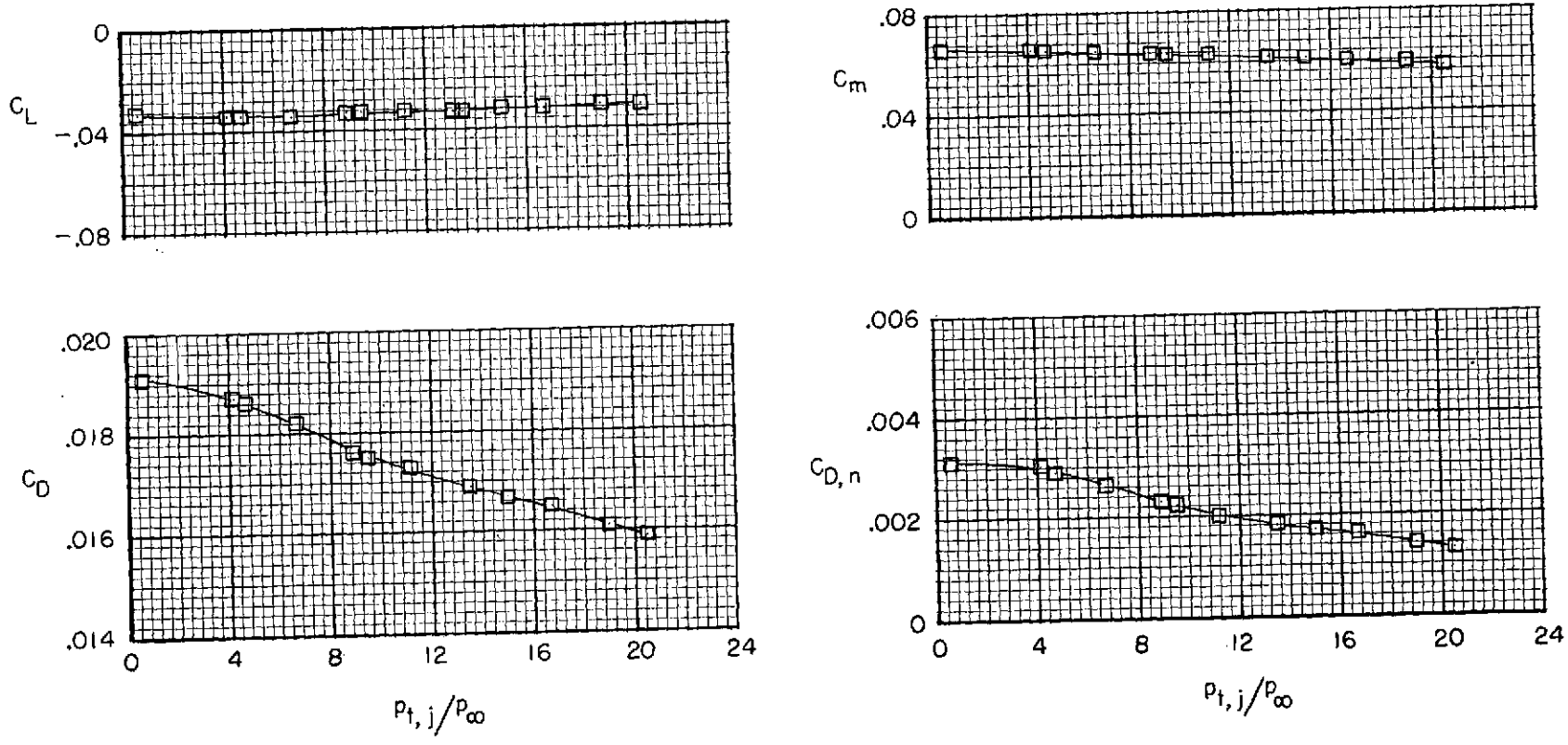

(e) M = 2.20.

Figure 14.- Concluded.

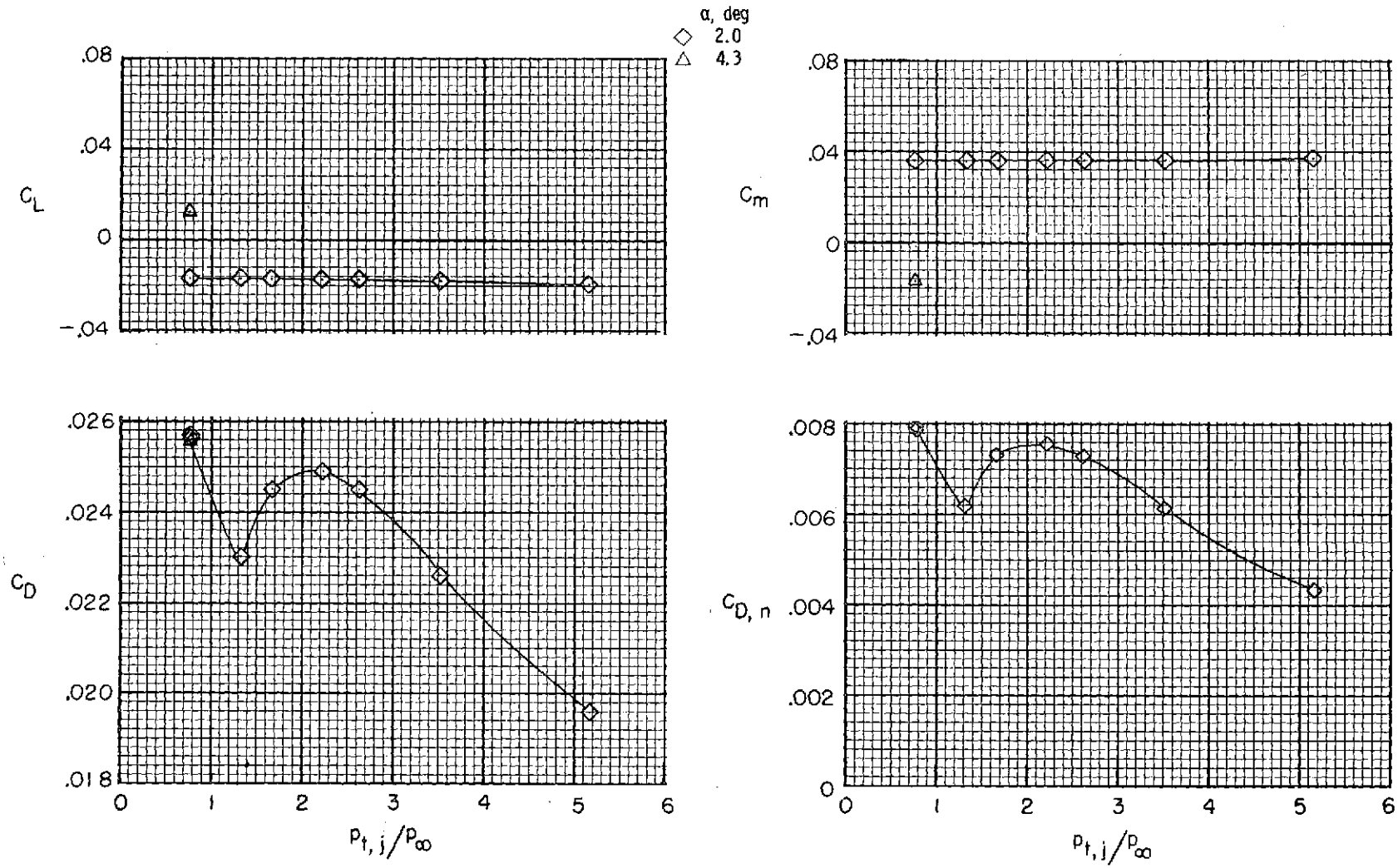

Figure 15.- Effect of jet total-pressure ratio on afterbody-nozzle aerodynamic forces and moments for type A maximum afterburning nozzles and interfairing 4 at M = 1.20.

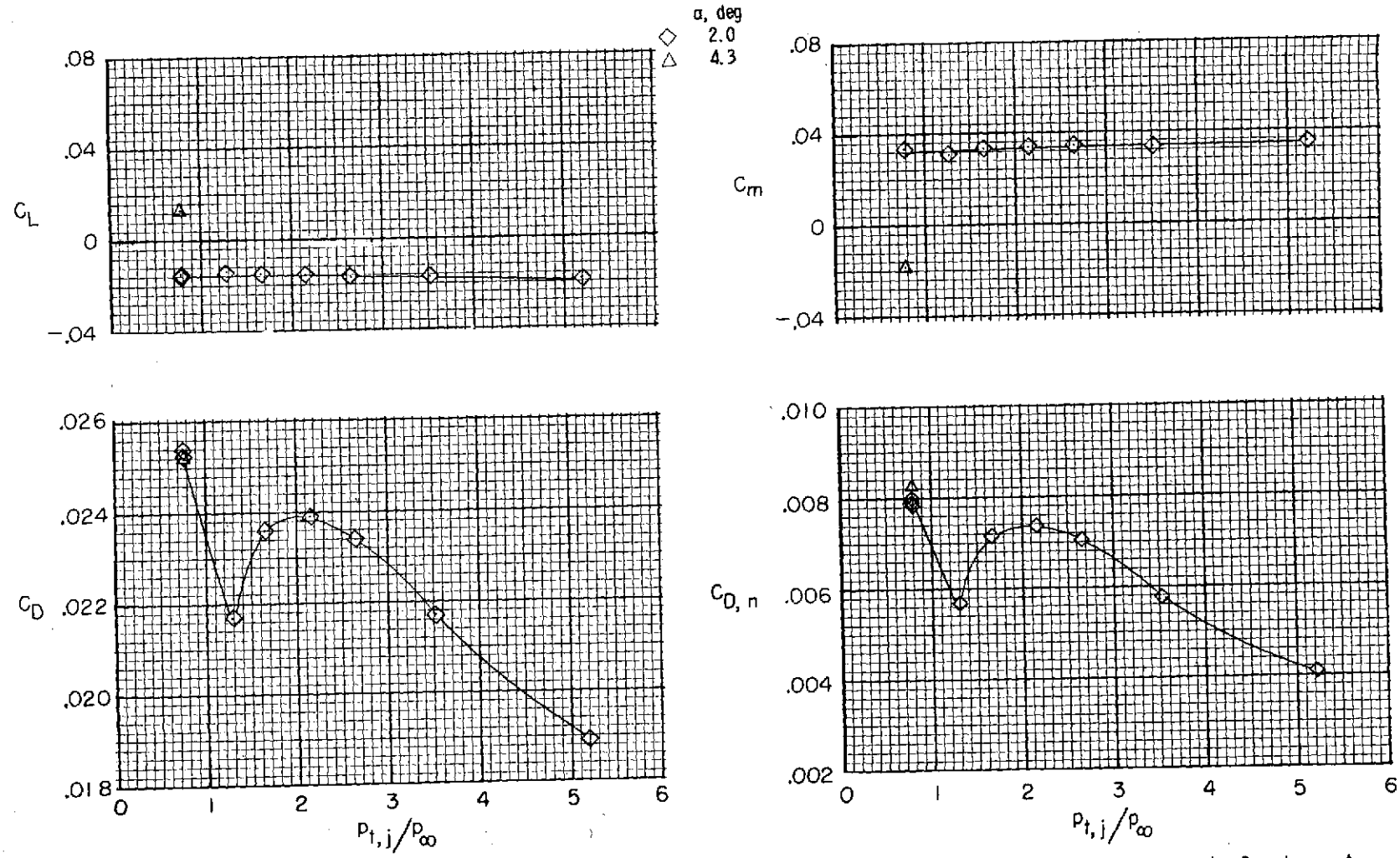

Figure 16.- Effect of jet total-pressure ratio on afterbody-nozzle aerodynamic forces and moments for type A maximum afterburning nozzles and interfairing 6 at M = 1.20.

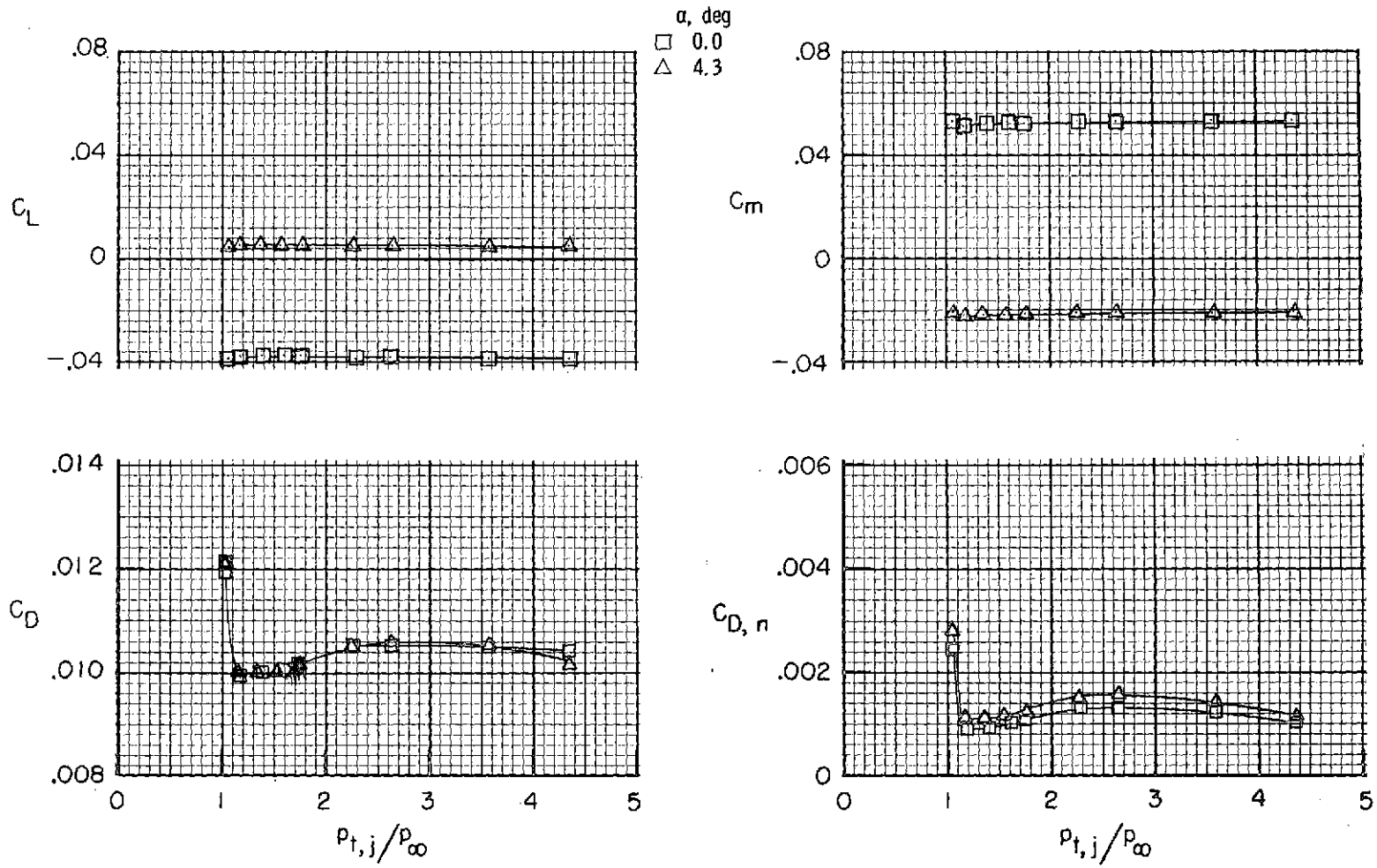

(a) M = 0.60.

Figure 17.- Effect of jet total-pressure ratio on afterbody-nozzle aerodynamic forces and moments for type B cruise nozzles and interfairing 1.

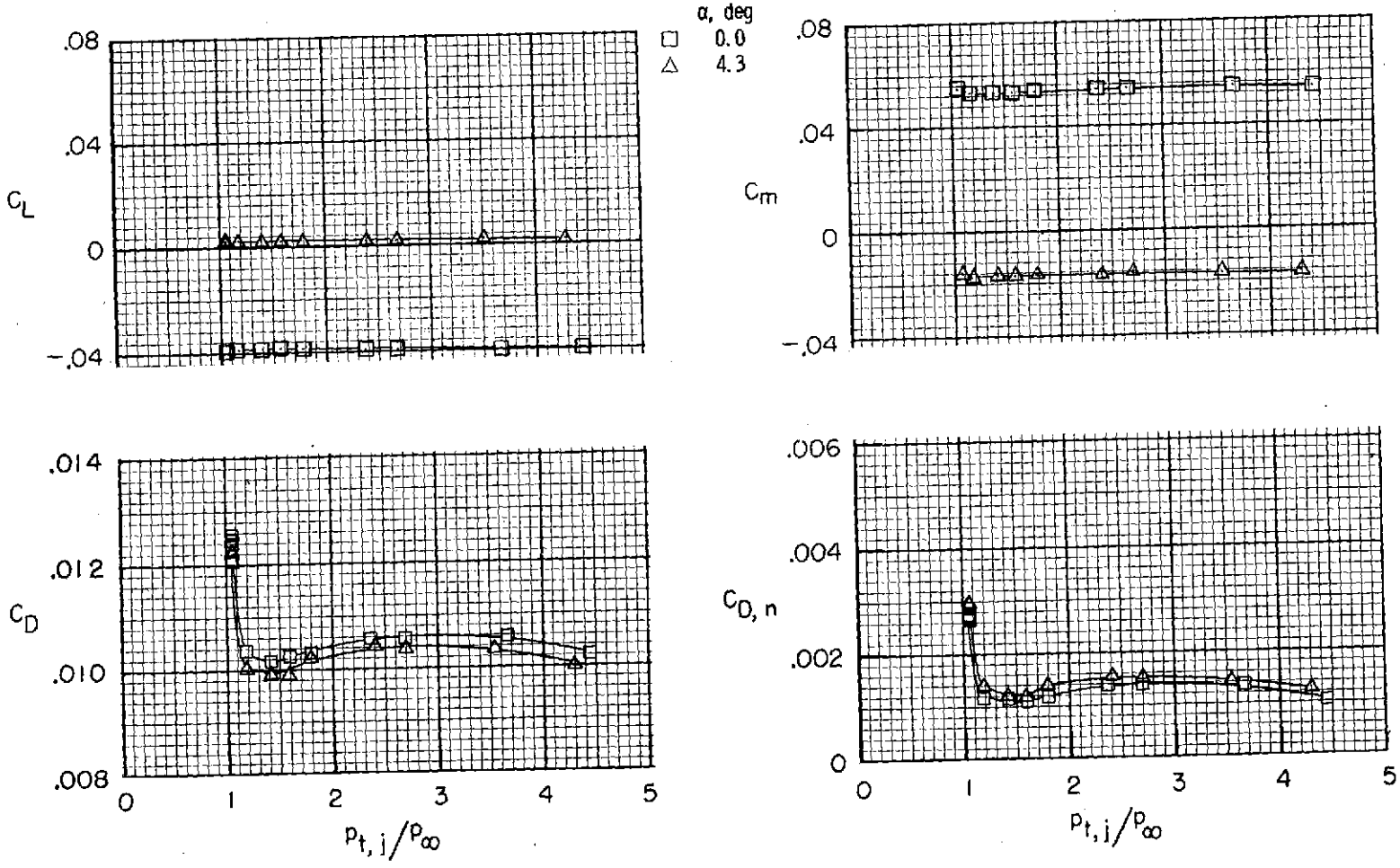

(b) M = 0.70.

Figure 17.- Continued.

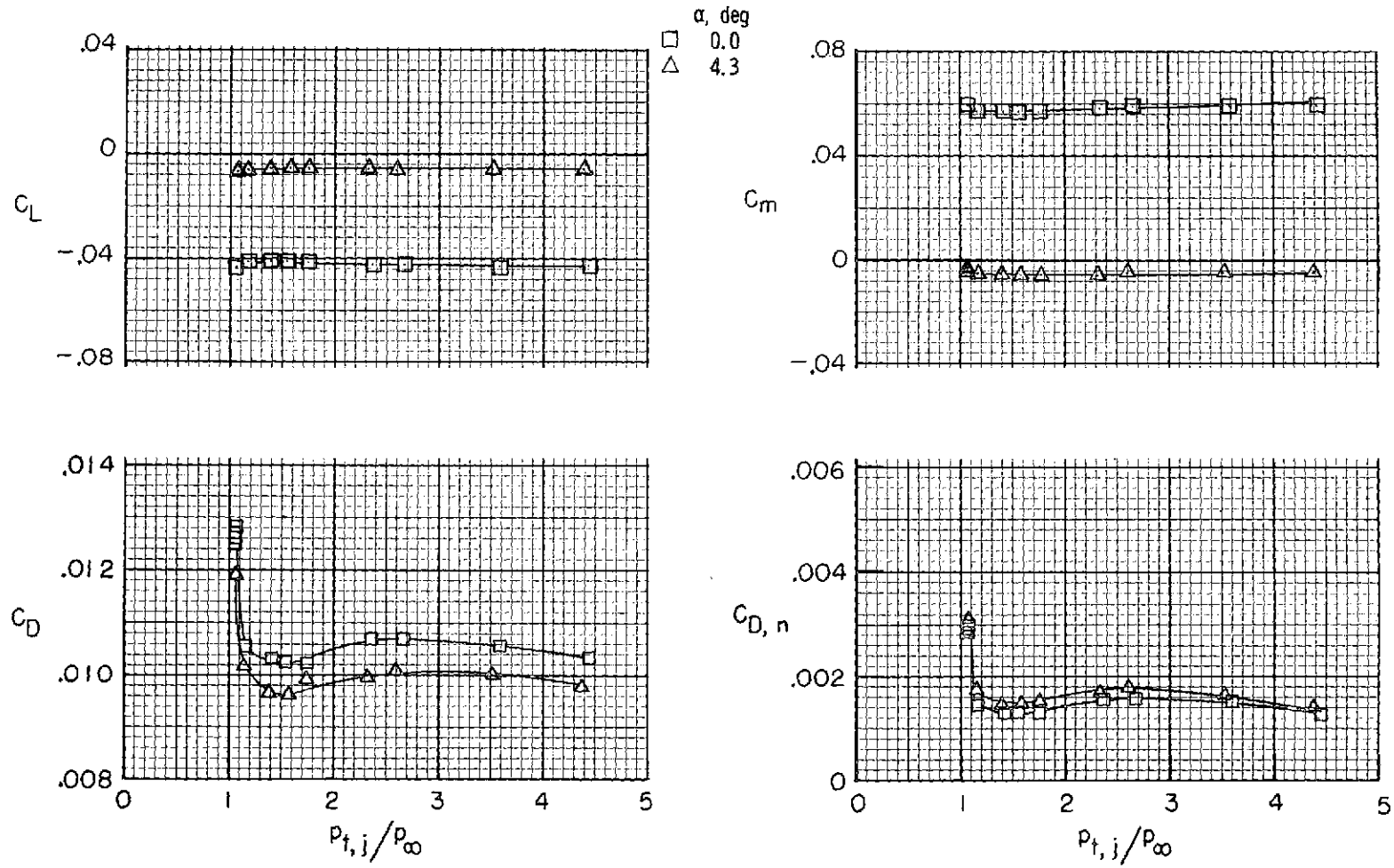

(c) M = 0.80.

Figure 17.- Continued.

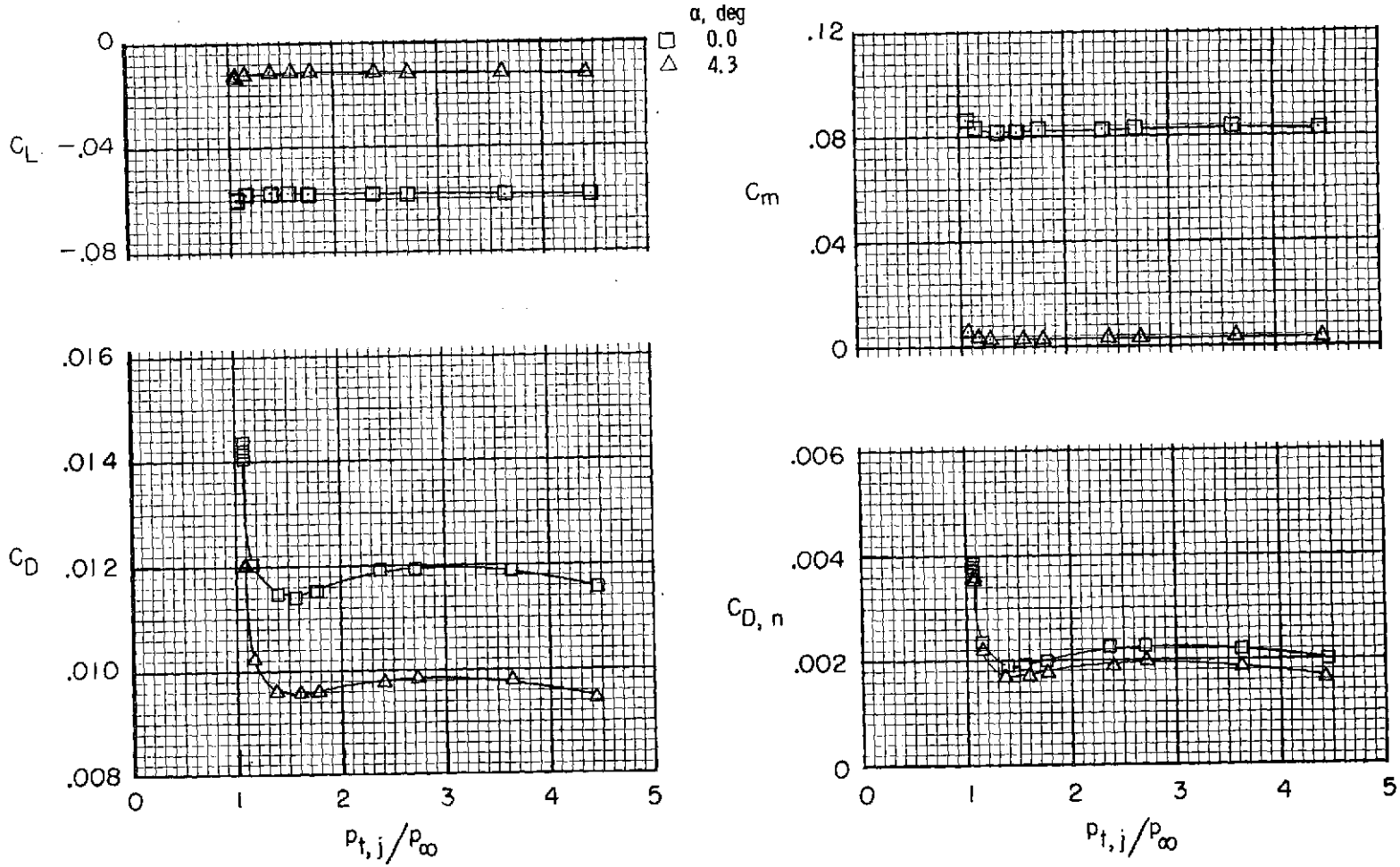

(d) M = 0.90.

Figure 17.- Concluded.

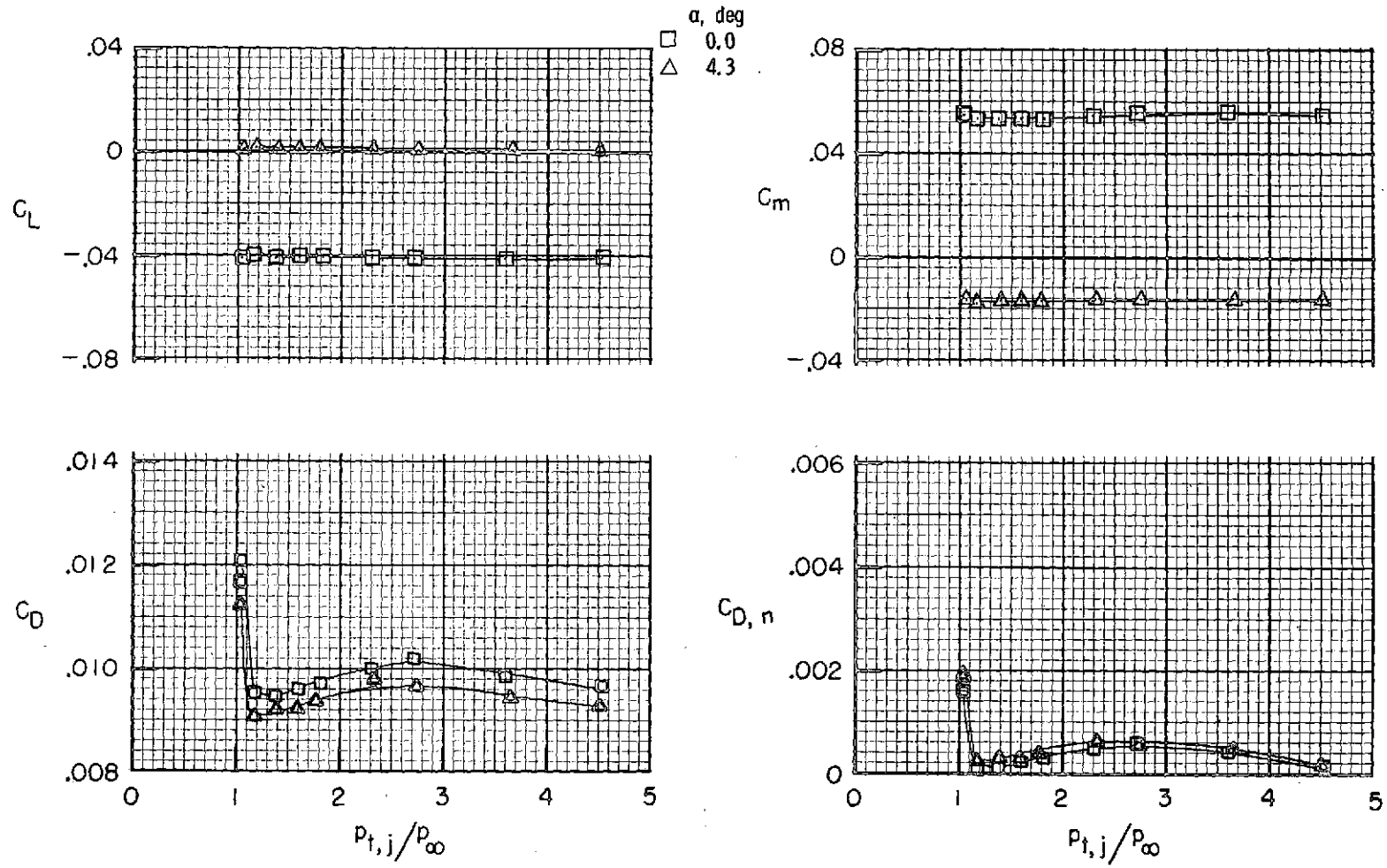

(a) M = 0.60.

Figure 18.- Effect of jet total-pressure ratio on afterbody-nozzle aerodynamic forces and moments for type B cruise nozzles and interfairing 2.

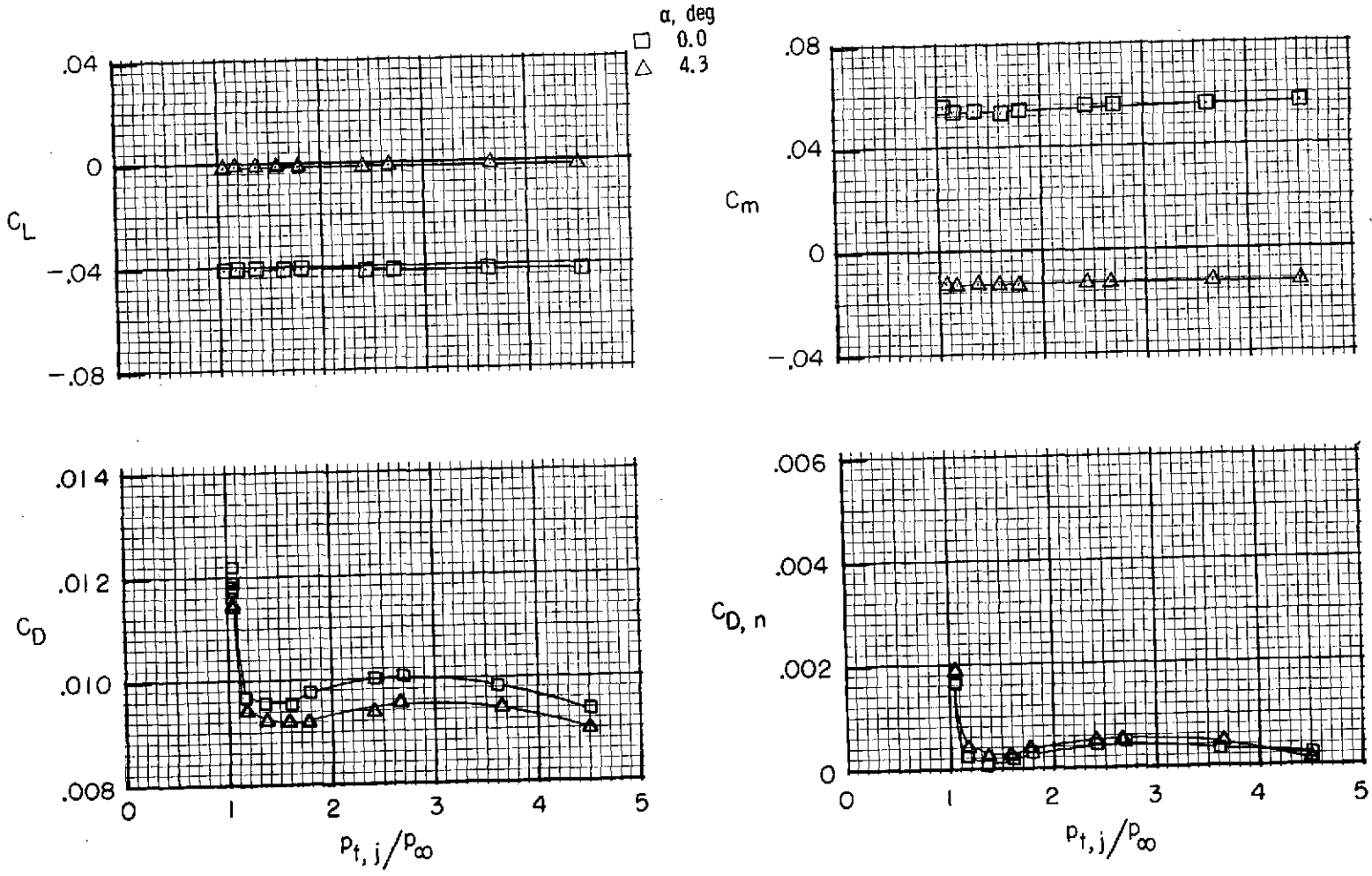

(b) M = 0.70.

Figure 18.- Continued.

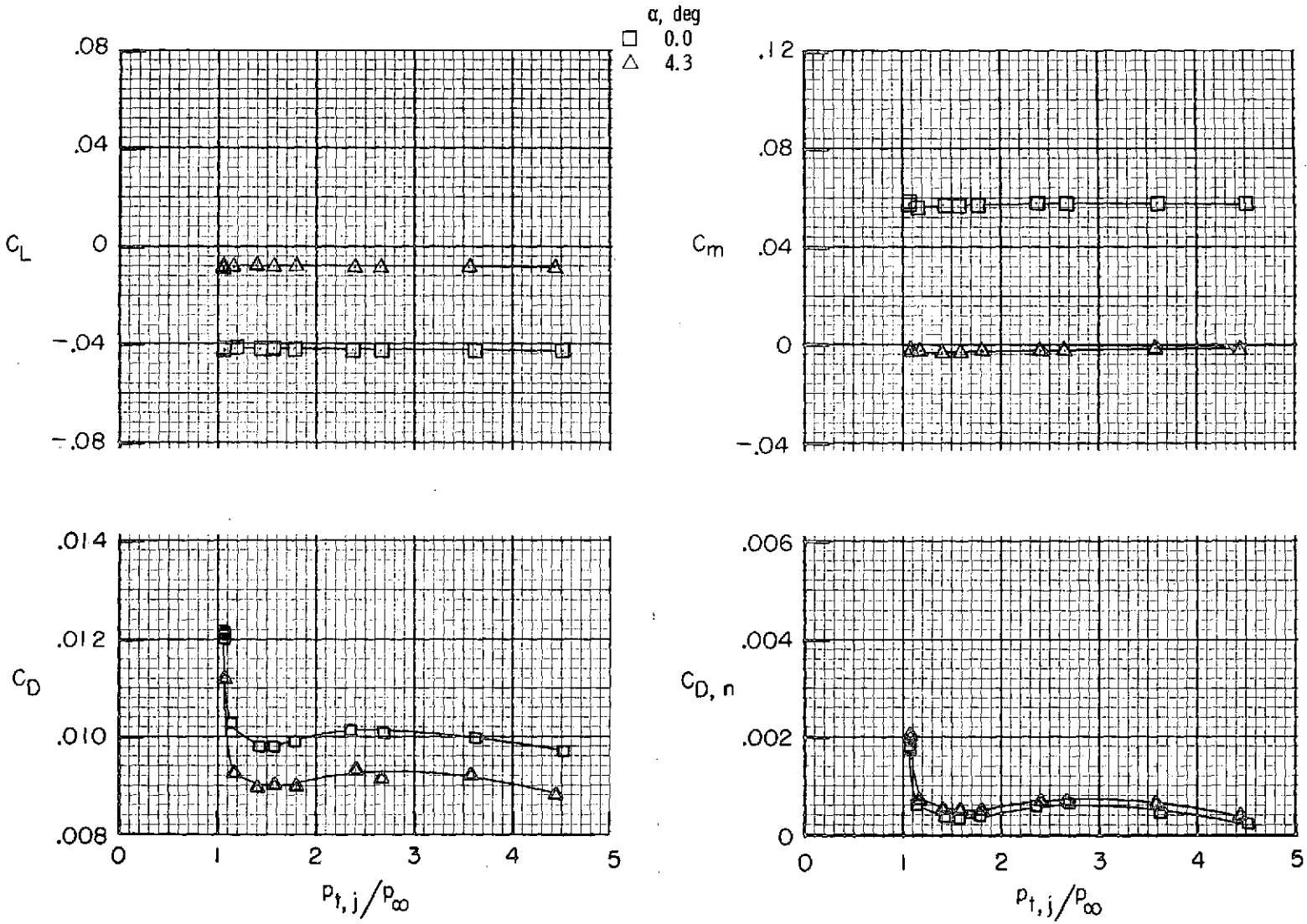

(c) M = 0.80.

Figure 18.- Continued.

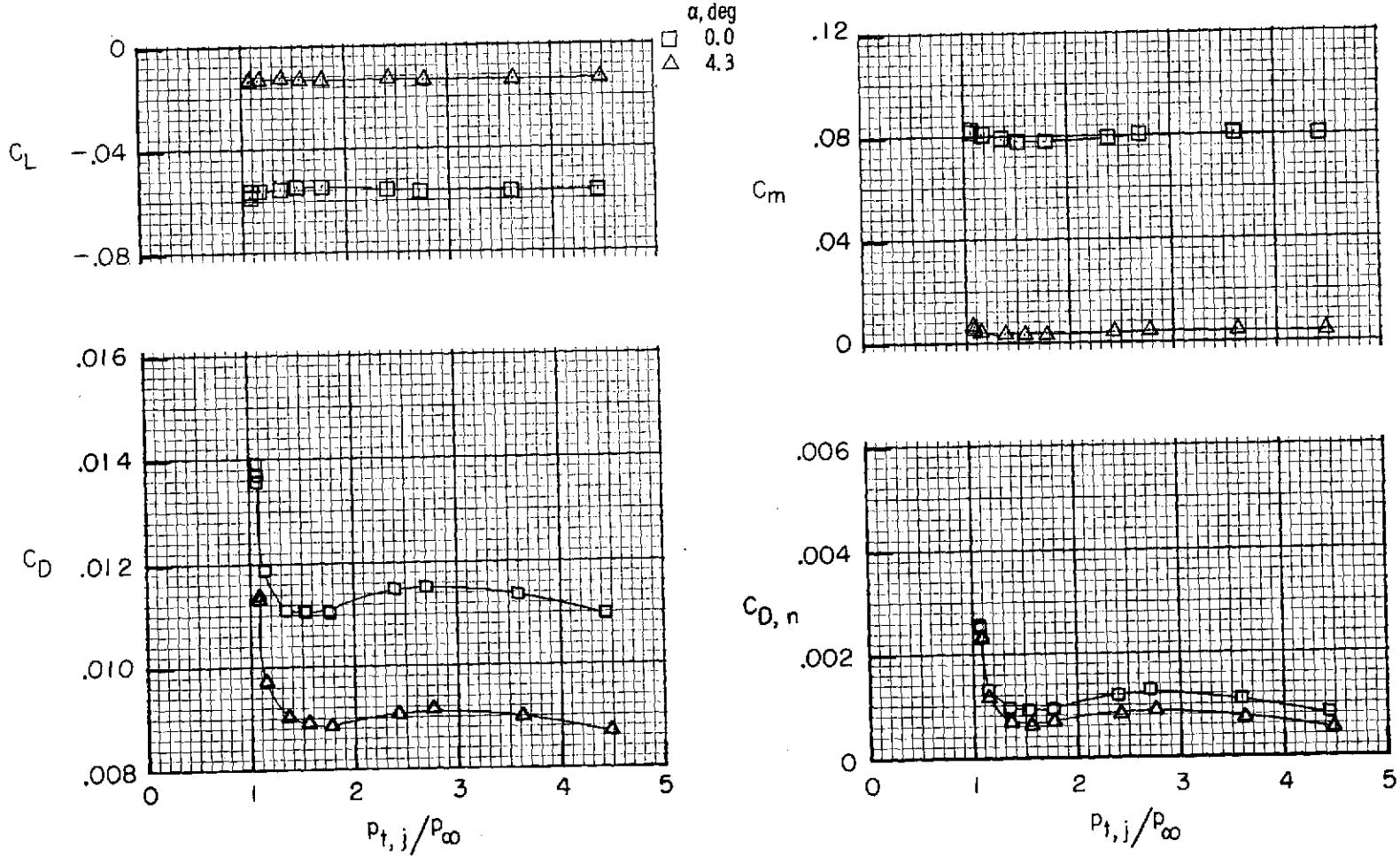

(d) M = 0.90.

Figure 18.- Concluded.

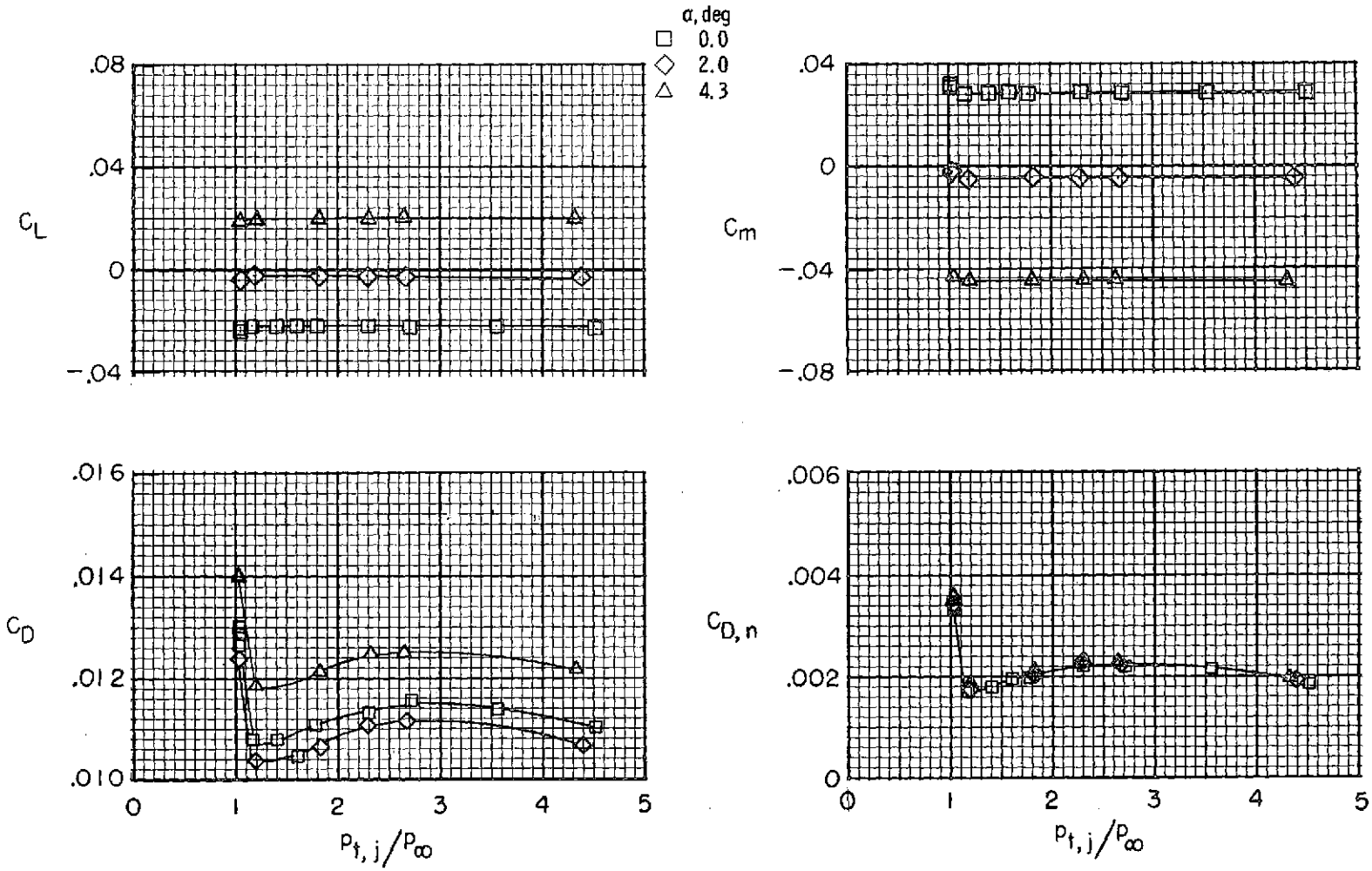

(a) M = 0.60.

Figure 19.- Effect of jet total-pressure ratio on afterbody-nozzle aerodynamic forces and moments for type B cruise nozzles and interfairing 3. Dashed line indicates possible fouling.

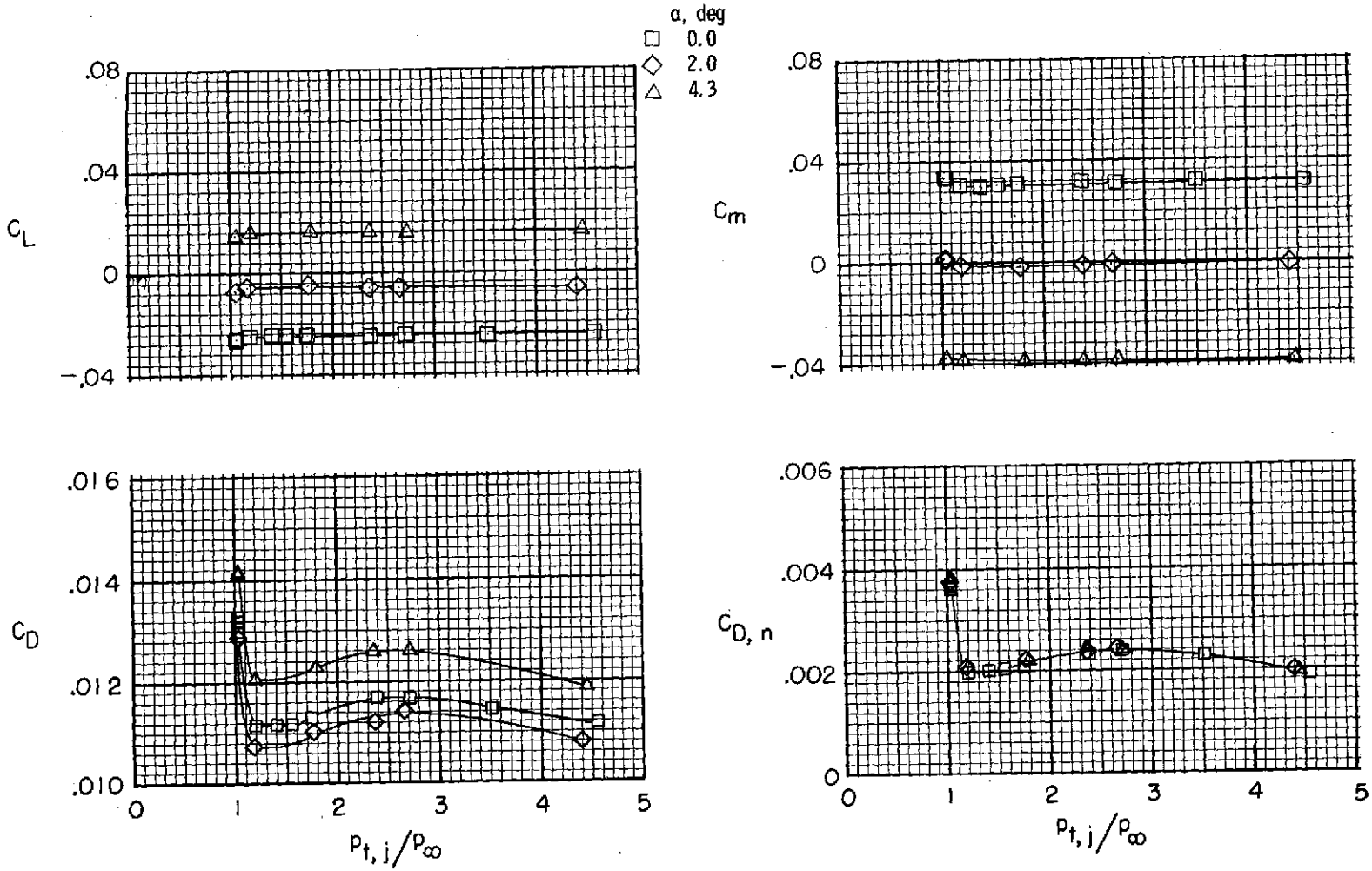

(b) M = 0.70.

Figure 19.- Continued.

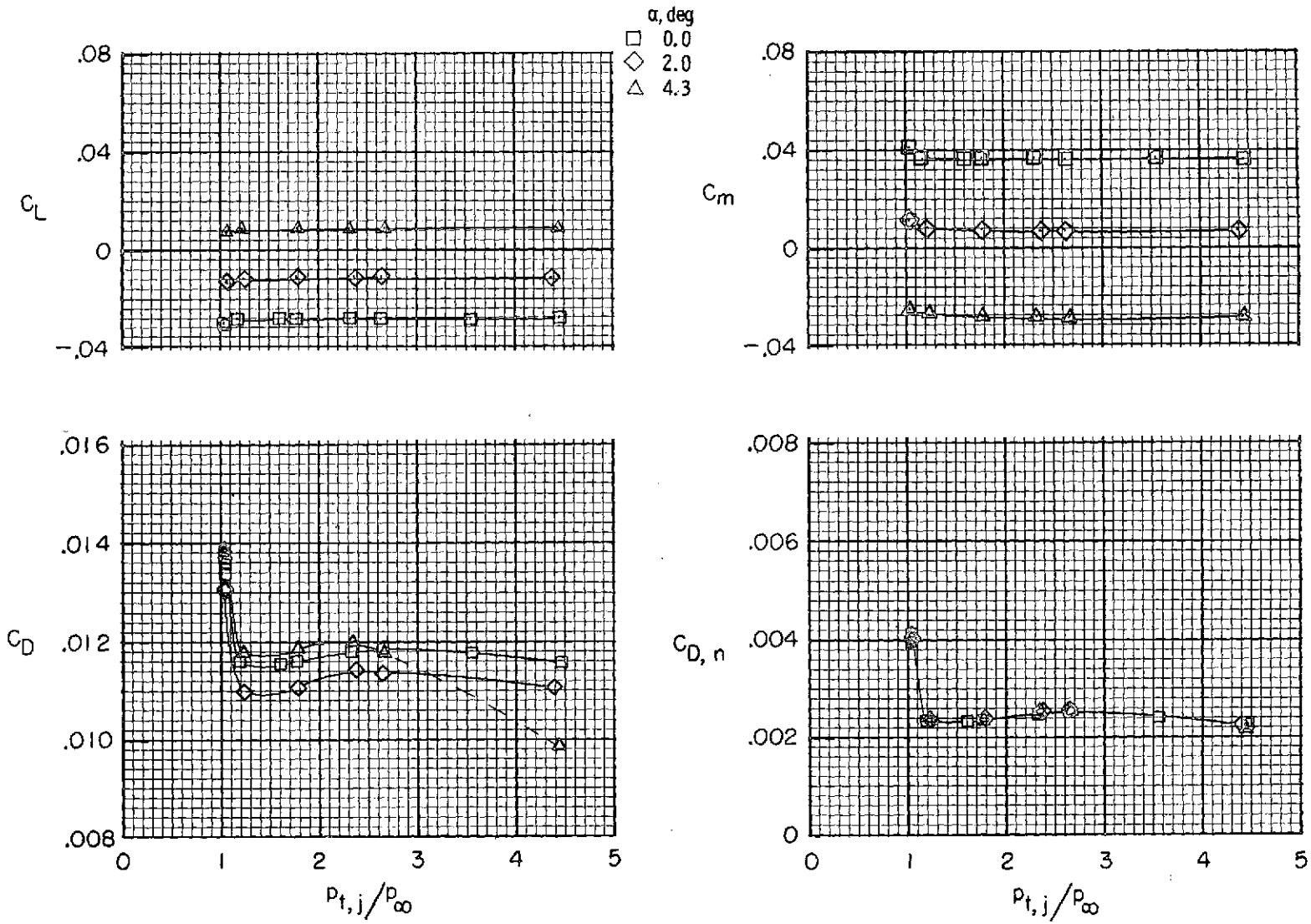

(c) M = 0.80.

Figure 19.- Continued.

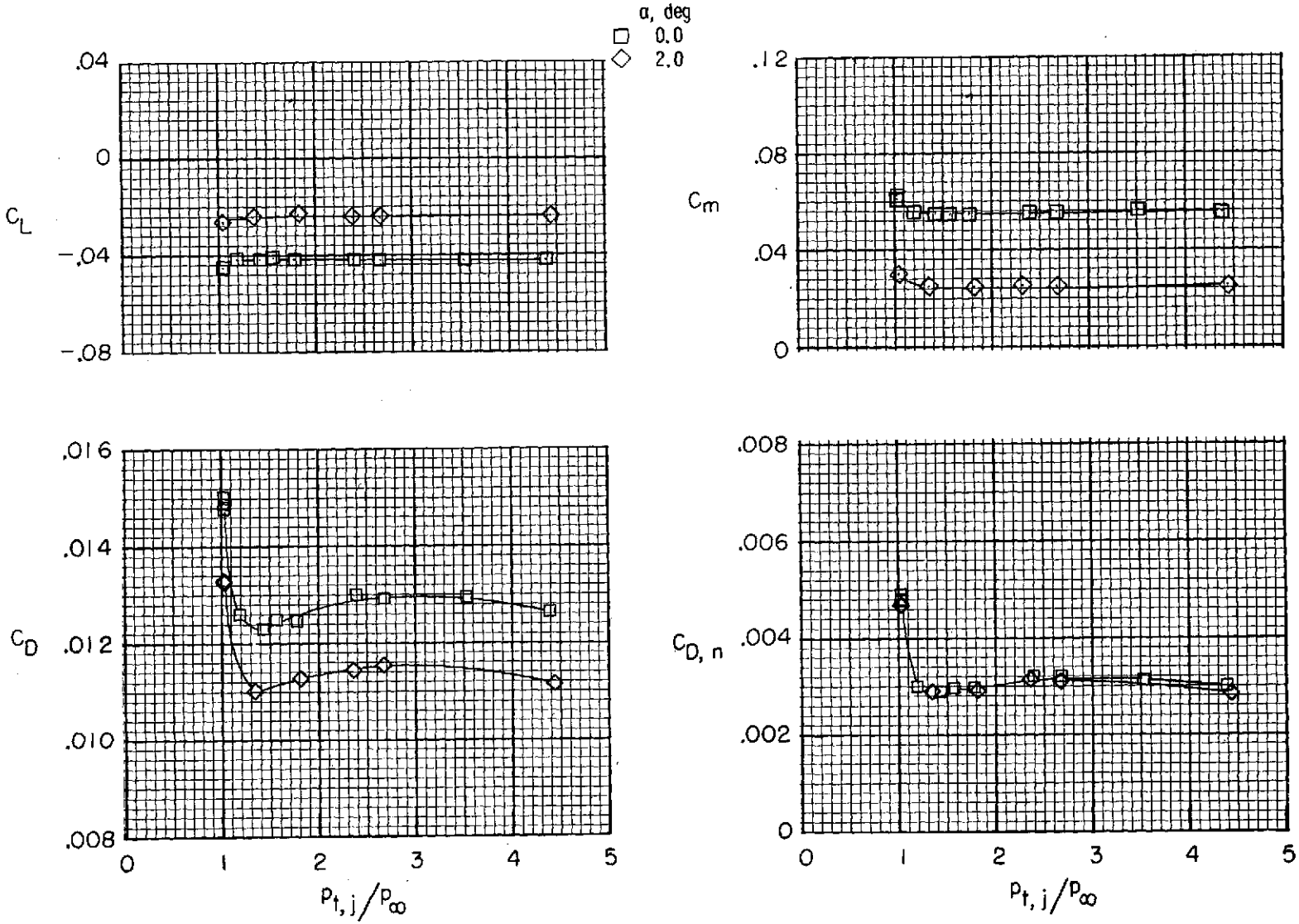

(d) M = 0.90.

Figure 19.- Concluded.

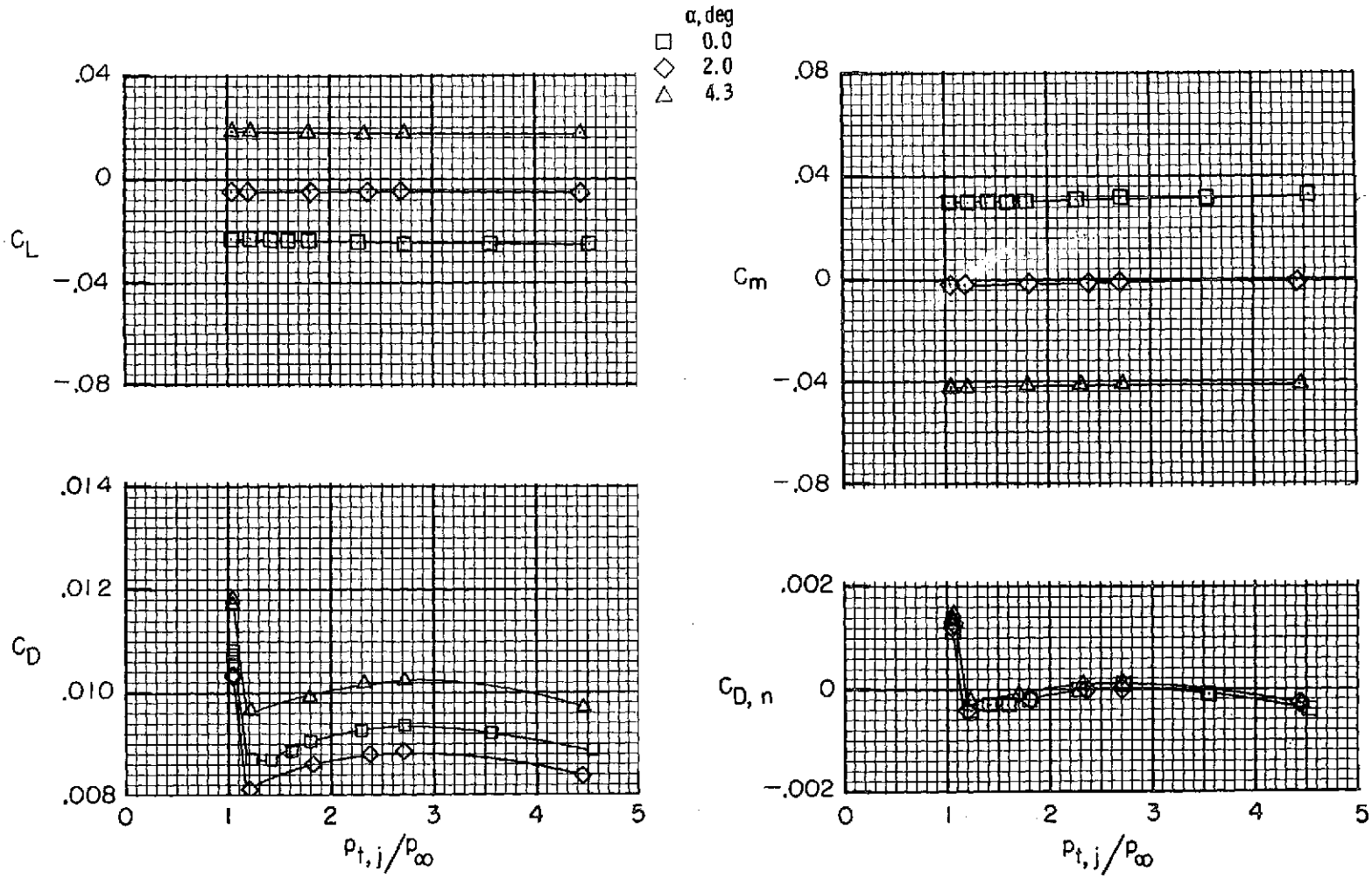

(a) M = 0.60.

Figure 20.- Effect of jet total-pressure ratio on afterbody-nozzle aerodynamic forces and moments for type B cruise nozzles and interfairing 4.

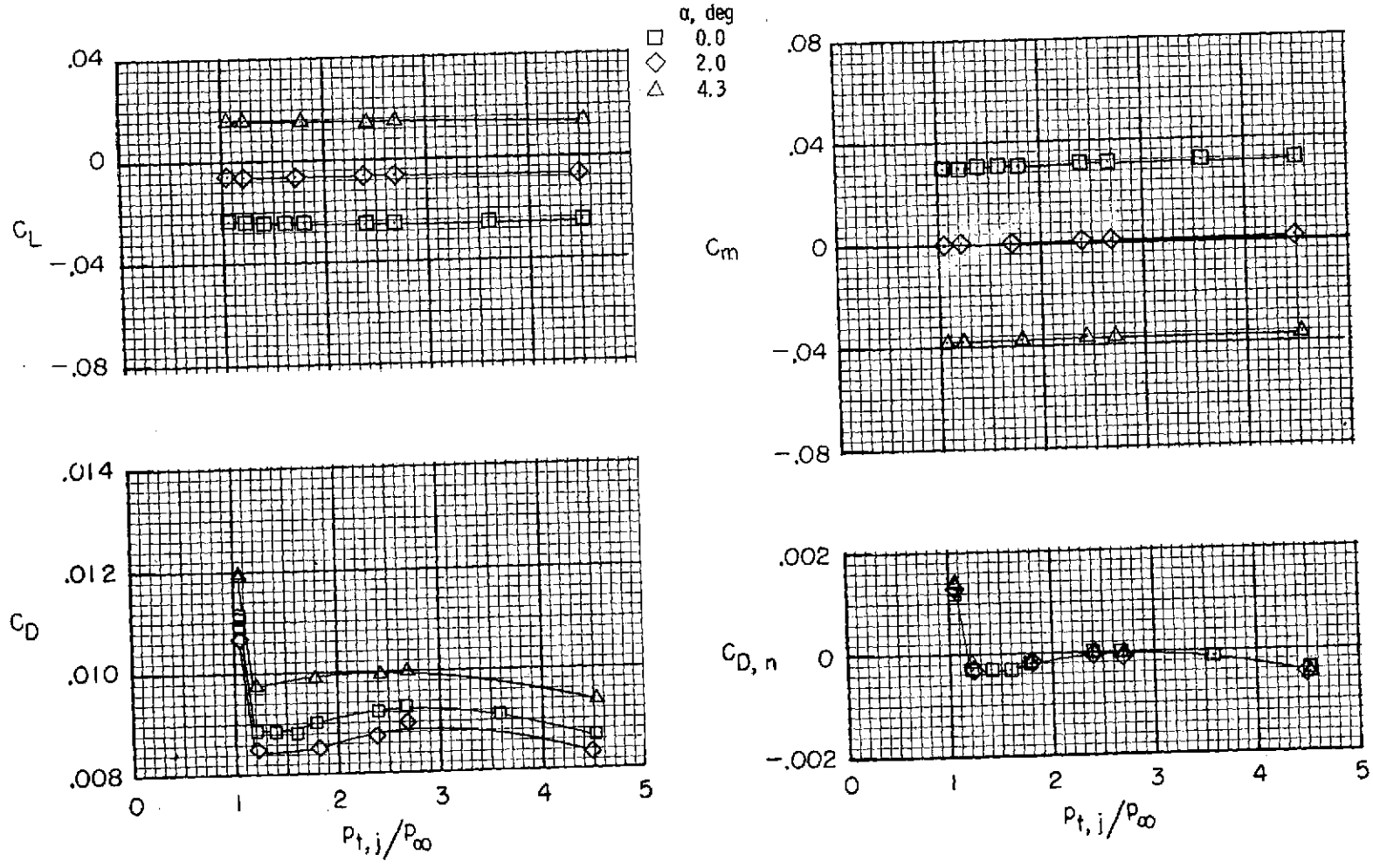

(b) M = 0.70.

Figure 20.- Continued.

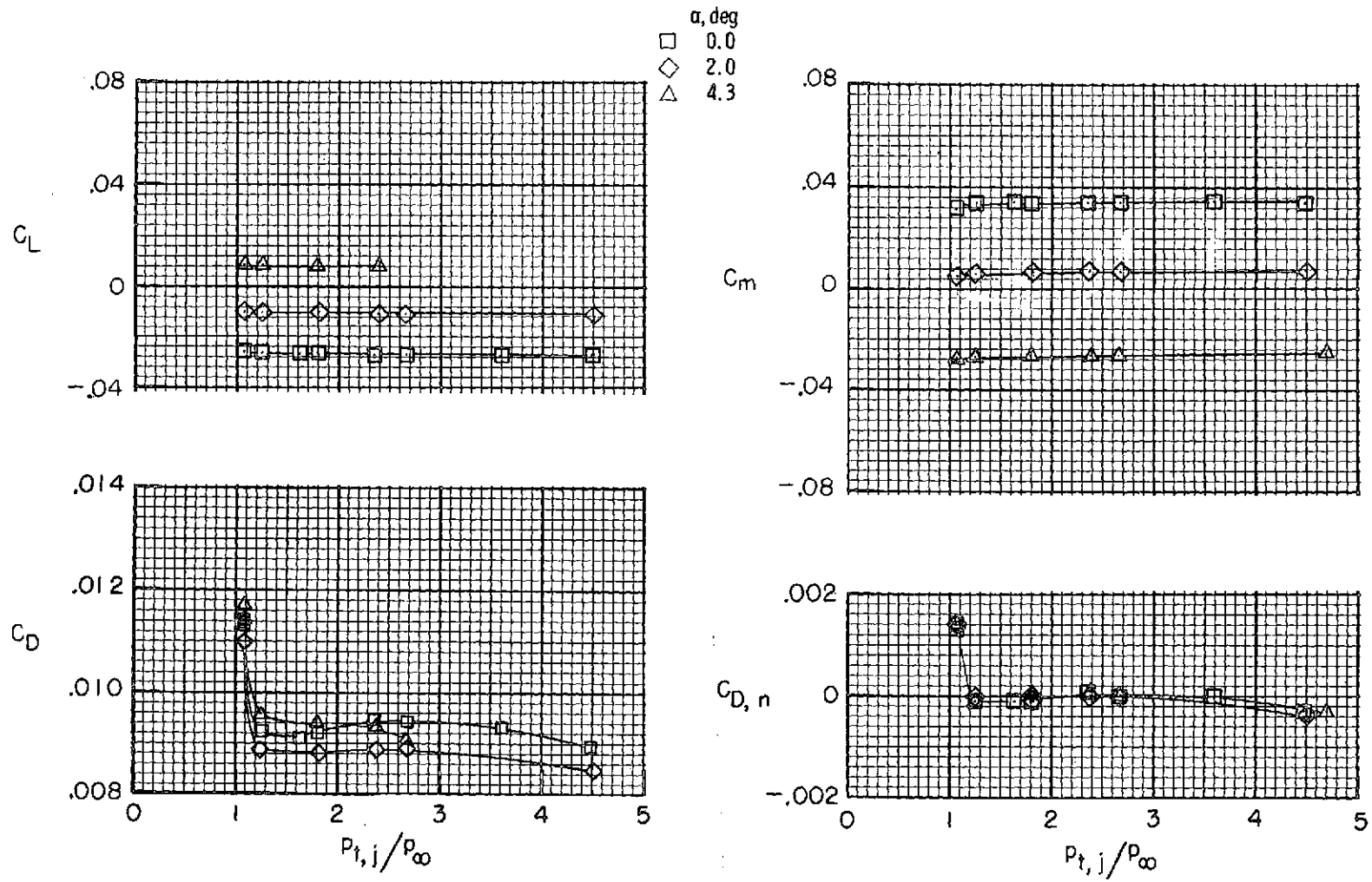

(c) M = 0.80.

Figure 20.- Continued.

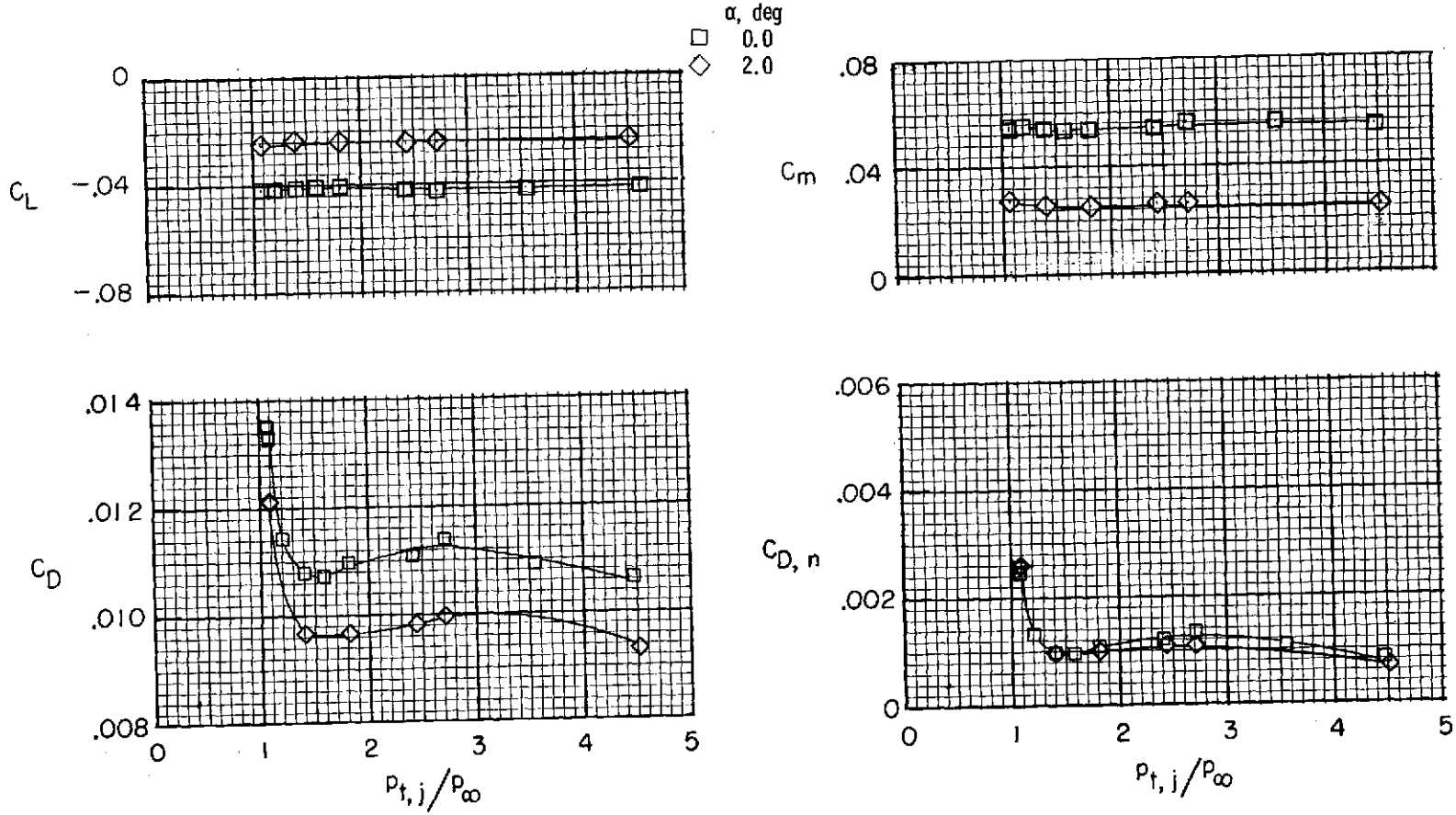

(d) M = 0.90.

Figure 20.- Concluded.

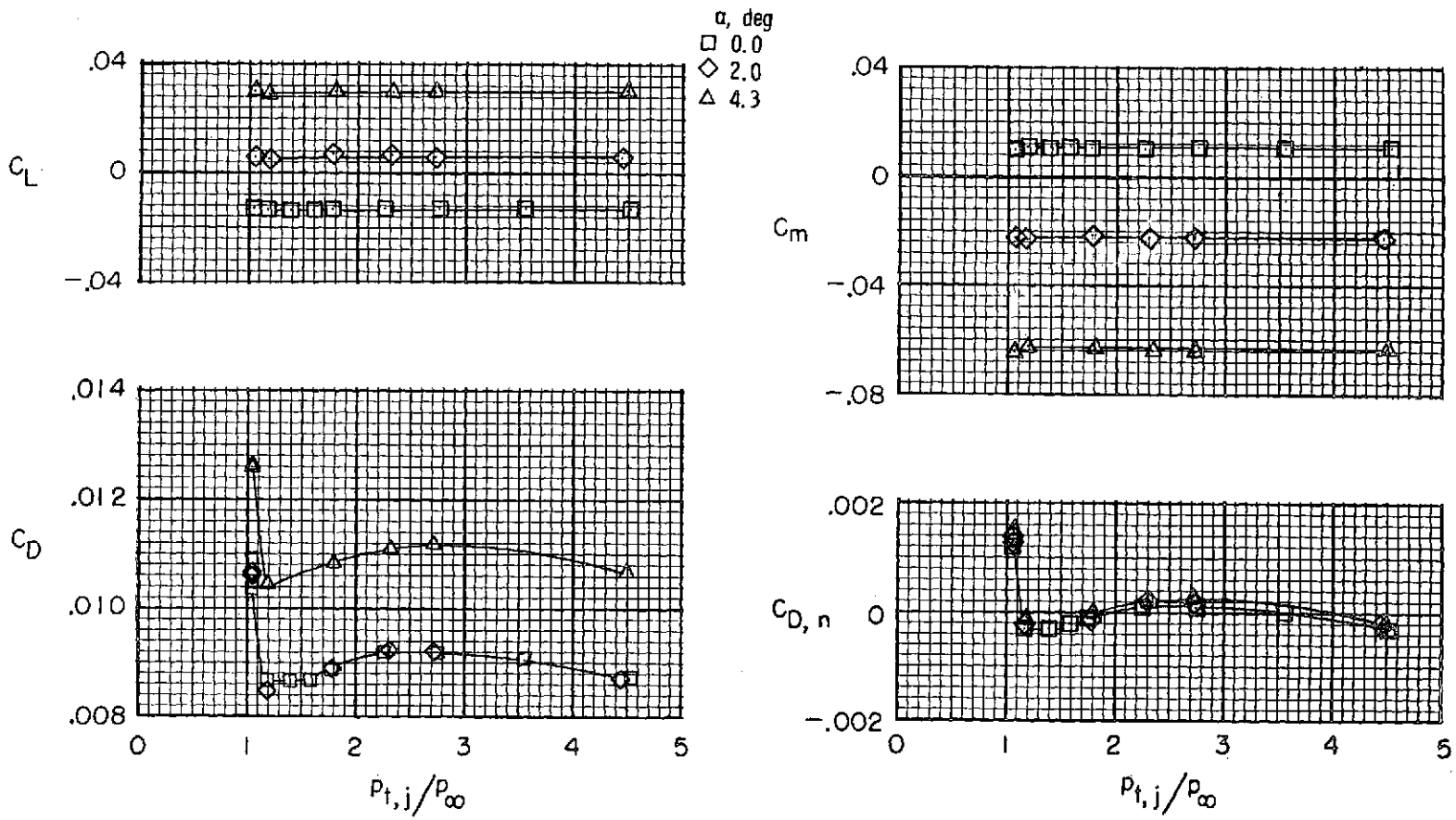

(a) M = 0.60.

Figure 21.- Effect of jet total-pressure ratio on afterbody-nozzle aerodynamic forces and moments for type B cruise nozzles and interfairing 5. Dashed line indicates possible fouling.

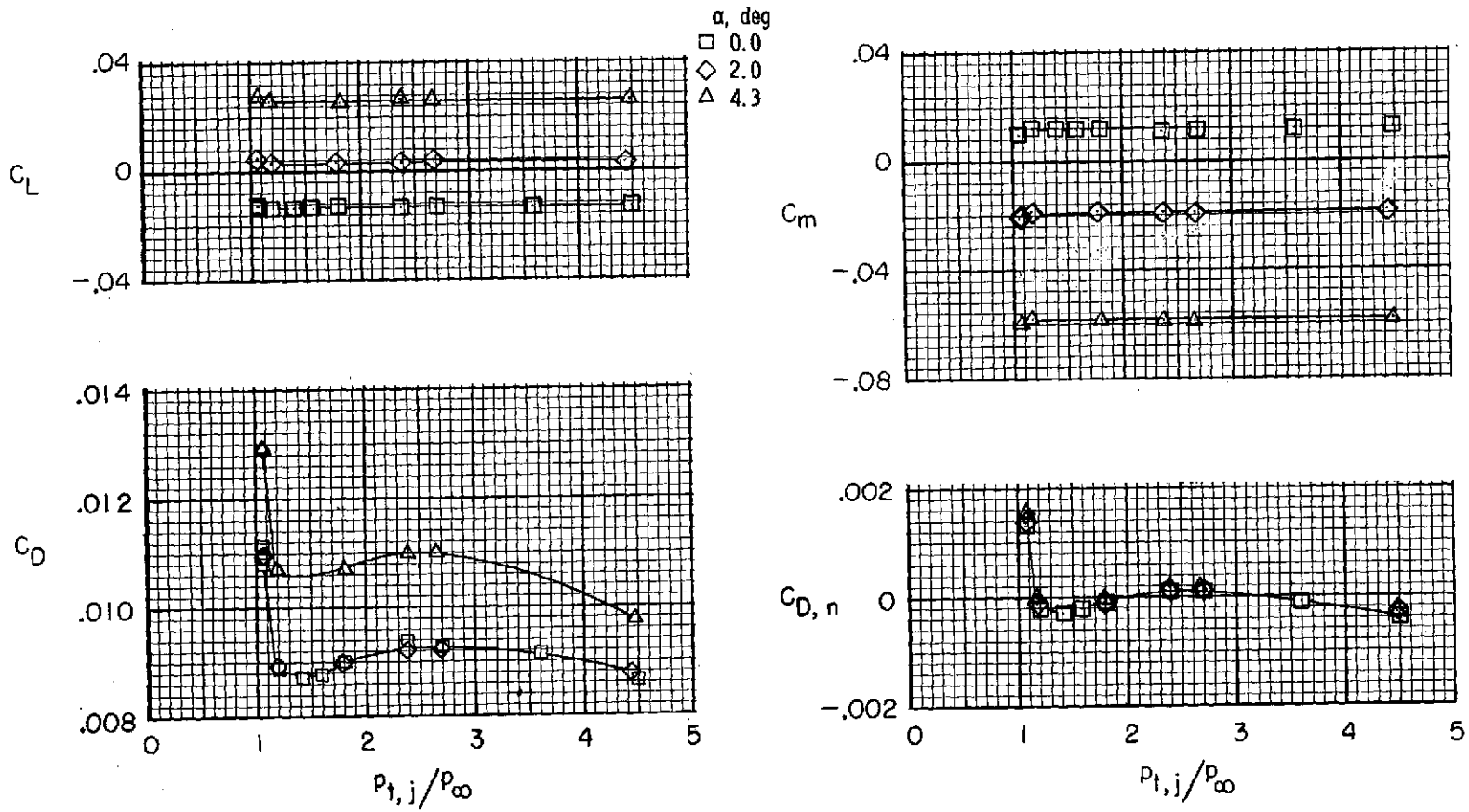

(b) M = 0.70.

Figure 21.- Continued.

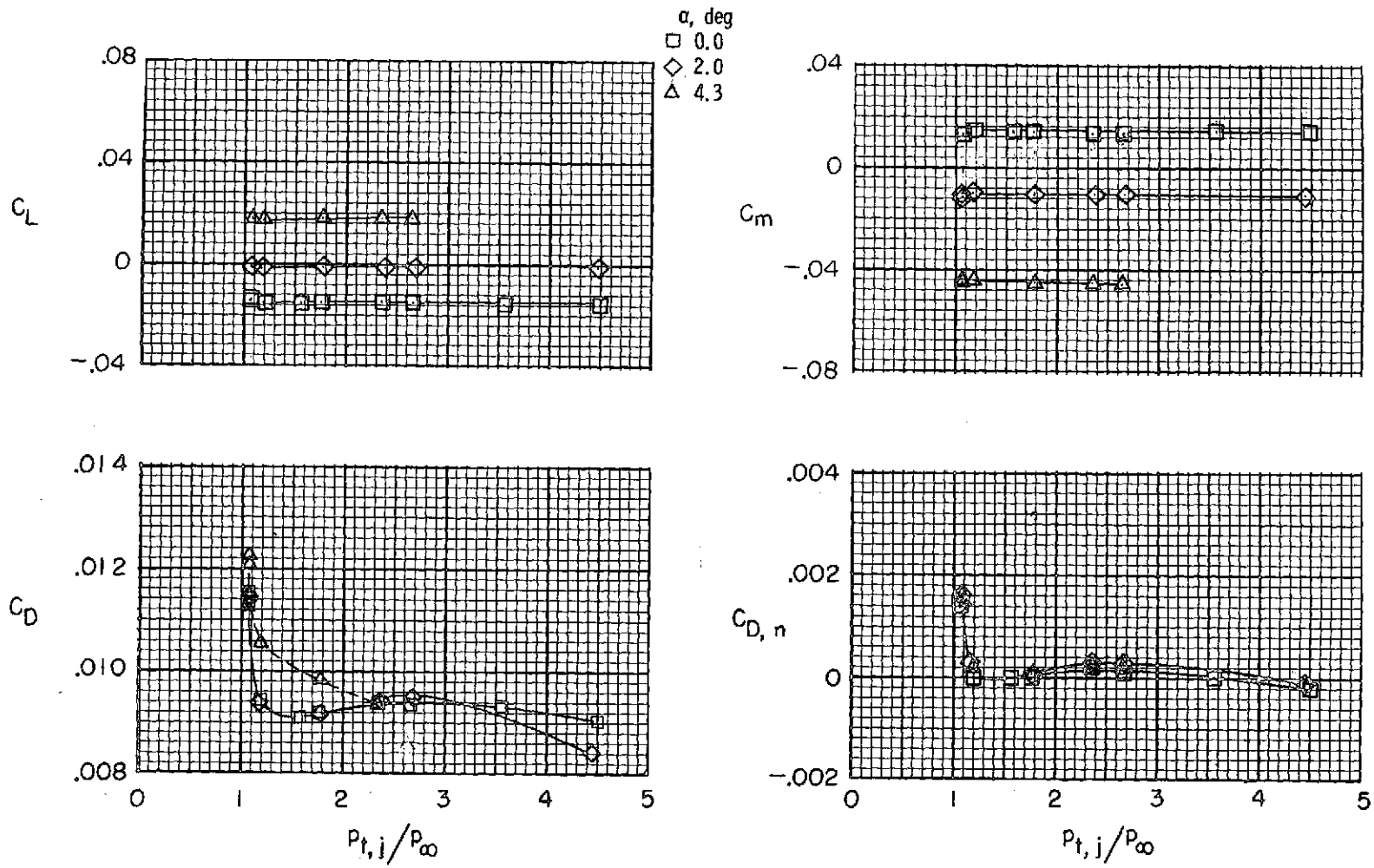

(c) M = 0.80.

Figure 21.- Continued.

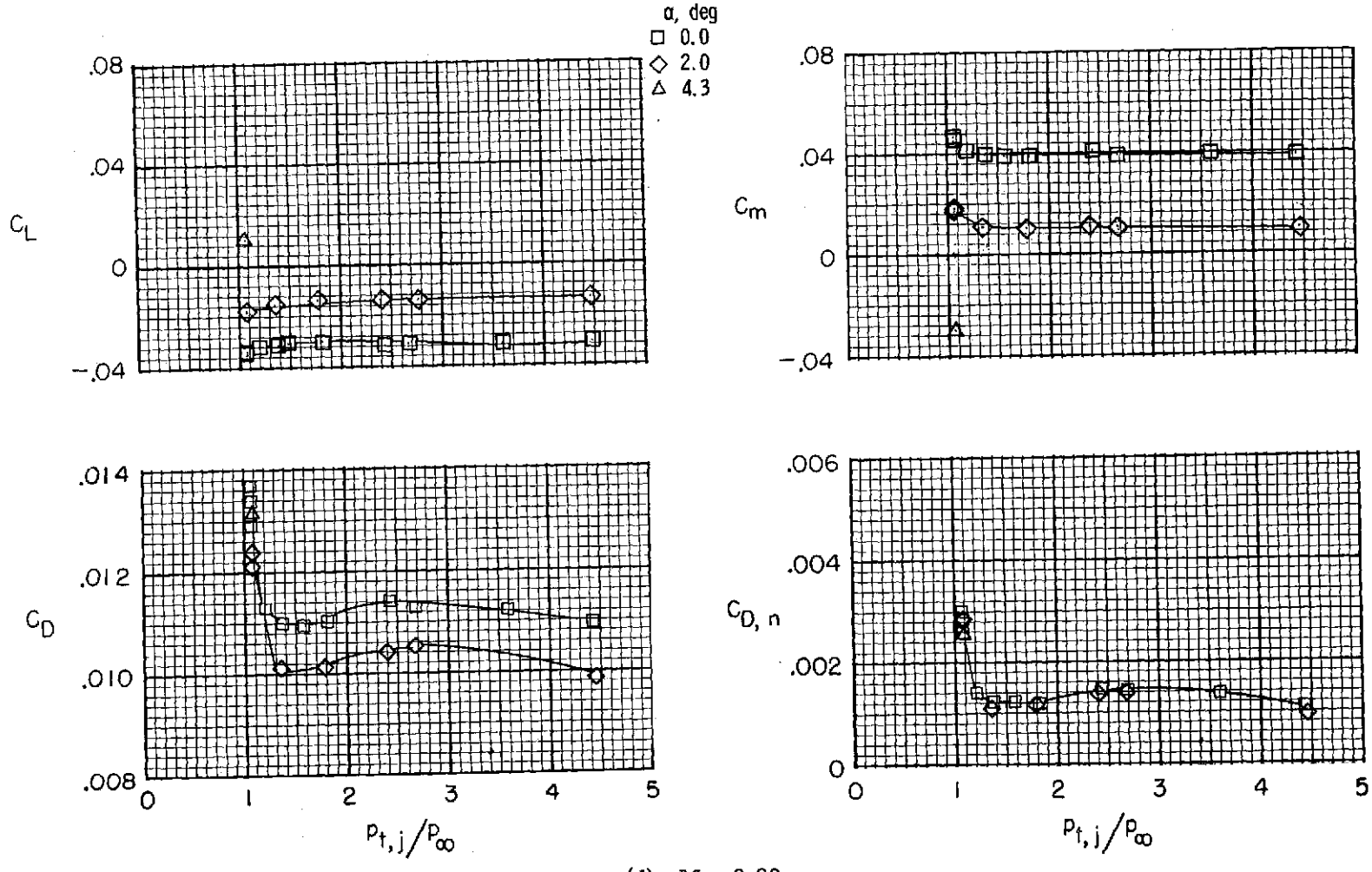

(d) M = 0.90.

Figure 21.- Concluded.

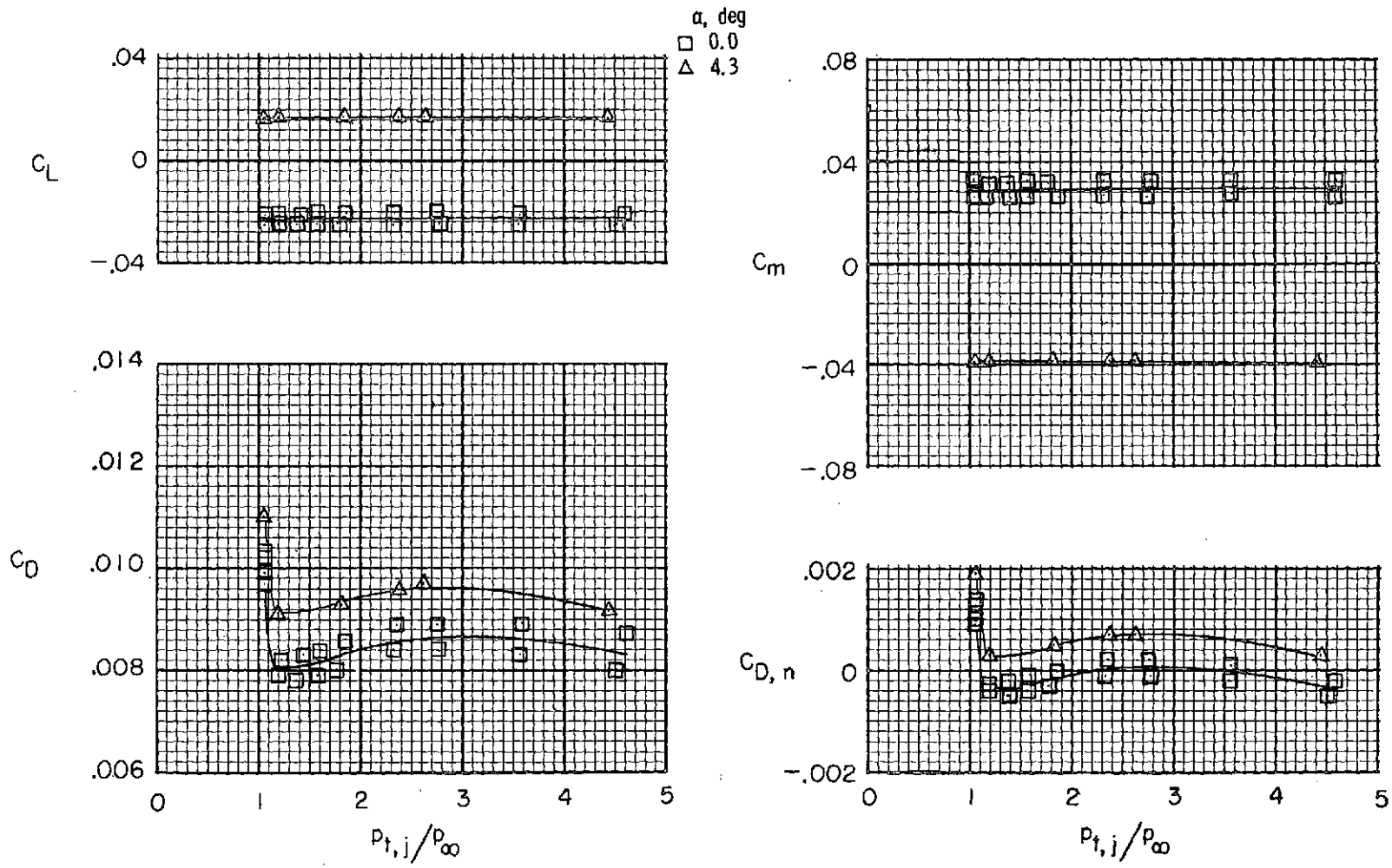

(a) M = 0.60.

Figure 22.- Effect of jet total-pressure ratio on afterbody-nozzle aerodynamic forces and moments for type B cruise nozzles and interfairing 6.

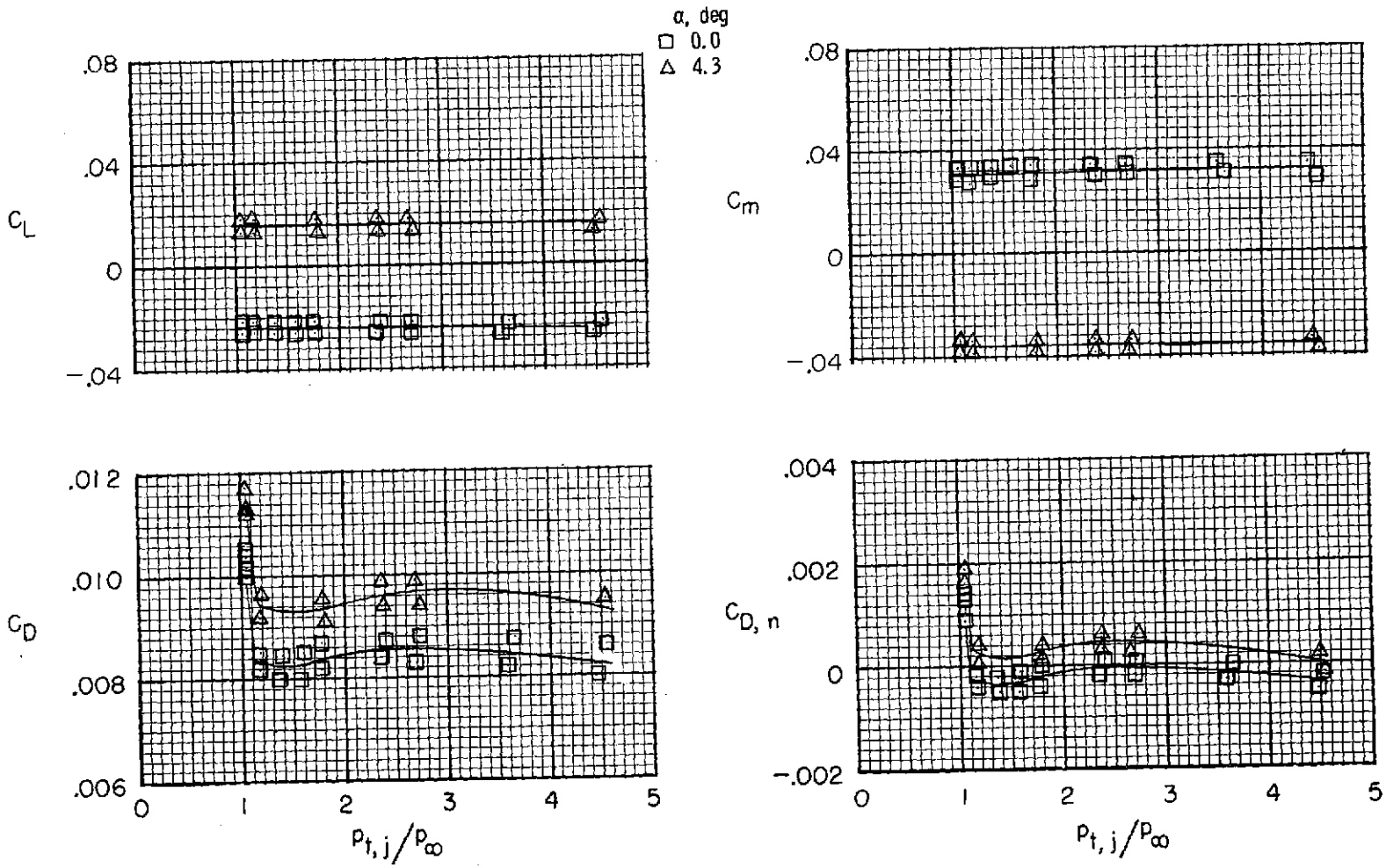

(b) M = 0.70.

Figure 22.- Continued.

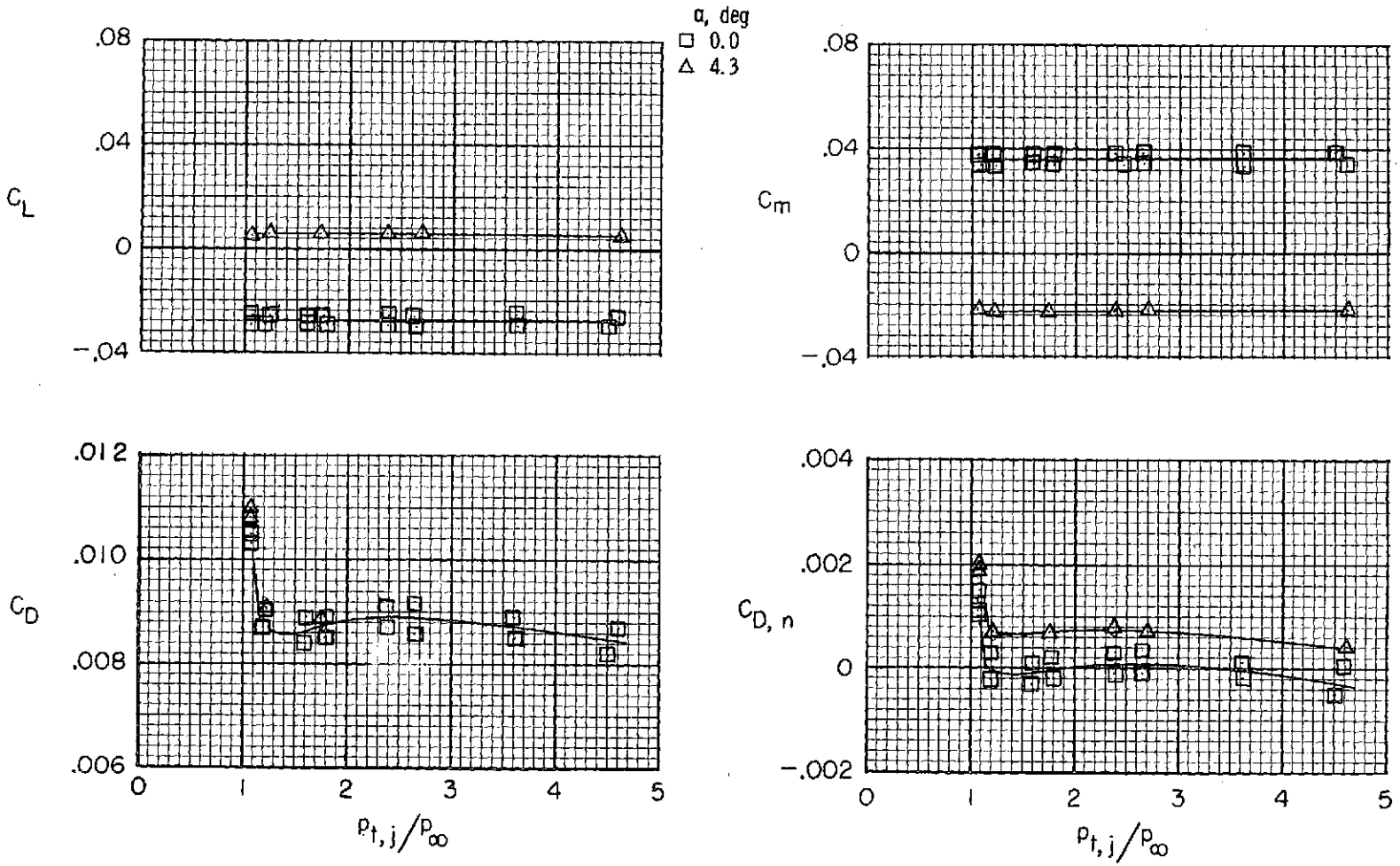

(c) M = 0.80.

Figure 22.- Continued.

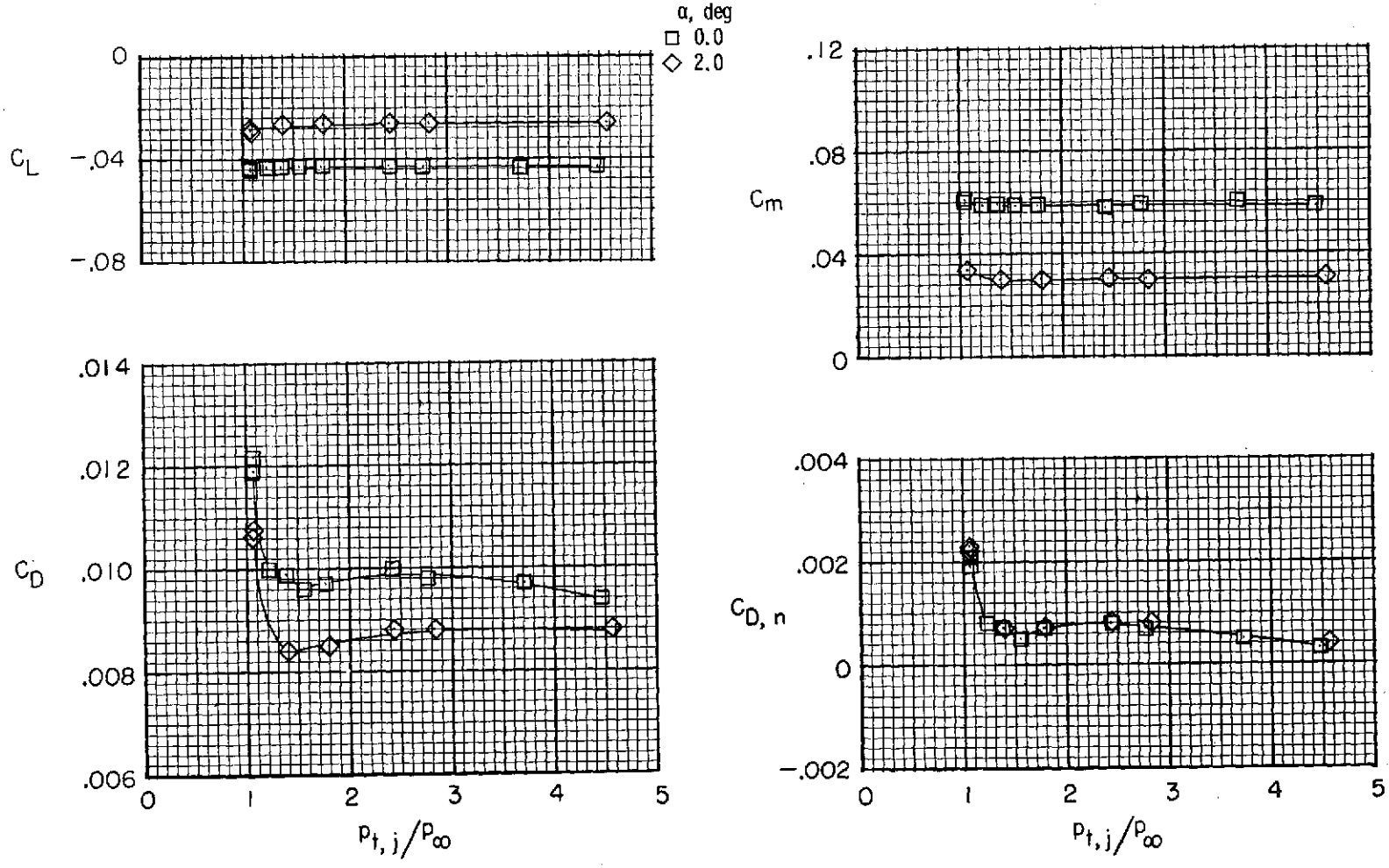

(d) M = 0.90.

Figure 22.- Concluded.

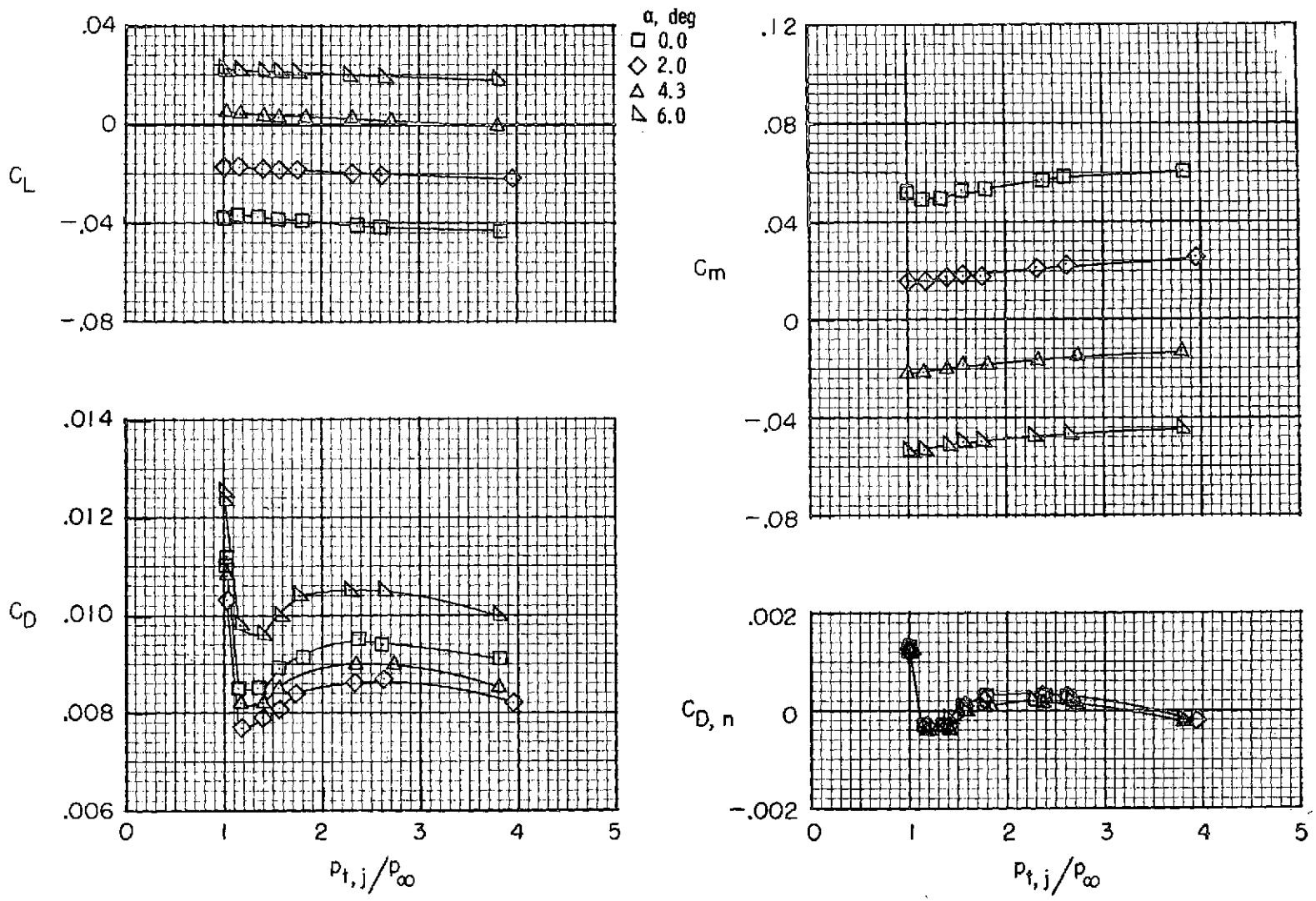

(a) M = 0.60.

Figure 23.- Effect of jet total-pressure ratio on afterbody-nozzle aerodynamic forces and moments for type B sea-level maximum afterburning nozzles and interfairing 2.

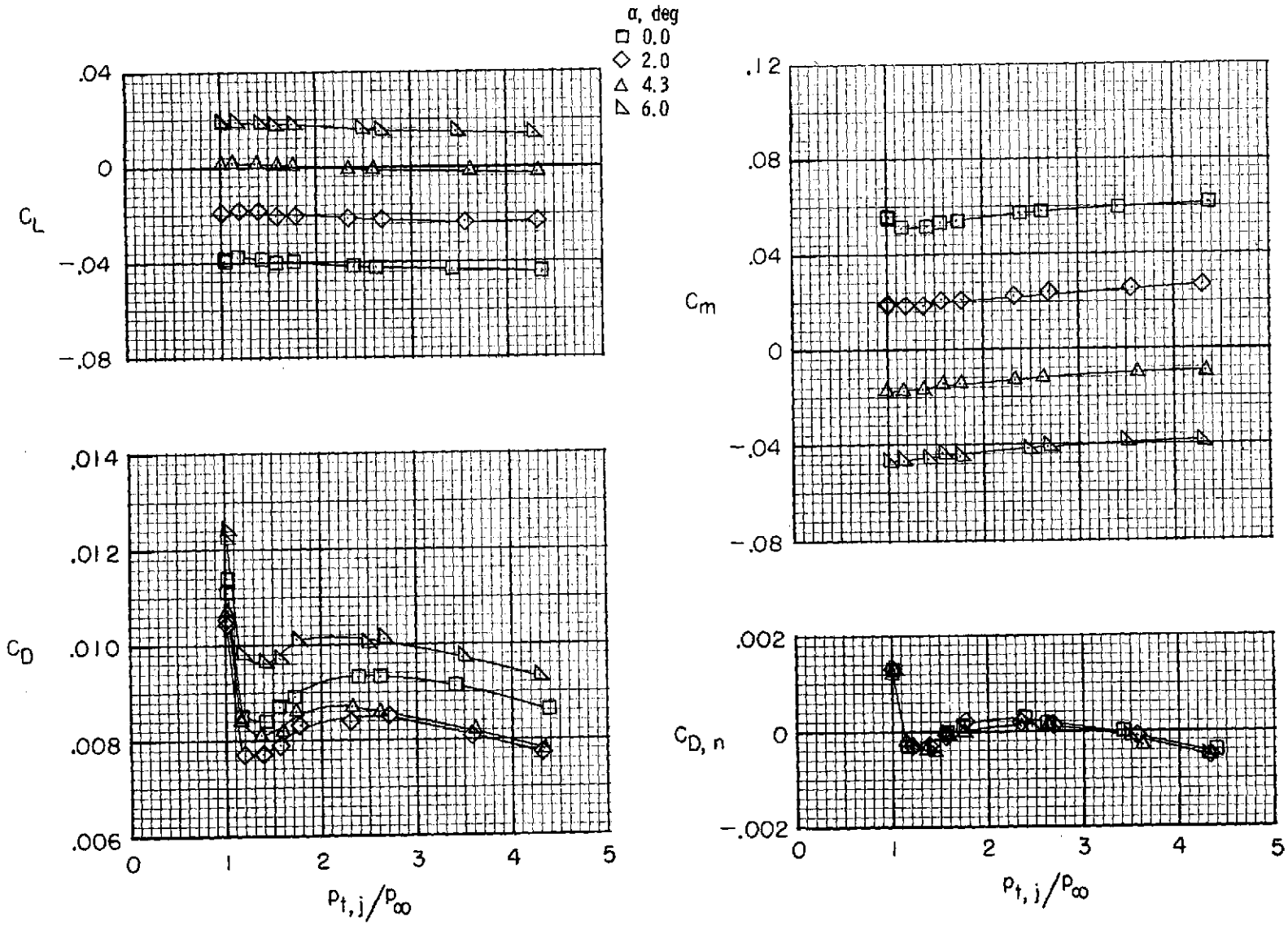

(b) M = 0.70.

Figure 23.- Continued.

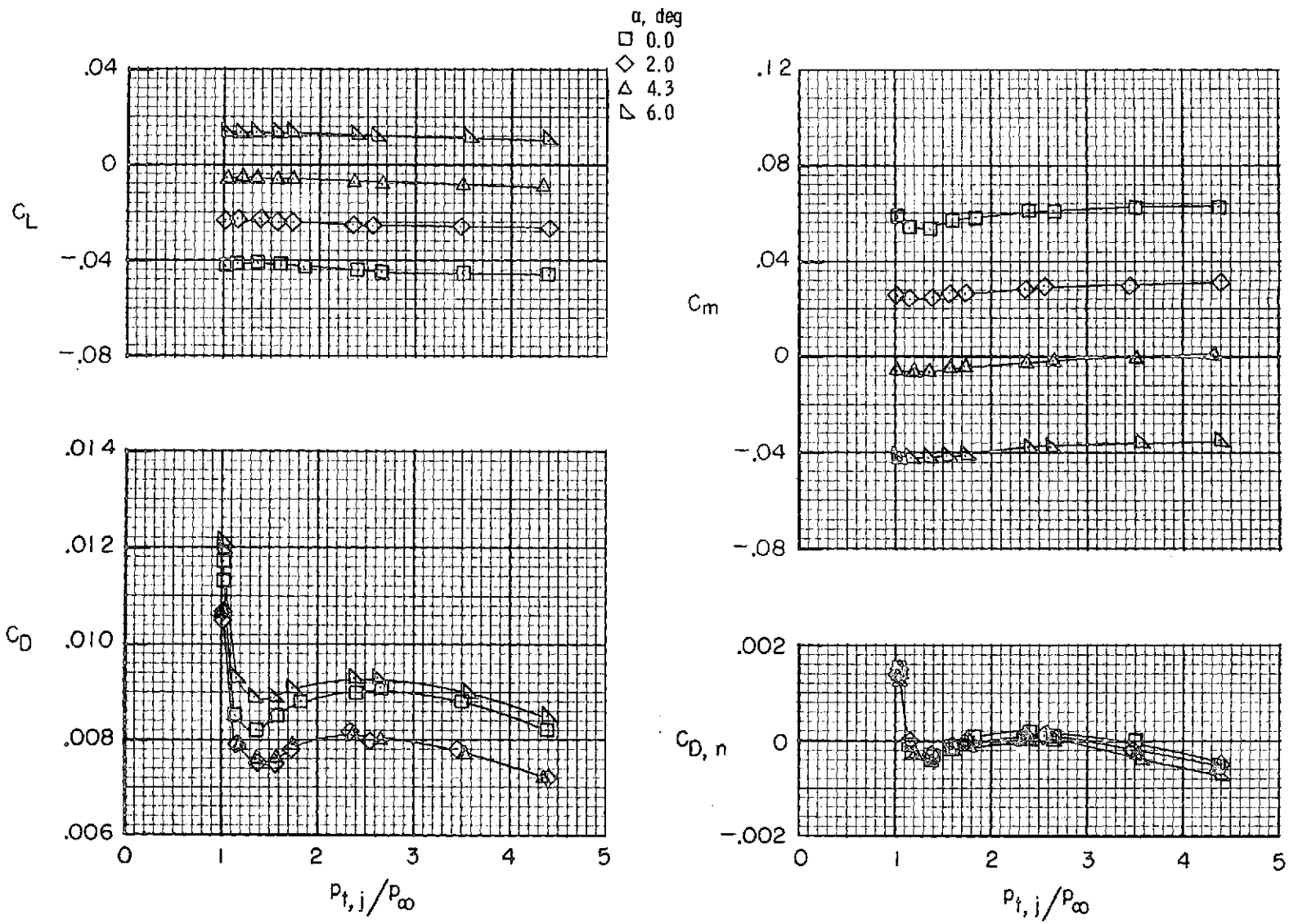

(c) M = 0.80.

Figure 23.- Continued.

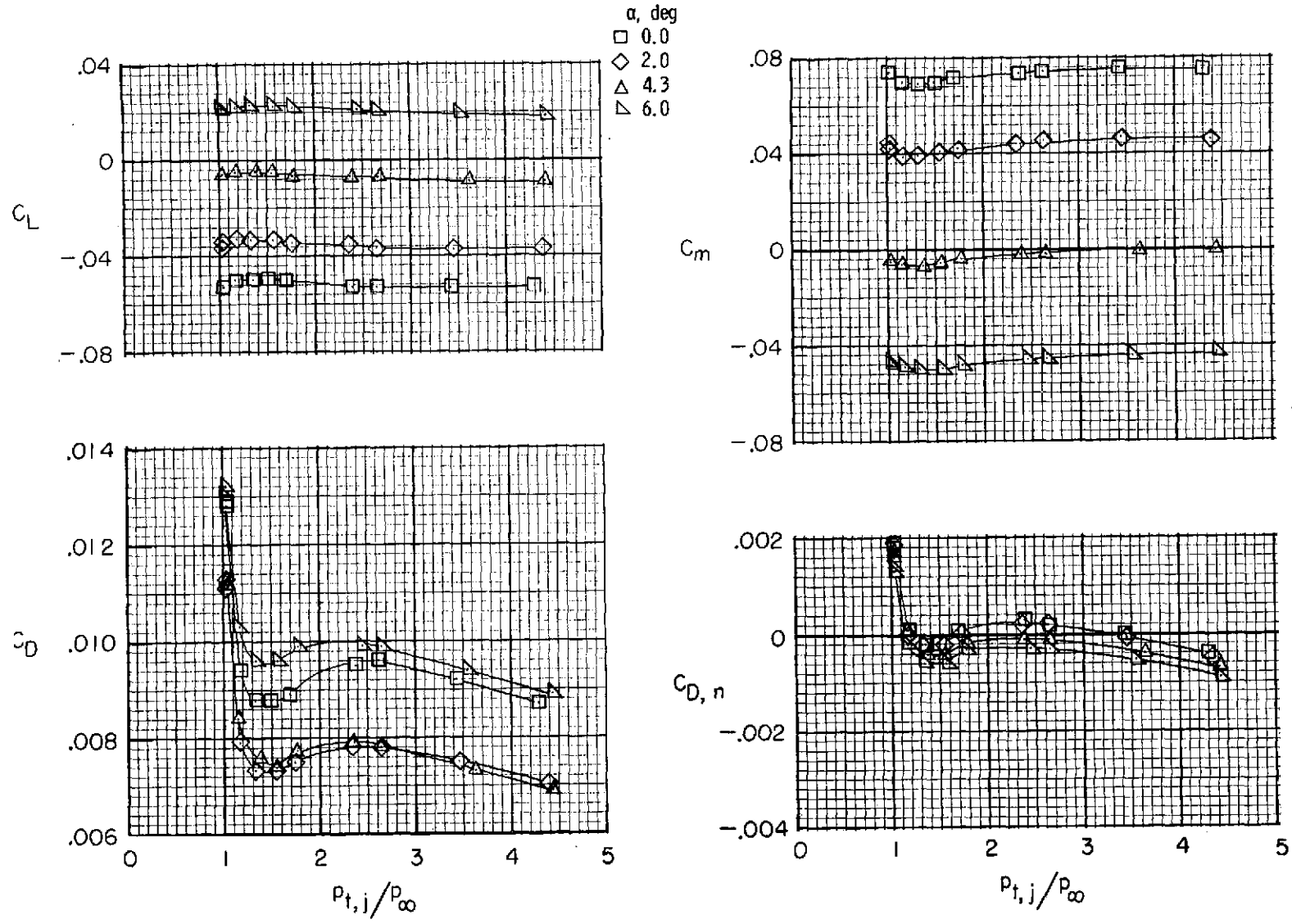

(d) M = 0.90.

Figure 23.- Concluded.

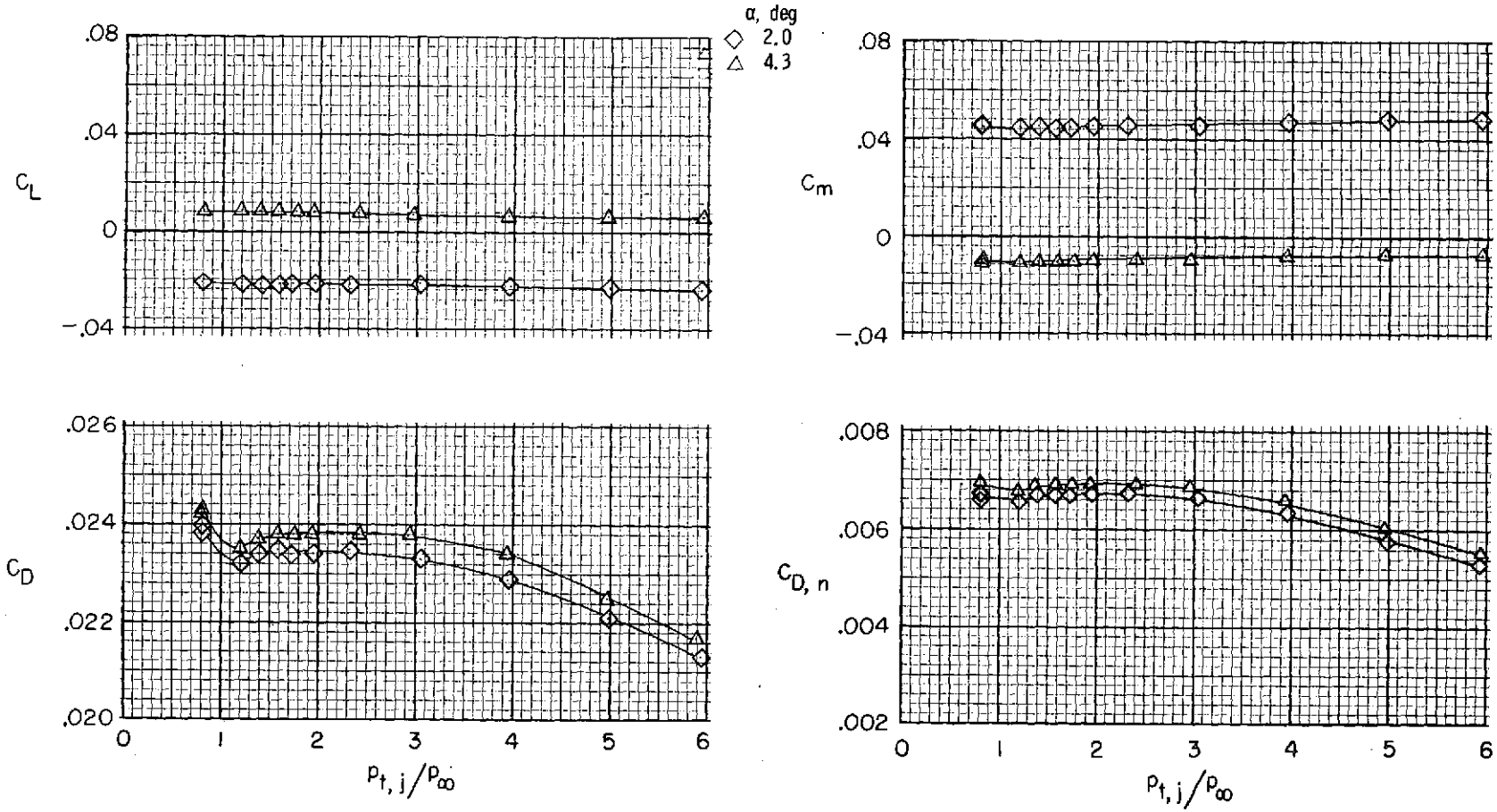

(a) M = 1.20.

Figure 24.- Effect of jet total-pressure ratio on afterbody-nozzle aerodynamic forces and moments for type B transonic maximum afterburning nozzles and interfairing 1.

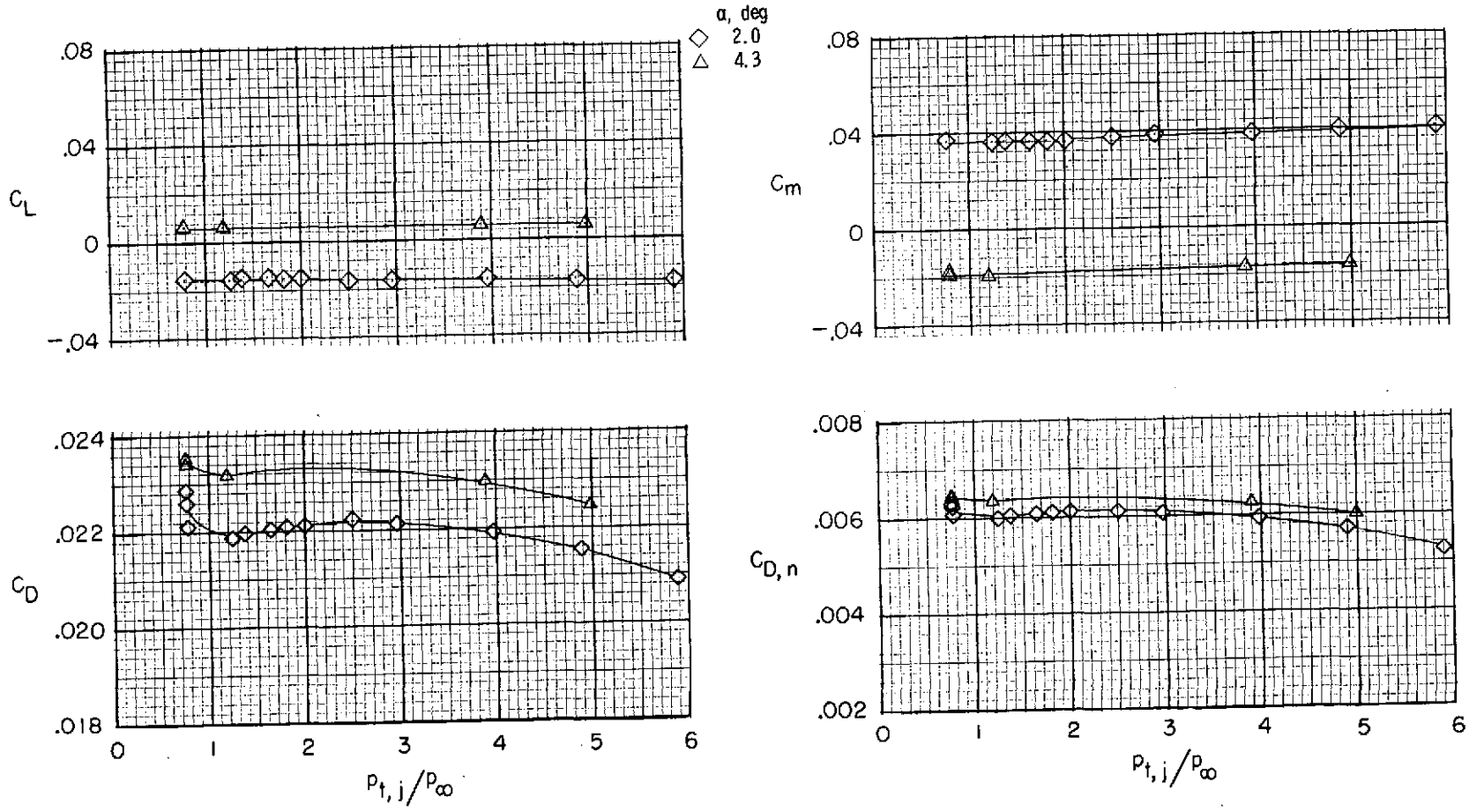

(b) M = 1.30.

Figure 24.- Concluded.

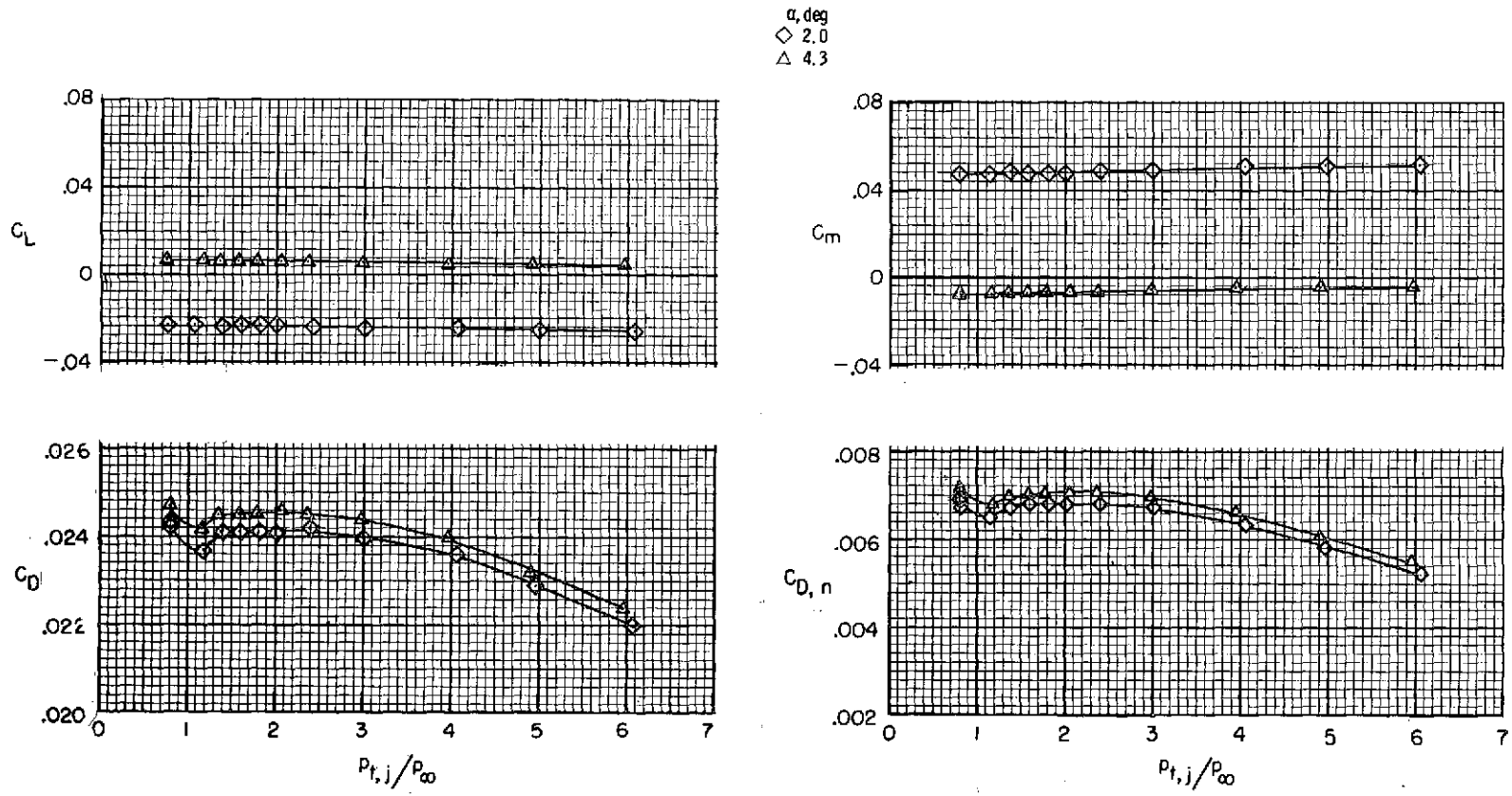

(a) M = 1.2.

Figure 25.- Effect of jet total-pressure ratio on afterbody-nozzle aerodynamic forces and moments for type B transonic maximum afterburning nozzles and interfairing 2.

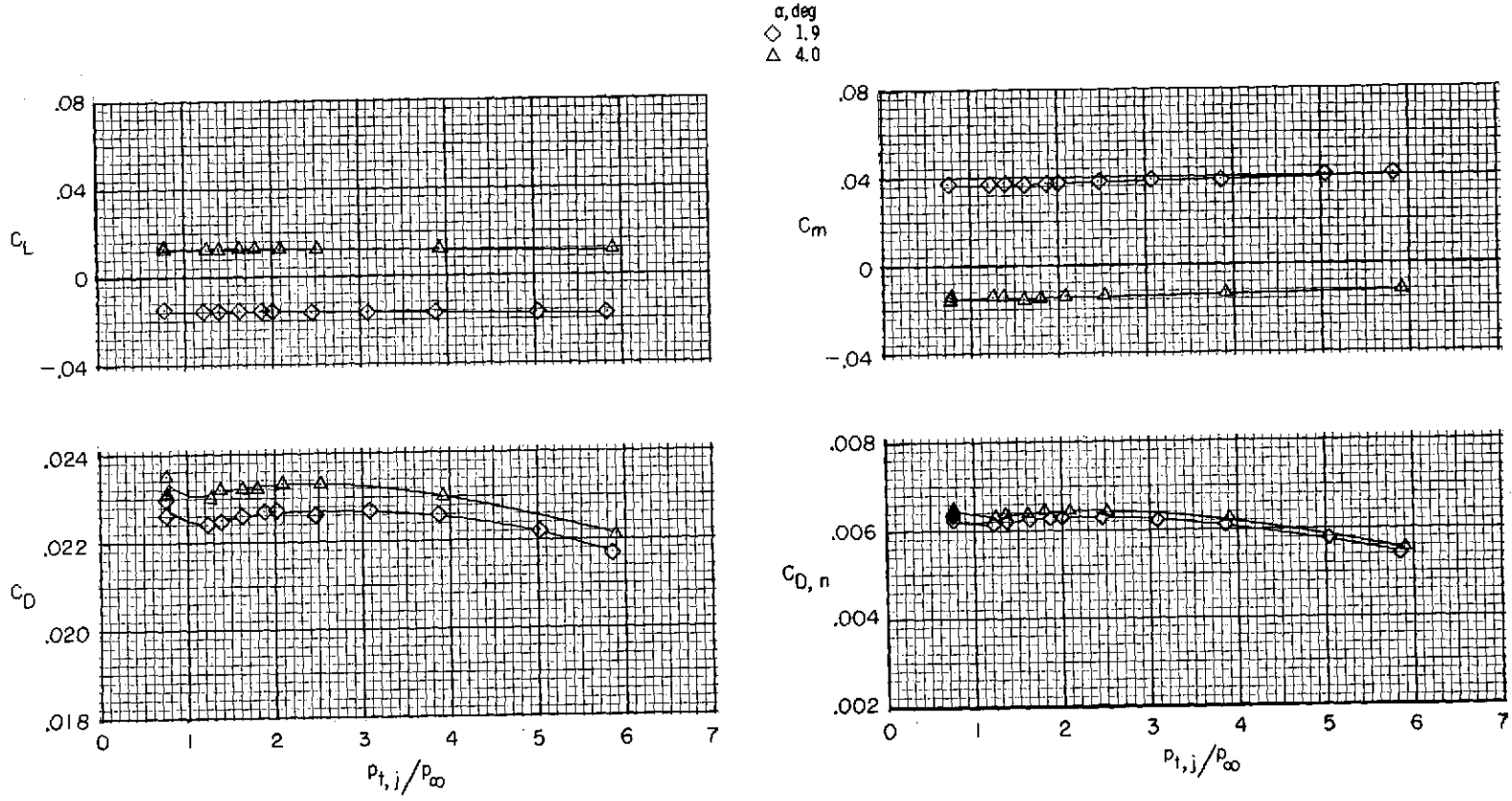

(b) M = 1.3.

Figure 25.- Concluded.

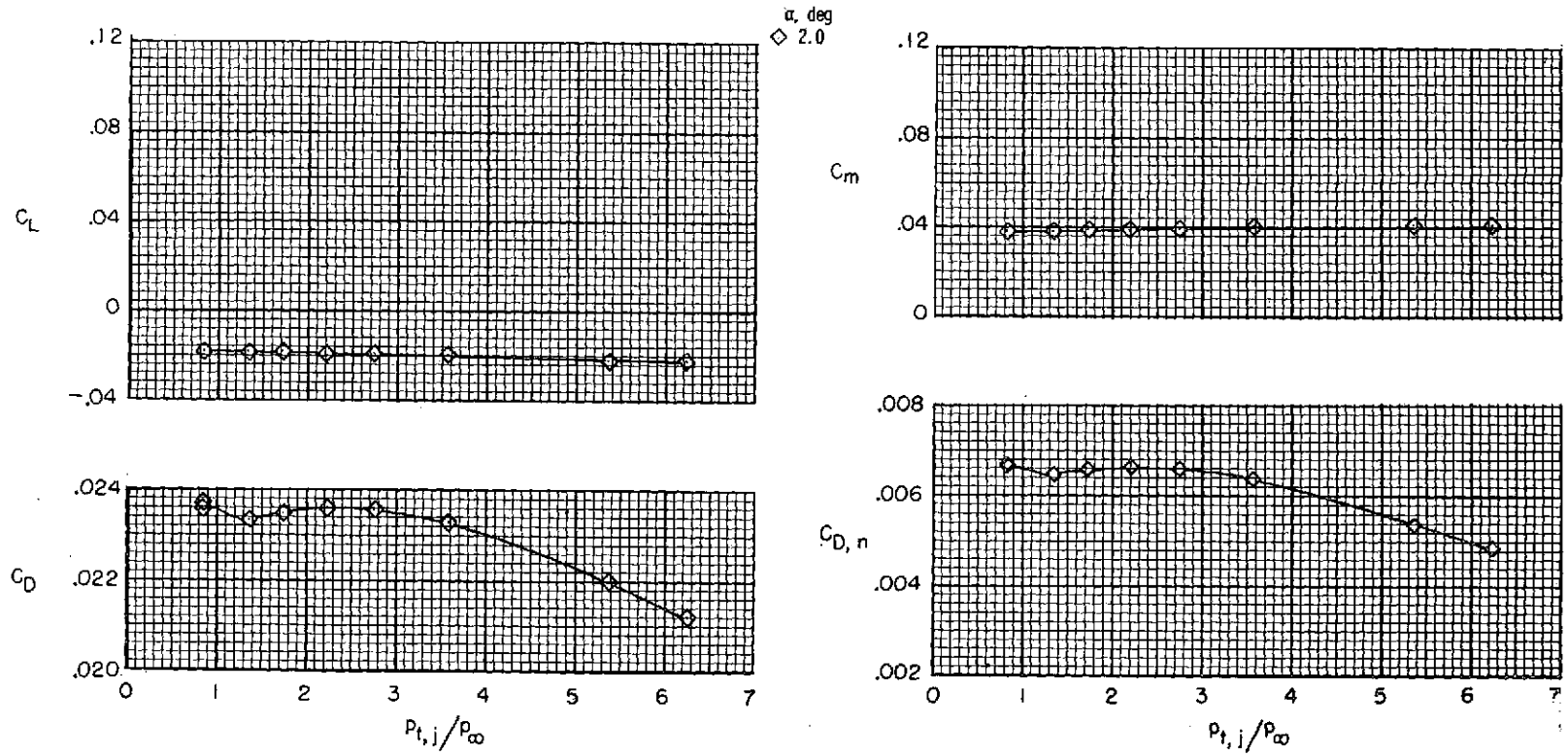

Figure 26.- Effect of jet total-pressure ratio on afterbody-nozzle aerodynamic forces and moments for type B transonic maximum afterburning nozzles and interfairing 4 at M = 1.20.

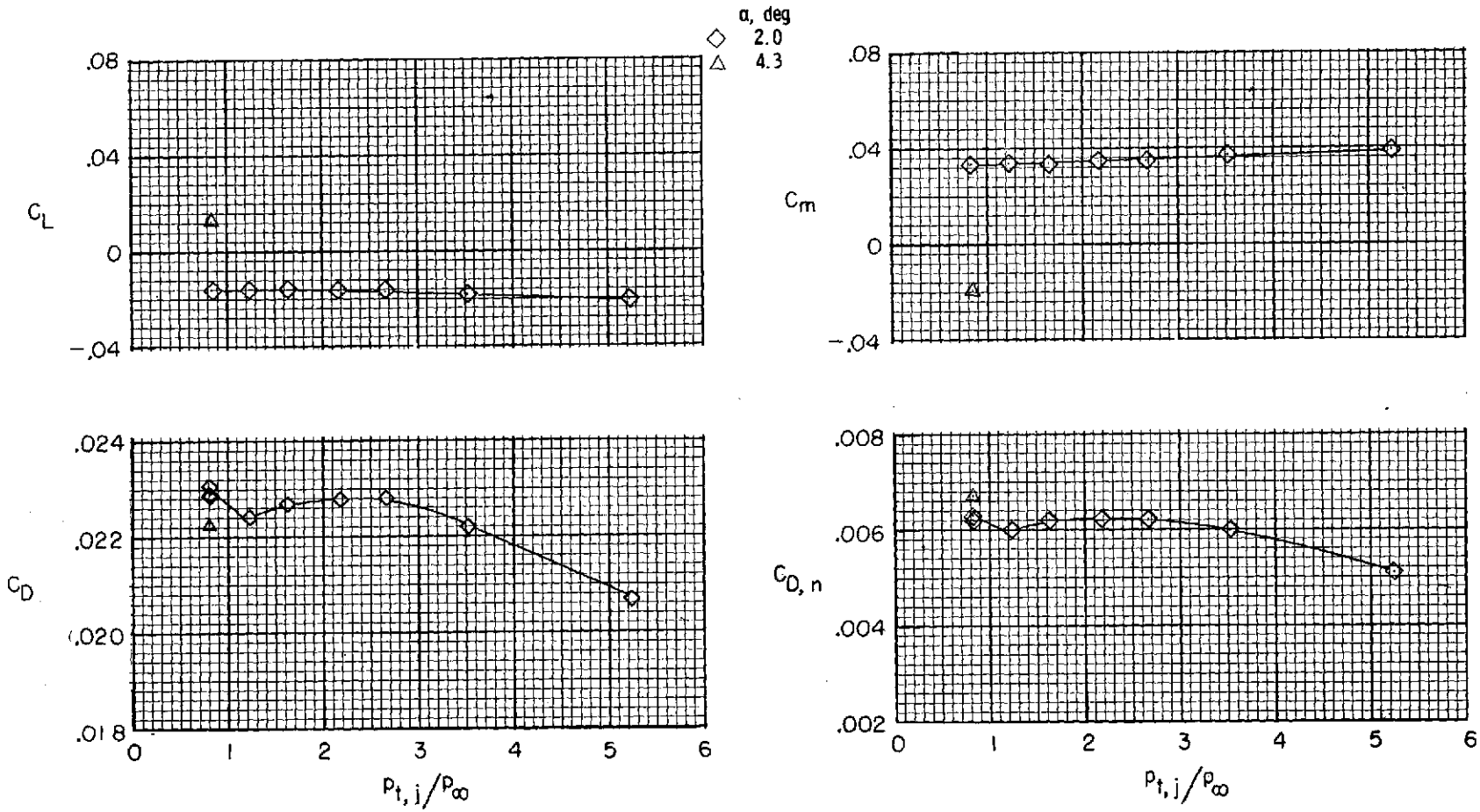

Figure 27.- Effect of jet total-pressure ratio on afterbody-nozzle aerodynamic forces and moments for type B transonic maximum afterburning nozzles and interfairing 6 at M = 1.20.

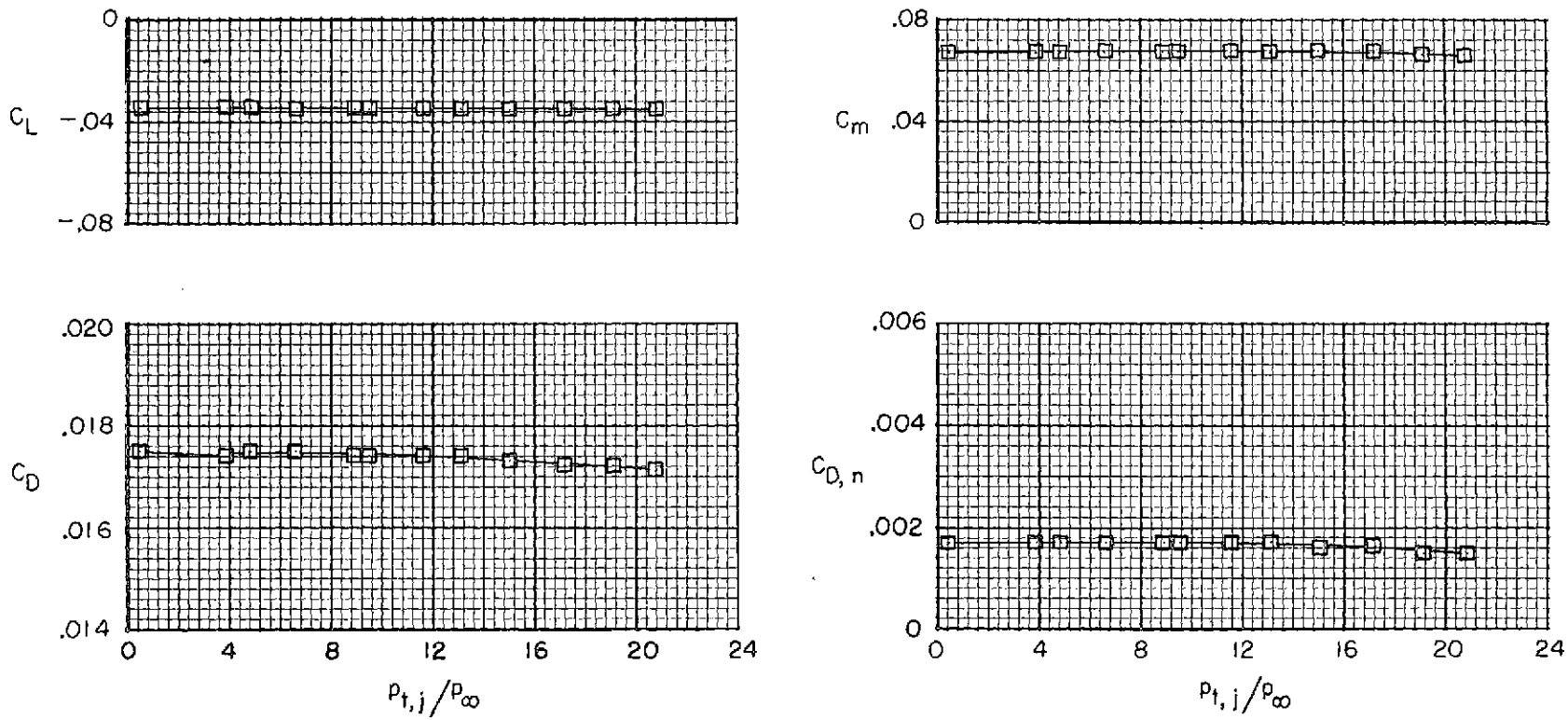

Figure 28.- Effect of jet total-pressure ratio on afterbody-nozzle aerodynamic forces and moments for type B supersonic maximum afterburning nozzles and interfairing 2 at M = 2.20.

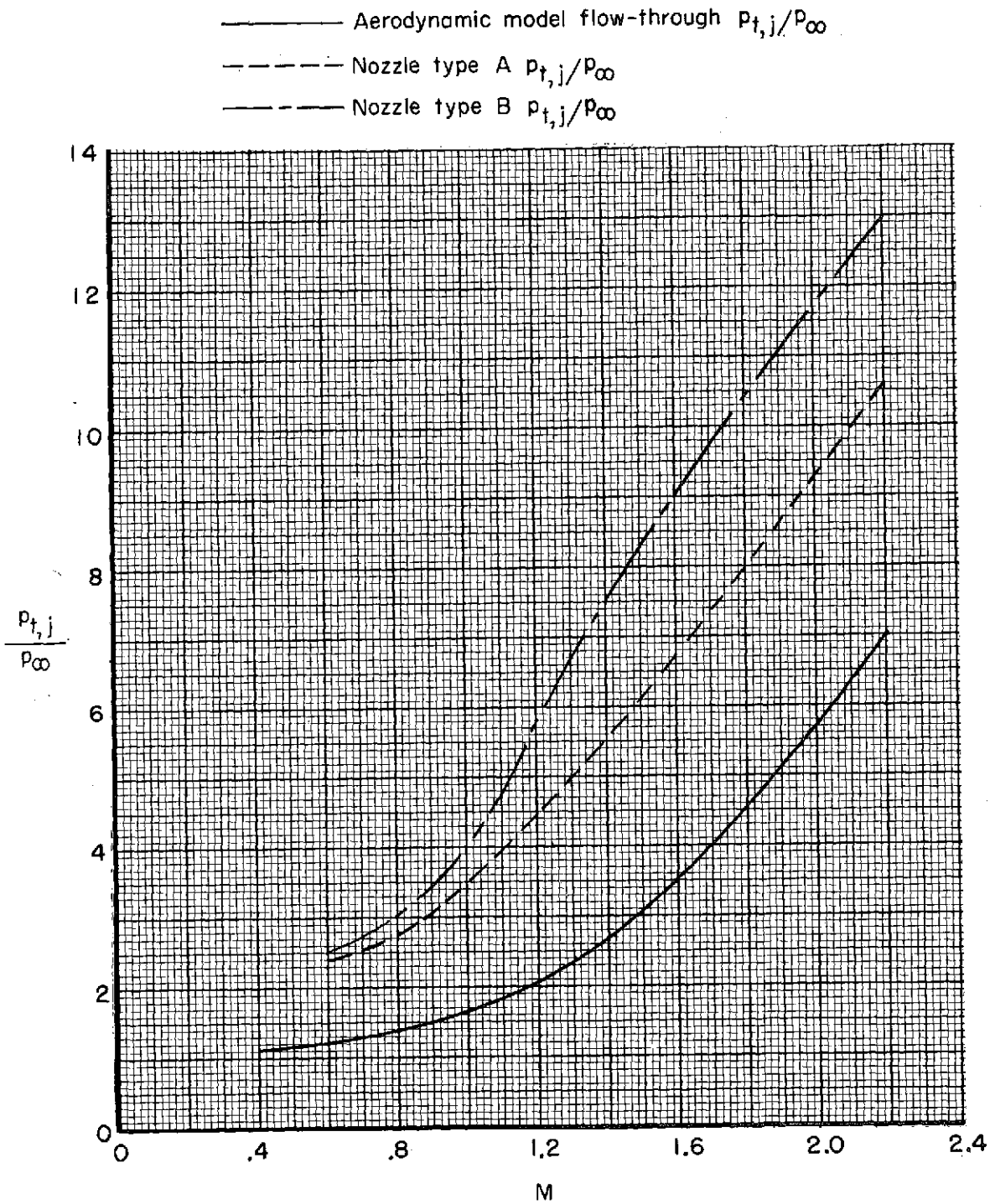

Figure 29.- Typical schedules of aerodynamic model flow-through and engine total-pressure ratios.

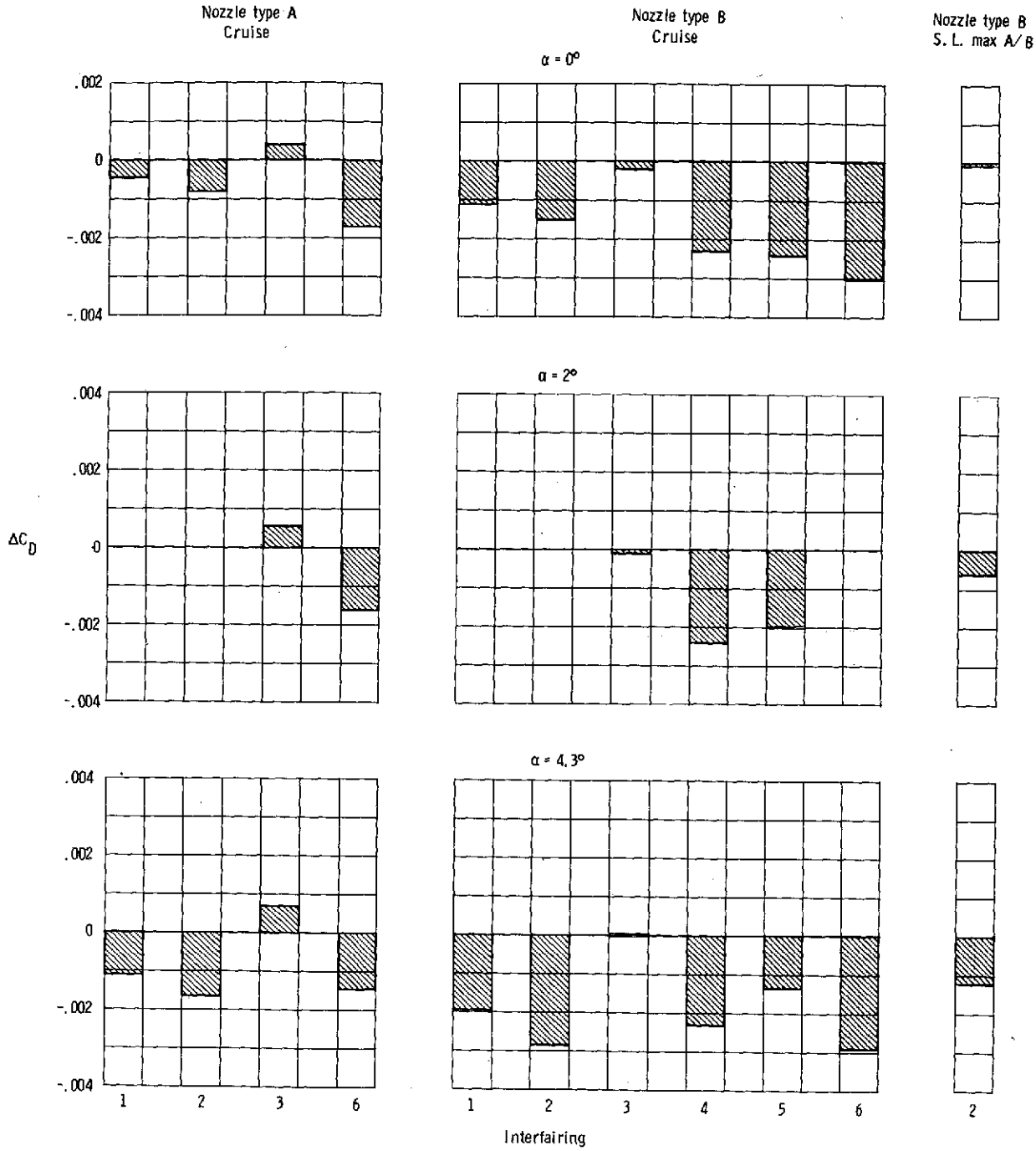

(a) M = 0.60.

Figure 30.- Afterbody-nozzle drag increment due to changing from basic interfairing to various modified interfairings.

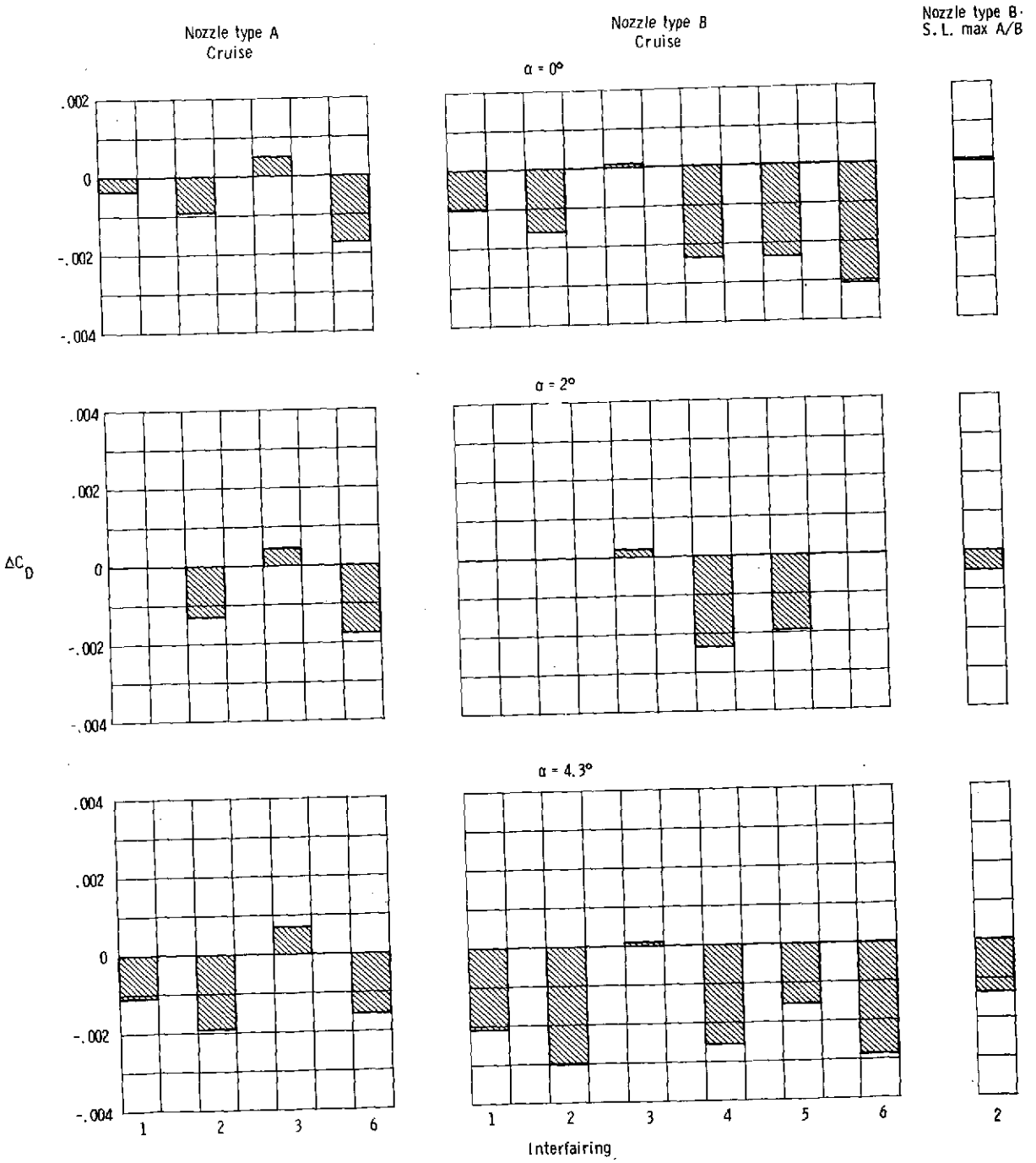

(b) M = 0.70.

Figure 30.- Continued.

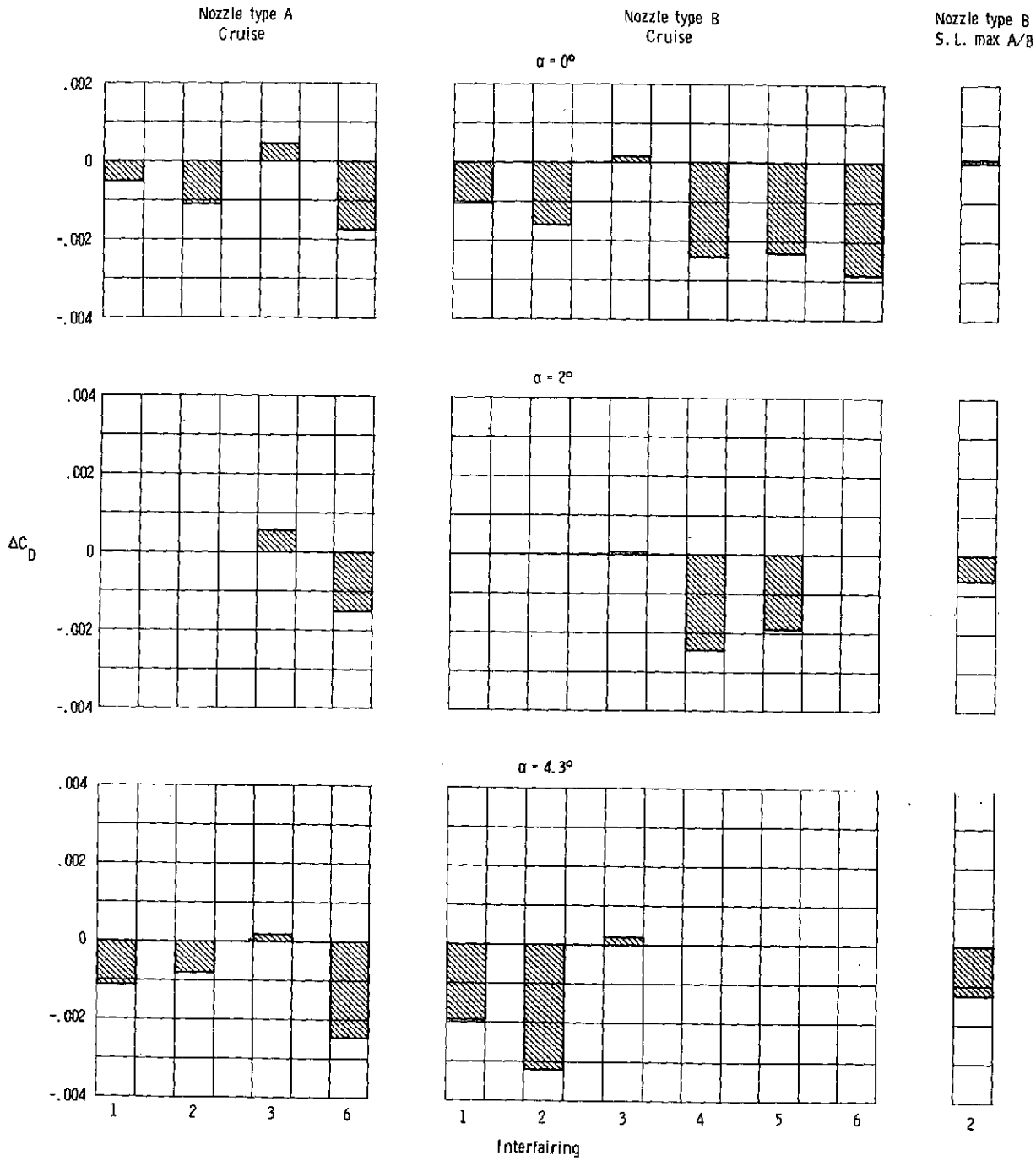

(c) M = 0.80.

Figure 30.- Continued.

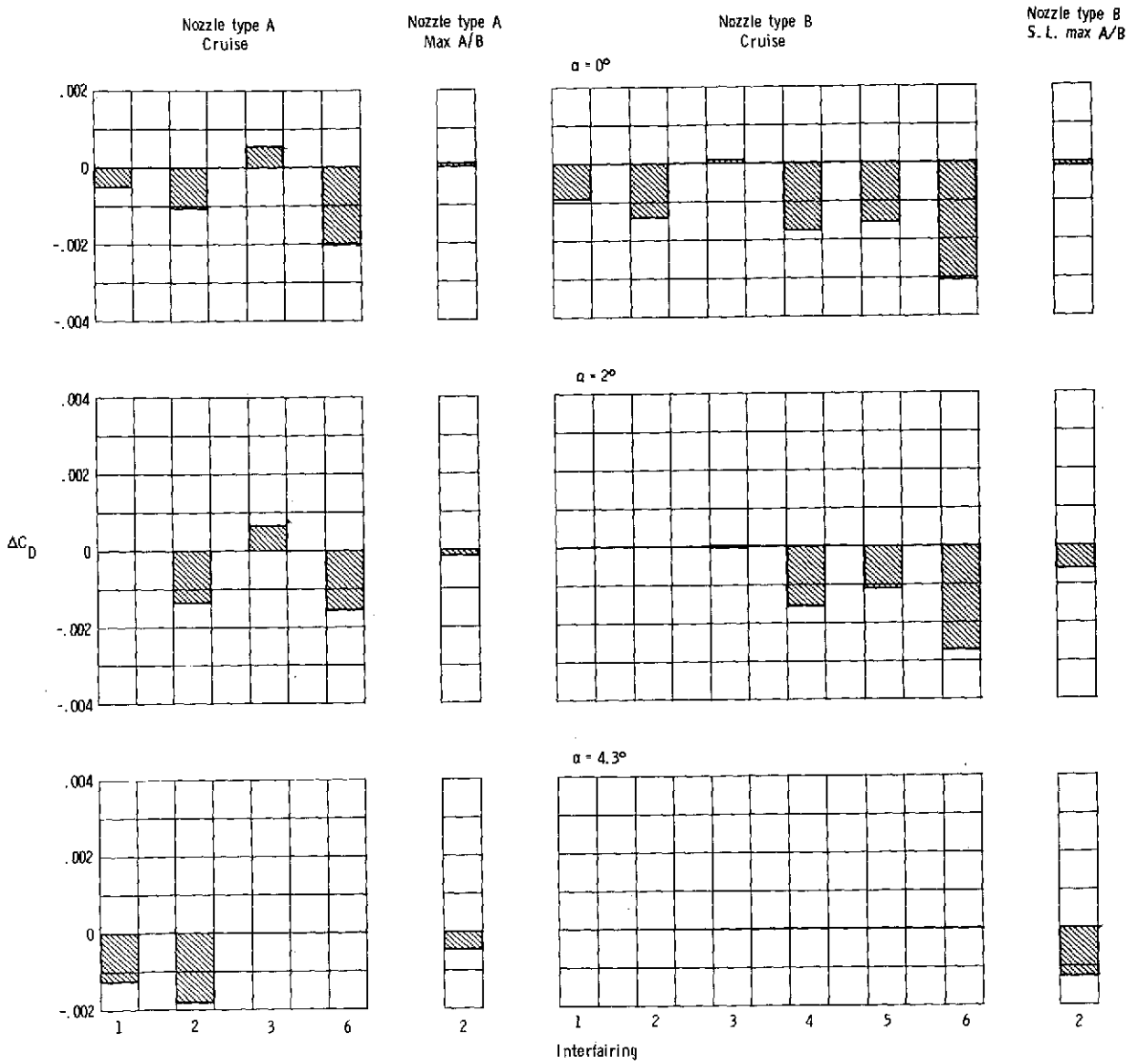

(d) M = 0.90.

Figure 30.- Concluded.

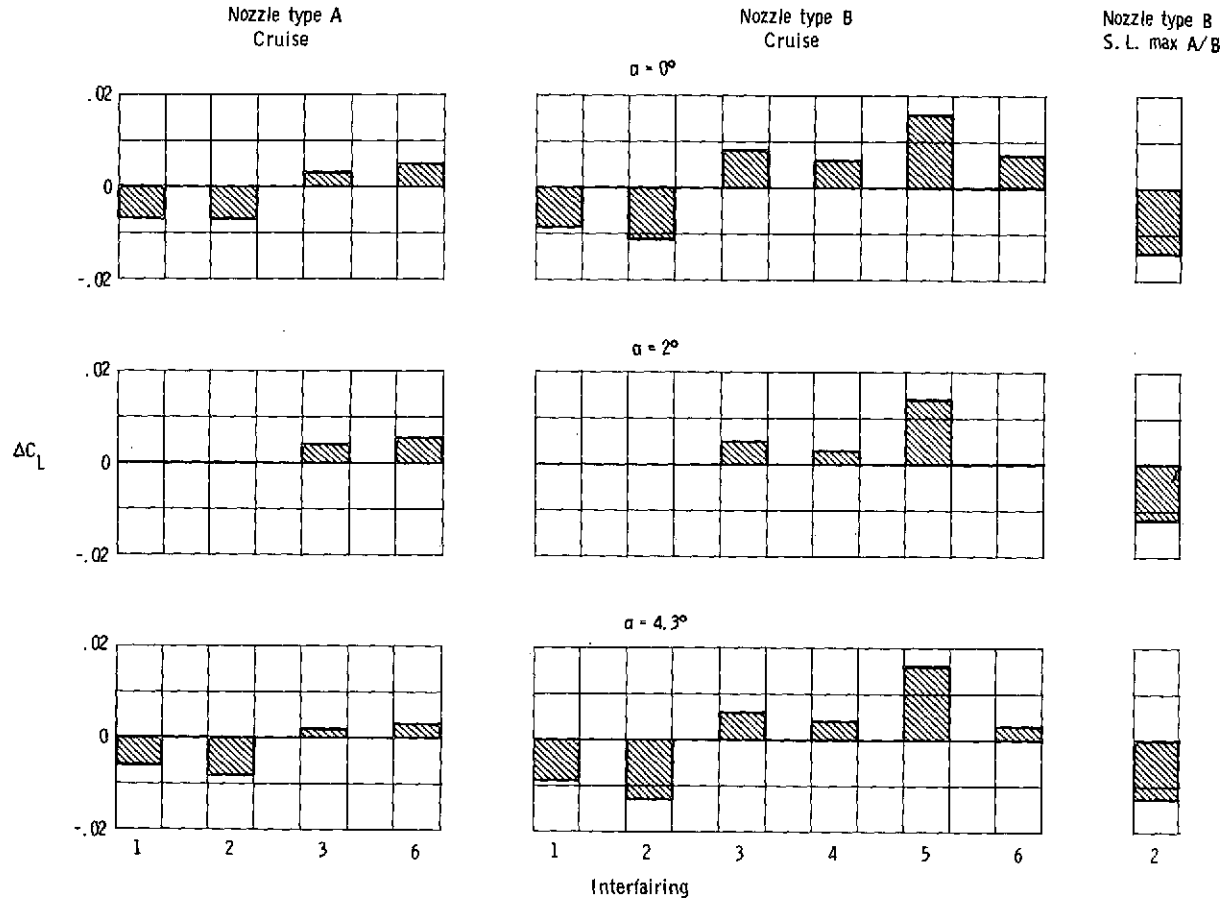

(a) M = 0.60.

Figure 31.- Afterbody-nozzle lift increment due to changing from basic interfairing to various modified interfairings.

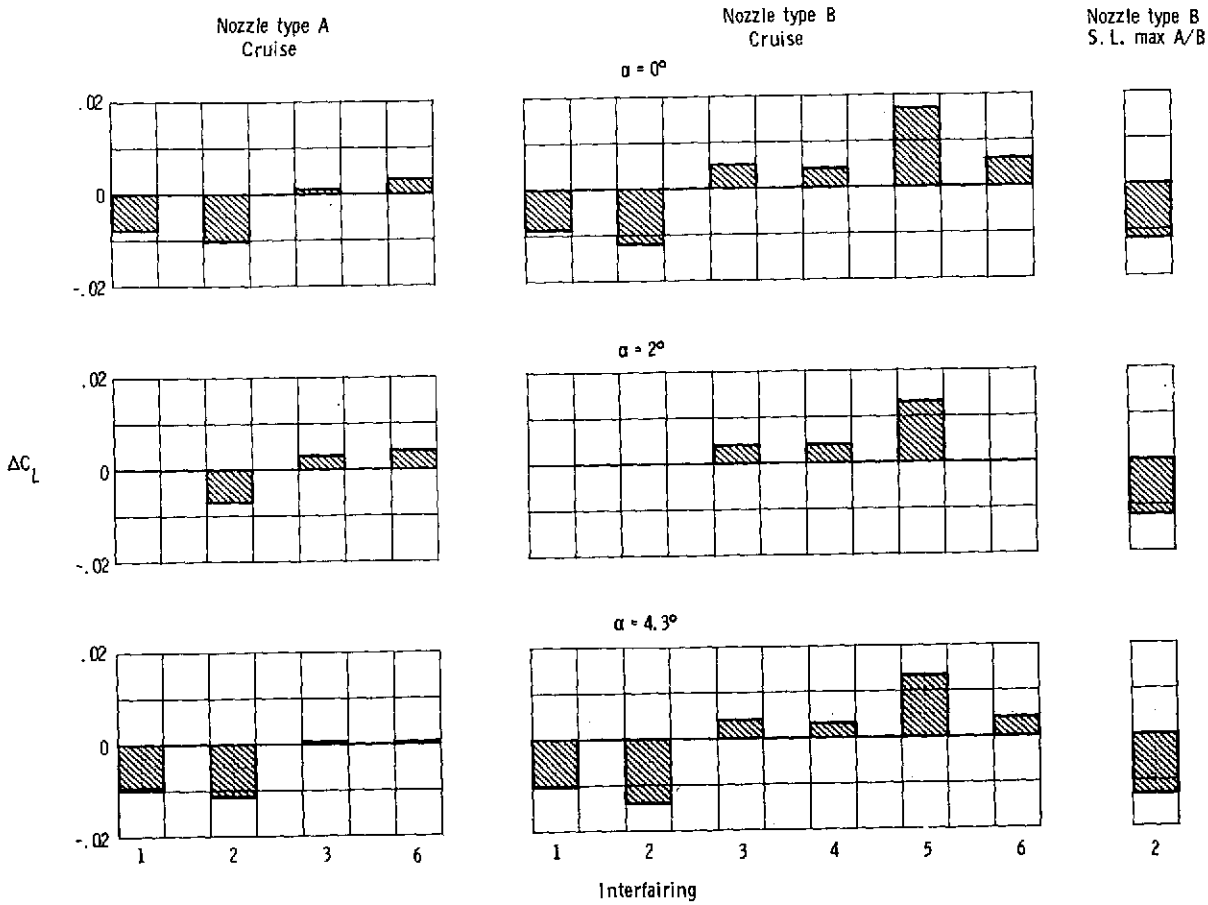

(b) M = 0.70.

Figure 31.- Continued.

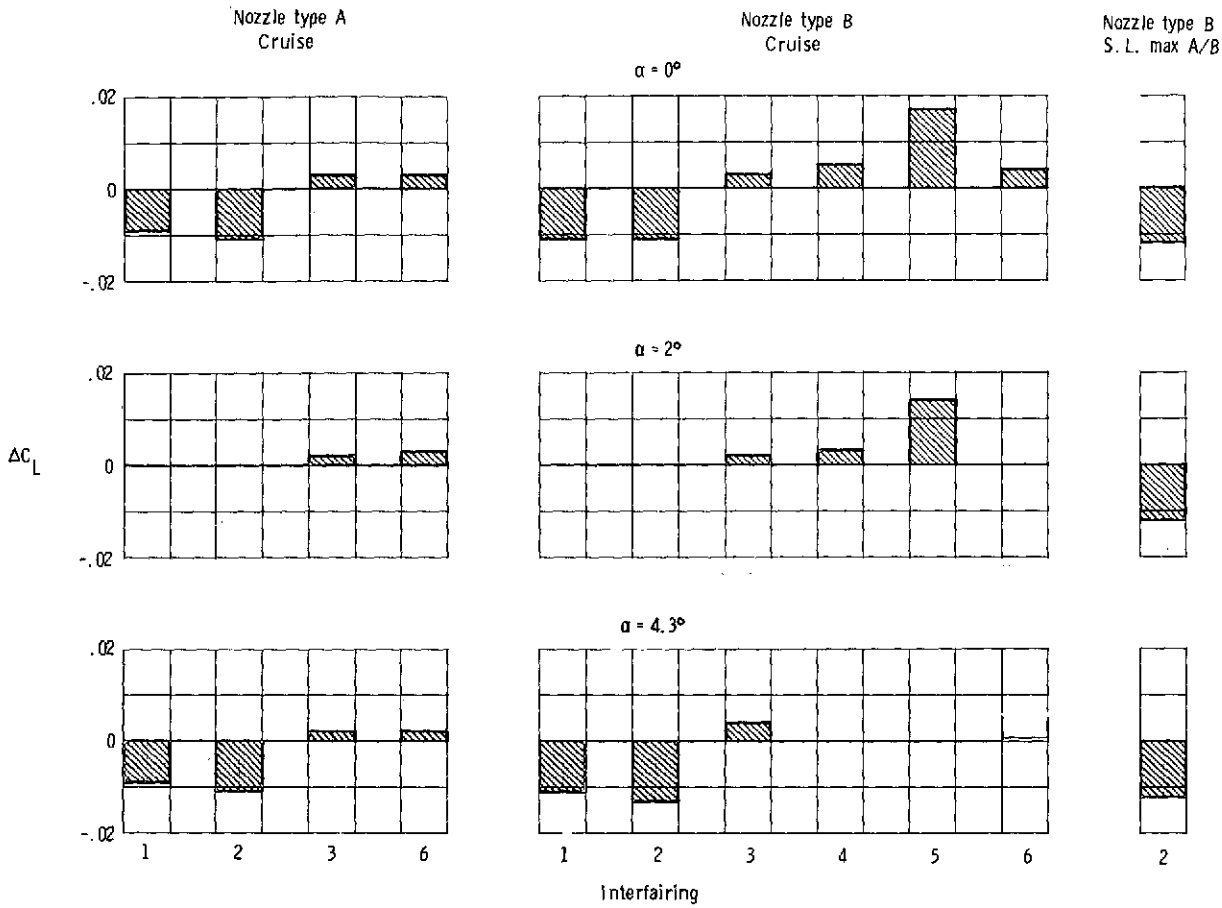

(c) M = 0.80.

Figure 31.- Continued.

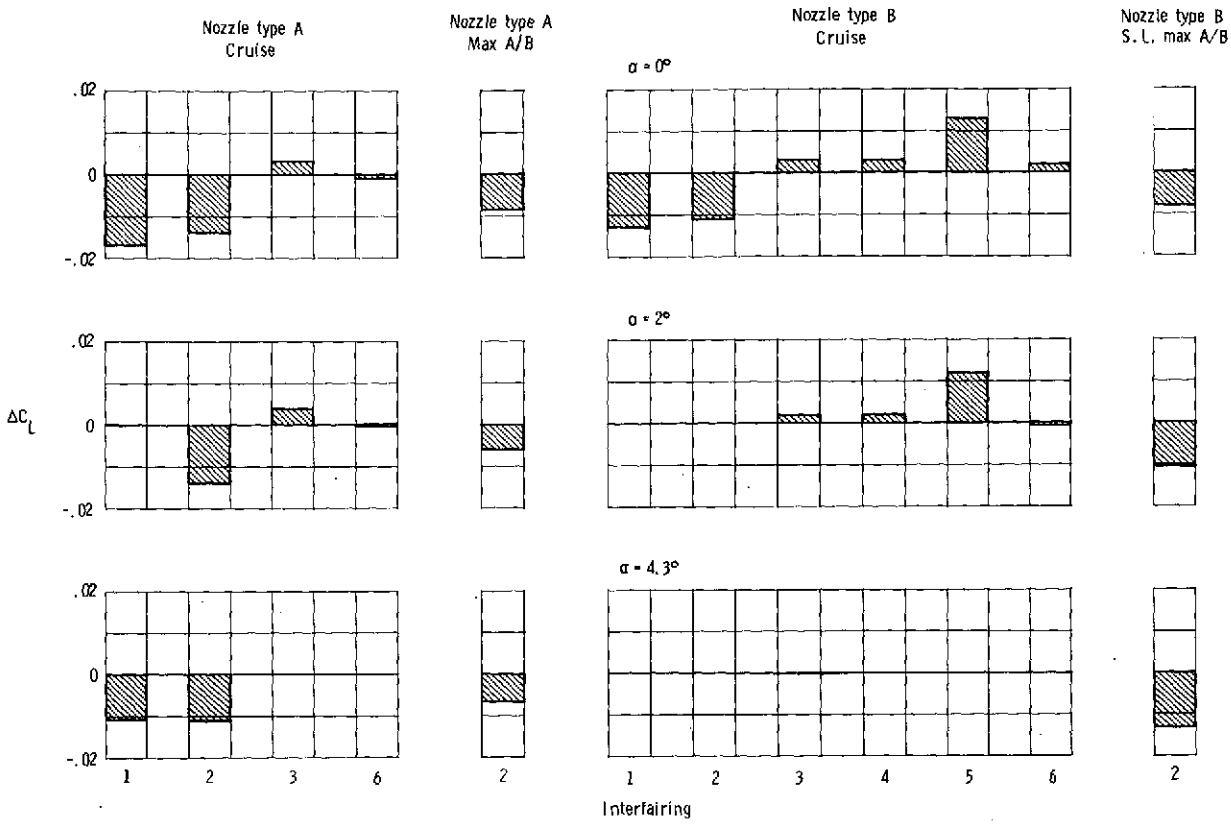

(d) M = 0.90.

Figure 31.- Concluded.

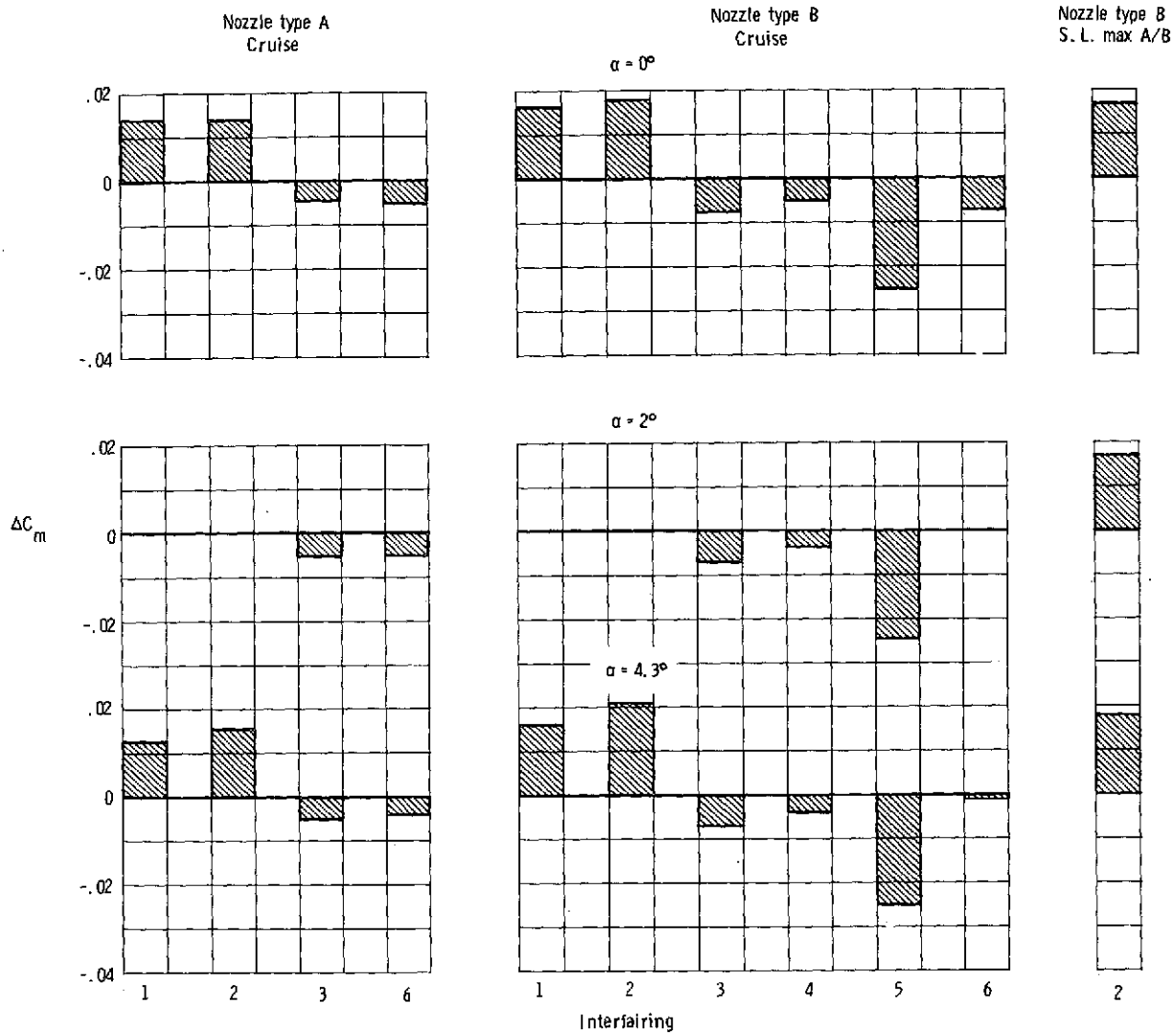

(a) M = 0.60.

Figure 32.- Afterbody-nozzle pitching-moment increment due to changing from basic interfairing to various modified interfairings.

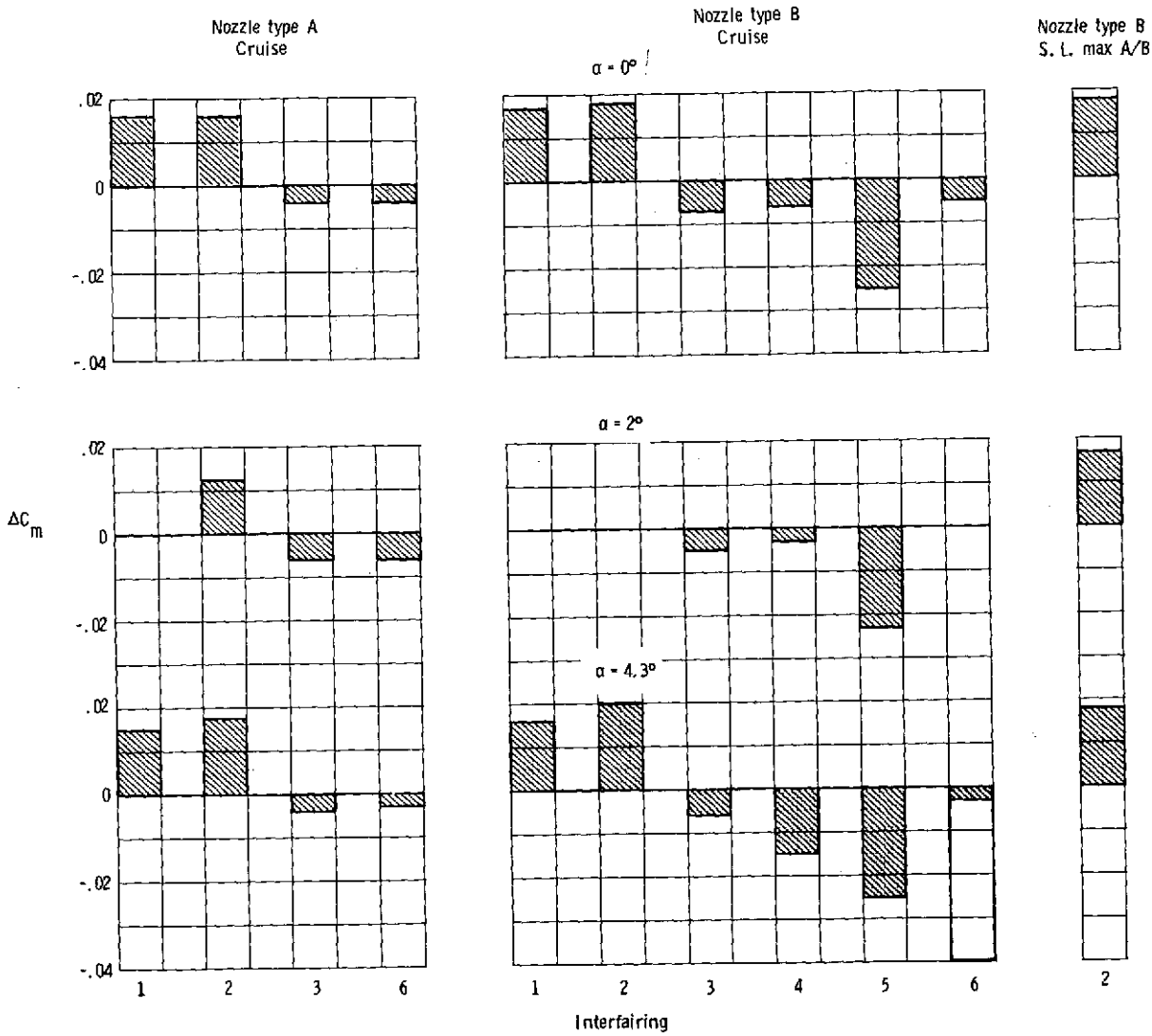

(b) M = 0.70.

Figure 32.- Continued.

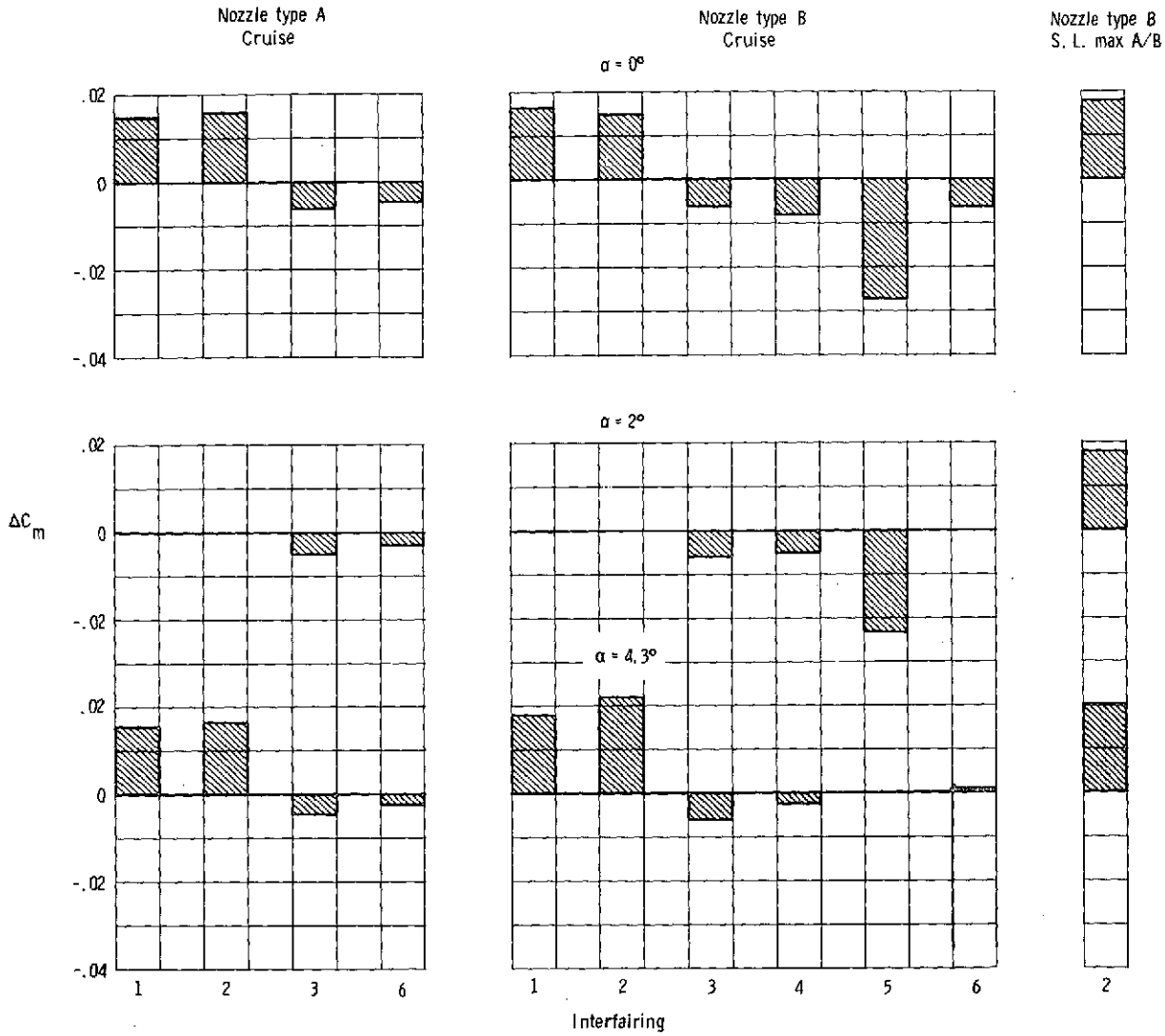

(c) M = 0.80.

Figure 32.- Continued.

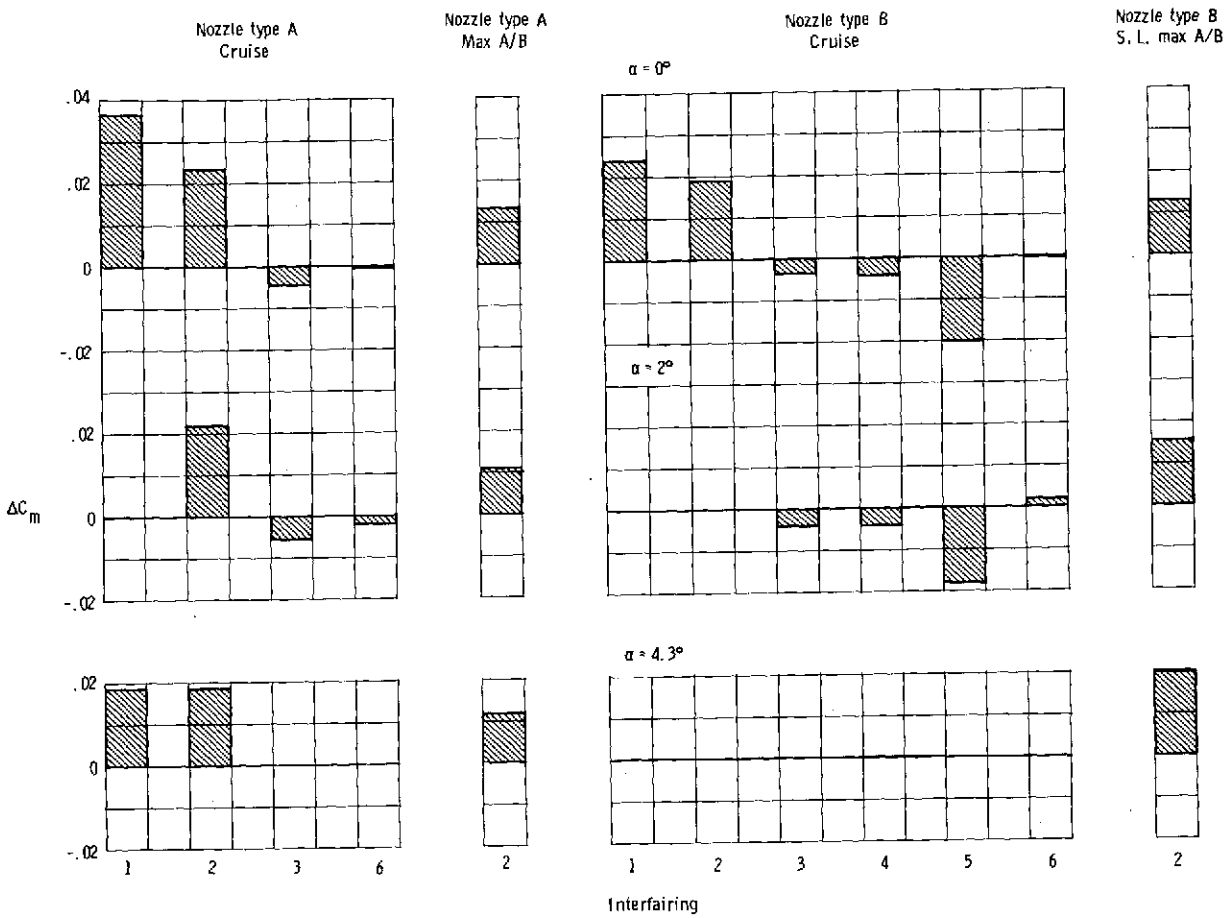

(d) M = 0.90.

Figure 32.- Concluded.

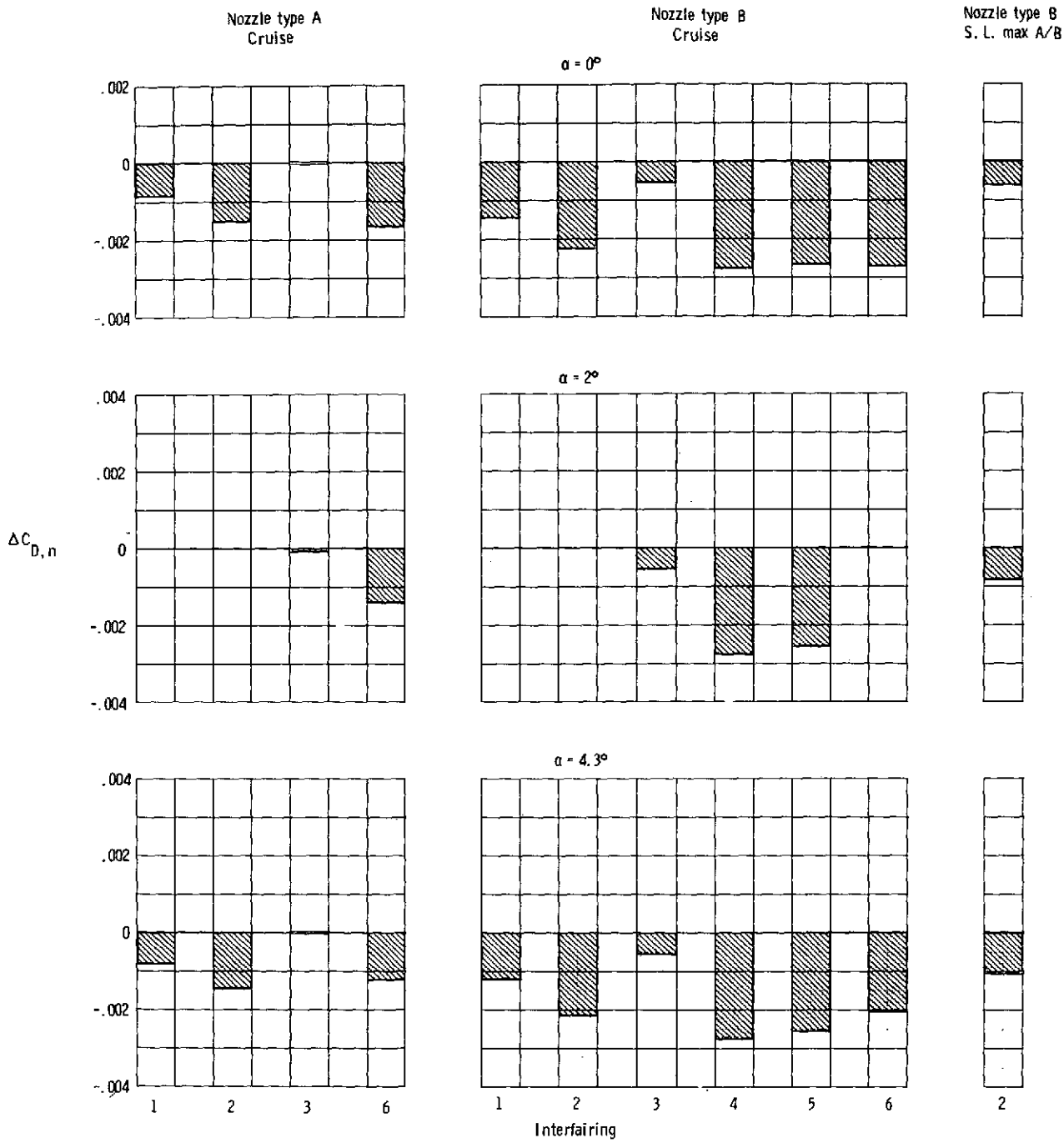

(a) M = 0.60.

Figure 33.- Nozzle drag increment due to changing from basic interfairing to various modified interfairings.

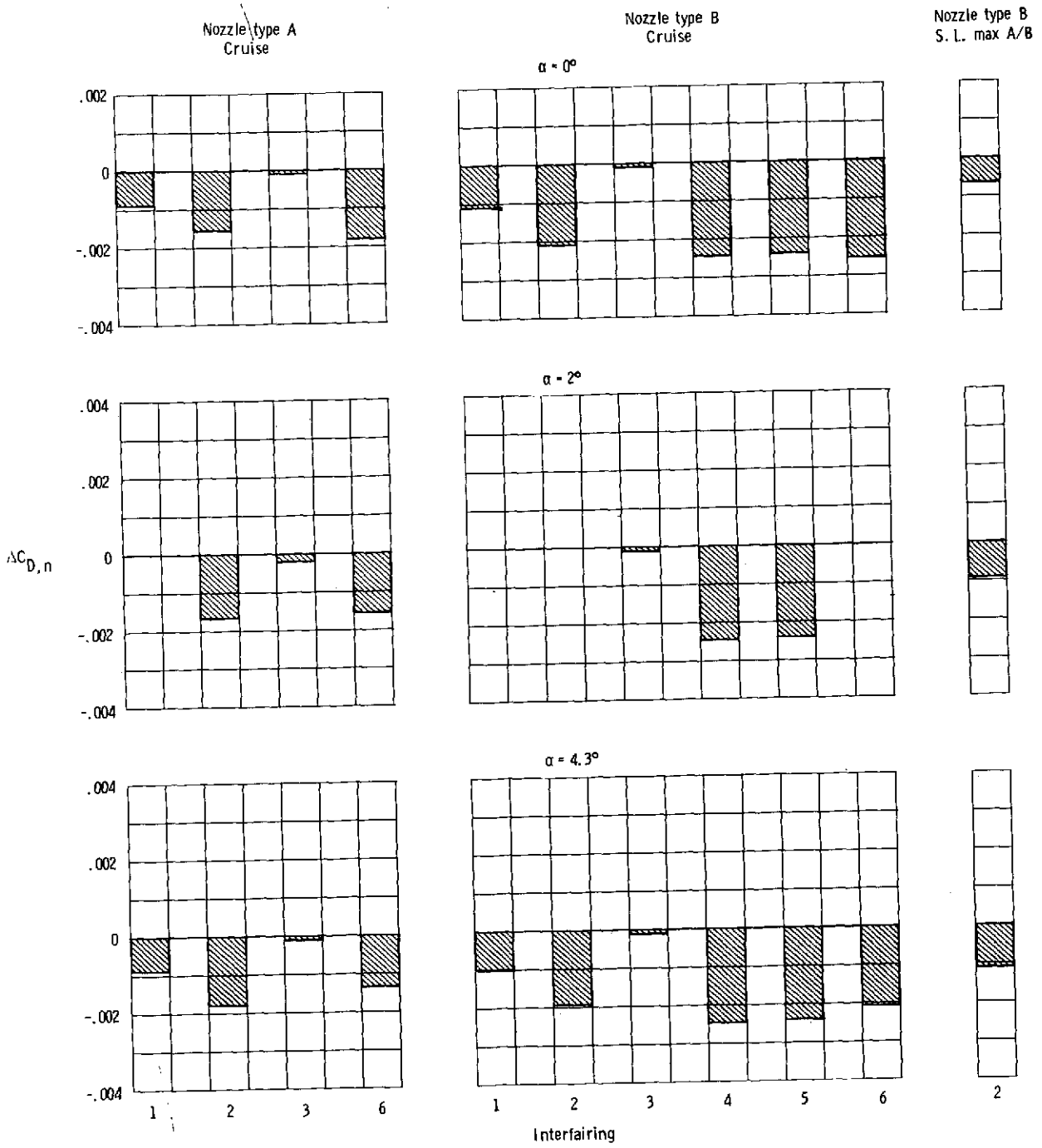

(b) M = 0.70.

Figure 33.- Continued.

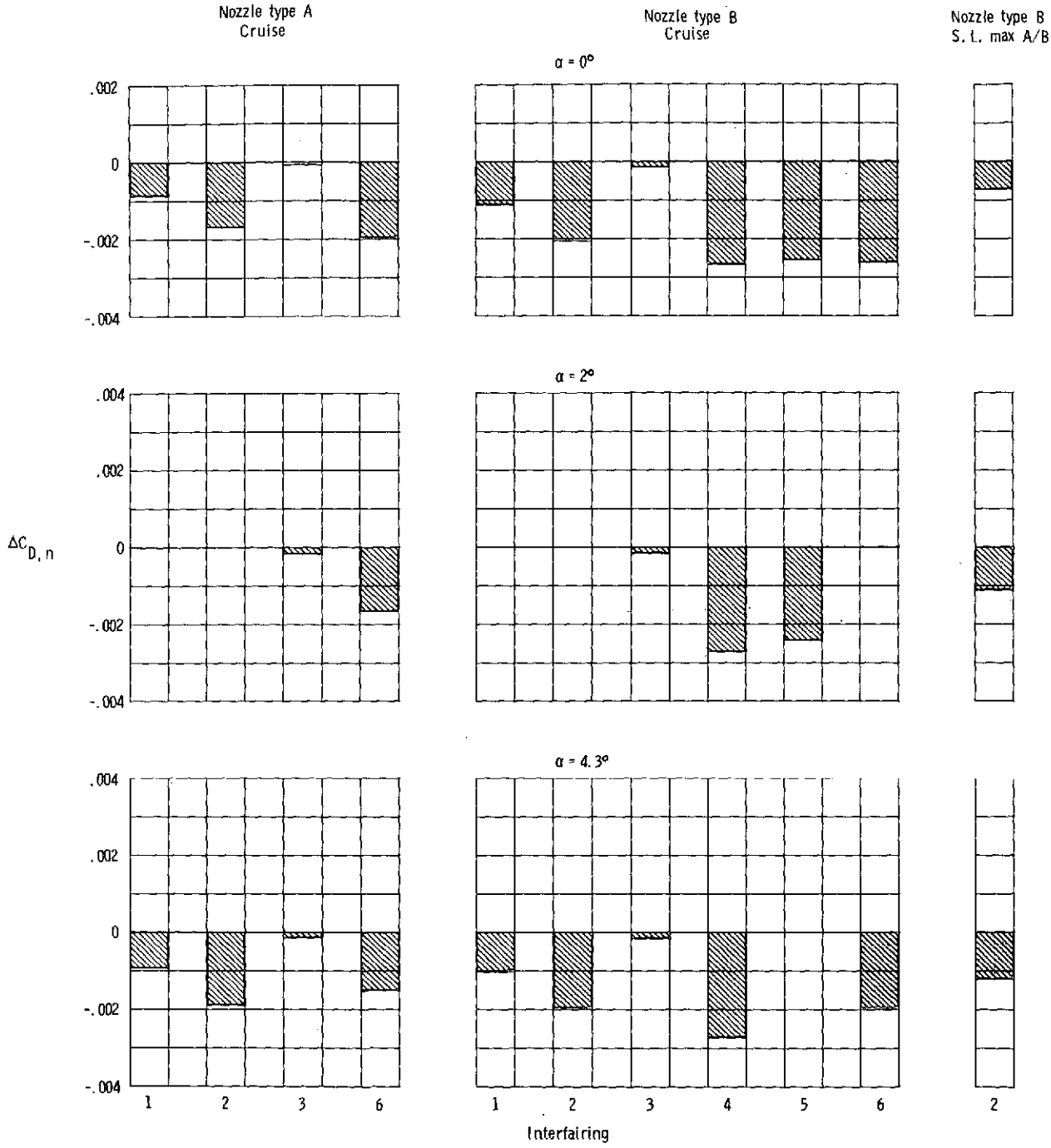

(c) M = 0.80.

Figure 33.- Continued.

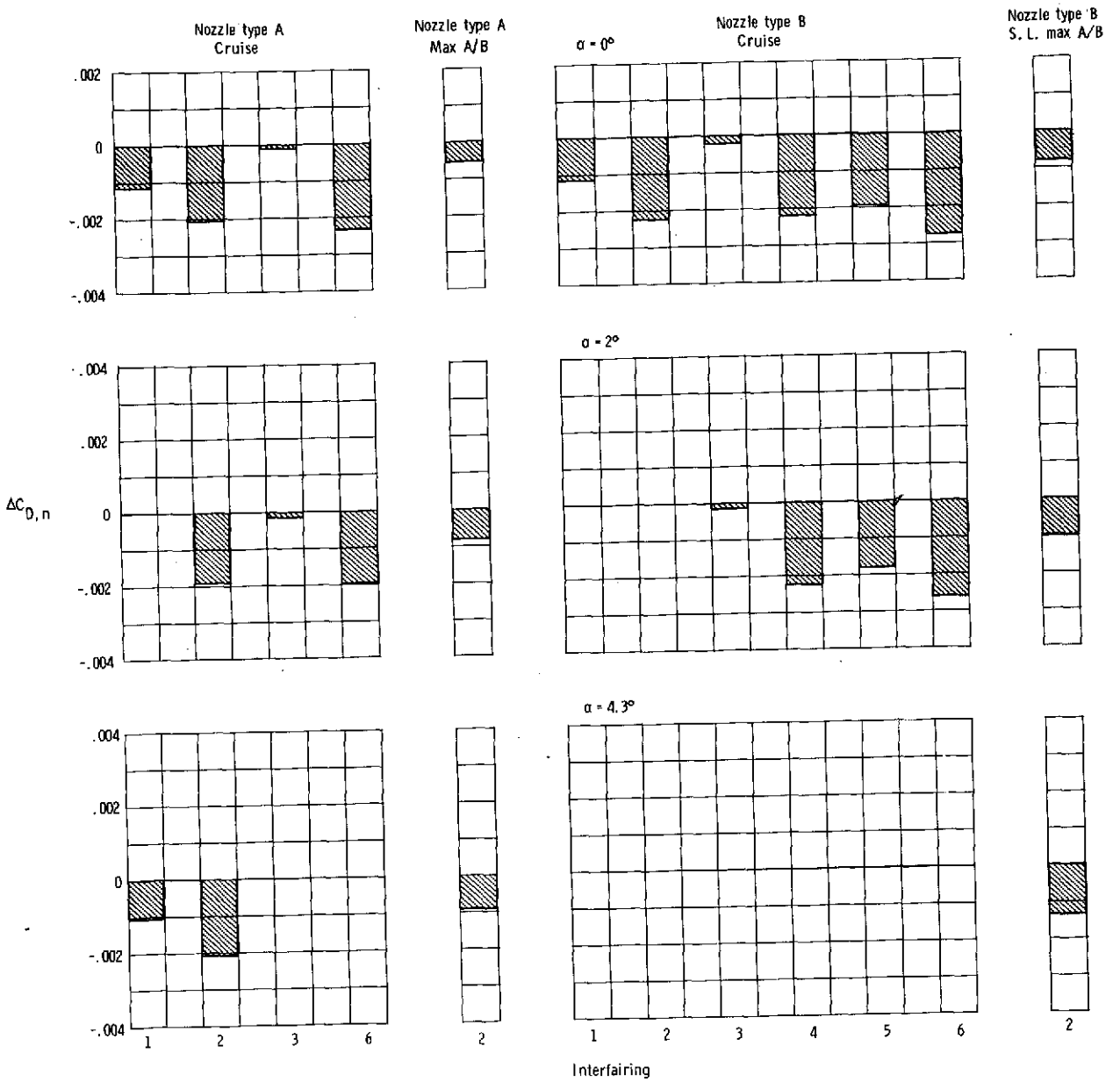

(d) M = 0.90.

Figure 33.- Concluded.

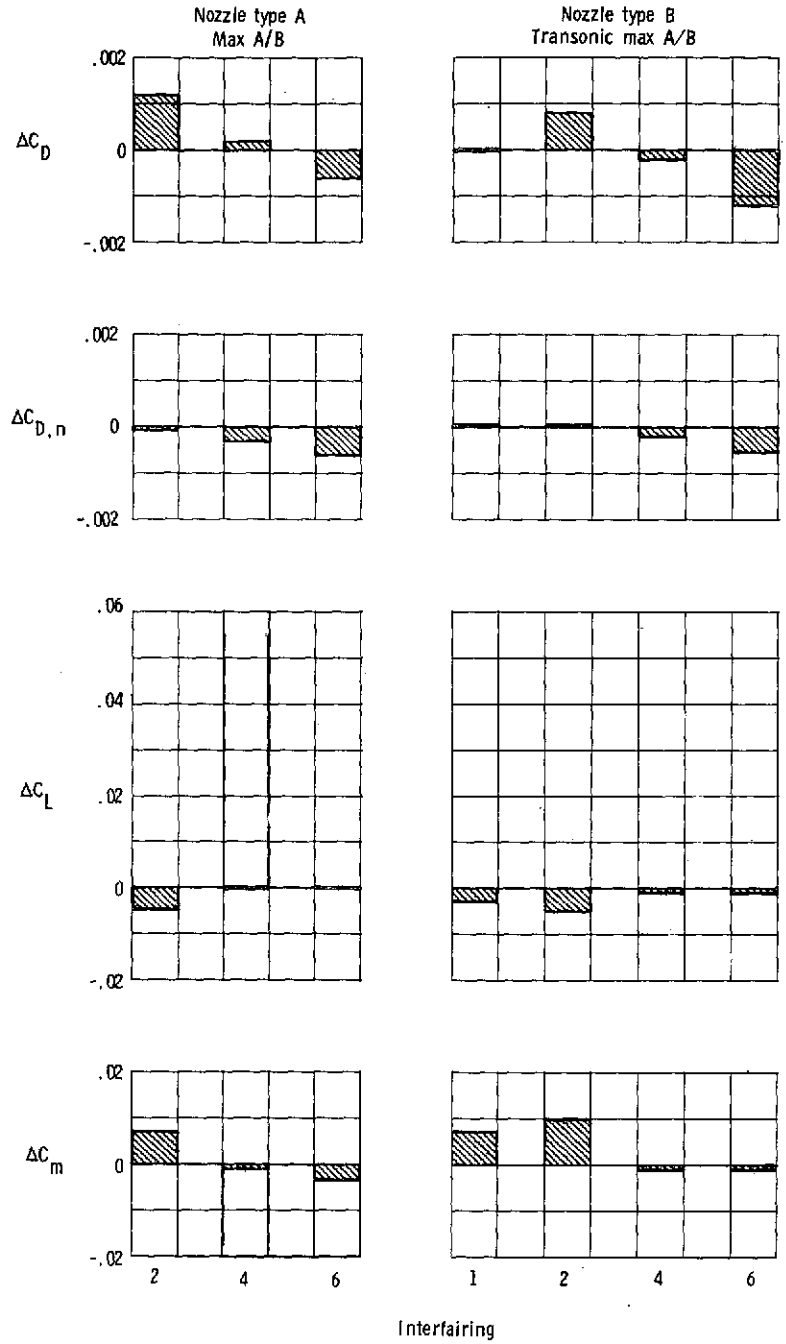

Figure 34.- Increments in afterbody-nozzle aerodynamic characteristics due to changing from basic interfairing to various modified interfairings at $M = 1.20$; $\alpha = 2^{o}$.

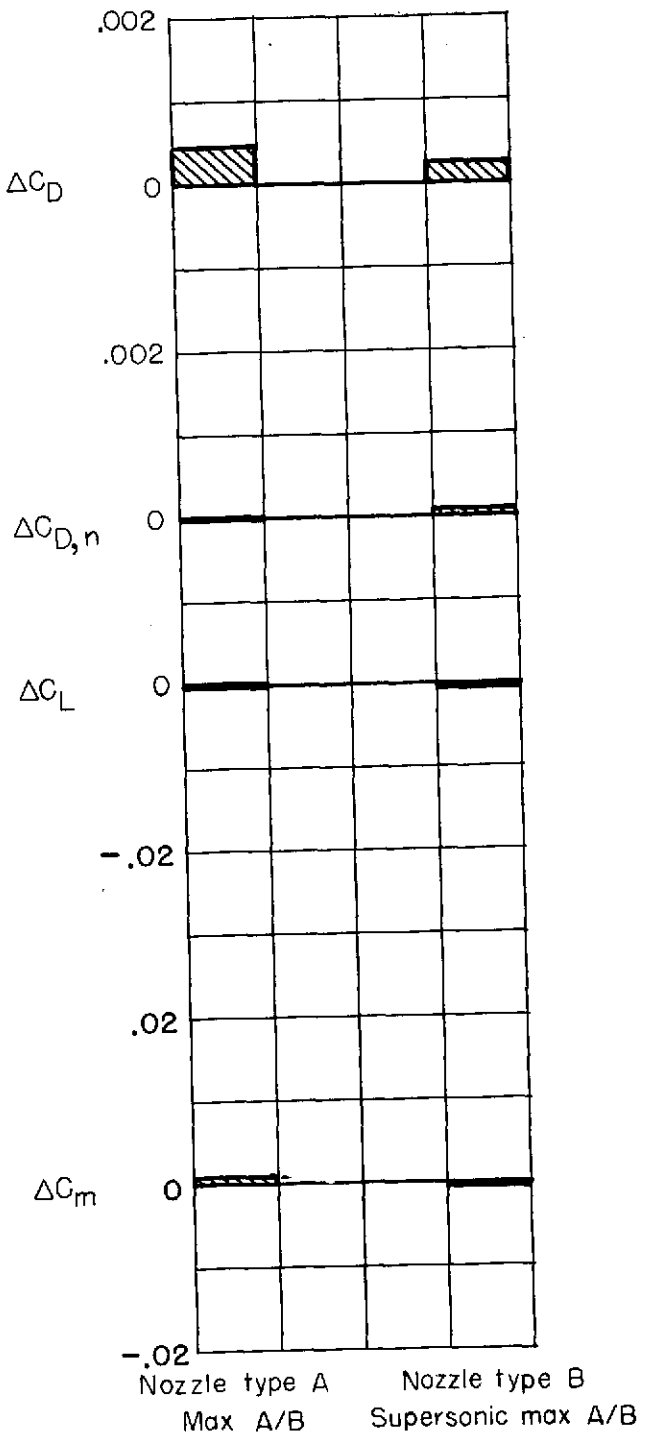

Figure 35.- Increments in afterbody-nozzle aerodynamic characteristics due to changing from basic interfairing to interfairing 2 at $M = 2.2$; $\alpha = 0^o$.

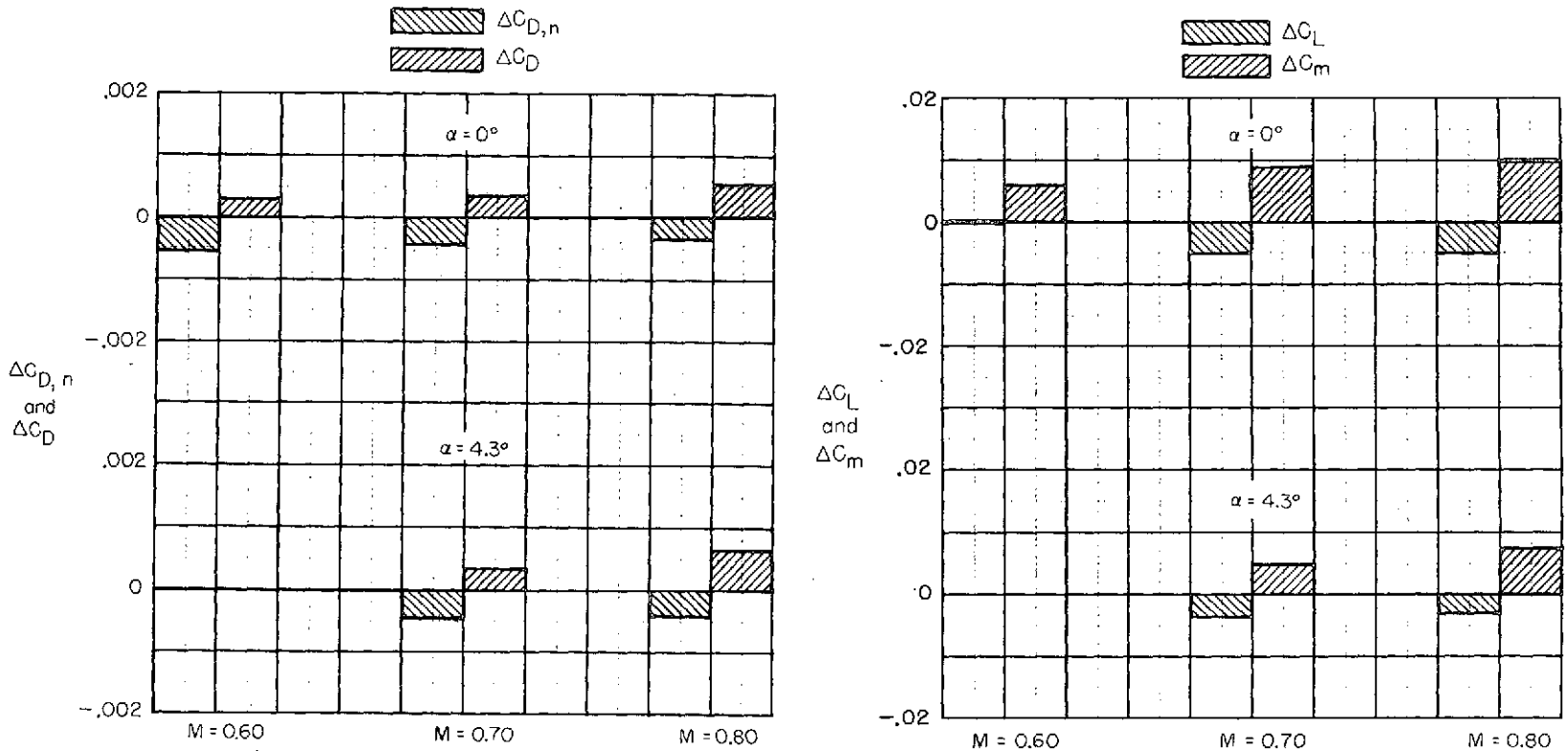

(a) Nozzle and afterbody-nozzle drag.

(b) Afterbody-nozzle lift and pitching moment.

Figure 36.- Increments in afterbody-nozzle aerodynamic characteristics due to addition of vortex generators to top of nacelles with type A cruise nozzles and basic interfairing.

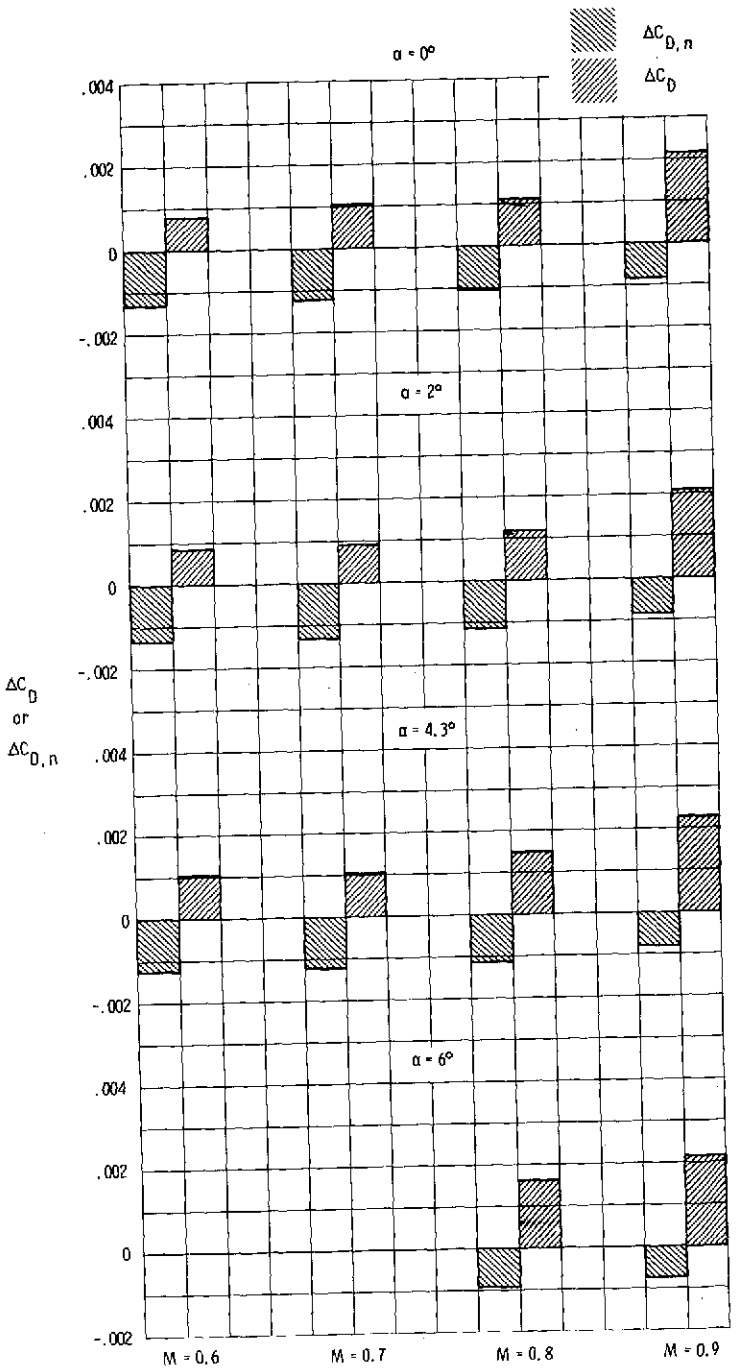

(a) Afterbody-nozzle and nozzle drag.

Figure 37.- Increments in afterbody-nozzle aerodynamic characteristics due to addition of vortex generators encircling nacelles with type A cruise nozzles and basic interfairing.

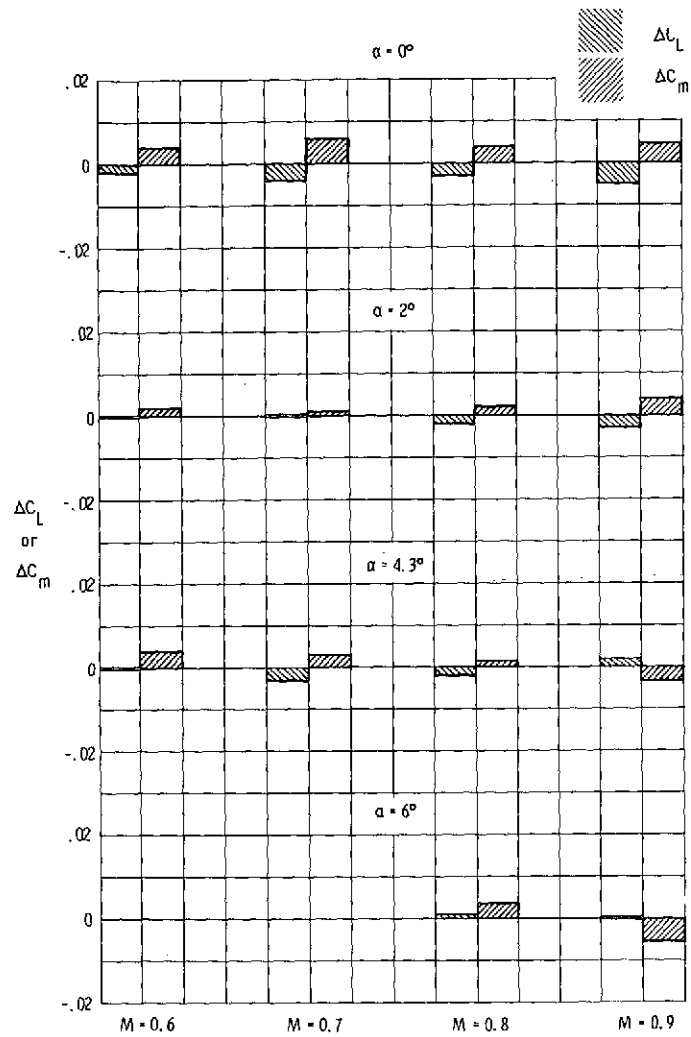

(b) Afterbody-nozzle lift and pitching moment.

Figure 37.- Concluded.

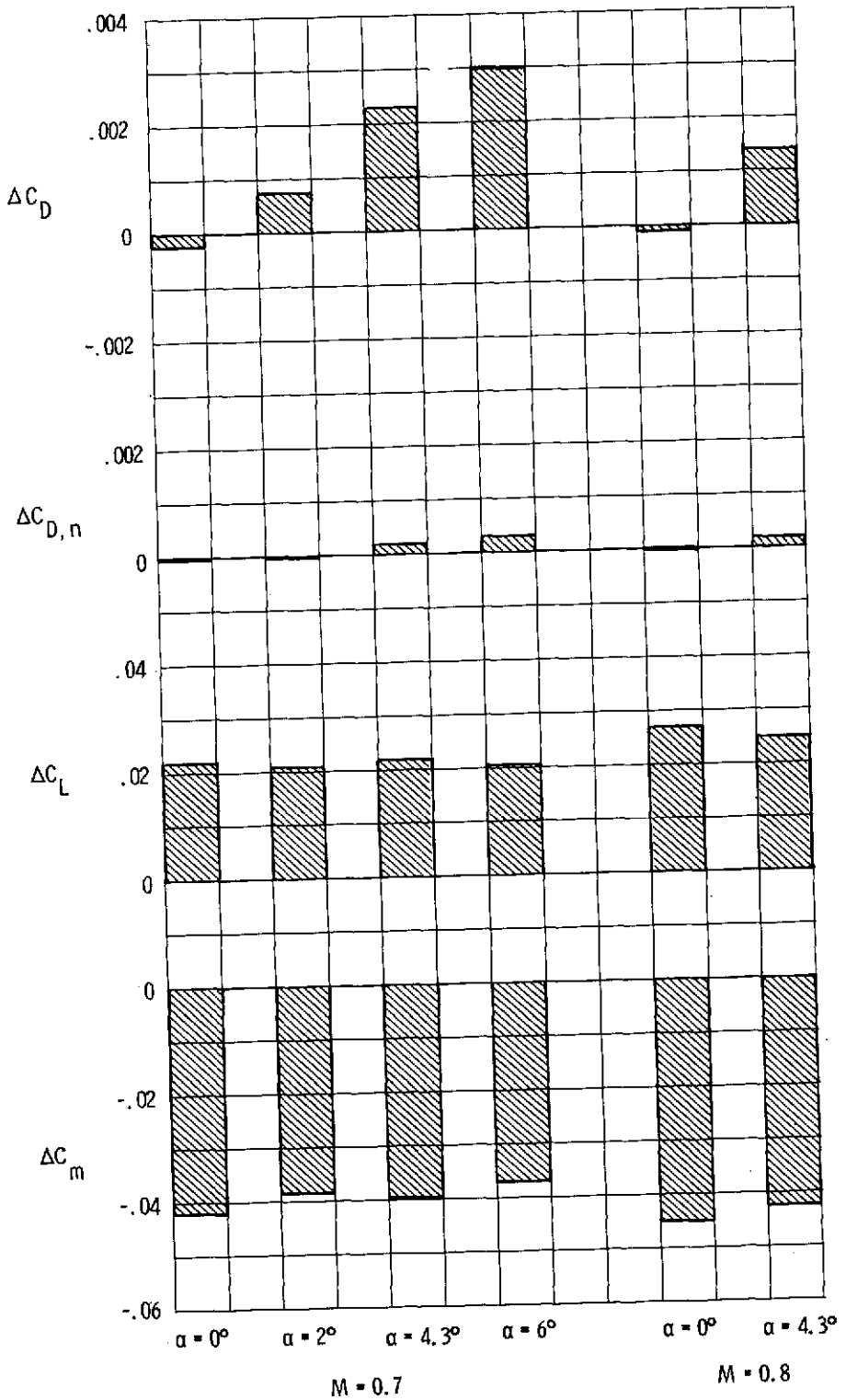

Figure 38.- Increments in afterbody-nozzle aerodynamic characteristics due to deflecting horizontal tails from 0^o to $+2^o$ with type A cruise nozzles and interfairing 2.

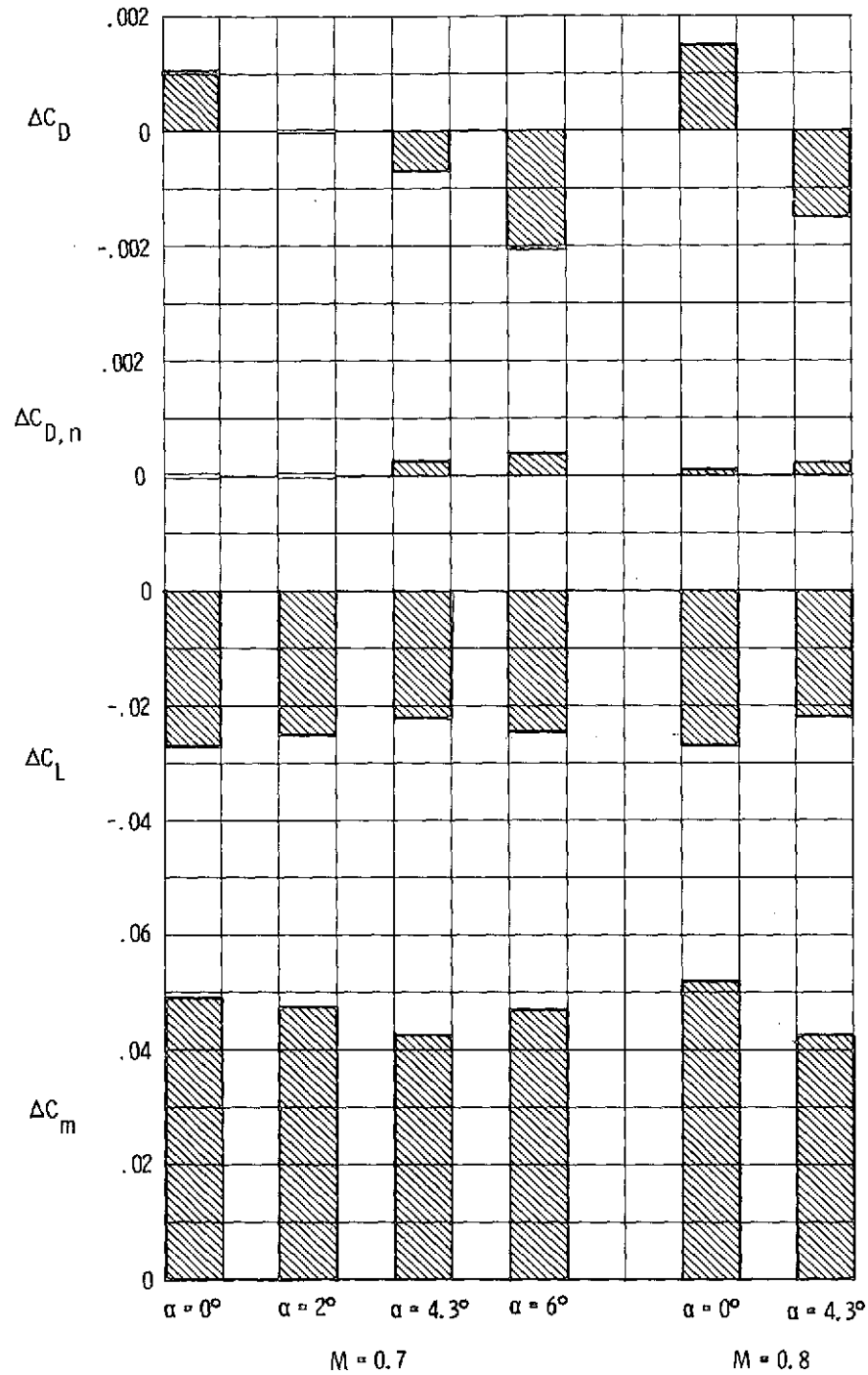

Figure 39.- Increments in afterbody-nozzle aerodynamic characteristics due to deflecting horizontal tails from 0^o to -2^o with type A cruise nozzles and interfairing 2.